frontiers | Research Topics

Genetic regulation of meat quality traits in livestock species

Edited by
Rajwali Khan, Anning Li and Sayed Haidar Abbas Raza

Published in
Frontiers in Veterinary Science
Frontiers in Genetics

ISSN 1664-8714
ISBN 978-2-83251-330-9
DOI 10.3389/978-2-83251-330-9

About Frontiers

Frontiers is more than just an open access publisher of scholarly articles: it is a pioneering approach to the world of academia, radically improving the way scholarly research is managed. The grand vision of Frontiers is a world where all people have an equal opportunity to seek, share and generate knowledge. Frontiers provides immediate and permanent online open access to all its publications, but this alone is not enough to realize our grand goals.

Frontiers journal series

The Frontiers journal series is a multi-tier and interdisciplinary set of open-access, online journals, promising a paradigm shift from the current review, selection and dissemination processes in academic publishing. All Frontiers journals are driven by researchers for researchers; therefore, they constitute a service to the scholarly community. At the same time, the *Frontiers journal series* operates on a revolutionary invention, the tiered publishing system, initially addressing specific communities of scholars, and gradually climbing up to broader public understanding, thus serving the interests of the lay society, too.

Dedication to quality

Each Frontiers article is a landmark of the highest quality, thanks to genuinely collaborative interactions between authors and review editors, who include some of the world's best academicians. Research must be certified by peers before entering a stream of knowledge that may eventually reach the public - and shape society; therefore, Frontiers only applies the most rigorous and unbiased reviews. Frontiers revolutionizes research publishing by freely delivering the most outstanding research, evaluated with no bias from both the academic and social point of view. By applying the most advanced information technologies, Frontiers is catapulting scholarly publishing into a new generation.

What are Frontiers Research Topics?

Frontiers Research Topics are very popular trademarks of the *Frontiers journals series*: they are collections of at least ten articles, all centered on a particular subject. With their unique mix of varied contributions from Original Research to Review Articles, Frontiers Research Topics unify the most influential researchers, the latest key findings and historical advances in a hot research area.

Find out more on how to host your own Frontiers Research Topic or contribute to one as an author by contacting the Frontiers editorial office: frontiersin.org/about/contact

Genetic regulation of meat quality traits in livestock species

Topic editors

Rajwali Khan — University of Agriculture, Peshawar, Pakistan

Anning Li — Northwest A&F University, China

Sayed Haidar Abbas Raza — South China Agricultural University, China

Citation

Khan, R., Li, A., Raza, S. H. A., eds. (2023). *Genetic regulation of meat quality traits in livestock species*. Lausanne: Frontiers Media SA. doi: 10.3389/978-2-83251-330-9

Table of contents

frontiers | Frontiers in Genetics

TYPE Editorial
PUBLISHED 04 January 2023
DOI 10.3389/fgene.2022.1092562

OPEN ACCESS

EDITED AND REVIEWED BY
Martino Cassandro,
University of Padua, Italy

*CORRESPONDENCE
Rajwali Khan,
rajwalikhan@aup.edu.pk

SPECIALTY SECTION
This article was submitted to Livestock Genomics,
a section of the journal
Frontiers in Genetics

RECEIVED 08 November 2022
ACCEPTED 02 December 2022
PUBLISHED 04 January 2023

CITATION
Khan R, Li A and Raza SHA (2023), Editorial: Genetic Regulation of Meat Quality Traits in Livestock Species. *Front. Genet.* 13:1092562. doi: 10.3389/fgene.2022.1092562

Editorial: Genetic Regulation of Meat Quality Traits in Livestock Species

Rajwali Khan[1]*, Anning Li[2] and Sayed Haidar Abbas Raza[2]

[1]Department of Livestock Management, Breeding and Genetics, The University of Agriculture Peshawar-Pakistan, Peshawar, Pakistan, [2]College of Animal Science and Technology, Northwest A&F University, Yangling, China

KEYWORDS

gene expression and regulation, meat quality, candidate gene, intramuscular fat (IMF), marker genes, differential gene expression

Editorial on the Research Topic
Genetic regulation of meat quality traits in livestock species

The increasing demand of the animal origin food for ever-expanding human population is an alarming call for the sustainable development in livestock productivity with high-quality animal proteins. In recent years, the application of modern technologies including advanced sequencing technologies, genome editing, genotype analysis, and genome profiling has promoted important changes in livestock genetic and breeding programs. These factors still fall short of accounting for the optimal level of variation that is required to achieve continued improvements in livestock productivity. The epigenome, which responds to internal and external environmental cues, is less explored but contains additional levels of variation that could be exploited for livestock traits of economic importance. Meat production and quality traits are strictly controlled by genetic factors, however their molecular mechanism is still needs to be explored. Intramuscular fat is a real challenge for the experts of animal science to improve meat quality traits. Research on the mechanism of adipogenesis provides invaluable information for the improvement of meat quality traits. In livestock species, the IM fat is considered one of the most important factors that determines carcass quality traits. Therefore, approaches for the improvement of Intramuscular fat deposition are crucial for the development of meat quality (Junjvlieke et al., 2020; Raza et al., 2020). Increasing the intramuscular fat content will increase the marbled texture of beef, and the tenderness and flavor of beef will become more palatable. Therefore, increasing the degree of fat deposition especially intramuscular fat in beef cattle is important research contents in the current beef cattle industry. Fat content is closely related to the number of fat cells and the volume of fat cells, and is regulated by the transcriptional expression of a large number of genes during the proliferation and differentiation of fat cells. At present, research on key regulatory genes in adipocyte differentiation and lipid metabolism is a focus of attention (Guo et al., 2018a; Guo et al., 2018b; Hongfang et al., 2022). Therefore, the current Research Topic was planned and researchers around the globe were invited to

explore the mechanism of genetic regulation of meat quality traits in livestock species. All important molecular mechanisms such as transcriptional and post-transcriptional regulation of adipogenic marker genes. RNAs, transcription factors, candidate genes, SNPs, sequencing, DNA methylation, DNA-Protein interaction for the improvement of meat quality traits were considered in this Research Topic. The Research Topic was published in 24 February 2022 with the titled "*Genetics regulation of meat quality traits in livestock species*", and closed on 31st of August 2022. A total of 09 manuscripts were published by 73 authors around the globe. Keeping in view the importance of molecular regulation of meat quality traits of meat obtained from different livestock species, we received manuscripts regarding cattle, buffalo, yak, sheep, pig and donkeys. We can summarize the published articles with the following description against each group of manuscript based on the target species of livestock.

In the first category, the manuscript related with beef quality from cattle were published in this Research Topic. The first manuscript explored the role of N^6-methyladenosine (m^6A) in bovine skeletal myoblast differentiation. They ascertained mRNA m^6A methylation exhibited declined changes during bovine skeletal myoblast differentiation, and both *MEF2C* mRNA expression and m^6A levels were significantly increased during myoblast differentiation. They also found that *MEF2C* with mutated m^6A sites significantly inhibited myoblast differentiation compared with wild-type *MEF2C*. METTL3 promoted MEF2C protein expression through posttranscriptional modification in an m^6A-YTHDF1-dependent manner. Moreover, MEF2C promoted the expression of METTL3 by binding to its promoter. These results revealed that there is a positive feedback loop between these molecules in myoblast differentiation. This manuscript provided new insights into skeletal muscle differentiation and fusion, which may provide an RNA methylation-based approach for molecular genetics and breeding in livestock as well as for the treatment of muscle-related diseases (Yang et al.). The second manuscript used bioinformatics tools for the exploration of differential genes in the regulation of adipogenesis. The authors downloaded the GSE116775 microarray dataset from Gene Expression Omnibus (GEO). The weighted gene co-expression network (WGCNA) was used to analyze the gene expression profile, and the key gene modules with the highest correlation with subcutaneous adipose tissue were identified, and the functional enrichment of the key modules was analyzed. Then, the "real" Hub gene was screened by in-module analysis and protein–protein interaction network (PPI), and its expression level in tissue samples and adipocytes was verified. The study showed that a total of nine co-expression modules were identified, and the number of genes in these modules ranged from 101 to 1,509. Among them, the blue module is most closely related to subcutaneous adipose tissue, containing 1,387 genes. These genes were significantly enriched in 10 gene ontologies including extracellular matrix organization, biological adhesion, and collagen metabolic process, and were mainly involved in pathways including ECM-receptor interaction, focal adhesion, cAMP signaling pathway, PI3K-AKT signaling pathway, and regulation of lipolysis in adipocytes. In the PPI network and coexpression network, five genes (CAV1, ITGA5, COL5A1, ABL1, and HSPG2) were identified as "real" Hub genes. Analysis of Hub gene expression by dataset revealed that the expression of these Hub genes was significantly higher in subcutaneous adipose tissue than in other tissues. In addition, real-time fluorescence quantitative PCR (qRT-PCR) analysis based on tissue samples and adipocytes also confirmed the above results. In this study, five key genes related to subcutaneous adipose tissue were discovered, which laid a foundation for further study of the molecular regulation mechanism of subcutaneous adipose tissue development and adipose deposition (Sheng et al.).

In this Research Topic two manuscripts were published regarding exploration of molecular mechanism in buffalo meat quality. In the first manuscript, the authors explore the role of Fatty acid transport 1 (FATP1) in intramuscular adipogenesis in buffalo. They investigated the effects of FATP1 on the differentiation and proliferation of adipocytes in five types of cells derived from muscle and adipose tissue and estimated the effects of FATP1 on intramuscular fat (IMF) deposition. This manuscript explored that FATP1 is mainly expressed in heart and muscle tissue in buffaloes as well as cells undergoing adipogenic differentiation. Interestingly, they found that FATP1 promoted the adipogenic differentiation of muscle-derived cells (buffalo myocytes and intramuscular preadipocytes and mouse C2C12 cells) but did not affect, or even inhibited, that of adipose-derived cells (buffalo subcutaneous preadipocytes and mouse 3T3-L1 cells, respectively). They concluded that FATP1 promotes IMF deposition and enhance the proliferative activity of all the assessed cells, except murine 3T3-L1 cells. These results provide new insights into the potential effects of FATP1 on IMF deposition, especially regarding its positive effects on meat quality in buffaloes and other livestock species (Huanget al.). In the second manuscript regarding buffalo meat quality, the authors used the bioinformatics tools along with the *in-vivo* and *in-vitro* analysis for the exploration of molecular mechanism in buffalo meat. In this study, weighted gene co-expression network analysis (WGCNA) was used to construct a circRNA co-expression network and revealed a candidate circRNA that may affect the IMF deposition of buffalo as determined by RT-qPCR, semiquantitative PCR and gain-of-function experiments. In this manuscript, the WGCNA determined that one module (turquoise module) is significantly associated with the growth and development stages of buffalo. Further analysis revealed a total of 191 overlapping circRNAs among differentially expressed (DE) circRNAs and the co-expression module. A candidate circRNA was found, 21:6969877|69753491 (circRNA_ID), with

a reported involvement in lipid metabolism. This circRNA is stably expressed and originates from the *MARK*3 gene, hence the name circMARK3. The circMARK3 is highly expressed in adipose tissue and mature adipocytes and is located in the cytoplasm. Gain-of-function experiments demonstrated that circMARK3 promoted adipogenic differentiation of buffalo adipocytes and 3T3-L1 cells by up-regulating the expression levels of adipogenic marker genes *PPARG, C/EBP*α and *FABP*4. They concluded that circMARK3 is a potential factor that promotes fat deposition by regulating adipocyte differentiation and adipogenesis in buffalo (Feng et al.).

In the third group of manuscripts, the articles related to donkey meat quality were included. One manuscript published in this category explored a total of 585,555 spectra from the six muscle samples. In total, 20,583 peptides were detected, including 15,279 unique peptides, and 2,540 proteins were identified. They, analyzed differentially abundant proteins (DAPs) between longissimus dorssi (LD) muscles of donkeys with high (H) and low (L) IMF content. They identified 30 DAPs between the H and L IMF content groups, of which 17 were upregulated and 13 downregulated in the H IMF group. Gene Ontology (GO) and Kyoto Encyclopedia of Genes and Genomes (KEGG) functional enrichment analysis of these DAPs revealed many GO terms (e.g., bone morphogenetic protein (BMP) receptor binding) and pathways (e.g., Wnt signaling pathway and Hippo signaling pathway) involved in lipid metabolism and adipogenesis. The construction of protein–protein interaction networks identified 16 DAPs involved in these networks. Our data provide a basis for future investigations into candidate proteins involved in IMF deposition and potential new approaches to improve meat quality in the donkey (Tan et al.).

The fourth group of published articles in this Research Topic included molecular regulation of mutton quality traits obtained from sheep. In one manuscript the authors characterized the miRNA transcriptome of the longissimus thoracis et lumborum muscle at several developmental time points such as at gestational d 85 (PN1), 110 (PN2), 133 (PN3), postnatal d 42 (PW1), 65 (PW2), and 243 (MAT) during muscle hypertrophy in lambs. They also examined the miR-29a expression and found that it is differentially regulated across development, loss of function on satellite cell proliferation and differentiation. Muscle fiber characteristics showed drastic increases ($p < 0.0001$) in fiber size and alterations in muscle fiber type occur during pre and postnatal development. miRNA sequencing comparisons were performed in developmental order (PN1 vs. PN2, PN2 vs. PN3, PN3 vs. PW1, PW1 vs. PW2, PW2 vs. MAT). There were 184 differentially expressed (Padj <0.05) miRNA, 142 unique miRNA, from all 5 comparisons made. The transitional stage (PN3 vs. PW1) had the largest number (115) of differentially expressed miRNA. Inhibition of miR-29a in satellite cell culture increased ($p < 0.05$) cell proliferation and differentiation capacity. Characterization of the miRNA transcriptome provides valuable insights into the miRNA involved in muscle fiber hypertrophy and the potential importance of the transitional period (Greene et al.). In another manuscript, in this category of sheep mutton quality the authors used high-throughput RNA sequencing to assess the expression profiles of coding and non-coding RNAs in muscle tissue of Tan sheep and Dorper sheep. To investigate the molecular processes involved in the formation of muscle fibers, they collected two different muscle tissues, longissimus dorsi and biceps femoris, from Tan sheep and Dorper sheep. The longissimus dorsi of Tan sheep and Dorper sheep displayed significantly differential expression levels for 214 lncRNAs, 25 mRNAs, 4 miRNAs, and 91 circRNAs. Similarly, 172 lncRNAs, 35 mRNAs, 12 miRNAs, and 95 circRNAs were differentially expressed in the biceps femoris of Tan sheep and Dorper sheep according to the expression profiling. GO and KEGG annotation revealed that these differentially expressed genes and non-coding RNAs were related to pathways of the formation of muscle fiber, such as the Ca^{2+}, FoxO, and AMPK signaling pathways. Several key genes are involved in the formation of muscle fibers, including ACACB, ATP6V0A1, ASAH1, EFHB, MYL3, C1QTNF7, SFSWAP, and FBXL5. RT-qPCR verified that the expression patterns of randomly selected differentially expressed transcripts were highly consistent with those obtained by RNA sequencing. A total of 10 lncRNAs, 12 miRNAs, 20 circRNAs, and 19 genes formed lncRNA/circRNA-miRNA-gene networks, indicating that the formation of muscle fiber in Tan sheep is controlled by intricate regulatory networks of coding and non-coding genes. Our findings suggested that specific ceRNA subnetworks, such as circ_0017336-miR-23a-FBXL5, may be critical in the regulation of the development of muscle fibers, offering a valuable resource for future study of the development of muscle fibers in this animal species. These findings increase our understanding of the variety in how muscle fibers originate in various domestic animals and lay the groundwork for future research into new systems that regulate the development of muscle (Cui et al.).

In this Research Topic the fifth category of published articles was regarding the exploration of molecular mechanism of pig meat quality. The first article the circRNA expression profiles between Huainan pigs (Chinese indigenous pigs, fat-type, HN) and Large White pigs (Western commercial pigs, lean-type, LW) in the longissimus dorsi (LD) muscle at 38, 58, and 78 days post conception (dpc) were compared by sequencing. In total, 39,887 circRNAs were identified in 18 samples, and 60, 78, and 86 differentially expressed circRNAs (DECs) were found at the three stages mentioned above between these two breeds. The parent genes of DECs were enriched in myogenesis, proliferation, adipogenesis and muscle fiber-type transition. The circRNA-miRNA interaction networks included 38 DECs and 47 miRNAs, and these miRNAs were involved in muscle development and lipid metabolism. Two shared DECs (circ_0030593 and circ_0032760) of these three stages were selected, their head-to-tail junction sites were validated by Sanger sequencing, and RT–qPCR results suggested that these two

DECs might be involved in intramuscular fat deposition. These findings provide a basis for understanding the role of circRNAs in meat quality (Wang et al.). In the second manuscript under this category, the authors analyzed lncRNAs in longissimus thoracis (LT) and semitendinosus (ST) muscles, being different in meat quality, with RNA-sequencing technology. A total of 500 differentially expressed lncRNAs (DELs) and 2,094 protein-coding genes (DEGs) were identified. Through KEGG analysis on DELs, they first made clear that fat deposition might be the main reason resulting in the differential phenotype of LT and ST, for which cGMP–PKG and VEGF signaling pathways were the most important ones. In total, forty-one key DELs and 50 DEGs involved in the differential fat deposition were then characterized. One of the key genes, cAMP-response element binding protein 1, was selected to confirm its role in porcine adipogenesis with molecular biology methods and found that it promotes the differentiation of porcine preadipocytes, consistent with its higher expression level and intramuscular fat contents in LT than that in ST muscle. Furthermore, through integrated analysis of DELs and DEGs, transcription factors important for differential fat deposition were characterized among which BCL6 has the most target DEGs while MEF2A was targeted by the most DELs. The results provide candidate genes crucial for meat quality, which will contribute to improving meat quality with molecular-breeding strategies (Sun et al.).

Author contributions

RK conceived the idea, wrote the manuscript, AL and SR edited the draft.

Conflict of interest

The authors declare that the research was conducted in the absence of any commercial or financial relationships that could be construed as a potential conflict of interest.

Publisher's note

All claims expressed in this article are solely those of the authors and do not necessarily represent those of their affiliated organizations, or those of the publisher, the editors and the reviewers. Any product that may be evaluated in this article, or claim that may be made by its manufacturer, is not guaranteed or endorsed by the publisher.

References

Guo, H., Khan, R., Raza, S. H. A., Ning, Y., Wei, D., Wu, S., et al. (2018a). KLF15 promotes transcription of KLF3 gene in bovine adipocytes. *Gene* 659, 77–83. doi:10.1016/j.gene.2018.03.049

Guo, H., Raza, S. H. A., Schreurs, N. M., Khan, R., Wei, D., Wang, L., et al. (2018b). Genetic variants in the promoter region of the KLF3 gene associated with fat deposition in Qinchuan cattle. *Gene* 672, 50–55. doi:10.1016/j.gene.2018.06.022

Hongfang, G., Khan, R., Raza, S. H. A., Nurgulsim, K., Suhail, S. M., Rahman, A., et al. (2022). Transcriptional regulation of adipogenic marker genes for the improvement of intramuscular fat in Qinchuan beef cattle. *Anim. Biotechnol.* 33 (4), 776–795. doi:10.1080/10495398.2020.1837847

Junjvlieke, Z., Khan, R., Mei, C., Cheng, G., Wang, S., Raza, S. H. A., et al. (2020). Effect of ELOVL6 on the lipid metabolism of bovine adipocytes. *Genomics* 112 (3), 2282–2290. doi:10.1016/j.ygeno.2019.12.024

Raza, S. H. A., Khan, S., Amjadi, M., Abdelnour, S. A., Ohran, H., Alanazi, K. M., et al. (2020). Genome-wide association studies reveal novel loci associated with carcass and body measures in beef cattle. *Arch. Biochem. Biophys.* 694, 108543. doi:10.1016/j.abb.2020.108543

frontiers | Frontiers in Veterinary Science

ORIGINAL RESEARCH
published: 28 April 2022
doi: 10.3389/fvets.2022.900924

MEF2C Expression Is Regulated by the Post-transcriptional Activation of the METTL3-m^{6}A-YTHDF1 Axis in Myoblast Differentiation

Xinran Yang[1], *Yue Ning*[1,2], *Sayed Haidar Abbas Raza*[1], *Chugang Mei*[1,3] *and Linsen Zan*[1,3]*

[1] College of Animal Science and Technology, Northwest A&F University, Xianyang, China, [2] College of Chemistry and Chemical Engineering, Xianyang Normal University, Xianyang, China, [3] National Beef Cattle Improvement Center, Northwest A&F University, Xianyang, China

N^6-methyladenosine (m^{6}A) plays an essential role in regulating gene expression. However, the effect of m^{6}A on skeletal myoblast differentiation and the underlying mechanisms are still unclear. Here, we ascertained mRNA m^{6}A methylation exhibited declined changes during bovine skeletal myoblast differentiation, and both *MEF2C* mRNA expression and m^{6}A levels were significantly increased during myoblast differentiation. We found that *MEF2C* with mutated m^{6}A sites significantly inhibited myoblast differentiation compared with wild-type *MEF2C*. METTL3 promoted MEF2C protein expression through posttranscriptional modification in an m^{6}A-YTHDF1-dependent manner. Moreover, MEF2C promoted the expression of METTL3 by binding to its promoter. These results revealed that there is a positive feedback loop between these molecules in myoblast differentiation. Our study provided new insights into skeletal muscle differentiation and fusion, which may provide an RNA methylation-based approach for molecular genetics and breeding in livestock as well as for the treatment of muscle-related diseases.

Keywords: N^6-methyladenosine, myoblast differentiation, MEF2C, METTL3, cattle

OPEN ACCESS

Edited by:
Honglin Jiang,
Virginia Tech, United States

Reviewed by:
Ayman Hassan Abd El-Aziz,
Damanhour University, Egypt
Rui-Si Hu,
University of Electronic Science and Technology of China, China

***Correspondence:**
Linsen Zan
zanlinsen@163.com

Specialty section:
This article was submitted to Livestock Genomics, a section of the journal Frontiers in Veterinary Science

Received: *21 March 2022*
Accepted: *06 April 2022*
Published: *28 April 2022*

Citation:
Yang X, Ning Y, Abbas Raza SH, Mei C and Zan L (2022) MEF2C Expression Is Regulated by the Post-transcriptional Activation of the METTL3-m^{6}A-YTHDF1 Axis in Myoblast Differentiation. Front. Vet. Sci. 9:900924. doi: 10.3389/fvets.2022.900924

INTRODUCTION

Research on the mechanisms underlying the growth, development and regeneration of skeletal muscle is of great significance to livestock meat production and meat quality improvements (1). The growth and development of skeletal muscle are extremely complex biological processes, which successively include directional differentiation of progenitor cells, myoblast proliferation, differentiation, and fusion of myocytes, and finally, formation of multinucleated muscle fibers with contractile function (2). Epigenetic changes such as DNA methylation and histone methylation, in addition to some myogenic-specific transcription factors, are known to play a key role in skeletal myogenesis (3, 4). Nonetheless, molecular selection breeding in beef cattle mostly focused on the exploration of some key genes, and rarely improved the breeding process from the perspective of RNA.

RNA methylation accounted for more than 60% of all identified chemical RNA modifications (5). Among these types of modification, N^6-methyladenosine (m^{6}A) is considered the most common mRNA modification in eukaryotes (6–12). m^{6}A is a dynamic and reversible posttranscriptional methylation modification, that is catalyzed by m^{6}A writer proteins

(methyltransferase complexes composed of METTL3, METTL14, and WTAP) and is demethylated by m^{6}A eraser proteins (FTO and ALKBH5) (13–17). The m^{6}A modification is functionally interpreted by m^{6}A "reader" proteins, such as the widely studied YTH-domain family proteins (18, 19). m^{6}A modification plays a variety of roles in mRNA metabolism, including mRNA translation efficiency, stability and splicing (19–23). A growing body of evidence suggested that m^{6}A influences a variety of biological processes, such as multiple cancer processes, mESC differentiation, antitumor immunity, cell fate determination, and adipogenesis (23–27). A series of recent studies, including ours, have published transcriptome profiles of m^{6}A modifications in muscle development in farm animals such as pigs, cattle, sheep and geese, revealing the important role of m^{6}A methylation modifications in skeletal muscle growth and development (28–36). However, the m^{6}A levels in the process of skeletal muscle myoblast differentiation and the detailed molecular mechanism underlying its role in this process are still unclear. Moreover, there are few reports on the biological functions of m^{6}A modification in cattle.

In the present study, we investigated the abundance, function and mechanism of m^{6}A modifications during myogenic differentiation in bovine myoblast. First, we found significant changes in the levels of m^{6}A modification in the mRNA of myoblasts and myotubes. We screened and identified the mechanism by which MEF2C expression was regulated by the METTL3-m^{6}A-YTHDF1 axis, and these findings were verified by MeRIP-seq, RNA-seq, and experiments. Then, it was found that MEF2C promotes the expression of METTL3 by directly binding to its promoter region. Our study identified the interaction of MEF2C and m^{6}A modification via a feedback loop during bovine skeletal muscle differentiation *in vitro*. Our findings make the mechanism of m^{6}A modification in skeletal myogenesis increasingly clear and provide an important basis for improving the molecular breeding of livestock from the perspective of RNA modification.

MATERIALS AND METHODS

Culture and Differentiation of Bovine Myoblasts

The cells used in this study were skeletal myoblasts of Qinchuan beef cattle preserved in our laboratory (36, 37). The myoblasts were cultured to 80–90% confluence in growth medium (GM), and then, myogenic differentiation was induced with differentiation medium (DM). The culture conditions were a humidified incubator (Thermo Fisher Scientific, MA, USA) containing 5% carbon dioxide at 37°C. The myoblast growth medium was composed of DMEM/F12 (HyClone, UT, USA), 20% fetal bovine serum (FBS, GIBCO, NY, USA) and 1% penicillin/streptomycin. The myoblast differentiation medium consisted of DMEM/F12 containing 2% horse serum (HS, GIBCO) and 1% penicillin/streptomycin. The medium was changed every 2 days.

RNA Isolation, CDNA Synthesis, and Real-Time Fluorescence Quantitative PCR (RT-QPCR)

RNAiso reagent (Takara, Dalian, China) was used to lyse proliferating myoblasts (named GM; 90% confluence, cultured in GM) and differentiated myotubes (named DM; cultured in DM for 4 d), and isolate the total RNA. PrimeScript RT reagent kit (Takara) was used to synthesize cDNA. The residual genomic DNA was removed at 42°C for 2 min, and then, the reverse transcription reaction was conducted at 37°C for 15 min and then at 85°C for 5 s. RT-qPCR was performed using the TB Green Premix Ex Taq II Kit (Takara) in the CFX Connect qPCR Detection System (BIO-RAD, CA, USA). Bovine *GAPDH* was used as the internal reference to standardize the data. Each sample analyzed by RT-qPCR was subjected to at least three biological repeats. Primers used for RT-qPCR are listed in **Supplementary Table 1**. Relative mRNA expression was calculated using the $2^{-\Delta\Delta Ct}$ method (38).

Analysis of the m^{6}A Levels in MRNA Using LC-MS/MS

Total RNA was purified using a PolyATtract mRNA Isolation Systems kit (Promega, WI, USA) following the manufacturer's protocols. About 200 ng of mRNA was digested in 25 μl buffer with nuclease P1 (2U; M0660S, NEB, MA, USA), 2.5 mM $ZnCl_2$ and 25 mM NaCl at 42°C for 2 h. Then alkaline phosphatase (0.5 U; Thermo Fisher, MA, USA) and NH_4HCO_3 (1 M, 3 ml) were added and incubated at 37°C for 2 h. Next, the sample was diluted 5-fold and filtered (pore size 0.22 mm; MilliporeSigma, MA, USA). A total of 5 μl of the solution was injected into an LC-MS/MS instrument. The total amount of m^{6}A in mRNA was assessed using an Agilent 1290 Infinity II-6470 (Agilent Technology, CA, USA) system as previously reported (15). The concentration of m^{6}A and A was calculated according to the standard curve, and then m^{6}A/A (%) was obtained.

Dot Blotting

The purified mRNA was diluted to to a concentration of 100 ∼ 200 ng/μl, denatured at 95°C for 3 min, and immediately put on ice. Approximately 1 μl mRNA or total RNA was spotted on a Hybond-N$^+$ membrane (GE Healthcarea, IL, USA) and UV-crosslinked for 15 min. After blocking with 5% non-fat milk for 2 h, the membranes were incubated with anti-m^{6}A antibody (202003, Synaptic Systems, Germany) overnight at 4°C. Then, the membranes and secondary antibodies incubation 2 h at room temperature. The membranes were imaged using the chemiluminescence method and the ChemiDoc XRS+ Imaging System (BIO-RAD, CA, USA). The developed membranes were stained with 0.02% methylene blue (MB) for 30 min to ensure equal of RNA loading.

Plasmid Construction, RNA Interference and Transfection

The coding sequences (CDS) of bovine *FTO* (NM_001098142), *METTL3* (NM_001102238), and *YTHDF1* (NM_001191416) were synthesized via PCR and cloned into the

pcDNA3.1 expression plasmid. The bovine *MEF2C* (ENSBTAT00000086206.1) CDS was synthesized and cloned into the pcDNA3.1-3xFlag-EGFP-C expression plasmid to generate the wild-type construct (*MEF2C*-WT). Nucleotide 1248 of the *MEF2C* CDS within the m^{6}A consensus sites was mutated from adenosine to cytosine (5′-GGACT-3′→ 5′-GGCCT-3′), and this sequence was synthesized by Sangon Biotech (Shanghai, China). All the primers are listed in **Supplementary Table 1**. Genepharma (Shanghai, China) synthesized all siRNAs for this study, and the sequences are shown in **Supplementary Table 2**.

To construct the wild-type *MEF2C* reporter plasmid, the entire sequence of *MEF2C* coding region was cloned into a psiCHECK2 vector (Promega) carrying Renilla luciferase and Firefly luciferase. Simultaneously, the adenosine (A) bases in the predicted m^{6}A common site were replaced with cytosine (C) bases to generate the *MEF2C* mutant reporter plasmid. Moreover, the amplified fragments of the *METTL3* promoter region containing the wild-type or mutated MEF2C-binding site were subcloned into a pGL3-promoter vector (Promega).

When the myoblasts reached 80-90% confluence, the cells were seeded in 6-well plates. The instantaneous transfection procedure was performed according to the protocol of the Lipofectamine 3000 transfection reagent (Invitrogen, CA, USA), and three replicate wells were transfected each time.

MRNA Stability Measurement

The cells were treated with actinomycin D (5 μg/ml, Selleck Chemicals, TX, USA) for 0, 3, 6, and 9 h before collection. Then total RNA was extracted, cDNA was synthesized, and the mRNA level was detected by RT-qPCR.

MeRIP-QPCR of Target Genes

m^{6}A immunoprecipitation assays were performed as previously described (39). In brief, 48 h after transfection, RNA from the cells was chemically digested into 200-nt fragments, and more than 200 μg of total RNA was subjected to immunoprecipitation with affinity-purified m^{6}A-specific antibody (202003, Synaptic Systems). The RNA fragments that bound to m^{6}A were separated by TRIzol reagent. Then the Input RNA and IP RNA were reverse transcribed, and the enriched sequences were detected by RT-qPCR. The ΔΔCt between the 10% input and the IP RNA was measured, and the relative fold change was calculated as $2^{-\Delta\Delta Ct}$. **Supplementary Table 1** lists the primers for amplification of the m^{6}A peak sequences.

Western Blotting

Cells were collected and lysed on ice in Western and IP cell lysis buffer (Beyotime Biotech, Shanghai, China) containing 1% PMSF (Solabio Life Sciences, Beijing, China) and 10% phosphatase inhibitor cocktail (Roche, Germany) for 30 min. The lysates were collected with a cell scraper and centrifuged at 14,000 g for 10 min at 4°C to collect the proteins in the supernatants. Then, the protein concentrations were determined by a BCA protein analysis kit (Beyotime Biotechnology). All the cell proteins were incubated at 100°C for 10 min in SDS-PAGE sample buffer. The proteins were separated by SDS-PAGE and transferred to PVDF membranes for immunoblotting. The membranes were incubated overnight with primary antibodies at 4°C and then with secondary antibodies at room temperature for 1.5 h. Western blotting was performed using the chemiluminescence method (ECL Plus detection system) and the band intensities were quantified by ImageJ (NIH, MD, USA) software. The antibodies are listed in **Supplementary Table 3**.

Immunofluorescence

Cultured myoblasts and myotubes were washed briefly with PBS and fixed with 4% paraformaldehyde at room temperature for 20 min, and then permeabilized with PBS containing 0.5% Triton X-100 for 15 min. The cells were subsequently washed three times with PBS. The cells were blocked with 0.3 M glycine, 10% donkey serum and 1% BSA in PBS for 1 h. Then, the cells were incubated with primary antibodies overnight at 4°C. After washing 3 times with PBS, the cells were incubated with fluorescent dye-conjugated secondary antibodies for 1.5 h at room temperature, and this step was performed in the dark. The cells were washed 3 times with PBS, stained with 0.1% DAPI (Sigma-Aldrich, MO, USA) for 15 min and then visualized under a fluorescence microscope [Olympus IX71 (Olympus Corporation, Japan) or Evos-fl-auto2 fluorescence microscopy imaging system (Thermo Fisher)]. The antibodies are listed in **Supplementary Table 3**.

Luciferase Reporter Assay

293A cells were inoculated in 24-well plates and transfected with a luciferase reporter, the pRL-TK Renilla luciferase vector (Promega), and the *METTL3* or *MEF2C* expression vectors. At least three biological replicates were set for each group. The relative luciferase activities were measured 48 h after transfection using a Dual-Luciferase Reporter Assay Kit (Promega).

RNA Immunoprecipitation Assay

RIP was performed as previously described (19). Bovine skeletal myoblasts transfected with pcDNA3.1-*YTHDF1* or the negative control were collected with cell scrapers (two 15-cm culture dishes for each group). Cell lysis and RNA immunoprecipitation and purification were performed according to the protocol of the Magna RIP RNA-Binding Protein Immunoprecipitation Kit (Sigma-Aldrich). The input mRNA and IP RNA of each sample were reverse transcribed, and enrichment was determined by RT-qPCR.

Chromatin Immunoprecipitation Assay

ChIP was performed using SimpleChIP Plus Sonication Chromatin IP Kit (Cell Signaling Technology, MA, USA) following the protocol of the manufacturer. In short, bovine skeletal myoblasts transfected with MEF2C expression vectors or empty vectors were fixed with 1% formaldehyde and then Quenching buffer was added to terminate the crosslinking reaction. The chromatin was sheared using a Covaris M220 focused-ultrasonicator (Woburn, MA, USA). The chromatin was incubated with either an anti-MEF2C polyclonal antibody (10056-1-AP, Proteintech, Wuhan, China) or an anti-IgG overnight at 4°C, and the IPs were bound to Protein G magnetic beads. Next, the chromatin was eluted from the antibody/protein G beads and de-crosslinked. The purified DNA and enriched

DNA sequences were detected using RT-qPCR with the primers listed in **Supplementary Table 1**. The data were expressed as a percentage of input.

Statistical Analysis

All results were displayed as the means ± standard deviation (SD) of at least three biological repetitions. Student's *t*-test (between two groups) or ANOVA (among multiple groups) were used to compare the significance of the means. $p < 0.01$ or $p < 0.05$ were considered the differences to be very significant or significant, respectively. GraphPad Prism 7.00 (GraphPad Software, CA, USA) software was used to analyze the results and produce images.

RESULTS

Identification of Bovine Skeletal Myoblasts and Detection of m^{6}A Levels During Differentiation

Myogenic differentiation and myogenesis are complex biological process. To verify whether the cells isolated from bovine longissimus dorsi muscles can undergo myogenic differentiation, we seeded the isolated cells in culture dishes, grew them to 80–90% confluence, and passaged them to a 6-well plate for further culture. After 48 h in growth medium, immunofluorescence showed that PAX7 and MYOD1 were simultaneously expressed, while the expression of MYOD1 was relatively low (**Figure 1A**), so we preliminarily identified the isolated cells as myoblasts. The myoblasts were cultured in growth medium to 90% confluence, and induce myogenic differentiation was induced with differentiation medium. Microscopic observation and fluorescence detection of the MYHC protein revealed that the myotubes formed by myoblast fusion gradually increased and became longer as the number of days of differentiation increased (**Figure 1B**). We evaluated the differentiation status of the myoblasts by detecting the mRNA levels of *MYOD1*, *MYOG*, *MYH3* (myosin heavy chain 3), and *MYMK* (myomaker, myoblast fusion factor), which are widely recognized marker genes of differentiated myoblasts and fused myotubes (40). The levels of *MYOG*, *MYH3*, and *MYMK* gradually increased during myogenic differentiation, while the levels of *MYOD1* peaked on D2 (**Figure 1C**). These findings were consistent with previous studies showing that MyoD1 plays a vital role in the proliferation and early differentiation of myoblasts (41). The trends in the expression of these pivotal genes were consistent with the differentiation stage. These results suggested that the isolated bovine skeletal myoblasts could undergo myogenic differentiation, and these cells can be used as a model for our follow-up study on myogenic differentiation. Meanwhile, we found the mRNA expression of *FTO* and *ALKBH5* increased during bovine myoblasts differentiation, while the levels of *METTL3* peaked on D2 (**Figure 1D**). Furthermore, using an LC-MS/MS assay, we detected the m^{6}A levels on days 0, 2, and 4 of myogenic differentiation (**Figure 1E**, **Supplementary Figures 1A,B**) and found that the levels of m^{6}A on D4 were significantly lower than those before differentiation (D0). The result may be related to the increased expression of *FTO* and *ALKBH5*. Alternatively, elevated *METTL3* expression did not lead to the increase of m^{6}A level in myoblast differentiation, implying that the regulation of m^{6}A modification in bovine myoblasts may be complex. The results of dot blotting also confirmed these same results (**Figure 1F**). Interestingly, dot blotting analysis showed that there was no obvious difference in the levels of m^{6}A on the total RNA (**Figure 1F**). These results indicated that m^{6}A modification may play a potential role in skeletal myogenic differentiation.

MeRIP-Seq and RNA-Seq Identify Potential Targets of m^{6}A Modification in Bovine Myoblasts Differentiation

To determine the role of m^{6}A in the process of myoblast differentiation, we extracted mRNA from pre-differentiation (GM, myoblasts, D0) and post-differentiation (DM, myotubes, D4) cells for MeRIP-seq and RNA-seq analyses (36). m^{6}A abundance has been reported to affect mRNA levels (9, 19, 42). To evaluate whether there was a potential correlation between m^{6}A mRNA methylation and gene transcript levels during myoblast differentiation, we compared the differentially expressed genes (DEGs) with the list of transcripts with altered m^{6}A levels. On the one hand, we found that among the 3,891 transcripts with higher m^{6}A levels in the DM group than in the GM group, only 119 transcripts showed higher expression levels while 94 transcripts exhibited lower expression levels (**Figure 2A**, **Supplementary Table 4**). On the other hand, among the 1,751 transcripts whose m^{6}A levels were decreased in the DM group compared to the GM group, 58 and 55 transcripts exhibited higher and lower expression levels, respectively (**Figure 2B**, **Supplementary Table 5**). The results suggested that the regulation of m^{6}A modification on gene expression during bovine myoblast differentiation may be complex. Gene overlap analysis in RNA-seq and MeRIP-seq data showed that 5,327 genes were modified with m^{6}A (**Figure 2C**). Among these 5,327 genes, the expression of 1,777 was upregulated. The skeletal muscle formation is known to be accompanied by the expression of many regulatory factors (43). Therefore, the genes with upregulated mRNA expression during myogenic differentiation were likely potential targets. Two genes, *KLF5* and *MEF2C*, that exhibited significantly increased expression in DM [$p < 0.05$, $\log_2(\text{FC}) \geq 2$] and are related to skeletal muscle cell differentiation were selected as potential candidates (**Figure 2C**). Finally, we selected *MEF2C* with increased m^{6}A level, as the target for our follow-up molecular mechanism research. Significant differences in the m^{6}A peaks were observed in MEF2C, as shown by IGV software (**Figure 2D**). MeRIP-qPCR was then used to verify the difference in the m^{6}A levels of *MEF2C* mRNA between the GM and DM groups. As expected, the m^{6}A level of *MEF2C* mRNA exhibited a significant increase in the DM group after myogenic differentiation (**Figure 2E**).

MEF2C Promotes the Myogenic Differentiation of Bovine Skeletal Myoblast

MEF2C has been reported to play an indispensable role in skeletal myogenesis and myoblast differentiation (44, 45). The expression of *MEF2C* was significantly increased in myoblast

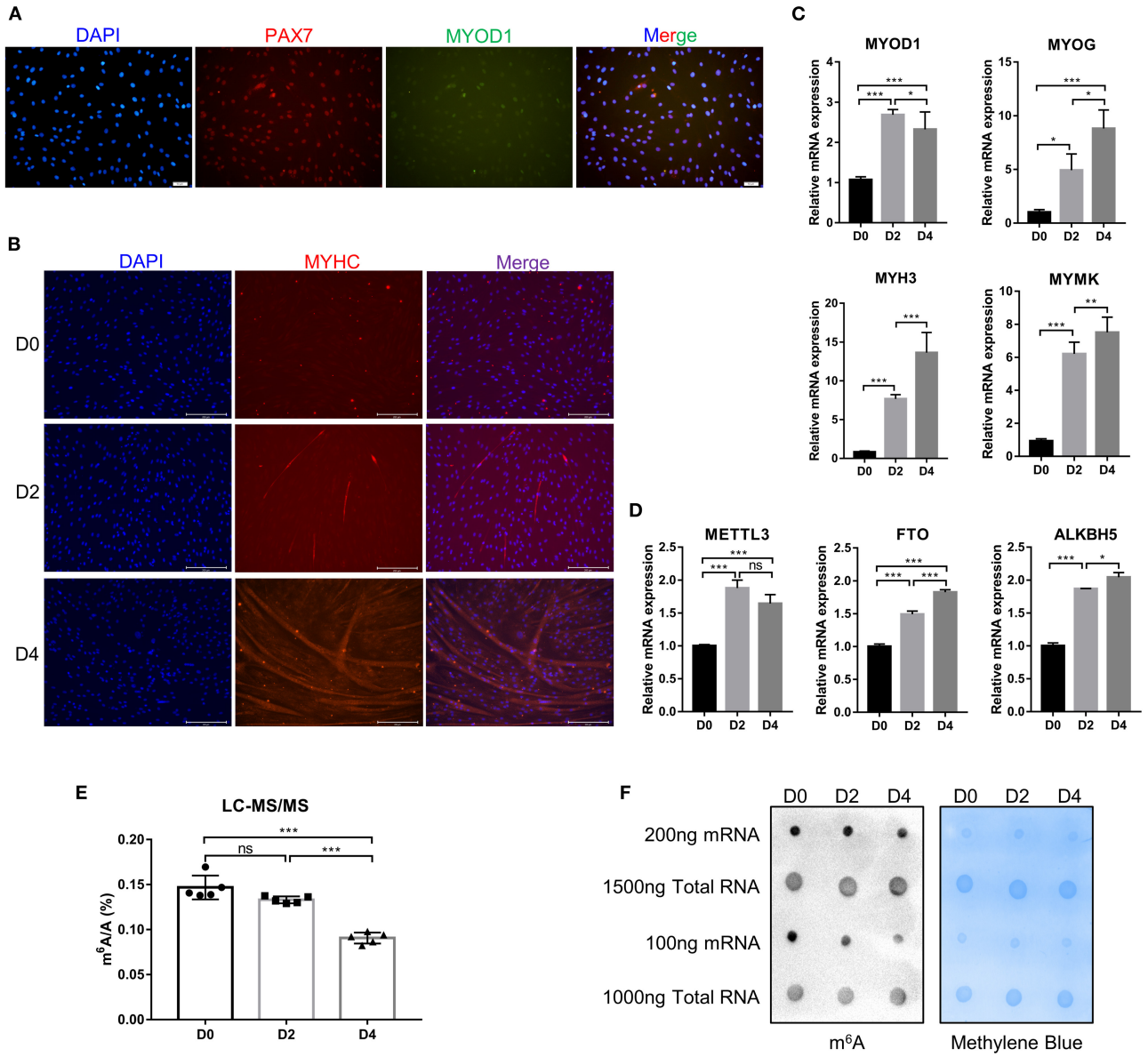

FIGURE 1 | Identification of bovine skeletal myoblasts and detection of m^{6}A levels during myogenic differentiation. **(A)** Identification of myoblasts based on PAX7 and MYOD1 expression in GM (scale bar: 50 μm, Olympus IX71). **(B)** Identification of differentiated myotubes based on MYHC expression after culture in DM for 0, 2, and 4 days (scale bar: 200 μm, Evos-fl-auto2 microscopy imaging system). **(C)** Relative mRNA expression of myogenic genes (*MYOD1*, *MYOG*, *MYH3*, and *MYMK)* during bovine skeletal myoblast differentiation. **(D)** Relative mRNA expression of *METTL3*, *FTO* and *ALKBH5* during myoblast differentiation. The results are presented as the means ± SD. **(E)** LC-MS/MS assay showed the amount of mRNA m^{6}A during myoblast differentiation. Data are presented as mean ± SD ($n = 5$). **(F)** Dot blotting was used to detect the m^{6}A modification of mRNA and total RNA at D0, D2, and D4 during bovine skeletal myoblasts differentiation. Methylene blue (MB) staining was used as a loading control. **(C–E)** $^*p < 0.05$, $^{**}p < 0.01$, $^{***}p < 0.001$, ns, no significance.

differentiation (**Figure 3A**). To verify the effects of MEF2C on bovine skeletal myoblast differentiation, siMEF2C for loss-of-function assays and *MEF2C*-WT for MEF2C overexpression were synthesized and constructed (**Supplementary Figure 2A**). MEF2C knockdown apparently inhibited myotube formation and fusion index at day 4 of myogenic differentiation in myoblast (**Figures 3B,C**). Meanwhile, MEF2C knockdown suppressed the mRNA expression of skeletal muscle-specific myogenic factors, such as *MYOD1*, *MYOG*, *MYH3*, and *MYMK*, and decreased the protein expression of MYH3 and MYOG (**Figures 3D–F**). In contrary, the overexpression of MEF2C obviously increased the mRNA and protein expression of these genes, and promoted myotubes formation and fusion index (**Figures 3H–L**, Vector and *MEF2C*-WT groups). Taken together, these results demonstrated that MEF2C plays a positive role in myogenic differentiation, which was consistent with expectations.

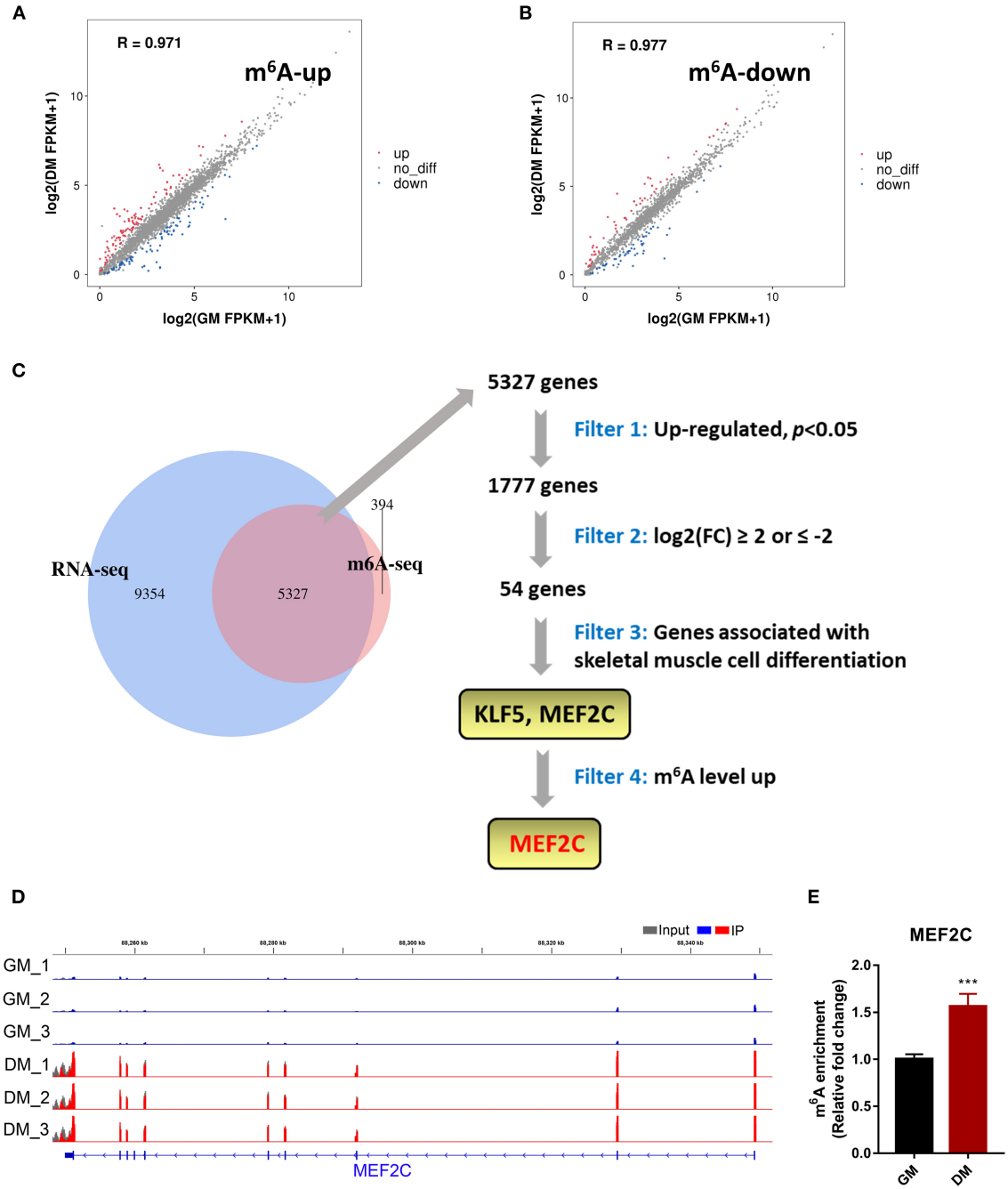

FIGURE 2 | m^{6}A methylome profiles of bovine skeletal muscle myoblasts (GM) and myotubes (DM). **(A,B)** Distribution of genes with significant differences in the both m^{6}A level and gene expression level between the GM and DM. **(C)** Venn diagram showed the overlapping genes identified by MeRIP-seq and RNA-seq, and bioinformatic analysis identified MEF2C as a target gene of m^{6}A modification during bovine skeletal myoblast differentiation. **(D)** IGV tracks displayed the distribution of m^{6}A peaks in the MEF2C transcript in all 6 groups. **(E)** Validations of the m^{6}A enrichment of MEF2C mRNA by MeRIP-qPCR. Data were presented as means ± SD. ***$p < 0.001$; Student's *t*-test.

m^{6}A Modification Facilitates MEF2C Protein Expression

In this study, we confirmed that the expression of *MEF2C* upregulated during myogenic differentiation, and the level of *MEF2C* mRNA m^{6}A modification was also significantly increased. Therefore, we speculated that m^{6}A modification was involved in the regulation of MEF2C expression. Considering the MeRIP-seq data and the m^{6}A peak map of *MEF2C*, we

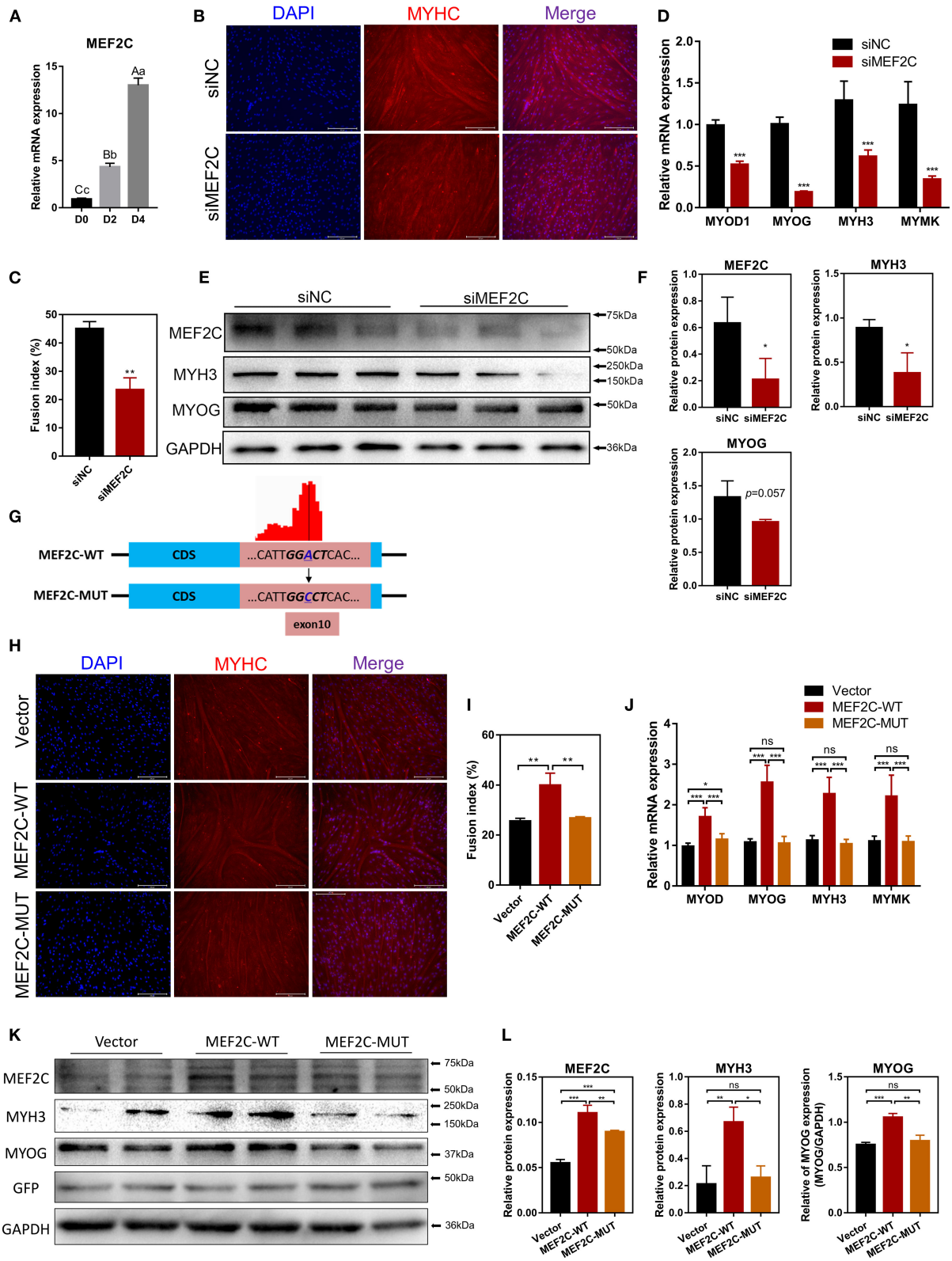

FIGURE 3 | MEF2C promotes bovine skeletal myoblast differentiation, and its expression and function in myoblast differentiation are regulated by m^{6}A modification. **(A)** Relative mRNA expression of *MEF2C* during bovine skeletal myoblast differentiation. **(B–F)** After myoblasts were transfected with siRNA for 24 h, myogenic

(Continued)

FIGURE 3 | differentiation was induced. **(B)** Myotube formation was observed on the 4th day of differentiation (scale bar: 200 μm). **(C)** The fusion index was calculated as the percentage of nuclei in fused myotubes out of the total nuclei. **(D)** Relative mRNA expression levels of *MYOD1*, *MYOG*, *MYH3*, and *MYMK* were measured on the fourth day of differentiation. **(E)** The protein expression of MEF2C, MYH3, MYOG, and GAPDH on the 4th day after myogenic induction. **(F)** Semi-quantitative analysis of the protein expression. **(G)** Synonymous mutations at the m^{6}A motif in the MEF2C CDS. **(H–L)** After transfection of the empty control, MEF2C-WT and MEF2C-MUT plasmids for 24 h, myoblasts were induced to differentiate. **(H)** Myotubes with MYHC expression on the 4th day after differentiation (scale bar: 200 μm). **(I)** The fusion index was counted. **(J)** Relative mRNA expression levels of *MYOD1*, *MYOG*, *MYH3*, and *MYMK* were measured. **(K,L)** The protein expression of MEF2C, MYH3, MYOG, GFP, and GAPDH after myogenic induction for 4 days. **(D,F,J,L)** The results were normalized to GAPDH levels and are presented as the means ± SD. $^*p < 0.05$, $^{**}p < 0.01$, $^{***}p < 0.001$, ns, no significance.

found that the m^{6}A-modified motif in *MEF2C* mRNA was in exon 10 (**Figures 2D**, **3G**). Subsequently, we replaced the N^6-methylated adenosine (A) in the m^{6}A peaks sequence of *MEF2C* mRNA (exon 10 of the CDS) with cytosine (C) to establish a synonymous mutant *MEF2C* that cannot be modified by m^{6}A (**Figure 3G**). **Figures 3H,I** show that *MEF2C*-MUT significantly inhibited the *MEF2C*-WT-induced myotube formation. Consistently, compared with *MEF2C*-WT, *MEF2C*-MUT markedly reduced the mRNA expression of *MYOD1*, *MYOG*, *MYH3*, and *MYMK* and decreased the protein expression of MYH3 and MYOG, but the mRNA expression of *MYOD1* in the *MEF2C*-MUT group was still higher than that of the control group (**Figures 3J–L**). It should be noted that *MEF2C*-MUT significantly increased the protein expression of MEF2C compared with the control, but decreased the protein expression of MEF2C compared with *MEF2C*-WT (**Figures 3K,L**). These results indicate that synonymous mutation of the m^{6}A motif in the *MEF2C* CDS inhibits the protein expression of MEF2C.

To further investigate how m^{6}A methylation modification regulates the expression of MEF2C, we performed loss-of-function and gain-of-function assays with both m^{6}A methyltransferase METTL3 and m^{6}A demethylase FTO (**Supplementary Figures 2B–D**). Myoblasts with FTO expression knocked down demonstrated significant upregulation of MEF2C protein expression, whereas FTO overexpression in myoblasts resulted in a reduction in the MEF2C protein levels (**Figures 4A,B**). In contrary, METTL3 knockdown inhibited the protein expression of MEF2C, while overexpression of METTL3 promoted the protein expression of MEF2C (**Figures 4C,D**). Additionally, MEF2C protein level was substantially decreased after 24 and 48 h of treatment with a global methylation inhibitor, 3-deazaadenosine (DAA) (4 μM, 86583-19-9, TargetMOI, MA, USA), without affecting its mRNA expression (**Figures 4E,F**, **Supplementary Figure 2E**). Together, these findings suggest that the m^{6}A modification of mRNA regulates MEF2C gene expression post-transcriptionally.

METTL3 Upregulates the Protein Expression of MEF2C in an m^{6}A-YTHDF1-Dependent Manner

Our results have shown that METTL3 could promote the protein expression of MEF2C (**Figures 4C,D**). Therefore, it is plausible to hypothesize that METTL3, an m^{6}A methyltransferase, could catalyze the methylation of *MEF2C* mRNA due to the increased m^{6}A level of *MEF2C* in DM after myogenic differentiation (**Figure 2E**). Similarly, in the luciferase assay, we replaced N^6-methylated adenosine with cytosine to synthesize a mutant *MEF2C*, and we ligated this sequence into the psiCHECK-2 dual-fluorescence vector. The relative luciferase activities of 293A cells transfected with the mutant *MEF2C* reporter were not significantly different when the cells were co-transfected with siMETTL3 or OE-METTL3. However, with the condition of the existence of the wild-type *MEF2C*-fused reporter, METTL3 knockdown and overexpression resulted in decreased and increased luciferase activity, respectively (**Figures 5A,B**). Thus, METTL3 was considered to regulate the m^{6}A level of *MEF2C*.

As the most widely studied m^{6}A readers, the m^{6}A-dependent functions of the members of the YTH protein family include, but are not limited to, the regulation of mRNA translation efficiency, stability and splicing (17). There was no difference in the half-life of *MEF2C* mRNA between the myoblasts in the *MEF2C*-WT and *MEF2C*-MUT groups at 0, 3, 6, and 9 h after actinomycin D treatment (**Figure 5C**), indicating that YTHDF2 did not regulate the stability of *MEF2C* mRNA. Moreover, YTHDF1 has been recognized to enhance the translation of m^{6}A-modified mRNAs and promote gene expression without changing the mRNA levels (22). To investigate whether MEF2C was modulated by YTHDF1, we examined the mRNA and protein levels of MEF2C after YTHDF1 knockdown and overexpression (**Supplementary Figures 3A,B**). Consistent with the reported functions of YTHDF1, overexpressing YTHDF1 improved the protein expression of MEF2C without affecting its mRNA level in myoblasts 4 days after the induction of differentiation. However, both the protein and mRNA levels of MEF2C were reduced after YTHDF1 expression was knocked down (**Figures 5D,E**, **Supplementary Figures 3C,D**). To further determine whether YTHDF1 functions as a direct m^{6}A reader of *MEF2C*, Western blotting was performed, and the results showed that the expression of MEF2C was significantly decreased after YTHDF1 expression was knocked down in myoblasts expressing *MEF2C*-WT, whereas no significant change was observed in the myoblasts expressing *MEF2C*-MUT (**Figures 5F,G**). Moreover, knockdown of YTHDF1 in the *MEF2C*-MUT group could reversed the inhibition of MYH3 observed in the *MEF2C*-WT group (**Figures 5F,G**). The results of immunofluorescence staining of myotubes with a MYHC antibody were also consistent with the protein expression of MEF2C in the 4 groups. Among these groups, the myotube formation in the *MEF2C*-WT single treatment group was the most obvious, while the formation of myotubes was significantly inhibited after YTHDF1 expression was knocked down or in the *MEF2C*-MUT group (**Figures 5H,I**). Next, YTHDF1 overexpression resulted

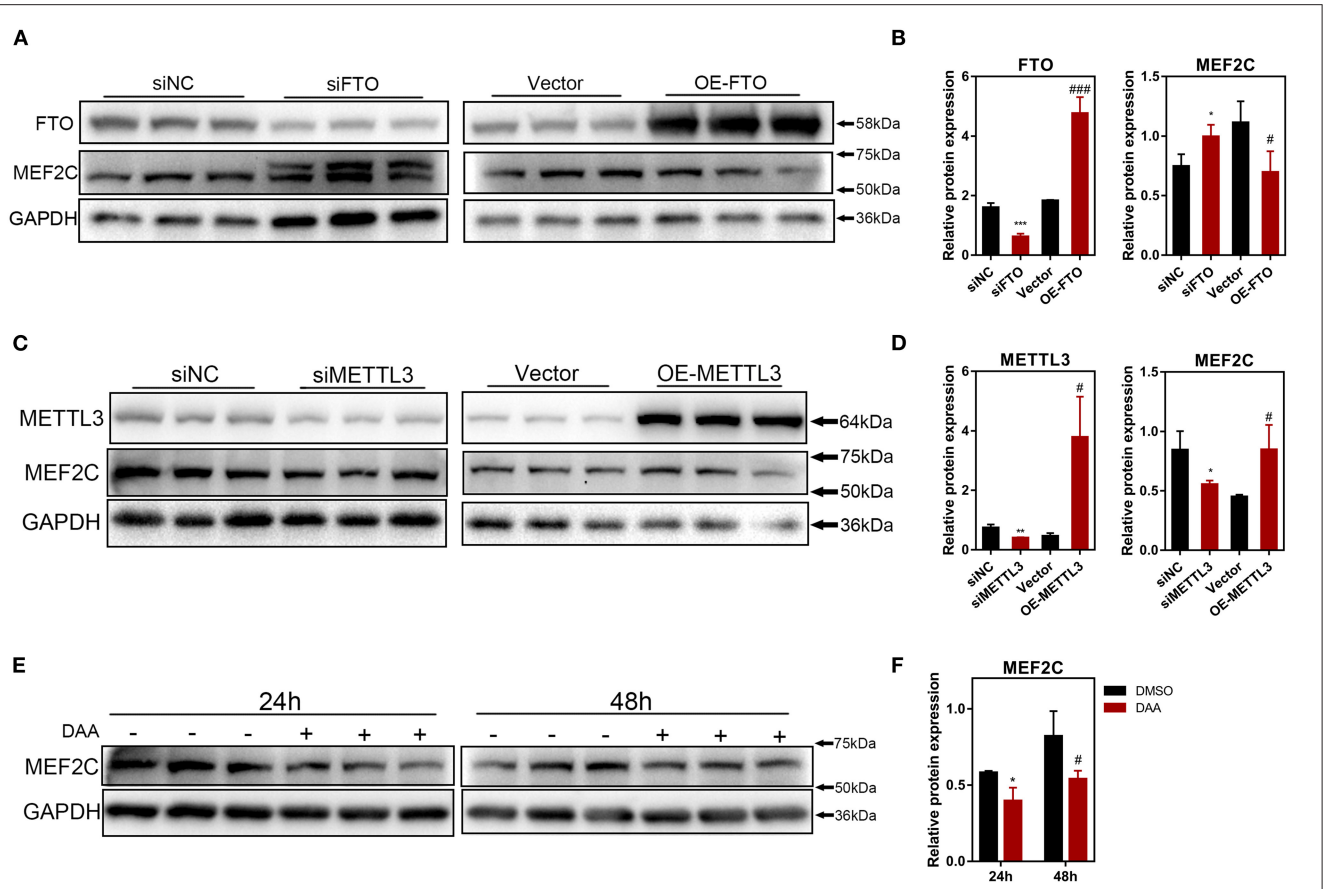

FIGURE 4 | The protein expression of MEF2C is regulated by m6A modification. **(A,B)** MEF2C and FTO protein levels after FTO knockdown and overexpression on the 4th day after differentiation. **(C,D)** MEF2C and METTL3 protein levels after METTL3 knockdown and overexpression for 4th day post differentiation. **(E,F)** Treatment with a global methylation inhibitor, 3-Deazaadenosine (DAA), for 24 and 48 h led to the downregulation of the MEF2C protein levels in bovine skeletal myoblasts. The results are presented as the means ± SD (*$p < 0.05$, **$p < 0.01$, ***$p < 0.001$, siNC vs. siRNA samples and DMSO vs. DAA at 24h; $^{\#}p < 0.05$, $^{\#\#\#}p < 0.001$, empty vector vs. overexpression plasmid samples and DMSO vs. DAA at 48h), using Student's *t* test.

in increased luciferase activity in the presence of the wild-type *MEF2C*-fused reporter (**Figure 5J**). RIP using an antibody against YTHDF1 and anti-IgG followed by qPCR revealed that the m^{6}A motif region in the *MEF2C* mRNA was effectively immunoprecipitated from bovine myoblasts overexpressing YTHDF1 (**Figure 5K**, **Supplementary Figure 3E**). These results indicated that YTHDF1 directly binds to *MEF2C* mRNA by recognizing the m^{6}A modification site to promote MEF2C expression at the translational level.

Some studies have reported that METTL3 regulated myogenesis (28, 33, 46). Our results shown that METTL3 markedly enhanced the differentiation of bovine skeletal myoblasts by promoting the expression of some key myogenic factors (such as *MYOD1*, *MYOG*, *MYH3*, and *MYMK*) (**Supplementary Figures 4A–D**). After knocking down METTL3 expression, the formation of multinuclear myotubes was also significantly inhibited (as assessed by the fluorescence of MYHC protein) (**Supplementary Figures 4E,F**). The results suggested that METTL3 may regulate myogenic differentiation by promoting the expression of MEF2C in an m^{6}A-YTHDF1-dependent manner. In general, these results indicate that METTL3 may increase the MEF2C protein levels by m^{6}A-YTHDF1-dependent mRNA translation.

MEF2C Promotes METTL3 Expression by Direct Binding Promoter DNA

As shown in **Figure 6A**, *METTL3* mRNA expression was enhanced on the 2nd and 4th days after the induction of differentiation in MEF2C overexpressing myoblasts. Western blotting showed that a significant decrease or increase in the METTL3 protein levels was observed in the MEF2C knockdown or overexpression cells, respectively (**Figures 6B,C**). Immunofluorescence staining revealed that knockdown of MEF2C expression reduced the m^{6}A levels in the total RNA of bovine myoblasts (**Figures 6D,E**). Meanwhile, Dot blot and LC-MS/MS showed that m^{6}A levels were decreased on day 3 of myogenic differentiation in siMEF2C myoblasts (**Figures 6F,G**).

MEF2C is a transcription factor that promotes the transcription of genes by recognizing and binding to transcription factor-binding sites (TFBS) of downstream

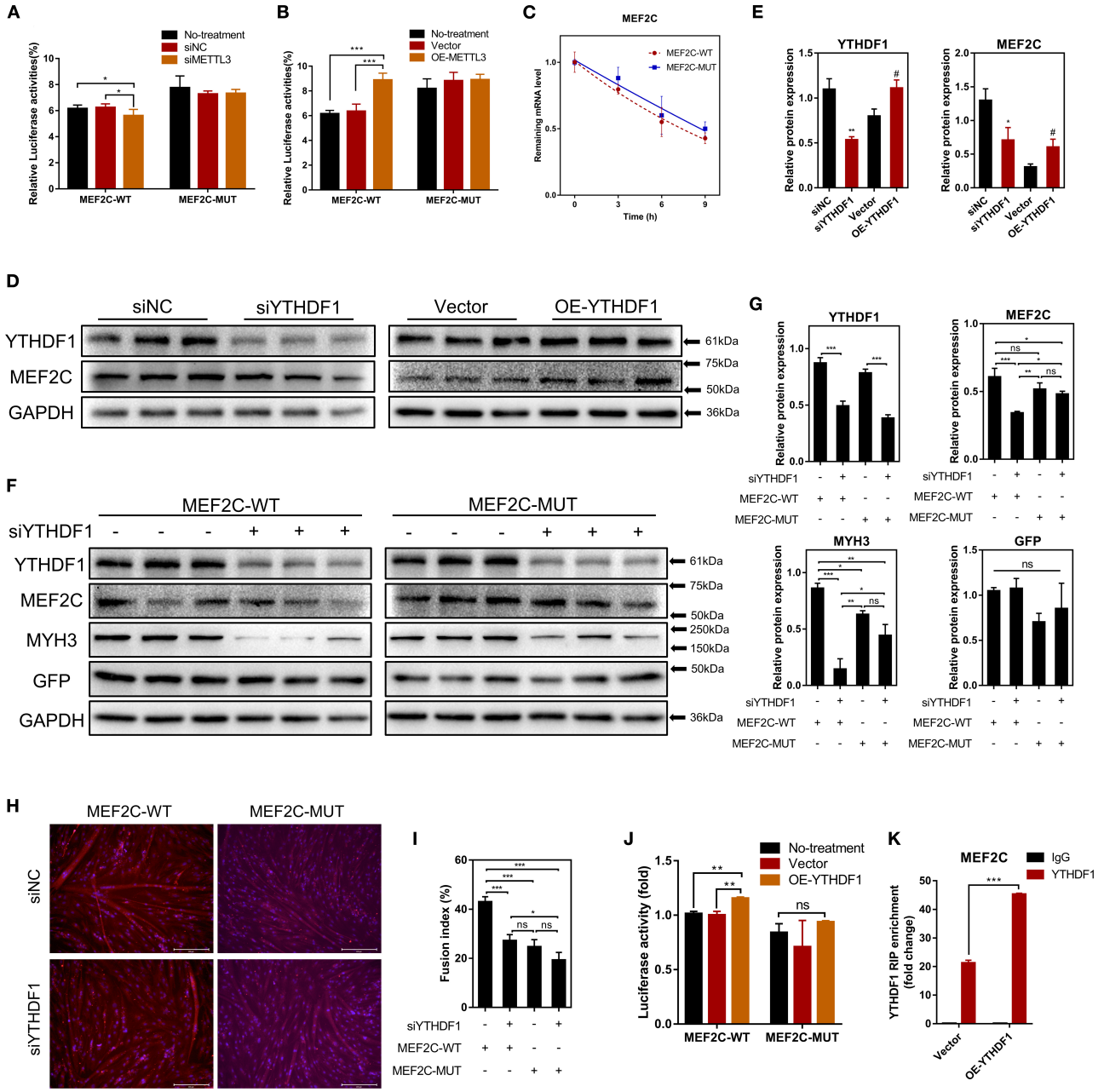

FIGURE 5 | METTL3 increases MEF2C protein expression in an m^{6}A-YTHDF1-dependent manner. **(A,B)** Relative dual-luciferase reporter activity of WT (MEF2C-WT) or mutated (MEF2C-MUT) reporters in METTL3 knockdown or overexpression 293A cells. **(C)** Representative mRNA profile of MEF2C in MEF2C-WT and MEF2C-MUT myoblasts at indicated time points after actinomycin D treatment. **(D,E)** MEF2C protein levels after YTHDF1 knockdown and overexpression on the 4th day after differentiation. $^*p < 0.05$, $^{**}p < 0.01$, siNC vs. siYTHDF1 samples; $^{\#}p < 0.05$, empty Vector vs. OE-YTHDF1 samples, using Student's *t*-test. **(F,G)** MEF2C, YTHDF1, MYH3, GFP, and GAPDH protein levels in MEF2C-WT or MEF2C-MUT with YTHDF1 expression knocked down after myogenic induction for 4 days. **(H)** Myotube formation in MEF2C-WT or MEF2C-MUT with YTHDF1 expression knocked down after myogenic induction for 4 days (scale bar: 200 μm). **(I)** The fusion index was counted. **(J)** Relative dual-luciferase reporter activity of MEF2C-WT or MEF2C-MUT reporters in YTHDF1 overexpression 293A cells. **(K)** RIP-qPCR detection of the binding of YTHDF1 to the transcript of MEF2C in myoblasts transfected with the empty vector and MEF2C-WT. The results are presented as the means ± SD. $^{***}p < 0.001$, using Student's *t*-test. **(A–C,G,I,J)** $^*p < 0.05$, $^{**}p < 0.01$, $^{***}p < 0.001$, ns, no significance, using one-way ANOVA with Tukey's correction for multiple comparisons.

target genes (44, 47). Two potential MEF2C-binding sites in the *METTL3* promoter were identified by genomic analysis and predicted with the JASPAR (48) and AnimalTFDB (49) online tools, and these results revealed the mechanisms underlying function of MEF2C (**Figures 6H,I**). Then, we designed two pairs of primers covering the two MEF2C-binding sites

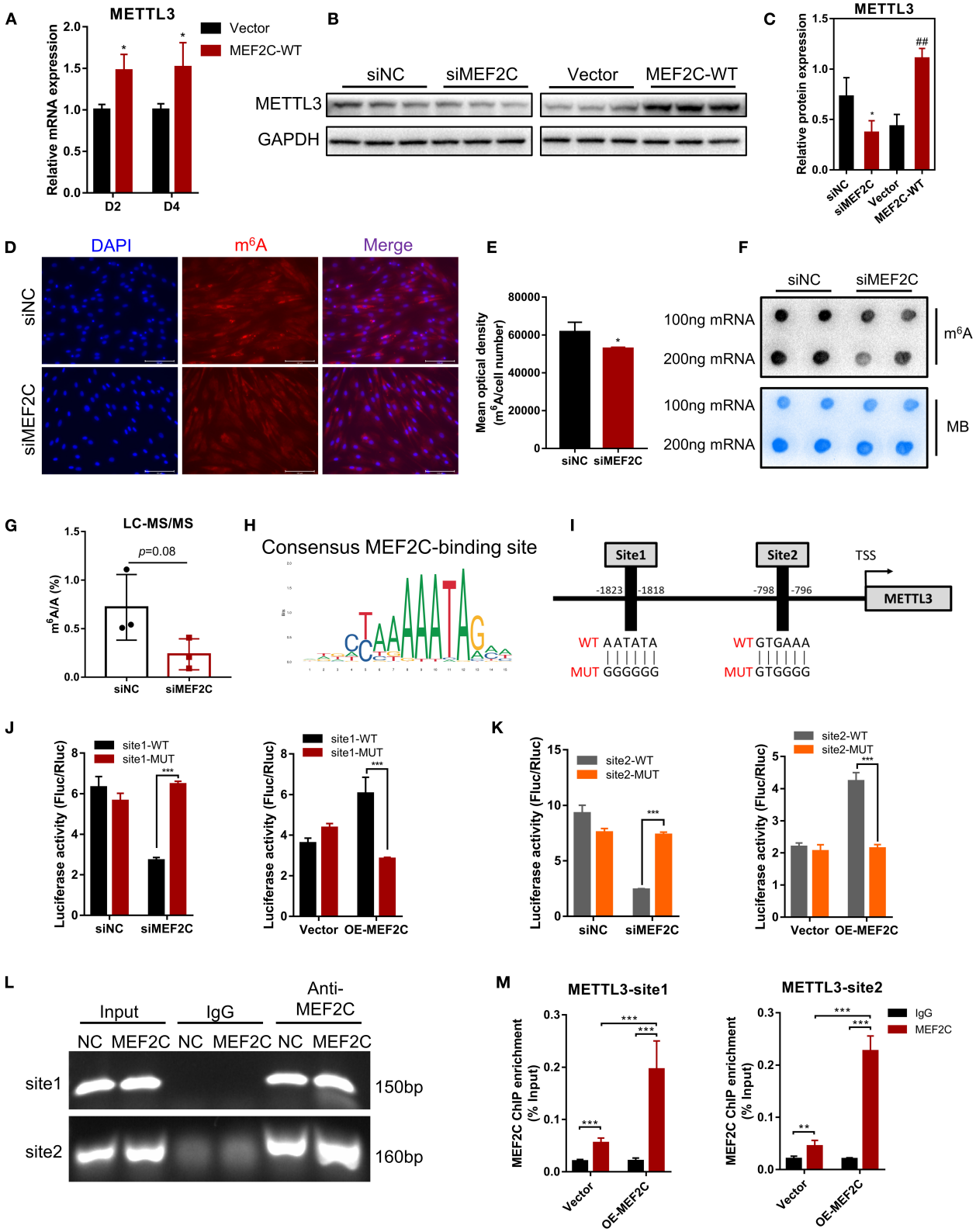

FIGURE 6 | Protein expression of METTL3 is regulated by MEF2C via direct DNA-binding. **(A)** Overexpression of MEF2C promotes the expression of METTL3 mRNA on the 2nd and 4th days after differentiation. **(B,C)** METTL3 protein levels after MEF2C knockdown and overexpression on the 4th day after differentiation. *$p < 0.05$,

(Continued)

FIGURE 6 | $^{**}p < 0.01$, siNC vs. siMEF2C samples; $^{\#\#}p < 0.01$, empty Vector vs. MEF2C-WT samples; Student's *t*-test. **(D)** Knockdown of MEF2C expression decreased the m^{6}A level of total RNA in bovine skeletal myoblasts after siRNA transfection for 3 days (scale bar: 100 μm). **(E)** Using Celleste Image Analysis Software (Invitrogen, USA), the average optical density was calculated as the cumulative optical density of m^{6}A red fluorescence divided by the number of nuclei, $n = 3$. **(F,G)** Dot blot and LC-MS/MS assays showed the level of m^{6}A after siMEF2C for 3 days. **(H,I)** The consensus MEF2C-binding site is indicated, and a schematic diagram illustrates two potential MEF2C-binding sites in the METTL3 promoter and the corresponding mutant sequences. **(J,K)** Luciferase assay with the wild-type or mutant sequences of METTL3 binding sites verified the activity of sites 1 and 2 in MEF2C knockdown or overexpression myoblasts. **(L)** ChIP and PCR analyses of myoblasts revealed the binding of MEF2C to two sites in the METTL3 promoter. **(M)** ChIP-qPCR detection of the binding of MEF2C to the 2 sites in the METTL3 promoter in myoblasts transfected with the empty vector and MEF2C-WT. **(A,E,G,J,K,M)** The results are presented as the means ± SD. $^{*}p < 0.05$, $^{**}p < 0.01$, $^{***}p < 0.001$, using Student's *t*-test.

(**Figure 6I**) and performed a luciferase assay in 293A cells transfected with siMEF2C or the MEF2C expression vector (OE-MEF2C). MEF2C expression increased the luciferase activities of cells expressing both wild-type promoters, while these effects were eliminated by a mutation in site 1 or site 2 (**Figures 6J,K**). To further confirm whether MEF2C can directly bind to the *METTL3* promoter, ChIP assays were carried out. As shown in **Figures 6L,M** the ChIP-qPCR results demonstrated that MEF2C bound to both sites. Collectively, these results provide evidence that MEF2C directly binds to the *METTL3* promoter as a transcription factor to increase METTL3 expression.

DISCUSSION

In recent years, the two extraordinary discoveries, i.e., the methylation modification of RNA is as reversible as DNA methylation (15) and the establishment of m^{6}A-specific methylated RNA immunoprecipitation coupled with next-generation sequencing (MeRIP-seq) (39, 50), have accelerated advances in research on m^{6}A modification in various fields. Meanwhile, a series of mechanisms in myogenic differentiation are also being uncovered uninterruptedly. However, the potential and detailed molecular mechanism underlying m^{6}A modification in myogenic differentiation is largely unknown. In the present study, we found that the level of m^{6}A decreased after myogenic differentiation in bovine skeletal myoblast, which was consistent with the results in C2C12 cells and sheep myoblasts (33, 34). To investigate the molecular mechanisms by which m^{6}A methylation influences myogenic differentiation, we further analyzed our previous sequencing data and found that the mRNA expression of MEF2C was up-regulated in myogenic differentiation, while the m^{6}A level was also significantly up-regulated. Further experiments demonstrated that MEF2C is regulated by METTL3-m^{6}A-YTHDF1 axis and METTL3 may promote myogenic differentiation by mediating the expression of MEF2C. In turn, MEF2C directly binds to the *METTL3* promoter, promoting *METTL3* transcription and thus affecting m^{6}A levels (**Figure 7**).

MEF2C, the member of the MEF2 family that is expressed first in skeletal muscle development, plays a positive role in skeletal muscle differentiation and regeneration (44, 45, 47, 51). We verified that MEF2C promoted the myogenic differentiation of bovine skeletal myoblasts by knockdown and overexpression assays, which was consistent with the findings of previous reports (44, 47). Furthermore, through synonymous mutation of the m^{6}A motif in the MEF2C coding region, we found that the m^{6}A modification was necessary for MEF2C protein expression and myotube formation. Then, we performed loss-of-function and gain-of-function assays to analyze the effects of active m^{6}A methyltransferase (METTL3) and demethylase (FTO), respectively, and found that the effects of METTL3 and FTO on the protein expression of MEF2C were opposite of those RNA methylation modification. Similarly, the protein expression of MEF2C was also affected by a methylation inhibitor (DAA). Multiple lines of evidence indicated that the protein expression of MEF2C was positively correlated with the level of m^{6}A. We then found that METTL3 regulates MEF2C expression by mediating m^{6}A methylation in myoblast differentiation. Some studies have found that METTL3 not only acts as m^{6}A writer, but also recognizes and binds m^{6}A sites to promote protein translation, and yet this generally occurs in the 3'UTR of the target transcripts (17), whereas the differentially methylated peaks of *MEF2C* are positioned in the CDS. Therefore, we speculated that YTHDF1, an m^{6}A reader protein, may be responsible for the increased expression of MEF2C. Our results demonstrated that YTHDF1 promoted the protein expression of MEF2C, and RIP assays indicated that YTHDF1 directly bound to *MEF2C* mRNA. Thus, multiple lines of evidence support our hypothesis that the *MEF2C* transcript was directly targeted by YTHDF1 and that METTL3 leads to high protein expression of MEF2C in an m^{6}A-YTHDF1-dependent manner in myoblast differentiation. Consistent with our findings, the previously reported next-generation sequencing data of m^{6}A, CLIP and RIP from the m6A2Target Database (http://m6a2target.canceromics.org/#/search/MEF2C) also identified *MEF2C* mRNA as a potential target of m^{6}A writers, erasers, and readers in humans and mice (GSE46705, GSE79577, GSE56010, GSE90914, GSE102493, GSE94098, GSE94148, and GSE100528). Furthermore, we aligned the m^{6}A modified sequence of bovine MEF2C mRNA with that of other species (including humans, mice, pigs and sheep) and found that the coding region and m^{6}A motif sequence of *MEF2C* were very conserved (**Supplementary Figure 5**). These findings suggest a possible general regulatory role of m^{6}A modifications in muscle development. Besides, we found a consequent alteration in METTL3 expression while conducting MEF2C knockdown and overexpression assays. As a well-known transcription activator, MEF2C was found to facilitate the expression of METTL3 by directly binding to the *METTL3* promoter during myogenic differentiation in our study.

Strikingly, the m^{6}A demethylase FTO also affected the expression of MEF2C, and two protein bands of similar size

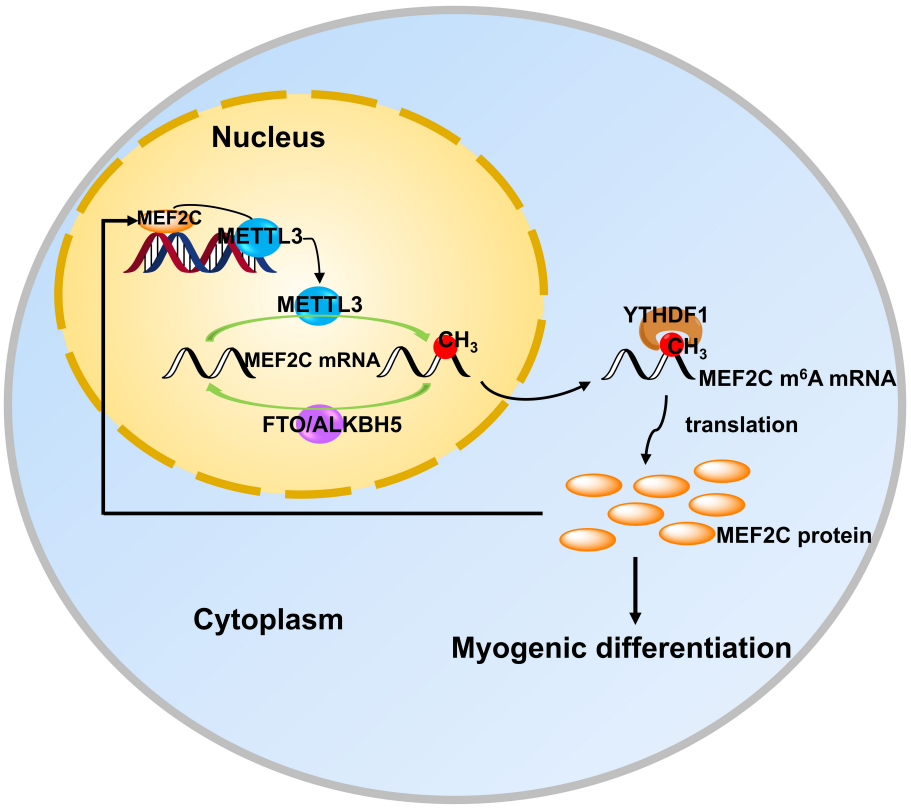

FIGURE 7 | MEF2C promotes the differentiation of bovine myoblasts by posttranscriptional activation of the METTL3-m^{6}A-YTHDF1 axis. METTL3 catalyzes the N^6-methylation of MEF2C mRNA, and YTHDF1 recognizes this modification site to promote the translation of MEF2C. Then, MEF2C can directly bind to the promoter region of METTL3 to activate its expression, suggesting that there is a positive feedback loop underlying the process of bovine skeletal myoblast differentiation.

appeared in MEF2C at day 4 of myogenic differentiation after knockdown of FTO (**Figure 4A**). Previous studies have found that m^{6}A demethylase FTO can regulate the splicing of the target transcripts (52, 53), so we speculated that FTO may regulate the translation of two different transcripts of *MEF2C*, which needs to be confirmed by subsequent studies. It could also be a protein modification that changes the weight of the protein.

Uniquely, our results showed that both m^{6}A methyltransferase (METTL3) and m^{6}A demethylases (FTO and ALKBH5) exhibited increased expression after the onset of differentiation. Simultaneously, overall m^{6}A levels were reduced, but METTL3 promoted myogenic differentiation of bovine myoblasts. These seemingly contradictory results imply that m^{6}A methylation modifications in skeletal myogenesis are dynamically changing and there may be a complex regulatory network of m^{6}A methylation. The combined analysis of MeRIP-seq and RNA-seq data showed no significant correlation between differential gene expression and differential m^{6}A abundance (**Figure 2A**), which is consistent with the N^6-methyladenosine methylome profile in porcine muscle development (54), whereas the m^{6}A modification profiles of goose embryonic muscle shown that m^{6}A methylation was negatively correlated with transcript level (55). These results indicate that the regulation of mRNA transcription by m^{6}A modification during myogenic differentiation was complicated.

Similarly, METTL3 is essential for *MyoD* mRNA expression in proliferating C2C12 myoblasts for skeletal muscle differentiation (28), is required for skeletal muscle regeneration (56) in mice and regulates the transitions of muscle stem cells/myoblasts (33). A recent study shown that METTL3 regulates skeletal muscle specific miRNAs at both the transcriptional and posttranscriptional levels (46). As suggested by these previous studies, METTL3 plays a critical role in skeletal muscle homeostasis and myogenic differentiation as a result of its function as a methyltransferase. However, some investigators identified that METTL3 inhibited differentiation of the C2C12 cells and primary mouse skeletal muscle cells (33, 35, 56). We analyzed the reasons for these differential results and found an intriguing result. Apart from the difference in the origin and type of cells, the different media used in cell culture are likely to be responsible for the opposite results of METTL3 regulation of myogenic differentiation. METTL3 promoted myogenic differentiation of cells cultured using growth medium with 20% FBS, including C2C12 cells (28) and the primary bovine skeletal myoblasts we used. The opposite result was obtained for studies using 10% or 15% FBS, i.e., METTL3 inhibited myogenic differentiation of C2C12 cells or primary

mouse skeletal myoblasts (33, 35, 56). It is also important to mention that the differentiation medium used in all these studies during myogenic differentiation of cells was 2% horse serum. These results implies that there is still a lot of work to be explored and developed in the field of RNA methylation.

In conclusion, we found that the protein expression of MEF2C was positively regulated by the METTL3-m^{6}A-YTHDF1 axis in myoblast differentiation. In addition, MEF2C promoted the expression of METTL3 by binding to its promoter, thus there may be a positive feedback loop between these molecules in myoblast differentiation (**Figure 7**). Our findings could provide new Q15insights into skeletal muscle development and livestock breeding. Moreover, it is becoming increasingly clear that the mechanisms of RNA methylation in skeletal myogenesis.

DATA AVAILABILITY STATEMENT

The original contributions presented in the study are included in the article/**Supplementary Material**, further inquiries can be directed to the corresponding author/s.

AUTHOR CONTRIBUTIONS

XY and LZ designed the experiment. XY performed most experiments, analyzed the data, and wrote the manuscript. YN provided bovine primary myoblasts and conducted partial cellular experiments. SA conducted partial molecular experiments. CM contributed to the discussion. All authors contributed to the article, provided constructive suggestions for manuscript writing, and approved the submitted version.

FUNDING

This work was supported by the National Key Research and Development Program of China (2018YFD0501700), National Natural Science Foundation of China (31972994), Key Research and Development Program of Ningxia Province (2019BEF02004), National Beef and Yak Industrial Technology System (CARS-37), and Key Research and Development Program of Shaanxi Province (2022NY-050 and 2022ZDLNY01-01).

ACKNOWLEDGMENTS

We are grateful to our colleagues of Zan's laboratory who provided expertise and contributed to this research, and sincerely thank Miss Zhao (Horticulture Science Research Center, Northwest A&F University, Yangling, China) for providing professional technical assistance with LC-MS/MS analysis.

SUPPLEMENTARY MATERIAL

The Supplementary Material for this article can be found online at: https://www.frontiersin.org/articles/10.3389/fvets.2022.900924/full#supplementary-material

REFERENCES

1. Picard B, Berri C, Lefaucheur L, Molette C, Sayd T, Terlouw C. Skeletal muscle proteomics in livestock production. *Brief Funct Genomics.* (2010) 9:259–78. doi: 10.1093/bfgp/elq005
2. Braun T, Gautel M. Transcriptional mechanisms regulating skeletal muscle differentiation, growth and homeostasis. *Nat Rev Mol Cell Biol.* (2011) 12:349–61. doi: 10.1038/nrm3118
3. Yang Y, Fan X, Yan J, Chen M, Zhu M, Tang Y, et al. A comprehensive epigenome atlas reveals DNA methylation regulating skeletal muscle development. *Nucleic Acids Res.* (2021) 49:1313–29. doi: 10.1093/nar/gkaa1203
4. McKinnell IW, Ishibashi J, Le Grand F, Punch VG, Addicks GC, Greenblatt JF, et al. Pax7 activates myogenic genes by recruitment of a histone methyltransferase complex. *Nat Cell Biol.* (2008) 10:77–84. doi: 10.1038/ncb1671
5. Cantara WA, Crain PF, Rozenski J, McCloskey JA, Harris KA, Zhang X, et al. The RNA modification database, Rnamdb: 2011 update. *Nucleic Acids Res.* (2011) 39 (Database issue):D195–201. doi: 10.1093/nar/gkq1028
6. Meyer KD, Jaffrey SR. The dynamic epitranscriptome: N6-methyladenosine and gene expression control. *Nat Rev Mol Cell Biol.* (2014) 15:313–26. doi: 10.1038/nrm3785
7. Jia G, Fu Y, He C. Reversible Rna adenosine methylation in biological regulation. *Trends Genet.* (2013) 29:108–15. doi: 10.1016/j.tig.2012.11.003
8. Luo GZ, MacQueen A, Zheng G, Duan H, Dore LC, Lu Z, et al. Unique features of the M6a methylome in arabidopsis thaliana. *Nat Commun.* (2014) 5:5630. doi: 10.1038/ncomms6630
9. Shen L, Liang Z, Gu X, Chen Y, Teo ZW, Hou X, et al. N(6)-Methyladenosine Rna modification regulates shoot stem cell fate in arabidopsis. *Dev Cell.* (2016) 38:186–200. doi: 10.1016/j.devcel.2016.06.008
10. Zhong S, Li H, Bodi Z, Button J, Vespa L, Herzog M, et al. Mta Is an arabidopsis messenger Rna adenosine methylase and interacts with a homolog of a sex-specific splicing factor. *Plant Cell.* (2008) 20:1278–88. doi: 10.1105/tpc.108.058883
11. Haussmann IU, Bodi Z, Sanchez-Moran E, Mongan NP, Archer N, Fray RG, et al. M(6)a potentiates Sxl alternative Pre-Mrna splicing for robust drosophila sex determination. *Nature.* (2016) 540:301–4. doi: 10.1038/nature20577
12. Schwartz S, Agarwala SD, Mumbach MR, Jovanovic M, Mertins P, Shishkin A, et al. High-Resolution mapping reveals a conserved, widespread, dynamic Mrna methylation program in yeast meiosis. *Cell.* (2013) 155:1409–21. doi: 10.1016/j.cell.2013.10.047
13. Liu J, Yue Y, Han D, Wang X, Fu Y, Zhang L, et al. A Mettl3-Mettl14 complex mediates mammalian nuclear Rna N6-adenosine methylation. *Nat Chem Biol.* (2014) 10:93–5. doi: 10.1038/nchembio.1432
14. Ping XL, Sun BF, Wang L, Xiao W, Yang X, Wang WJ, et al. Mammalian Wtap is a regulatory subunit of the Rna N6-methyladenosine methyltransferase. *Cell Res.* (2014) 24:177–89. doi: 10.1038/cr.2014.3
15. Jia G, Fu Y, Zhao X, Dai Q, Zheng G, Yang Y, et al. N6-Methyladenosine in nuclear Rna is a major substrate of the obesity-associated Fto. *Nat Chem Biol.* (2011) 7:885–7. doi: 10.1038/nchembio.687
16. Zheng G, Dahl JA, Niu Y, Fedorcsak P, Huang CM, Li CJ, et al. Alkbh5 is a mammalian Rna demethylase that impacts Rna metabolism and mouse fertility. *Mol Cell.* (2013) 49:18–29. doi: 10.1016/j.molcel.2012.10.015
17. Shi H, Wei J, He C. Where, when, and how: context-dependent functions of Rna methylation writers, readers, and erasers. *Mol Cell.* (2019) 74:640–50. doi: 10.1016/j.molcel.2019.04.025
18. Zhang Z, Theler D, Kaminska KH, Hiller M, de la Grange P, Pudimat R, et al. The Yth domain is a novel Rna binding domain. *J Biol Chem.* (2010) 285:14701–10. doi: 10.1074/jbc.M110.104711

19. Wang X, Lu Z, Gomez A, Hon GC, Yue Y, Han D, et al. N6-Methyladenosine-dependent regulation of messenger Rna stability. *Nature.* (2014) 505:117–20. doi: 10.1038/nature12730
20. Fu Y, Dominissini D, Rechavi G, He C. Gene expression regulation mediated through reversible M(6)a Rna methylation. *Nat Rev Genet.* (2014) 15:293–306. doi: 10.1038/nrg3724
21. Meyer KD, Patil DP, Zhou J, Zinoviev A, Skabkin MA, Elemento O, et al. 5' Utr M(6)a promotes cap-independent translation. *Cell.* (2015) 163:999–1010. doi: 10.1016/j.cell.2015.10.012
22. Wang X, Zhao BS, Roundtree IA, Lu Z, Han D, Ma H, et al. N(6)-Methyladenosine modulates messenger Rna translation efficiency. *Cell.* (2015) 161:1388–99. doi: 10.1016/j.cell.2015.05.014
23. Zhao X, Yang Y, Sun BF, Shi Y, Yang X, Xiao W, et al. Fto-Dependent demethylation of N6-methyladenosine regulates Mrna splicing and is required for adipogenesis. *Cell Res.* (2014) 24:1403–19. doi: 10.1038/cr.2014.151
24. Batista PJ, Molinie B, Wang J, Qu K, Zhang J, Li L, et al. M(6)a Rna modification controls cell fate transition in mammalian embryonic stem cells. *Cell Stem Cell.* (2014) 15:707–19. doi: 10.1016/j.stem.2014.09.019
25. Lin S, Choe J, Du P, Triboulet R, Gregory RI. The M(6)a methyltransferase mettl3 promotes translation in human cancer cells. *Mol Cell.* (2016) 62:335–45. doi: 10.1016/j.molcel.2016.03.021
26. Wang Y, Gao M, Zhu F, Li X, Yang Y, Yan Q, et al. Mettl3 is essential for postnatal development of brown adipose tissue and energy expenditure in mice. *Nat Commun.* (2020) 11:1648. doi: 10.1038/s41467-020-15488-2
27. Han D, Liu J, Chen C, Dong L, Liu Y, Chang R, et al. Anti-Tumour immunity controlled through Mrna M(6)a methylation and Ythdf1 in dendritic cells. *Nature.* (2019) 566:270–4. doi: 10.1038/s41586-019-0916-x
28. Kudou K, Komatsu T, Nogami J, Maehara K, Harada A, Saeki H, et al. The requirement of Mettl3-promoted myod mrna maintenance in proliferative myoblasts for skeletal muscle differentiation. *Open Biol.* (2017) 7:170119. doi: 10.1098/rsob.170119
29. Zhang X, Yao Y, Han J, Yang Y, Chen Y, Tang Z, et al. Longitudinal epitranscriptome profiling reveals the crucial role of N(6)-methyladenosine methylation in porcine prenatal skeletal muscle development. *J Genet Genomics.* (2020) 47:466–76. doi: 10.1016/j.jgg.2020.07.003
30. Wang X, Huang N, Yang M, Wei D, Tai H, Han X, et al. Fto is required for myogenesis by positively regulating Mtor-Pgc-1alpha pathway-mediated mitochondria biogenesis. *Cell Death Dis.* (2017) 8:e2702. doi: 10.1038/cddis.2017.122
31. Mathiyalagan P, Adamiak M, Mayourian J, Sassi Y, Liang Y, Agarwal N, et al. Fto-Dependent N(6)-methyladenosine regulates cardiac function during remodeling and repair. *Circulation.* (2019) 139:518–32. doi: 10.1161/CIRCULATIONAHA.118.033794
32. Dorn LE, Lasman L, Chen J, Xu X, Hund TJ, Medvedovic M, et al. The N(6)-methyladenosine mrna methylase mettl3 controls cardiac homeostasis and Hypertrophy. *Circulation.* (2019) 139:533–45. doi: 10.1161/CIRCULATIONAHA.118.036146
33. Gheller BJ, Blum JE, Fong EHH, Malysheva OV, Cosgrove BD, Thalacker-Mercer AE. A defined N6-methyladenosine (M(6)a) profile conferred by mettl3 regulates muscle stem cell/myoblast state transitions. *Cell Death Discov.* (2020) 6:95. doi: 10.1038/s41420-020-00328-5
34. Deng K, Fan Y, Liang Y, Cai Y, Zhang G, Deng M, et al. Fto-Mediated demethylation of gadd45b promotes myogenesis through the activation of P38 Mapk pathway. *Mol Ther Nucleic Acids.* (2021) 26:34–48. doi: 10.1016/j.omtn.2021.06.013
35. Xie SJ, Lei H, Yang B, Diao LT, Liao JY, He JH, et al. Dynamic M(6)a mrna methylation reveals the role of mettl3/14-M(6)a-Mnk2-Erk signaling axis in skeletal muscle differentiation and regeneration. *Front Cell Dev Biol.* (2021) 9:744171. doi: 10.3389/fcell.2021.744171
36. Yang X, Wang J, Ma X, Du J, Mei C, Zan L. Transcriptome-Wide N (6)-methyladenosine methylome profiling reveals M(6)a regulation of skeletal myoblast differentiation in cattle (bos taurus). *Front Cell Dev Biol.* (2021) 9:785380. doi: 10.3389/fcell.2021.785380
37. Yang X, Ning Y, Mei C, Zhang W, Sun J, Wang S, et al. The role of bambi in regulating adipogenesis and myogenesis and the association between its polymorphisms and growth traits in cattle. *Mol Biol Rep.* (2020) 47:5963–74. doi: 10.1007/s11033-020-05670-6
38. Livak KJ, Schmittgen TD. Analysis of relative gene expression data using real-time quantitative Pcr and the 2(-delta delta C(T)) method. *Methods.* (2001) 25:402–8. doi: 10.1006/meth.2001.1262
39. Dominissini D, Moshitch-Moshkovitz S, Schwartz S, Salmon-Divon M, Ungar L, Osenberg S, et al. Topology of the human and mouse M6a Rna methylomes revealed by M6a-Seq. *Nature.* (2012) 485:201–6. doi: 10.1038/nature11112
40. Millay DP, O'Rourke JR, Sutherland LB, Bezprozvannaya S, Shelton JM, Bassel-Duby R, et al. Myomaker is a membrane activator of myoblast fusion and muscle formation. *Nature.* (2013) 499:301–5. doi: 10.1038/nature12343
41. Weintraub H. The myod family and myogenesis: redundancy, networks, and thresholds. *Cell.* (1993) 75:1241–4. doi: 10.1016/0092-8674(93)90610-3
42. Zhao BS, Roundtree IA, He C. Post-Transcriptional gene regulation by mrna modifications. *Nat Rev Mol Cell Biol.* (2017) 18:31–42. doi: 10.1038/nrm.2016.132
43. Buckingham M. Myogenic progenitor cells and skeletal myogenesis in vertebrates. *Curr Opin Genet Dev.* (2006) 16:525–32. doi: 10.1016/j.gde.2006.08.008
44. Estrella NL, Desjardins CA, Nocco SE, Clark AL, Maksimenko Y, Naya FJ. Mef2 transcription factors regulate distinct gene programs in mammalian skeletal muscle differentiation. *J Biol Chem.* (2015) 290:1256–68. doi: 10.1074/jbc.M114.589838
45. Liu N, Nelson BR, Bezprozvannaya S, Shelton JM, Richardson JA, Bassel-Duby R, et al. Requirement of Mef2a, C, and D for skeletal muscle regeneration. *Proc Natl Acad Sci USA.* (2014) 111:4109–14. doi: 10.1073/pnas.1401732111
46. Diao LT, Xie SJ, Lei H, Qiu XS, Huang MC, Tao S, et al. Mettl3 regulates skeletal muscle specific mirnas at both transcriptional and post-transcriptional levels. *Biochem Biophys Res Commun.* (2021) 552:52–8. doi: 10.1016/j.bbrc.2021.03.035
47. Taylor MV, Hughes SM. Mef2 and the skeletal muscle differentiation program. *Semin Cell Dev Biol.* (2017) 72:33–44. doi: 10.1016/j.semcdb.2017.11.020
48. Fornes O, Castro-Mondragon JA, Khan A, van der Lee R, Zhang X, Richmond PA, et al. Jaspar 2020: update of the open-access database of transcription factor binding profiles. *Nucleic Acids Res.* (2020) 48:D87–92. doi: 10.1093/nar/gkz1001
49. Hu H, Miao YR, Jia LH, Yu QY, Zhang Q, Guo AY. Animaltfdb 3.0: a comprehensive resource for annotation and prediction of animal transcription factors. *Nucleic Acids Res.* (2019) 47:D33–8. doi: 10.1093/nar/gky822
50. Meyer KD, Saletore Y, Zumbo P, Elemento O, Mason CE, Jaffrey SR. Comprehensive analysis of mrna methylation reveals enrichment in 3' utrs and near stop codons. *Cell.* (2012) 149:1635–46. doi: 10.1016/j.cell.2012.05.003
51. Naya FJ, Olson E. Mef2: a transcriptional target for signaling pathways controlling skeletal muscle growth and differentiation. *Curr Opin Cell Biol.* (1999) 11:683–8. doi: 10.1016/S0955-0674(99)00036-8
52. Bartosovic M, Molares HC, Gregorova P, Hrossova D, Kudla G, Vanacova S. N6-Methyladenosine demethylase fto targets pre-mrnas and regulates alternative splicing and 3'-end processing. *Nucleic Acids Res.* (2017) 45:11356–70. doi: 10.1093/nar/gkx778
53. Merkestein M, Laber S, McMurray F, Andrew D, Sachse G, Sanderson J, et al. Fto influences adipogenesis by regulating mitotic clonal expansion. *Nat Commun.* (2015) 6:6792. doi: 10.1038/ncomms7792
54. Tao X, Chen J, Jiang Y, Wei Y, Chen Y, Xu H, et al. Transcriptome-Wide N (6) -methyladenosine methylome profiling of porcine muscle and adipose tissues reveals a potential mechanism for transcriptional regulation and differential methylation pattern. *BMC Genomics.* (2017) 18:336. doi: 10.1186/s12864-017-3719-1
55. Xu T, Xu Z, Lu L, Zeng T, Gu L, Huang Y, et al. Transcriptome-Wide study revealed M6a regulation of embryonic muscle development in dingan goose (anser cygnoides orientalis). *BMC Genomics.* (2021) 22:270. doi: 10.1186/s12864-021-07556-8
56. Liang Y, Han H, Xiong Q, Yang C, Wang L, Ma J, et al. Mettl3-Mediated M(6)a methylation regulates muscle stem cells and muscle

regeneration by notch signaling pathway. *Stem Cells Int.* (2021) 2021:9955691. doi: 10.1155/2021/9955691

Conflict of Interest: The authors declare that the research was conducted in the absence of any commercial or financial relationships that could be construed as a potential conflict of interest.

Publisher's Note: All claims expressed in this article are solely those of the authors and do not necessarily represent those of their affiliated organizations, or those of the publisher, the editors and the reviewers. Any product that may be evaluated in this article, or claim that may be made by its manufacturer, is not guaranteed or endorsed by the publisher.

frontiers | Frontiers in Veterinary Science

ORIGINAL RESEARCH
published: 22 June 2022
doi: 10.3389/fvets.2022.914848

Weighted Gene Co-Expression Network Analysis Identifies Key Modules and Central Genes Associated With Bovine Subcutaneous Adipose Tissue

Hui Sheng[1], *Cuili Pan*[1], *Shuzhe Wang*[1], *Chaoyun Yang*[1], *Junxing Zhang*[1], *Chunli Hu*[1], *Honghong Hu*[1], *Xue Feng*[1], *Mengli Yang*[1], *Zhaoxiong Lei*[1], *Yuhong Gao*[1], *Zhong Wang*[1] *and Yun Ma*[1,2*]

[1] *Key Laboratory of Ruminant Molecular and Cellular Breeding, School of Agriculture, Ningxia University, Yinchuan, China,*
[2] *College of Life Sciences, Xinyang Normal University, Xinyang, China*

Background: Fat deposition is an important economic trait in livestock and poultry production. However, the relationship between various genes and signal pathways of fat deposition is still unclear to a large extent. The purpose of this study is to analyze the potential molecular targets and related molecular pathways in bovine subcutaneous adipose tissue.

Results: We downloaded the GSE116775 microarray dataset from Gene Expression Omnibus (GEO). The weighted gene co-expression network (WGCNA) was used to analyze the gene expression profile, and the key gene modules with the highest correlation with subcutaneous adipose tissue were identified, and the functional enrichment of the key modules was analyzed. Then, the "real" Hub gene was screened by in-module analysis and protein–protein interaction network (PPI), and its expression level in tissue samples and adipocytes was verified. The study showed that a total of nine co-expression modules were identified, and the number of genes in these modules ranged from 101 to 1,509. Among them, the blue module is most closely related to subcutaneous adipose tissue, containing 1,387 genes. These genes were significantly enriched in 10 gene ontologies including extracellular matrix organization, biological adhesion, and collagen metabolic process, and were mainly involved in pathways including ECM-receptor interaction, focal adhesion, cAMP signaling pathway, PI3K-AKT signaling pathway, and regulation of lipolysis in adipocytes. In the PPI network and coexpression network, five genes (CAV1, ITGA5, COL5A1, ABL1, and HSPG2) were identified as "real" Hub genes. Analysis of Hub gene expression by dataset revealed that the expression of these Hub genes was significantly higher in subcutaneous adipose tissue than in other tissues. In addition, real-time fluorescence quantitative PCR (qRT-PCR) analysis based on tissue samples and adipocytes also confirmed the above results.

Conclusion: In this study, five key genes related to subcutaneous adipose tissue were discovered, which laid a foundation for further study of the molecular regulation mechanism of subcutaneous adipose tissue development and adipose deposition.

Keywords: fat deposition, WGCNA, Hub gene, focal adhesion, PI3K-AKT

OPEN ACCESS

Edited by:
Anning Li,
Northwest A&F University, China

Reviewed by:
Gefeng Xu,
Chinese Academy of Fishery Sciences, China
Elena De Felice,
University of Camerino, Italy

***Correspondence:**
Yun Ma
mayun_666@126.com

Specialty section:
This article was submitted to Livestock Genomics, a section of the journal Frontiers in Veterinary Science

Received: *07 April 2022*
Accepted: *13 May 2022*
Published: *22 June 2022*

Citation:
Sheng H, Pan C, Wang S, Yang C, Zhang J, Hu C, Hu H, Feng X, Yang M, Lei Z, Gao Y, Wang Z and Ma Y (2022) Weighted Gene Co-Expression Network Analysis Identifies Key Modules and Central Genes Associated With Bovine Subcutaneous Adipose Tissue. Front. Vet. Sci. 9:914848. doi: 10.3389/fvets.2022.914848

INTRODUCTION

Adipose tissue is an active metabolic organ that secretes numerous protein factors, such as resistin and lipocalin, which are essential for lipid accumulation, energy expenditure, glucose, and insulin metabolism, and hormonal regulation, and have a profound role in regulating the body's glucolipid metabolic homeostasis and maintaining energy homeostasis (1, 2). However, due to the complex molecular mechanism of adipose tissue formation and deposition, there are relatively few studies on adipose deposition-related genes in cattle, which need to be further explored.

Adipose tissue not only plays a necessary role in the development of individuals but also plays an important role in the study of beef quality. Adipose tissue is classified as intramuscular fat, visceral fat, intermuscular fat, and subcutaneous fat according to its distribution. Among them, intramuscular fat (IMF) plays an indispensable role in meat quality, which affects meat taste, juicy, shear force, and so on (3, 4). Subcutaneous adipose tissue is an important source of essential fatty acids and plays a role in the transport of fat-soluble vitamins, which constitute the main source of energy and insulating substances for the animal's body. Studies have shown that fat deposition in backfat is related to body fat percentage, carcass cross-sectional fat area ratio, intramuscular fat, and flavor and juiciness of beef (5, 6). In Japanese Wagyu cattle, IMF content in the longest dorsal muscle was found to be positively correlated with the percentage of subcutaneous fat and maturity *in vivo* (7, 8). Therefore, the identification of key genes related to subcutaneous adipose tissue by a new method is an important strategy for carcass and meat quality genetic improvement.

Weighted gene coexpression network analysis (WGCNA) is an efficient and accurate method for bioinformatics and biological data mining (9). It helps to create free-scale gene co-expression networks to identify associations between different gene collections or between gene collections and clinical features (10). At present, it is widely used in genetics, cancer, and brain imaging research and analysis (11). By using WGCNA, we can create a coexpression network to identify differentially related gene clusters and analyze gene specificity (12).

This study constructed a gene co-expression network using transcriptome data from multiple tissues and identified the modules of gene co-expression related to subcutaneous adipose tissue. The interested module was analyzed by gene ontology (GO) and Kyoto Encyclopedia of Genes and Genomes (KEGG) pathway analysis, and the Hub gene in the module was determined. Then the expression of the Hub gene was analyzed, and the accuracy of selection was preliminarily verified. This study provides a starting point for further exploration of the molecular regulatory mechanism of fat deposition.

MATERIALS AND METHODS

Data Collection and Preprocessing

We downloaded the GSE116775 microarray dataset from the Gene Expression Omnibus (GEO) database (**Supplementary Table 1**), which consists of approximately 1.2 Tb of high-quality RNA-Seq transcriptome data from four key metabolic tissues (rumen epithelium, liver, muscle, and subcutaneous fat) and data on the content of 49 fatty acids in backfat, to explore the molecular regulatory mechanisms of these tissues in fatty acid formation in cattle (13). In our study, the GSE116775 dataset was used to construct co-expression networks and identify hub genes associated with bovine subcutaneous adipose tissue. The data set provides gene expression profiles of 185 samples containing four tissue types of three breeds of cattle. All the datasets were normalized independently using Robust Multiarray Average (RMA) followed by log2 transformation and quantile normalization.

Construction of Co-Expression Network

Phenotype-correlated gene modules associated with adiposity were identified by WGCNA. The top 10,000 genes with the highest expression levels were used to construct the WGCNA network using the WGCNA package in R. Firstly, a similarity matrix was constructed by calculating the Pearson's correlation coefficient to measure the similarity between all samples. Then, based on the free-scale topological criterion, the similarity matrix is transformed into an adjacency matrix, and a scale-free co-expression network based on the soft threshold parameter β is constructed by using the adjacency matrix. In this study, the free-scale topology was $R^2 = 0.80$ with a soft threshold equal to 12. The topological overlap matrix (TOM) was used to define modules based on dissimilarity (1-TOM). The minimum number of genes in each module is 30. For module grouping, the partition threshold used is 0.25. Finally, a color is assigned to each gene module, and genes that are not assembled into any module are grouped into gray modules (14).

Identification of the Module of Interest and Functional Annotation

In order to clarify the potential biological significance of genes in key modules and further explore the functions of genes in the most related modules of subcutaneous adipose tissue, we analyzed GO terms and KEGG pathways using the "clusterProfiler" software package in R software. In addition, only when the p.adjust of the GO or KEGG terms is >0.01, they are considered important.

Hub Genes Identification

The degree of module members (MM) is defined as the correlation between gene expression profiles and module eigengenes (Mes). Gene significance (GS) is defined as the absolute value of the correlation between genes and external traits. Genes with both high MM and high GS are considered to be candidate central genes. Then, all the genes in the interested module are uploaded to the STRING website to create a PPI network, and the CytoHubba plug-in of Cytoscape software is used to identify the central genes in the PPI network. Hub genes that co-occurred in the co-expression network and Cytoscape software analysis were considered as "real" Hub genes and were selected for subsequent analysis (15, 16).

Validation of the Hub Genes

The expression levels of Hub genes in the dataset were analyzed by differential expression patterns. At the same time, qRT-PCR was used to further verify the expression level of Hub gene in bovine subcutaneous adipose tissue and bovine preadipocytes at different induction stages. The R package ggpubr was used to calculate difference significance and visualization.

Sample Collection and Cell Culture

The tissue samples (rumen epithelium, liver, muscle, and subcutaneous fat) and bovine subcutaneous adipocytes were provided by the Key Laboratory of Ruminant Molecular Cell breeding of Ningxia University. All the experiments were carried out in strict accordance with the recommendations in the guidelines for Animal Protection and Utilization of Ningxia University and approved by the Animal Welfare Committee of Ningxia University (IACUC-NXU1098). The isolated cells were cultured in a growth medium containing 90% Dulbecco's modified Eagle medium (DMEM, Gibco) and 10% fetal bovine serum (FBS, Gibco) until cell density reached approximately 80%. Then 90% DMEM, 10% FBS, 3.5 mg/ml insulin (Sigma), 0.01% dexamethasone (Sigma), 1% Isobutylmethylxanthine (Sigma) and 0.01% rosiglitazone (Sigma) were mixed together to form a differentiation medium to induce cell differentiation. After 2 days of differentiation, the cells were cultured in maintenance medium (95% DMEM, 5% FBS, 3.5 mg/mL insulin, 0.01% rosiglitazone).

Oil Red O Staining

Oil red O was used to observe the morphology of bovine preadipocytes after 0 and after 10 days of differentiation. The storage solution of oil red O (oil red O + isopropanol) was diluted into a working solution at 2:3 with Phosphate-Buffered Saline (PBS), and the cells were sfixed with 10% formalin and stained (17).

RNA Extraction and qRT-PCR

Total RNA was extracted from tissue samples and cultured cells using TRIZOL reagent (Invitgen, USA). PrimeScript II first strand cDNA synthesis kit (Takara, Dalian, China) was used to prepare first strand cDNA. QRT-PCR was performed using All-in-One™ qRT-PCR Mix (Genocopoeia, Guangzhou, China) in a LightCycler® 96 Instrument (Roche, Germany) to detect the expression level of mRNAs. All the primers used are listed in **Supplementary Table 2**.

Statistical Analysis

According to the characteristics of data distribution, a nonparametric test or t-test was used to analyze the statistical significance of gene expression in four tissues. Tissue and cellular qRT-PCR experiments were performed using mRNA of β-actin as an endogenous control at basal levels, and the relative expression levels of genes were calculated using the $2^{-\Delta\Delta Ct}$ method and were considered statistically significant when the $p < 0.05$.

RESULTS

Construction of Weighted Gene Co-Expression Network

This study performed a WGCNA analysis based on the GSE116775 dataset. The clustering analysis of the selected samples is shown in **Figure 1**. A total of 185 samples were divided into four independent clusters, each corresponding to a tissue type, indicating that different tissue types were the main reason for the differences between samples, and thus the results of the analysis are expected to uncover modules and Hub genes specific to bovine subcutaneous adipose tissue. When 0.8 is used as the correlation coefficient threshold, the soft threshold power is selected as 12 (**Figure 2A**). Then, on the basis of the determined soft threshold, the weighted gene co-expression network is constructed, the co-expression modules are divided by dynamic cutting and module merging, and finally, nine co-expression modules are obtained. The modules with the most genes were turquoise modules (1,509), followed by blue modules (1,387), brown modules (1,157), and yellow modules (1,058) (**Figure 2B**). In addition, we have drawn adjacency heat maps of all the analyzed genes, which show that these modules are independent of other modules (**Figure 2C**).

Identification of Key Modules

We calculated the correlation coefficient and the corresponding statistical significance between modular feature genes and clinical traits and displayed the results with a heat map (**Figure 3A**). According to the aim of the study, we found the highest correlation between the blue module and bovine subcutaneous adipose tissue ($r = 0.88$, $p = 3e\text{-}61$). **Figure 3B** shows that the genes in the blue module are of great significance for the study of subcutaneous fat (**Supplementary Table 4**). **Figure 3C** shows that the expression level of genes related to subcutaneous adipose tissue in the blue module is significantly higher than that in other tissues, so the blue module is selected for further analysis.

Functional Annotation of the Key Co-Expression Module

We carried out GO and KEGG pathway enrichment analysis of the genes in the blue module in order to find out the main biological processes and signal pathways of enrichment. **Figure 4** shows the first 10 terms for GO-BP and KEGG enrichment analysis (all enriched terms and explanations for the first 10 terms can be found in **Supplementary Tables 5**, **6**). GO-BP functional enrichment analysis showed that the genes in the blue module were mainly enriched in extracellular matrix tissue, bioadhesion, and collagen metabolism (**Figure 4A**). KEGG analysis showed that ECM receptor interaction, focal adhesions, cAMP signal pathway, PI3K-AKT signal pathway and the regulation of lipolysis of adipocytes were the obvious ways of gene enrichment in the blue module (**Figure 4B**).

Excavation of the Hub Gene

In this study, 56 genes with high clinical trait relationships (GS ≥ 0.88) and high linkage (MM ≥ 0.92) in the blue module were selected as pivotal genes for WGCNA (**Supplementary Table 7**;

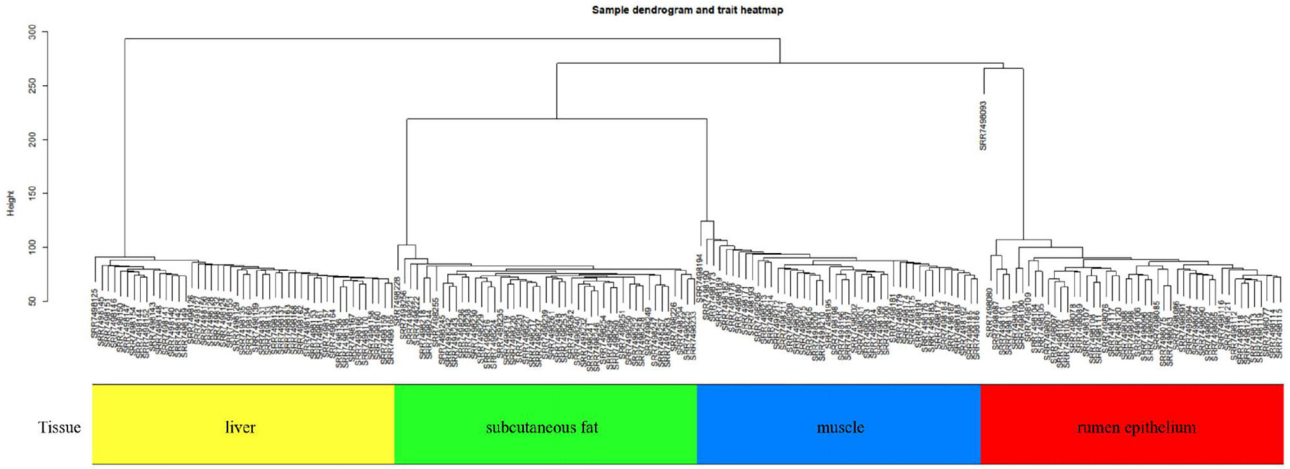

FIGURE 1 | Sample dendrogram and trait heatmap in GSE116775.

Figure 5). According to the STRING database, all the genes in the module are used to build the PPI network using Cytoscape software (**Supplementary Table 8**; **Figure 6A**), and the 20 genes with the highest connectivity are defined as the Hub genes in the PPI network. Then, the five common genes (CAV1, ITGA5, COL5A1, ABL1, and HSPG2) in the co-expression network and PPI network are defined as "real" Hub genes (**Figure 6B**).

Induction of Differentiation of Bovine Subcutaneous Adipocytes

By inducing the differentiation of bovine subcutaneous adipocytes, qRT-PCR and oil red O staining were used to detect the sequential expression of adipogenic marker genes in the induced cells for 0–10 days. The results showed that compared with that before induction, the expression levels of PPARγ, C/EBPβ, and FABP4 increased significantly after induction ($p < 0.01$) (**Figure 7C**), and the content of lipid droplets in cells increased significantly ($p < 0.01$) (**Figures 7A,B**), indicating that the model of inducing differentiation of bovine subcutaneous adipocytes was successfully established.

Validation of the Hub Genes

We discussed the differential expression level of Hub gene in the data set. The results showed that Hub gene expression was significantly higher in subcutaneous adipose tissue than in rumen epithelium, liver, and muscle tissue ($p < 0.01$) (**Figure 8**). QRT-PCR was used to detect the expression level of the Hub gene in tissues and induced subcutaneous adipocytes. The results showed that the Hub gene was highly expressed in adipose tissue (**Figure 9**); and compared with that before induction, the expression level of the Hub gene increased significantly after cell induction ($p < 0.01$) (**Figure 10**). These results suggest that these Hub genes play an important role in the study of adipose tissue development.

DISCUSSION

Fat deposition is a qualitative trait typically regulated by multiple genes that function by interacting with each other. In traditional unidimensional studies, it is difficult to find the key genes for this trait and their mechanisms of action. However, WGCNA is a powerful statistical method based on gene correlation that can be used to construct gene networks, detect modules, identify pivotal genes, and screen candidate genes as biomarkers (10). In the statistical process, WGCNA focuses on dealing with a group of gene modules rather than individual genes, which avoids the disadvantage of only dealing with single genes and neglecting molecular transcriptional networks. Therefore, using WGCNA to study the co-expression network of multiple tissue phenotypes can identify the marker genes in subcutaneous adipose tissue and provide a research basis for exploring the molecular mechanism of fat deposition.

In this study, we downloaded 185 samples belonging to the GSE116775 dataset from the GEO database, and obtained nine modules by using the WGCNA method. According to the correlation study of the topological overlap matrix (TOM) graph (**Figure 2**), each module is proved to be independent of the other modules. In addition, after trait-module correlation analysis, the blue module was identified as the key module positively related to subcutaneous adipose tissue, which means that the gene expression in this module is closely related to subcutaneous adipose tissue. Subsequent GO analysis showed that the genes in fat-related modules were mainly enriched in the extracellular matrix organization, biological adhesion, collagen metabolic process, and other biological functions. KEGG enrichment showed that these genes were mainly involved in ECM receptor interaction, focal adhesions, cAMP signal pathway, PI3K-AKT signal pathway, and the regulation of lipolysis of adipocytes. In addition, adipose tissue-related "real" Hub genes (CAV1 and ITGA5) are mainly involved in KEGG pathways related to extracellular matrix organization and cell surface receptor signaling transduction pathways (**Figure 11**).

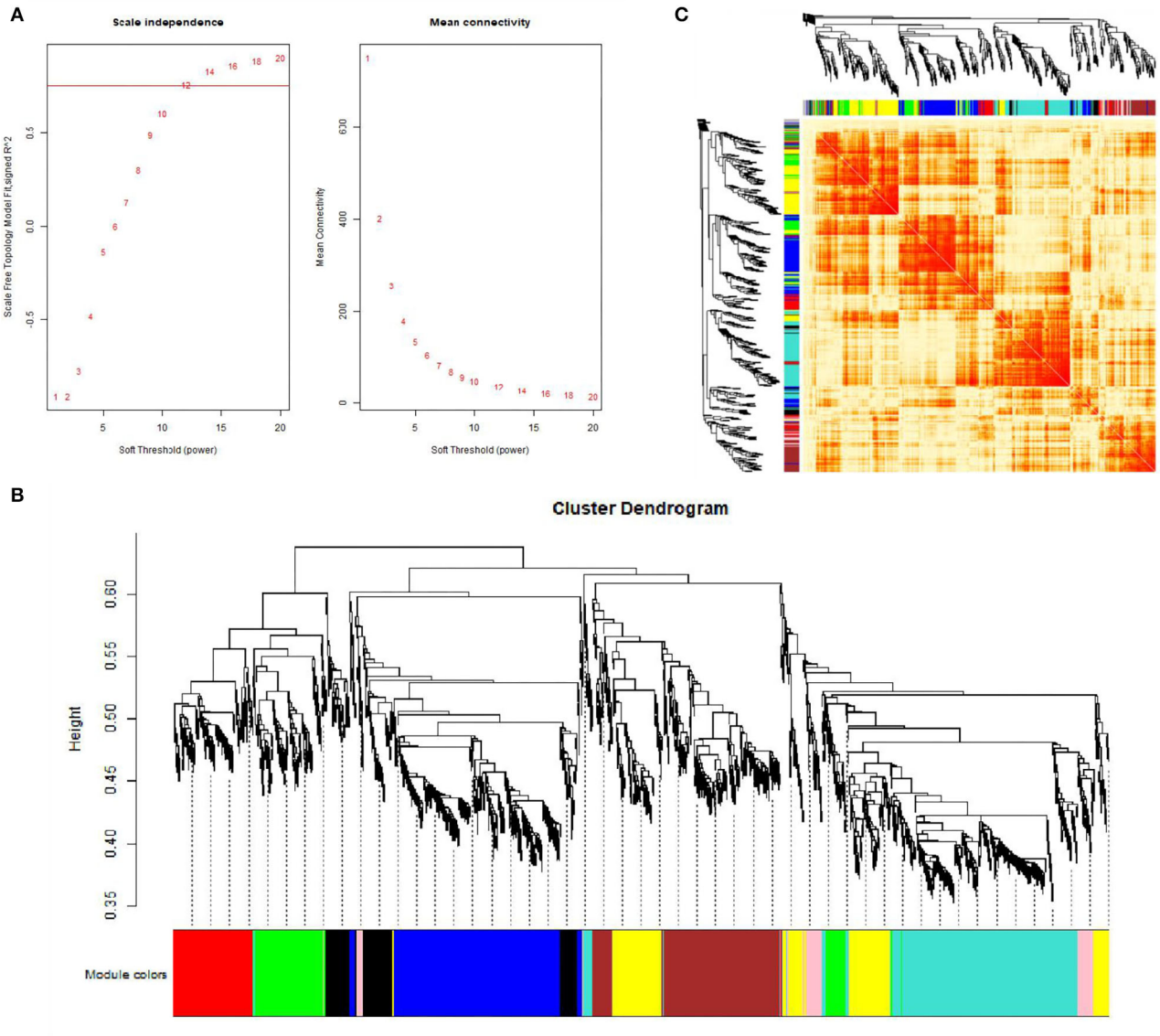

FIGURE 2 | Gene co-expression networks in subcutaneous adipose tissue (GSE116775). **(A)** Analysis of the scale-free fit index for soft-thresholding powers (left) and the mean connectivity for various soft-thresholding powers (right); **(B)** Gene expression clustering tree and recognition module in co-expression network; **(C)** Network heatmap plot in the co-expression modules.

Through literature research, we found that the composition and distribution of the extracellular matrix changed in the process of adipocyte differentiation, suggesting that organizing the components of the extracellular matrix into a suitable structure is a necessary condition for adipocyte differentiation and maintenance. Among the extracellular matrix components, the extracellular network of fibronectin (FN) is the first to form but gradually degrades as adipocytes differentiate. The type I collagen network is the last to form and remains well organized during the later stages of adipocyte differentiation. The extracellular network of type III, V, and VI collagen was formed in the middle stage of adipocyte differentiation and maintained until the late stage of adipocyte differentiation. The reticular structures of type IV collagen and laminin were degraded during differentiation and located on the surface of globular cells (18). And with regard to adipose tissue regeneration, appropriate ECM may be needed to support cell attachment, proliferation, and differentiation until adipocytes can secrete their own ECM (19). In addition, ECM is also an important part of the focal adhesions pathway and PI3K-AKT pathway. Focal adhesions are cell-matrix adhesion structures mediated by integrins whose functions include anchoring the ends of actin filaments, promoting strong attachment to the matrix, and functioning as an integrin signaling platform (20). A PI3K-AKT signaling pathway is involved in many biological processes, including cell cycle, apoptosis, angiogenesis, and

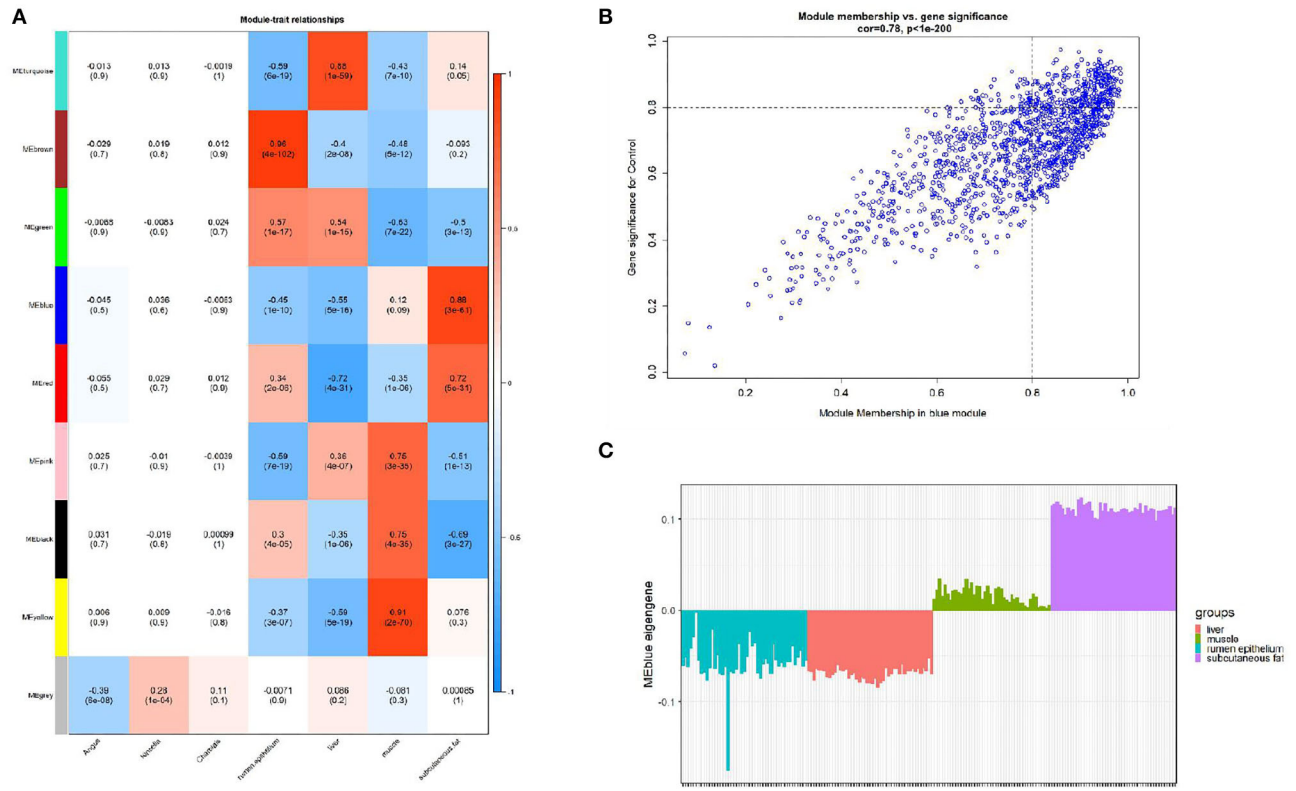

FIGURE 3 | Module-trait correlations analysis in subcutaneous adipose tissue (GSE116775). **(A)** The correlation heat map between the module and subcutaneous adipose tissue (each unit contains the correlation coefficient and the corresponding P value); **(B)** The significance of genes related to subcutaneous adipose tissue in the blue module (a dot represents the genes in the blue module); **(C)** Module eigengene (y-axis) across samples (x-axis) from the blue module (associated to Subcutaneous fat tissue).

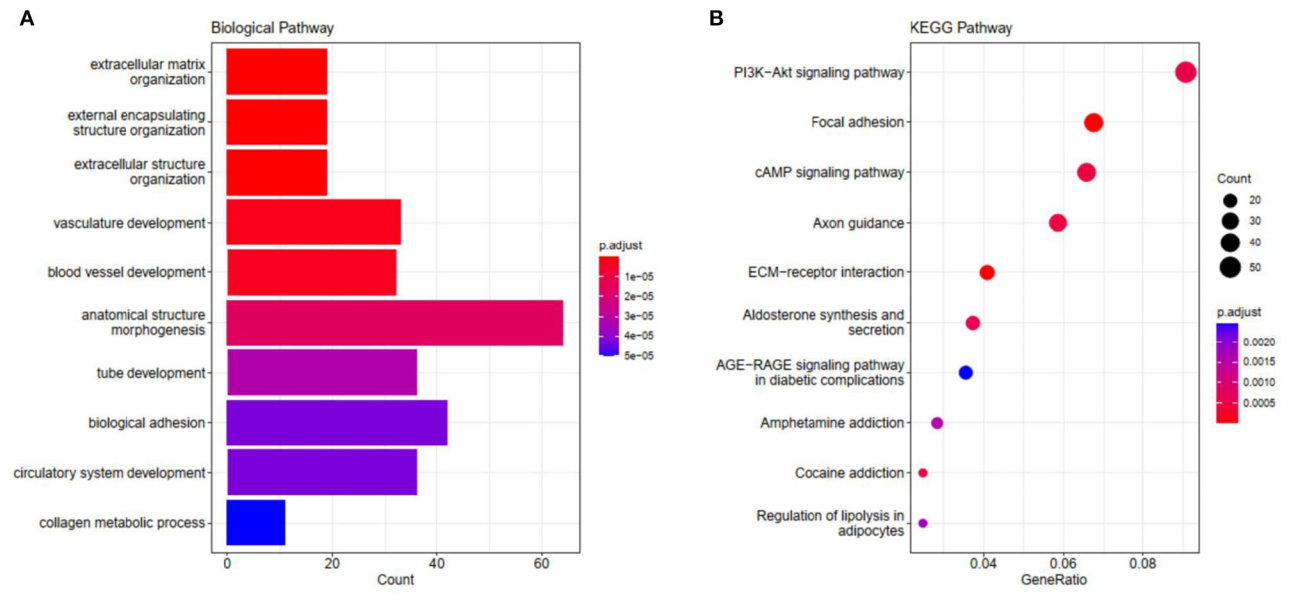

FIGURE 4 | The visualization results of **(A)** partial GO biological function analysis and **(B)** partial KEGG analysis of the blue module. The top 10 significant enriched pathways were shown.

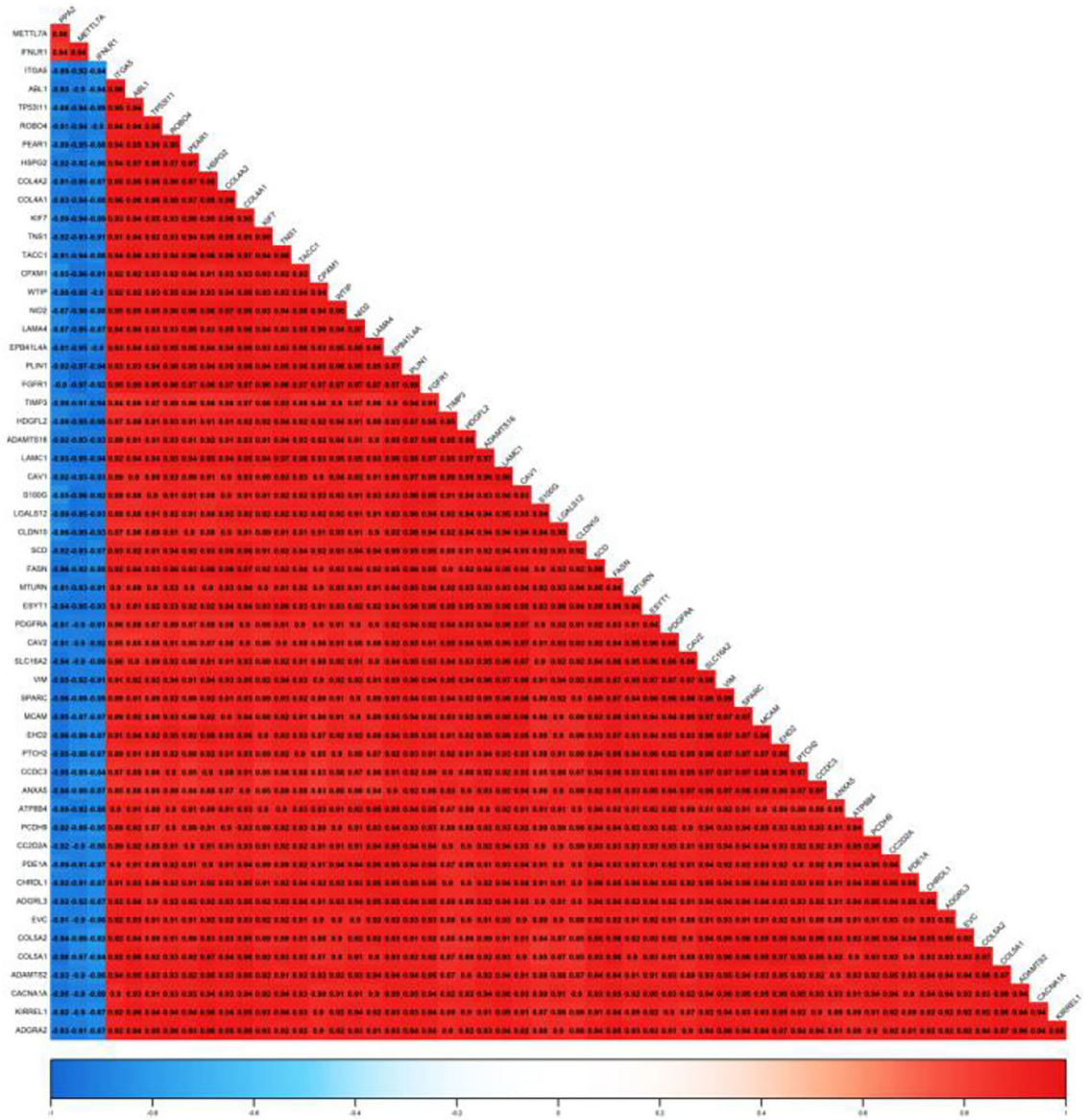

FIGURE 5 | Correlation of the top 56 genes with high MM and GS in the blue module.

glucose metabolism, which is essential for cell proliferation and apoptosis (21, 22). And the cAMP signaling pathway has been reported to play an important role in the regulation of energy homeostasis with its involvement in adipogenesis and lipid metabolic processes (23–26).

With regard to the identified central genes, the functional studies of CAV1, ITGA5, COL5A1, ABL1, and HSPG2 in the process of fat deposition are insufficient. Caveolae are small flask-shaped invaginations of the plasma membrane that are found with remarkable abundance in endothelial cells, myotubes, and adipocytes (27). They are considered a subset of the so-called lipid raft domains and segregate a number of membrane-related processes (28). The Caveolae protein family has three highly related members (caveolin-1 through-3). In adipocytes, Caveolin-1 expression was found to be a key step in increasing caveolae density, increasing the ability of adipocytes to accommodate larger lipid droplets, and promoting cell expansion through increased glucose utilization (29). COL5A1 and ITGA5 are important constituents of ECM. COL5A1 is differentially expressed before and after bariatric surgery, which may be a new candidate gene for regulating adipose tissue function (30). ITGA5 is expressed in different degrees in mesenchymal stem cells isolated from adipose tissue and white mature adipocytes, which is related to the Hippo pathway, while the Hippo pathway controls tissue growth and regulates cell proliferation, differentiation, and cell death (31–33). ABL1 is highly expressed

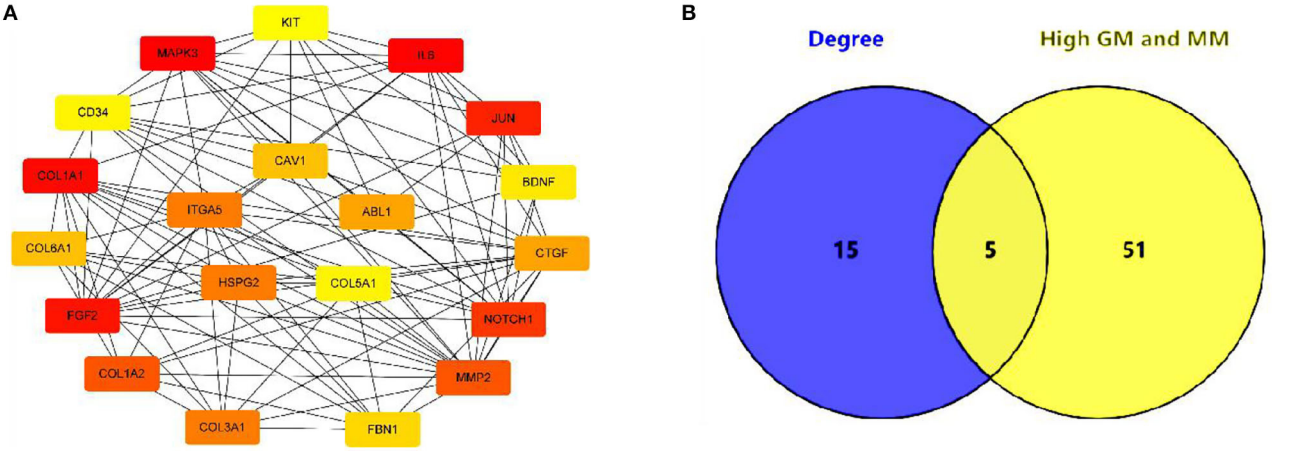

FIGURE 6 | Identification of Hub gene. **(A)** The top 20 genes with the highest connectivity identified by Cytoscape software; **(B)** Identify the common genes in the co-expression network and PPI network.

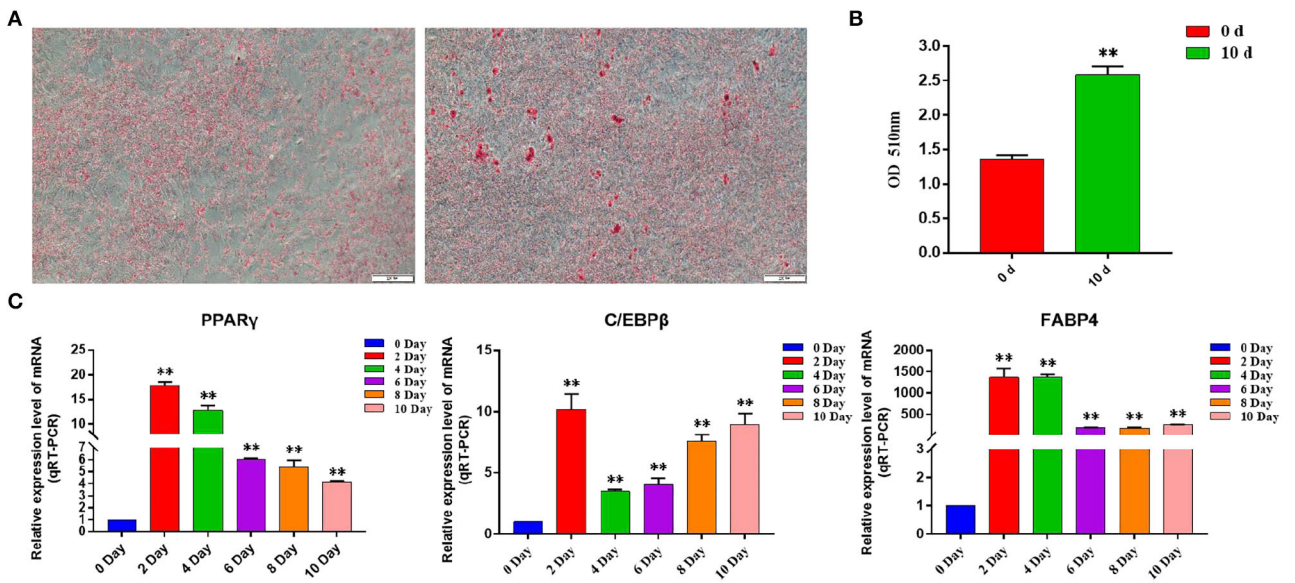

FIGURE 7 | Induction of primary adipocyte differentiation. **(A)** Bovine adipocytes were stained with oil red O at 0 d (left) and 10 d (right) after adipogenic differentiation; **(B)** Absorbance measurements at 510 nm. Control: isopropyl alcohol, 0 d: adipocyte extracts from 0 day of induced differentiation, 10 d: adipocyte extracts from 10 day of induced differentiation; **(C)** Expression of adipogenic marker genes in the process of adipogenic differentiation. Compared with the control, "*" means significant difference ($p < 0.05$), and "**" means extremely significant difference ($p < 0.01$).

in the subcutaneous fat of obese humans and high-fat diet-induced obese mice, and it is able to regulate diet-induced obesity by improving insulin sensitivity in subcutaneous fat (34). HSPG2 is a heparan sulfate proteoglycan, which is a component of the basement membrane and participates in a variety of biological activities. It was found that the mass and cell size of white adipose tissue in HSPG2 knockout mice were smaller than those in the control group, which may regulate the catabolism of lipids and glucose by transforming the composition of muscle fibers into oxidized fibers (35).

Adipose tissue is mainly composed of adipocytes and matrix components around the cells. Peroxisome proliferator-activated receptor gamma (PPARγ) and CCAAT enhanced binding protein (C/EBP) have been proved to be the main regulatory factors involved in adipocyte differentiation. Adipocytes rapidly induce the expression of C/EBPβ and C/EBPδ proteins within 4 h of induced differentiation and then activate the transcription of PPARγ and CEBPα (36). The expression of PPARγ and C/EBPα regulates a variety of genes in coordination, which determines the phenotype of

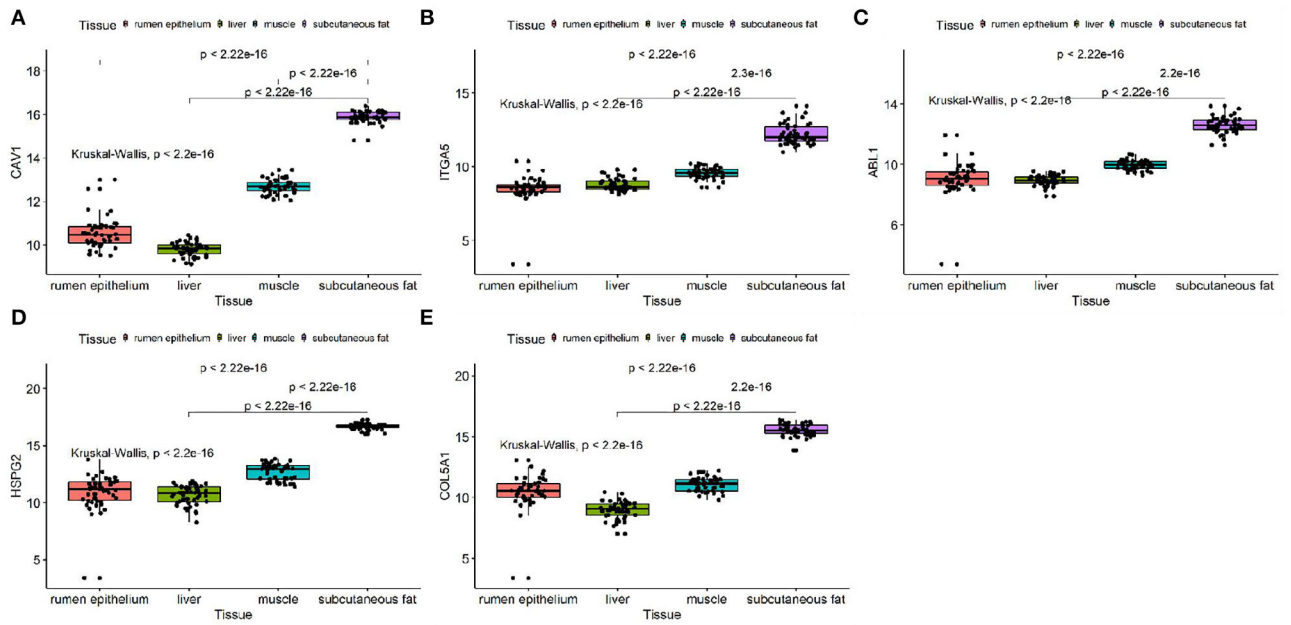

FIGURE 8 | Expression of Hub genes in dataset GSE116775. **(A–E)** Expression levels of **(A)** CAV1, **(B)** ITGA5, **(C)** ABL1, **(D)** HSPG2, and **(E)** COL5A1 were significantly increased in Subcutaneous fat tissue.

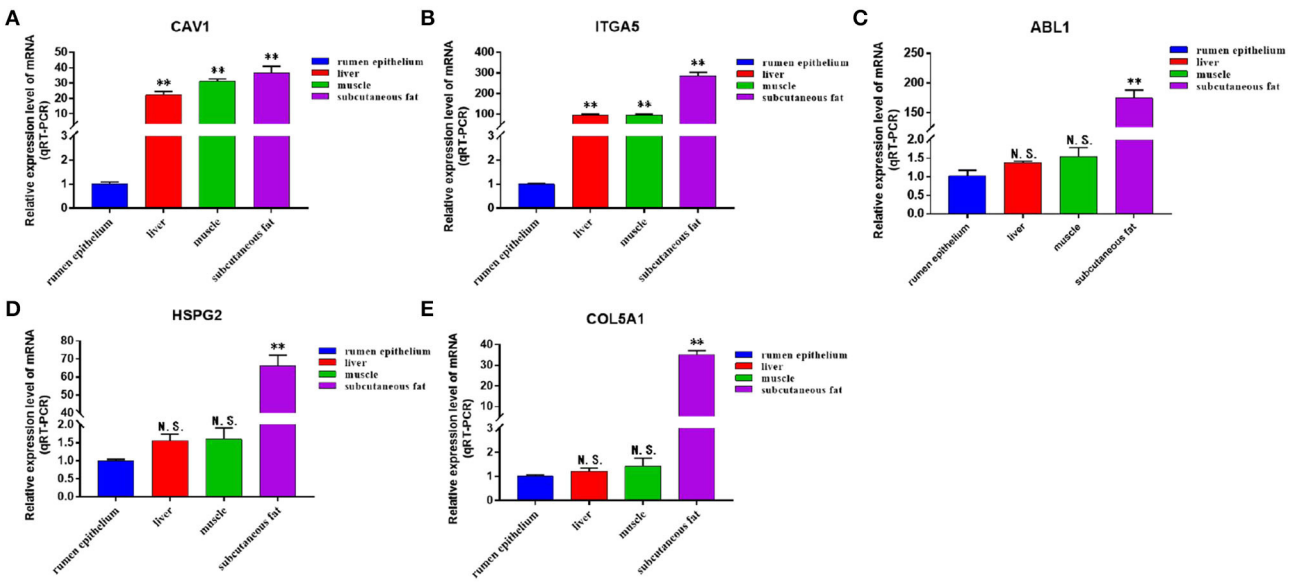

FIGURE 9 | The expression level of Hub gene in different tissue samples. **(A–E)** Compared with other tissues, the expression levels of **(A)** CAV1, **(B)** ITGA5, **(C)** ABL1, **(D)** HSPG2, and **(E)** COL5A1 in subcutaneous adipose tissue were significantly increased. Compared with the control, "*" means significant difference ($p < 0.05$), "**" means extremely significant difference ($p < 0.01$), and "N.S." indicates non-significant difference.

cell differentiation (37). Fatty acid binding protein 4 (FABP4) gene is highly expressed during adipocyte differentiation and can bind and transport long-chain fatty acids, which plays an important role in the synthesis and decomposition of triglycerides. In this study, by constructing the differentiation model of bovine subcutaneous adipocytes, the expression level of the adipogenic marker gene and the formation of lipid droplets were detected by the qRT-PCR technique. The results showed that compared with that before induction, the expression levels of adipogenic marker genes PPARγ, C/EBPα and FABP4 in induced subcutaneous adipocytes were all at a high level, and the number of lipid droplets

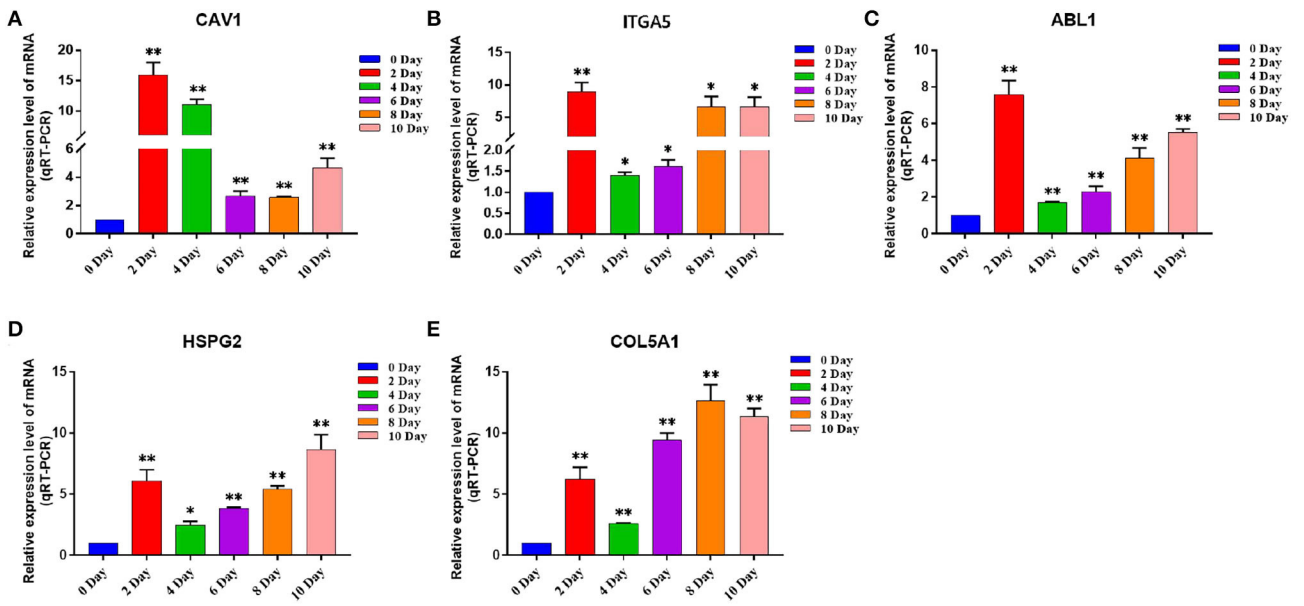

FIGURE 10 | The expression level of Hub gene in different differentiation stages of adipocytes. **(A–E)** Compared with that before induction, the expression levels of **(A)** CAV1, **(B)** ITGA5, **(C)** ABL1, **(D)** HSPG2, and **(E)** COL5A1 were significantly increased after induction. Compared with the control, "*" means significant difference ($p < 0.05$), "**" means extremely significant difference ($p < 0.01$), and "N.S." indicates non-significant difference.

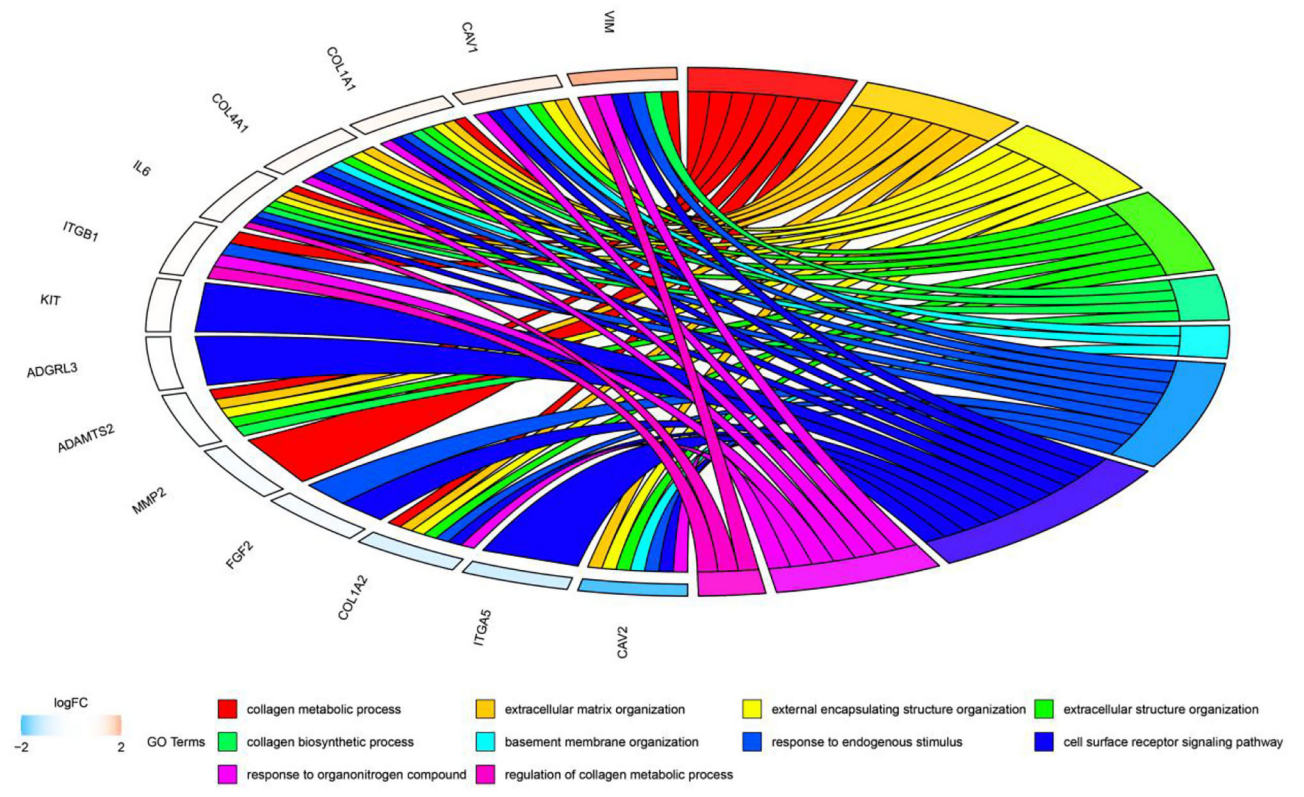

FIGURE 11 | Circos plot to indicate the relationship between hub genes and KEGG pathways.

increased significantly after induction, which proved that we successfully established the induced differentiation model of bovine subcutaneous adipocytes. Subsequently, the expression of Hub gene (CAV1, ITGA5, COL5A1, ABL1, and HSPG2) in bovine subcutaneous adipocytes was detected, and it was found that the expression level of five Hub genes increased significantly after cell induction, especially on the second day of induction, which was consistent with the expression of adipogenic marker genes, which may be due to the effect of changing induction medium to stimulate adipocyte differentiation. It is suggested that these five Hub genes may play the same role as adipogenic marker genes in the process of adipocyte differentiation.

In summary, CAV1, ITGA5, COL5A1, ABL1, and HSPG2 from the blue module are candidate genes related to subcutaneous adipose tissue, and their expression levels are related to adipocyte proliferation and differentiation, which may regulate adipose tissue growth and development by mediating extracellular matrix tissue and cell surface receptor signal transduction pathway. Although many studies have reported that these genes play an important role in fat development, the specific mechanism is not clear. Finally, we verified our results using tissue samples and adipocyte samples obtained by real-time fluorescence quantitative PCR and found that these Hub genes were highly expressed in adipose tissue and induced differentiated adipocytes. Therefore, these five candidate genes can be regarded as new biomarkers of subcutaneous adipose tissue. The results of this study will provide a new perspective on adipose tissue development and adipose deposition.

DATA AVAILABILITY STATEMENT

The original contributions presented in the study are included in the article/**Supplementary Material**, further inquiries can be directed to the corresponding author.

ETHICS STATEMENT

The animal study was reviewed and approved by the Animal Welfare Committee of Ningxia University.

AUTHOR CONTRIBUTIONS

HS and CP: made the same contribution to the work and analyzed the data. YM and HS: conceived and designed the research. HS: wrote the manuscript. SW, CY, JZ, CH, HH, XF, MY, ZL, YG, ZW, and YM: modified the manuscript. All authors read and approved the final manuscript.

FUNDING

This study was supported by grants from the National Natural Science Foundation of China (32072720-31672403), the Leading Talents Fund in Science and Technology Innovation in Henan Province (No. 194200510022), the Key Research and Talent Introduction Project of Ningxia Hui Autonomous Region (2019YCZX0068, 2021BEF01002, and 2021NXZD1), and the Cultivation Project for Talents in Science and Technology Innovation of Ningxia Hui Autonomous Region (2020GKLRLX02). The funding bodies played no role in the design of the study, collection, analysis, and interpretation of data and writing the manuscript.

ACKNOWLEDGMENTS

We would also like to express our gratitude to all the participants.

SUPPLEMENTARY MATERIAL

The Supplementary Material for this article can be found online at: https://www.frontiersin.org/articles/10.3389/fvets.2022.914848/full#supplementary-material

REFERENCES

1. Ferhat M, Funai K, Boudina S. Autophagy in adipose tissue physiology and pathophysiology. *Antioxid Redox Signal.* (2019) 31:487–501. doi: 10.1089/ars.2018.7626
2. Galic S, Oakhill JS, Steinberg GR. Adipose tissue as an endocrine organ. *Mol Cell Endocrinol.* (2010) 316:129–39. doi: 10.1016/j.mce.2009.08.018
3. Purchas RW, Burnham DL, Morris ST. Effects of growth potential and growth path on tenderness of beef longissimus muscle from bulls and steers. *J Anim Sci.* (2002) 80:3211–21. doi: 10.2527/2002.80123211x
4. Okeudo NJ, Moss BW. Interrelationships amongst carcass and meat quality characteristics of sheep. *Meat Sci.* (2005) 69:1–8. doi: 10.1016/j.meatsci.2004.04.011
5. Silva-Vignato B, Coutinho LL, Cesar ASM, Poleti MD, Regitano LCA, Balieiro JCC. Comparative muscle transcriptome associated with carcass traits of nellore cattle. *BMC Genomics.* (2017) 18:506. doi: 10.1186/s12864-017-3897-x
6. Xing K, Zhu F, Zhai L, Liu H, Wang Z, Hou Z, et al. The Liver Transcriptome of two full-sibling songliao black pigs with extreme differences in backfat thickness. *J Anim Sci Biotechnol.* (2014) 5:32. doi: 10.1186/2049-1891-5-32
7. Liu L, Cao P, Zhang L, Qi M, Wang L, Li Z, et al. Comparisons of adipogenesis- and lipid metabolism-related gene expression levels in muscle, adipose tissue and liver from wagyu-cross and holstein steers. *PLoS ONE.* (2021) 16:e0247559. doi: 10.1371/journal.pone.0247559
8. Yamada T, Kamiya M, Higuchi M. Fat depot-specific effects of body fat distribution and adipocyte size on intramuscular fat accumulation in wagyu cattle. *Anim Sci J.* (2020) 91:e13449. doi: 10.1111/asj.13449
9. Zhang B, Horvath S. A general framework for weighted gene co-expression network analysis. *Stat Appl Genet Mol Biol.* (2005) 4. doi: 10.2202/1544-6115.1128
10. Langfelder P, Horvath S. Wgcna: An R package for weighted correlation network analysis. *BMC Bioinformatics.* (2008) 9:559. doi: 10.1186/1471-2105-9-559
11. Ravasz E, Somera AL, Mongru DA, Oltvai ZN, Barabasi AL. Hierarchical organization of modularity in metabolic networks. *Science.* (2002) 297:1551–5. doi: 10.1126/science.1073374
12. Bakhshi S, Gupta A, Sharma MC, Khan SA, Rastogi S. Her-2/Neu, P-53, and their coexpression in osteosarcoma. *J Pediatr Hematol Oncol.* (2009) 31:245–51. doi: 10.1097/MPH.0b013e318197947e
13. Sun HZ, Zhu Z, Zhou M, Wang J, Dugan MER, Guan LL. Gene co-expression and alternative splicing analysis of key metabolic tissues to unravel the regulatory signatures of fatty acid composition in cattle. *RNA Biol.* (2021) 18:854–62. doi: 10.1080/15476286.2020.1824060

14. Gao Z, Ding R, Zhai X, Wang Y, Chen Y, Yang CX, et al. Common gene modules identified for chicken adiposity by network construction and comparison. *Front Genet.* (2020) 11:537. doi: 10.3389/fgene.2020.00537
15. Li B, Pu K, Wu X. Identifying novel biomarkers in hepatocellular carcinoma by weighted gene co-expression network analysis. *J Cell Biochem.* (2019). doi: 10.1002/jcb.28420
16. Lu DL, Bai X, Zou QY, Gan ZH, Lv YF. Identification of the association between hmmr expression and progression of hepatocellular carcinoma via construction of a co-expression network. *Oncol Lett.* (2020) 20:2645–54. doi: 10.3892/ol.2020.11844
17. Yang M, Gao X, Ma Y, Wang X, Lei Z, Wang S, et al. Bta-Mir-6517 promotes proliferation and inhibits differentiation of pre-adipocytes by targeting Pfkl. *J Anim Physiol Anim Nutr (Berl).* (2021). doi: 10.1111/jpn.13662
18. Kubo Y, Kaidzu S, Nakajima I, Takenouchi K, Nakamura F. Organization of extracellular matrix components during differentiation of adipocytes in long-term culture in vitro. *Cell Dev Biol Anim.* (2000) 36:38–44. doi: 10.1290/1071-2690(2000)036<0038:OOEMCD>2.0.CO;2
19. Ting ACH, Craft RO, Palmer JA, Gerrand YW, Penington AJ, Morrison WA, et al. The adipogenic potential of various extracellular matrices under the influence of an angiogenic growth factor combination in a mouse tissue engineering chamber. *Acta Biomater.* (2014) 10:1907–18. doi: 10.1016/j.actbio.2013.11.019
20. Guo W, Giancotti FG. Integrin signalling during tumour progression. *Nat Rev Mol Cell Biol.* (2004) 5:816–26. doi: 10.1038/nrm1490
21. Xie Y, Shi X, Sheng K, Han G, Li W, Zhao Q, et al. Pi3k/Akt Signaling transduction pathway, erythropoiesis and glycolysis in hypoxia (Review). *Mol Med Rep.* (2019) 19:783–91. doi: 10.3892/mmr.2018.9713
22. Spangle JM, Roberts TM, Zhao JJ. The emerging role of pi3k/akt-mediated epigenetic regulation in cancer. *Biochim Biophys Acta Rev Cancer.* (2017) 1868:123–31. doi: 10.1016/j.bbcan.2017.03.002
23. Altarejos JY, Montminy M. Creb and the Crtc co-activators: sensors for hormonal and metabolic signals. *Nat Rev Mol Cell Biol.* (2011) 12:141–51. doi: 10.1038/nrm3072
24. Bruno NE, Kelly KA, Hawkins R, Bramah-Lawani M, Amelio AL, Nwachukwu JC, et al. Creb coactivators direct anabolic responses and enhance performance of skeletal muscle. *EMBO J.* (2014) 33:1027–43. doi: 10.1002/embj.201386145
25. Lee K, Jin H, Chei S, Oh HJ, Choi SH, Nah SY, et al. The gintonin-enriched fraction of ginseng regulates lipid metabolism and browning via the camp-protein kinase a signaling pathway in mice white adipocytes. *Biomolecules.* (2020) 10. doi: 10.3390/biom10071048
26. Ravnskjaer K, Madiraju A, Montminy M. Role of the camp pathway in glucose and lipid metabolism. *Handb Exp Pharmacol.* (2016) 233:29–49. doi: 10.1007/164_2015_32
27. Palade GE. Blood capillaries of the heart and other organs. *Circulation.* (1961) 24:368–88. doi: 10.1161/01.CIR.24.2.368
28. Parton RG, Simons K. The multiple faces of caveolae. *Nat Rev Mol Cell Biol.* (2007) 8:185–94. doi: 10.1038/nrm2122
29. Briand N, Prado C, Mabilleau G, Lasnier F, Le Liepvre X, Covington JD, et al. Caveolin-1 expression and cavin stability regulate caveolaedynamics in adipocyte lipid store fluctuation. *Diabetes.* (2014) 63:4032–44. doi: 10.2337/db13-1961
30. Dankel SN, Fadnes DJ, Stavrum AK, Stansberg C, Holdhus R, Hoang T, et al. Switch from stress response to homeobox transcription factors in adipose tissue after profound fat loss. *PLoS ONE.* (2010) 5:e11033. doi: 10.1371/journal.pone.0011033
31. Morandi EM, Verstappen R, Zwierzina ME, Geley S, Pierer G, Ploner C. Itgav and Itga5 diversely regulate proliferation and adipogenic differentiation of human adipose derived stem cells. *Sci Rep.* (2016) 6:28889. doi: 10.1038/srep28889
32. Chen CS, Mrksich M, Huang S, Whitesides GM, Ingber DE. Geometric control of cell life and death. *Science.* (1997) 276:1425–8. doi: 10.1126/science.276.5317.1425
33. Folkman J, Moscona A. Role of cell shape in growth control. *Nature.* (1978) 273:345–9. doi: 10.1038/273345a0
34. Wu R, Sun JG, Wang JQ Li B, Liu Q, Ning G, et al. C-Abl Inhibition mitigates diet-induced obesity through improving insulin sensitivity of subcutaneous fat in mice. *Diabetologia.* (2017) 60:900–10. doi: 10.1007/s00125-016-4202-2
35. Yamashita Y, Nakada S, Yoshihara T, Nara T, Furuya N, Miida T, et al. Perlecan, a heparan sulfate proteoglycan, regulates systemic metabolism with dynamic changes in adipose tissue and skeletal muscle. *Sci Rep.* (2018) 8:7766. doi: 10.1038/s41598-018-25635-x
36. Chondronikola M, Sidossis LS. Brown and beige fat: from molecules to physiology. *Biochim Biophys Acta Mol Cell Biol Lipids.* (2019) 1864:91–103. doi: 10.1016/j.bbalip.2018.05.014
37. Hausman GJ, Dodson MV, Ajuwon K, Azain M, Barnes KM, Guan LL, et al. Board-invited review: the biology and regulation of preadipocytes and adipocytes in meat animals. *J Anim Sci.* (2009) 87:1218–46. doi: 10.2527/jas.2008-1427

Conflict of Interest: The authors declare that the research was conducted in the absence of any commercial or financial relationships that could be construed as a potential conflict of interest.

Publisher's Note: All claims expressed in this article are solely those of the authors and do not necessarily represent those of their affiliated organizations, or those of the publisher, the editors and the reviewers. Any product that may be evaluated in this article, or claim that may be made by its manufacturer, is not guaranteed or endorsed by the publisher.

frontiers | Frontiers in Veterinary Science

ORIGINAL RESEARCH
published: 07 July 2022
doi: 10.3389/fvets.2022.946447

Weighted Gene Co-expression Network Analysis Revealed That CircMARK3 Is a Potential CircRNA Affects Fat Deposition in Buffalo

Xue Feng[1†], *Jinhui Zhao*[2†], *Fen Li*[1†], *Bandar Hamad Aloufi*[3], *Ahmed Mohajja Alshammari*[3] *and Yun Ma*[1,2*]

[1] *Key Laboratory of Ruminant Molecular and Cellular Breeding of Ningxia Hui Autonomous Region, School of Agriculture, Ningxia University, Yinchuan, China,* [2] *College of Life Sciences, Xinyang Normal University, Xinyang, China,* [3] *Department of Biology, College of Science, University of Hail, Hail, Saudi Arabia*

OPEN ACCESS

Edited by:
Sayed Haidar Abbas Raza, Northwest A&F University, China

Reviewed by:
Rajwali Khan, University of Agriculture, Pakistan
Lupei Zhang, Institute of Animal Sciences (CAAS), China
Rui-Si Hu, University of Electronic Science and Technology of China, China
Ali Raza Jahejo, Shanxi Agricultural University, China

***Correspondence:**
Yun Ma
mayun_666@126.com

[†] *These authors have contributed equally to this work*

Specialty section:
This article was submitted to Livestock Genomics, a section of the journal Frontiers in Veterinary Science

Received: *17 May 2022*
Accepted: *13 June 2022*
Published: *07 July 2022*

Citation:
Feng X, Zhao J, Li F, Aloufi BH, Alshammari AM and Ma Y (2022) Weighted Gene Co-expression Network Analysis Revealed That CircMARK3 Is a Potential CircRNA Affects Fat Deposition in Buffalo. Front. Vet. Sci. 9:946447. doi: 10.3389/fvets.2022.946447

Background: Buffalo meat is increasingly widely accepted for consumption as it shares several quality attributes with cattle meat (beef). Hence, there is a huge opportunity for growth in the buffalo meat industry. However, buffalo meat has relatively low intramuscular fat (IMF) content, affecting its flavor, tenderness and juiciness. As there is a dearth of information on factors that control fat deposition, this study was undertaken to provide new candidate factor associated with buffalo fat deposition. Circular RNA (circRNA) is a novel class of non-coding RNA with a closed-loop structure, and play an important role in fat deposition.

Methods: In this study, weighted gene co-expression network analysis (WGCNA) was used to construct a circRNA co-expression network and revealed a candidate circRNA that may affect the IMF deposition of buffalo as determined by RT-qPCR, semiquantitative PCR and gain-of-function experiments.

Results: Herein, WGCNA determined that one module (turquoise module) is significantly associated with the growth and development stages of buffalo. Further analysis revealed a total of 191 overlapping circRNAs among differentially expressed (DE) circRNAs and the co-expression module. A candidate circRNA was found, 21:6969877|69753491 (circRNA_ID), with a reported involvement in lipid metabolism. This circRNA is stably expressed and originates from the *MARK*3 gene, hence the name circMARK3. circMARK3 is highly expressed in adipose tissue and mature adipocytes and is located in the cytoplasm. Gain-of-function experiments demonstrated that circMARK3 promoted adipogenic differentiation of buffalo adipocytes and 3T3-L1 cells by up-regulating the expression levels of adipogenic marker genes *PPARG*, *C/EBPα* and *FABP*4.

Conclusion: These results indicate that circMARK3 is a potential factor that promotes fat deposition by regulating adipocyte differentiation and adipogenesis in buffalo.

Keywords: buffalo, circRNA, WGCNA, adipocytes, adipogenesis

INTRODUCTION

Beef (cattle meat) is the third most widely consumed meat worldwide. It is a consumer favorite because of its "flavor," "tenderness," "juiciness," and "rich in nutrition" properties (1). Buffalo meat has the same nutritional values as beef (2), but it is not widely accepted by consumers because of its low intramuscular fat (IMF) content which negatively affects its flavor, tenderness, and juiciness (3). Since China is the most populous country in the world, beef is often in short supply. Therefore, enhancing IMF deposition in buffalo meat has become one of the major goals in current buffalo breeding activity.

Adipogenesis is a well-orchestrated multistep process that involves the action of a large number of transcription factors (4–6), and in particular the PPAR (PPARγ, PPARα) (4, 7–10) and C/EBP family (C/EBPα, C/EBPβ, and C/EBPδ) (4, 9, 11) are enriched for adipogenesis regulated transcription factors in many animals species. Among them, PPARG (PPARγ) and C/EBPα, as key transcription factors in adipogenesis, are involved in a single pathway of adipocyte development with PPARγ being the proximal effector of adipogenesis (12). The master regulatory factors affecting adipogenesis have been widely studied, but it is far from enough to analyze the molecular regulatory mechanism of fat deposition only by transcription factors. Currently, several new factors are being proposed as regulators or influencers of adipogenesis. For example, sterol regulatory element binding protein (SREBP) transcription factor (13), phosphoenolpyruvate carboxykinase1 (*PCK1*) (3, 14), and fatty acid binding protein (*FABP4*) (9). In addition, non-coding RNAs (miRNAs, lncRNAs, and circRNAs) also play an important role in regulating the economic traits of livestock and poultry, and they interact with coding RNAs to form a regulatory network to jointly regulate fat deposition (15).

circRNAs, a type of endogenous non-coding RNA with covalently closed loop structure (16, 17), have become a research hotspot in recent years. They have been recently reported to be involved in multiple biological processes, such as cancer (18–20), ontogenesis (21, 22) and adipogenesis (23, 24). RNA sequencing technology has been instrumental to show that circRNAs modulate fat deposition in livestock animals (25–27). In pig, the potential lncRNAs/circRNAs-miRNAs-mRNAs regulatory networks shared *MYOD1*, *PPARD*, miR-423-5p and miR-874, which were associated with skeletal muscle muscular proliferation, differentiation/regeneration, and adipogenesis (28). In chicken, several reference circRNAs, such as circLCLAT1, circFNDC3AL, circCLEC19A, and circARMH1, potentially affect adipogenesis by regulating miRNAs via PPAR and fatty acid metabolism-related pathways (26). Recent studies have shown that circINSR inhibits preadipocyte adipogenesis in bovine by alleviating inhibition of miR-15/16 against target genes (29, 30). In this study, a candidate circRNA 21:6969877|69753491(circMARK3) was found through weighted gene co-expression network analysis (WGCNA), and further gain-of-function experiments demonstrated that circMARK3 promoted the adipogenic differentiation of buffalo adipocytes by up-regulating the adipogenesis relative gene. In summary, we propose a potential circRNA that plays an important role in buffalo fat deposition, which provides a molecular basis for beef quality improvement.

Abbreviations: WGCNA, Weighted gene co-expression network analysis; DE, Differentially expressed; MARK3, microtubule affinity regulating kinase 3; PPARγ or PPARG, peroxisome proliferator activated receptor gamma; C/EBPα, CCAAT/enhancer-binding protein α; FABP4, fatty acid binding protein 4; IMF, intramuscular fat; SREBP1, sterol regulatory element binding protein; THRSP, thyroid hormone responsive; PRDM16, PR/SET domain 16; PCK1, phosphoenolpyruvate carboxykinase 1; MYOD1, Myogenic Differentiation 1; PBS, phosphate buffer saline; GAPDH, Glyceraldehyde-3-phosphate dehydrogenase; SD, Standard Deviation; MAD, median absolute deviation; ceRNA, endogenous RNA; SE, standard error.

MATERIALS AND METHODS

Animal Ethics

Six Chinese swamp buffaloes were bred for commercial use, rather than for experimental reasons, and they were slaughtered according to the food industry-approved halal food quality certified protocol by a Muslim cleric according to the law of Islam. Thus, no ethics approval was required by a specific committee (31).

Animals and Tissue Samples

Six Chinese swamp buffaloes were raised at the Xinyang buffalo farm (Xinyang, Henan, China) with equivalent forage and feeding management conditions. Animals were weaned at 6 months of age and slaughtered at 30 months of age. Tissues, i.e., heart, liver, spleen, lung, kidney, longissimus dorsi muscle, and back subcutaneous fat, were sampled immediately after slaughter and were frozen in liquid nitrogen for RT-qPCR experiments. For primary adipocyte isolation, fresh back subcutaneous fat tissue was sampled, kept in phosphate buffer saline (PBS) with 1% streptomycin and penicillin, and taken back to the lab for isolation and culture of adipose tissue-derived mesenchymal stem cells.

CircRNA Bioinformatics Analysis

The circRNAs expression matrix and DE circRNAs obtained from RNA-seq analysis have been reported previously (31). The WGCNA package in R4.1.0 provides a comprehensive set of functions for performing weighted correlation network analysis (32), and phenotypic information used in WGCNA is shown in **Supplementary Table S1**. The overlapping circRNAs among DE circRNAs and co-expression modules were analyzed using VENNY 2.1(https://bioinfogp.cnb.csic.es/tools/venny/index.html).

Weighted Gene Co-expression Network Analysis

The co-expression network of the circRNAs was constructed base-on-base using the circRNAs expression matrix (33) and traits characteristic data (**Supplementary Table S1**). To allow direct comparison between sample, circRNAs in each sample were normalized as the number of back-spliced reads per million mapped reads (RPM) (31, 34, 35). The soft threshold for co-expression network construction was determined and

the adjacency matrix was defined. The adjacency matrix was subsequently converted to a topological overlap matrix (TOM) and the corresponding dissimilarity TOM (dissTOM) was calculated. For modules with high TOM, the adaptive dynamic pruning algorithm was used to merge the modules. The soft-free network was constructed using the module function, after which module partition analysis was performed to identify the gene co-expression modules. Gene significance (GS) and module membership (MM) values were calculated. MM is the correlation coefficient between a gene and the genes for trait characteristics within the module and can be used to screen for important genes in the module. When GS and MM values of a gene in a module show significant correlation, it suggests that the gene may be a hub gene that is highly correlated with the target trait.

RNA Isolation and cDNA Synthesis

Total RNA was isolated by TRIzol (Invitrogen, Carlsbad, CA, United States) according to the manufacturer's instructions. RNA quality was measured with NanoDrop 2000 (Nanodrop, Wilmington, DE, USA) and 1.5% agarose gels. RNA with $1.8 < 260/280$ value < 2.0 was used for further analysis. Elimination of linear RNA was performed by Lucigen RNR07250 Ribonuclease R kit (RNase R, Lucigen-Simplifying Genomics). RNase R reaction system according to the manufacturer's instructions. Isolation of nuclear and cytoplasmic RNA was performed using the PARIS kit (Life Technologies, Carlsbad, CA, United States) according to the manufacturer's instructions. The total RNA was transcribed into cDNA using the PrimeScript^{TM} RT Master Mix (Takara, Dalian, China).

RT-qPCR Analysis

Glyceraldehyde-3-phosphate dehydrogenase (*GAPDH*) and *β-actin* were used as reference genes. Furthermore, *β-actin* was used as a cytoplasmic marker in both nucleus and cytoplasm for cell localization. RT-qPCR was performed using TB Green^{TM} Premix Ex Taq^{TM} II (Dalian, China, Takara Bio) and LightCycler® 96 (Switzerland, Roche) with two-step reactions according to the manufacturer's recommended protocol. The $2^{\Delta\Delta Ct}$ method was used to calculate the relative expression level of circRNA. Three replicates were run per sample and the RT-qPCR experiment was performed three times. Among them, primers were designed using the "pick primers" function from NCBI (https://www.ncbi.nlm.nih.gov/tools/primer-blast/) and Primer 5.0 (**Supplementary Table S2**).

Vector Construction and Adenovirus Packaging

For 3T3-L1 cells, mouse-circMARK3 (mouse-source sequence) overexpression was achieved by using pCD2.1-ciR vector. Mouse pCD2.1-circRNA was amplified from cDNA of mouse adipose tissue. The sequence of mouse circRNA (**Supplementary Text S1**) was cloned into the KpnI and BamHI restriction sites of the pCD2.1-ciR vector. However, due to the fact that buffalo primary adipocytes are difficult to efficiently transfect, the overexpression of buffalo-circMARK3 (buffalo-source sequence) was achieved by adenovirus packaging experiments (36). Adenovirus packaging was performed at Hanbio Biotechnology Co., Ltd. (Shanghai, China). Briefly, full length buffalo-circRNAs (**Supplementary Text S1**) were synthesized and ligated to the AdMax system to obtain Ad-circRNA. EGFP was used as an indicator for transduction efficiency and Ad-EGFP was used as a negative control.

Cell Transfection, Adenovirus Transduction, Oil Red O Staining and Quantification

For 3T3-L1 preadipocytes, transfection with mouse pCD2.1-circRNA was performed using Lipofectamine 3000 (Invitrogen, Carlsbad, CA, United States) when cells reached 80% confluence, following the manufacturer's protocol. Forty-eight hours after transfection, 3T3-L1 primary adipocytes were treated for 2 days with inducing medium containing 1 μM dexamethasone (Sigma, USA), 0.5 mM IBMX, 10 μg/mL insulin and 1 μM rosiglitazone (Sigma, Milwaukee, WI, USA). Then, 3T3-L1 cells were treated with a maintenance medium containing 10 μg/mL insulin and 1 μM rosiglitazone. The maintenance medium was replaced every 2 days for a total of 6 days, until induction of differentiation. Similar to cell transfection, adenovirus transfection buffalo Ad-circRNA was performed when buffalo adipocytes reached 80% confluence according to the adenovirus transduction manufacturer's protocol. Two days after transfection, buffalo adipose-derived mesenchymal stem cells were treated with inducing medium for 2 days. For a further 4 days, they were treated with maintenance medium, which was changed every 2 days. After inducing with adipogenic agents for 6 days, Oil Red O staining and quantification were performed as described (36).

Statistical Analysis

Comparisons were analyzed using SPSS software. P-value < 0.05 was considered to indicate statistical significance. Results are represented as the mean ± SD ($n = 3$) and plotted with GraphPad Prism7 software.

RESULTS

Weighted Gene Co-expression Network Analysis

WGCNA analyzed 5,141 circRNAs obtained from RNA-seq (31) and was used to construct 21 co-expression modules (**Figure 1A**). Among them, the soft-thresholding power we chose was 9 as the correlation coefficient threshold, and 30 was chosen as the minimum number of circRNA in modules. To merge possible similar modules, we defined 0.25 as the threshold for cut height. The modules comprising most genes were turquoise, followed by blue, brown, and yellow (**Supplementary Table S3**). Moreover, the dissTOM obtained was subjected to hierarchical clustering, resulting in a hierarchical clustering tree (5,000 circRNAs), and these modules were independent of other modules (**Figure 1B**). Module-trait correlation analysis showed that the turquoise module was related to month and weight (**Figure 1C**). The significance of these circRNAs in the turquoise module is

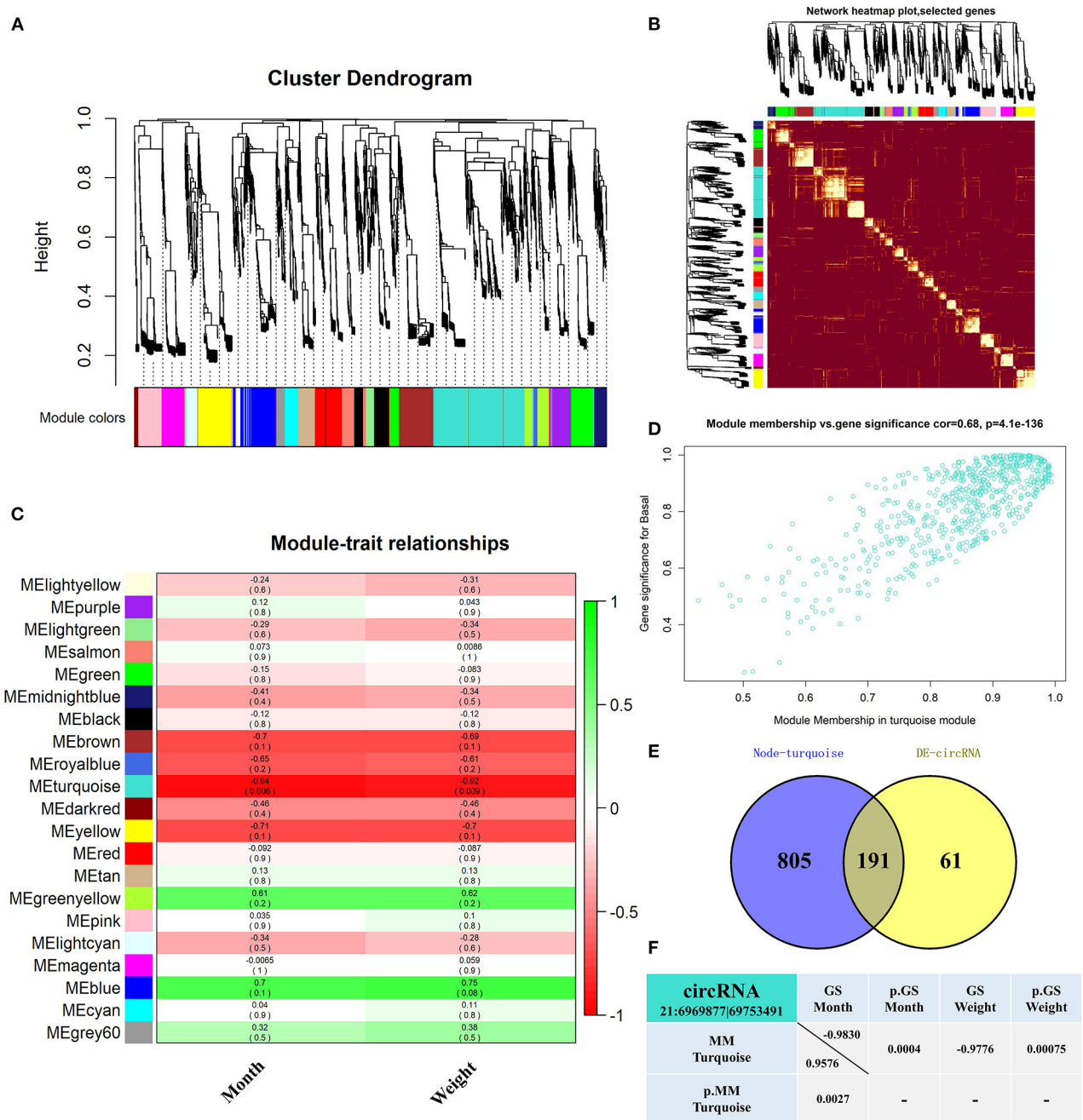

circRNA 21:6969877|69753491	GS Month	p.GS Month	GS Weight	p.GS Weight
MM Turquoise	-0.9830 / 0.9576	0.0004	-0.9776	0.00075
p.MM Turquoise	0.0027	-	-	-

FIGURE 1 | Screened-out circRNAs significantly associated to buffalo fat deposition. **(A–D)** CircRNA co-expression network of adipose tissue in the Xinyang buffalo revealed by WGCNA; **(A)** Hierarchical cluster tree of co-expression modules, where every leaf on a tree is a circRNA and main branches are made up of 21 color-coded modules; **(B)** Construction of co-expression modules by WGCNA. Progressively more saturated red colors indicate higher overlap among these functional modules and blocks of lighter color along the diagonal are the gene modules. Module assignment gene and dendrograms are at the top and left, respectively; **(C)** Association analysis of gene co-expression network modules with trait, where each row corresponds to a module (name displayed on the left) and each column corresponds to a particular trait. Colors of the row/column intersection cells indicate the correlation coefficient between module and trait (positive-green and negative-red); **(D)** Scatterplot of Gene Significance (GS) For Traits vs. Module Membership (MM) in the turquoise module, with a highly significant correlation between GS and MM (one dot represents one gene in the turquoise module); **(E)** Overlapping circRNAs between DE circRNAs and co-expression turquoise module; **(F)** CircRNA 21:6969877|69753491 GS and MM values.

shown in **Figure 1D** and **Supplementary Table S4**. We found 191 overlapping circRNAs between the DE circRNAs list (31) and the turquoise module (**Supplementary Table S5**; **Figure 1E**). Among these, circRNA 21:6969877|69753491 has been shown to be involved in lipid metabolism in a previous study, therefore it likely affects fat deposition. Gene significance (GS>0.8) (37, 38)

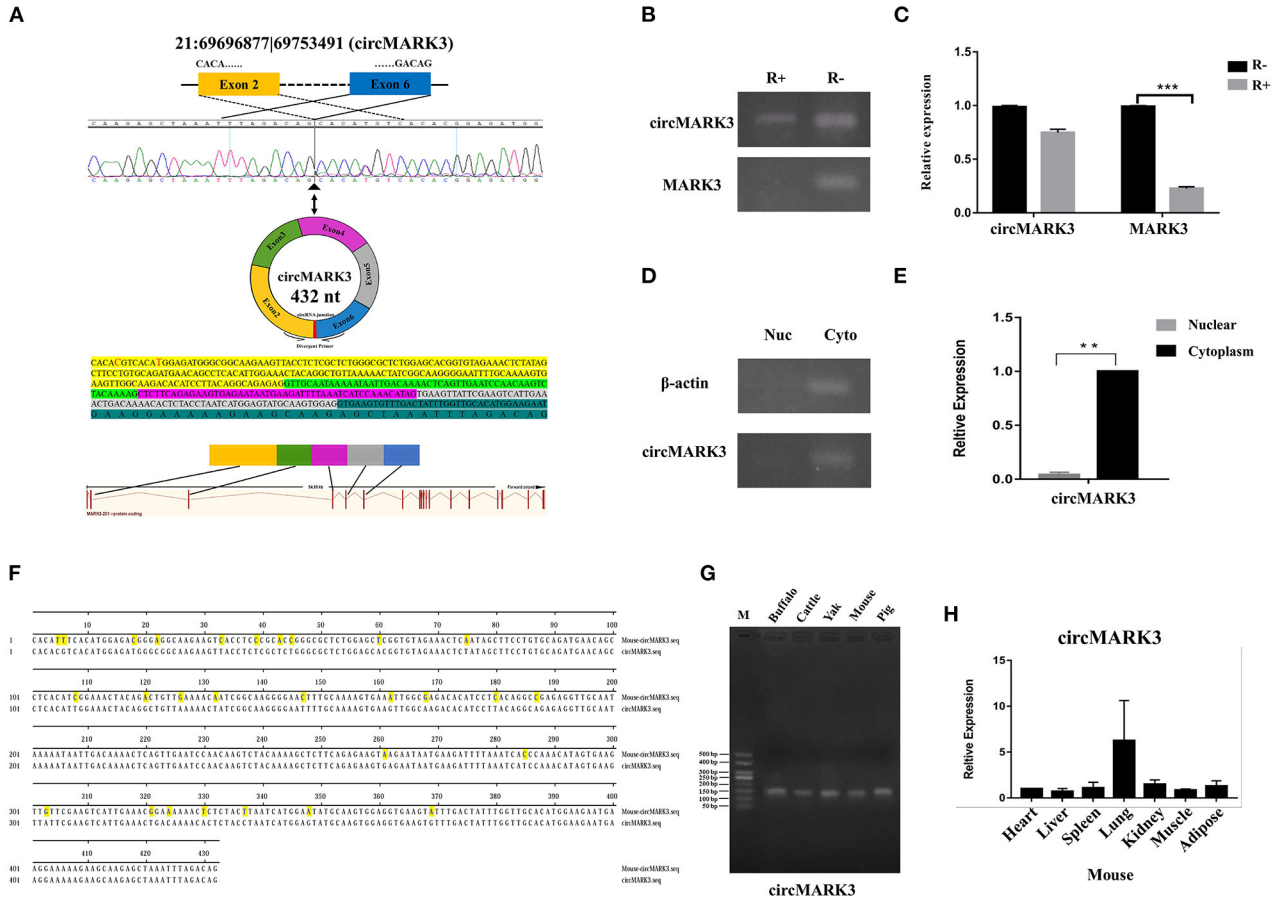

FIGURE 2 | Characteristic analysis of circMARK3. **(A)** Basic information of circMARK3 composition structure (bases C and T labeled red were mutated into T and C in the sequence); **(B)** Semiquantitative PCR results of circMARK3 and *MARK3* before and after RNase R treatment; **(C)** RT-qPCR results of circMARK3 and *MARK3* before and after RNase R treatment; **(D)** Cell localization of circMARK3 by semiquantitative PCR; **(E)** Cell localization of circMARK3 by RT-qPCR; **(F)** Sequence alignment results of circMARK3 in mouse and buffalo; **(G)** CircMARK3 conservation in adipose tissues of different species by semiquantitative PCR detection; **(H)** Expression profile of circMARK3 in heart, liver, spleen, lung, kidney, muscle and adipose tissues of mouse. In panels B-E, bovine-*β-actin* was used to normalize the expression level of the reference gene. In panel H, mouse-*β-actin* was used to normalize the expression level of the reference gene. Data are presented as the mean ± SD, $n = 3$, $^{**}P < 0.01$, $^{***}P < 0.001$. **(B–D)** The samples derive from the same experiment and gels were processed in parallel.

and module membership (MM>0.8) (37–39) values showed a high correlation between circRNA 21:6969877|69753491 and two traits (month and weight) of buffalo **Figure 1F**.

Characteristic Analysis of CircMARK3

Since circRNA 21:6969877|69753491 (432 nt) is formed by splicing and circularizing exons 2–6 of the microtubule affinity regulating kinase 3 (*MARK3*) gene (**Figure 2A**), we have named it circMARK3. Semiquantitative PCR results show the latter still exists in primary adipocytes by the RNase R digestion linear RNA (**Figure 2B**). The RT-qPCR results show that circMARK3 is still highly expressed in cells treated by the RNase R (**Figure 2C**). These results show that circMARK3 is stably expressed as circRNA (**Figures 2B,C**). Also, semiquantitative PCR and RT-qPCR results of isolated nuclear and cytoplasm of adipocytes show that circMARK3 is mainly expressed in the cytoplasm (**Figures 2D,E**). Conservation in different species was assessed by semiquantitative PCR and RT-qPCR detection: circMAK3 is conserved in buffalo, cattle, yak, mouse and pig (**Figure 2G**), and is ubiquitously expressed in different tissues of mice (**Figure 2H**). Sequence alignment shows that circMARK3 in mouse and buffalo are partially conserved, and the homology was 93.51% (**Figure 2F**).

The Expression Pattern of CircMARK3

circMARK3 is mainly expressed in adipose tissue of buffalo (**Figure 3A**, $p < 0.001$). Primary adipocytes cultured *in vitro* are ideal cell models for studying the molecular regulatory mechanism of adipogenesis. Therefore, buffalo adipocytes were successfully isolated and cultured (**Figures 3B–D**). By inducing the culture medium, they successfully differentiated to produce lipid droplets (**Figure 3E**). During adipogenic

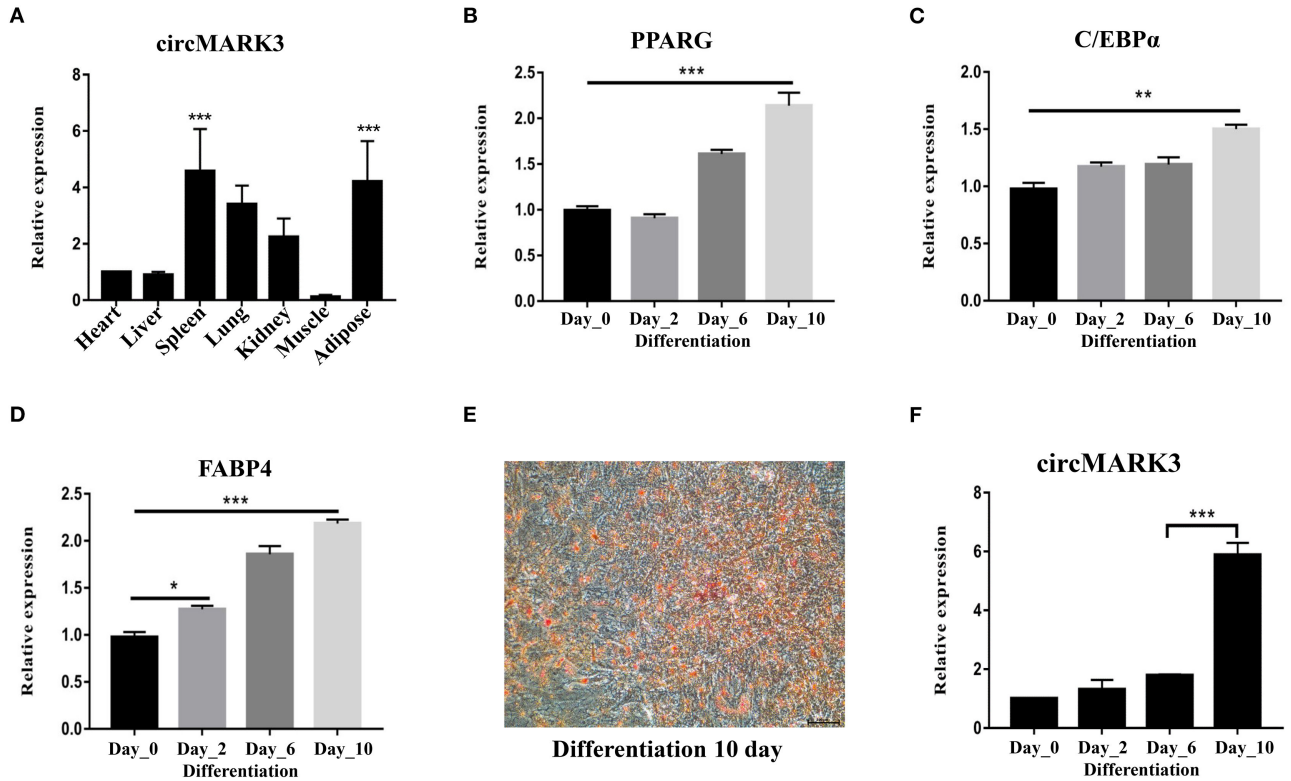

FIGURE 3 | Expression pattern of circMARK3 in tissues and adipocytes of buffalo. **(A)** Expression profile of circMARK3 in heart, liver, spleen, lung, kidney, muscle and adipose tissues of buffalo; **(B–D)** expression pattern during buffalo adipocyte differentiation of *PPARG* (after 0, 2, 6, and 10 days) **(B)**, *C/EBPα* **(C)** and *FABP4* **(D)**; **(E)** Oil Red O staining for detection of buffalo adipocyte lipid deposition (differentiation day 10); **(F)** Expression pattern of circMARK3 during buffalo adipocyte differentiation. In **(A–D)** and **(F)**, bovine-*GAPDH* was used to normalize the expression level of the reference gene. In panel **(A)**, data was normalized to the heart. In panels **(B–D)** and **(F)**, all data were normalized to day 0. Data are presented as the mean ± SD, $n = 3$, #:no significance, $^{*}P < 0.05$, $^{**}P < 0.01$, $^{***}P < 0.001$.

differentiation, circMARK3 was up-regulated in the mature adipocytes (**Figure 3F**).

CircMARK3 Promotes the Adipogenic Differentiation of 3T3-L1 Cells

The sequences of mouse and buffalo circMARK3 show high homology (**Figures 2F,H**). Therefore, the role of circMARK3 in fat deposition was investigated by performing gain-of-function experiments for mouse-circMARK3 in 3T3-L1 cells. The strategy of transfection, adipogenic differentiation, RT-qPCR and Oil Red O staining is shown in **Figure 4A**. Consistent with a higher lipid accumulation in the mouse pCD2.1-circMARK3 group than in the pCD2.1-ciR group (**Figures 4B,C**, $P < 0.01$), the former group showed much higher circMARK3 mRNA expression (**Figure 4D**, $P < 0.001$) and significant higher up-regulation of *PPARG*, *C/EBPα*, and *FABP4* (**Figures 4E–G**, $P < 0.001$).

CircMARK3 Promotes the Adipogenic Differentiation of Buffalo Adipocytes

To evaluate the effect of circMARK3 on fat deposition in buffalo, full length buffalo-circMARK3 was packaged into an adenovirus system for overexpression (Ad_circMARK3), following the same scheme shown in **Figure 4A**. The indicator GFP was highly expressed 2 days after adenoviral transduction (**Figure 5A**). Expression of circMARK3 in Ad_circMARK3 was significantly higher than in the Ad_EGFP group on day 2 of cell transfection (**Figure 5D**, $P<0.001$). At the same time, lipid accumulation in Ad_circMARK3 was significantly enhanced (**Figures 5B,C**, $P<0.01$), whereas mRNA expression of *PPARG*, *C/EBPα*, and *FABP4* was slightly up-regulated on day 2 after transfection (**Figures 5E–G**, $P < 0.01$).

DISCUSSION

Fat deposition is closely related to growth and development (40, 41), and IMF is a key factor affecting beef quality (42). Compared to beef, however, the IMF content in buffalo meat is significantly lower (3). Since buffalo is abundant in China, it would be desirable to increase its IMF content. It is known that the IMF correlates with maturity (43) and percentage (44) of back subcutaneous fat, which therefore may be used as IMF indicator. Therefore, determining the related factors affecting subcutaneous fat deposition can provide theoretical basis for improving meat quality.

WGCNA is an efficient and accurate method based on RNA-seq used for biological data mining (45, 46). This method is

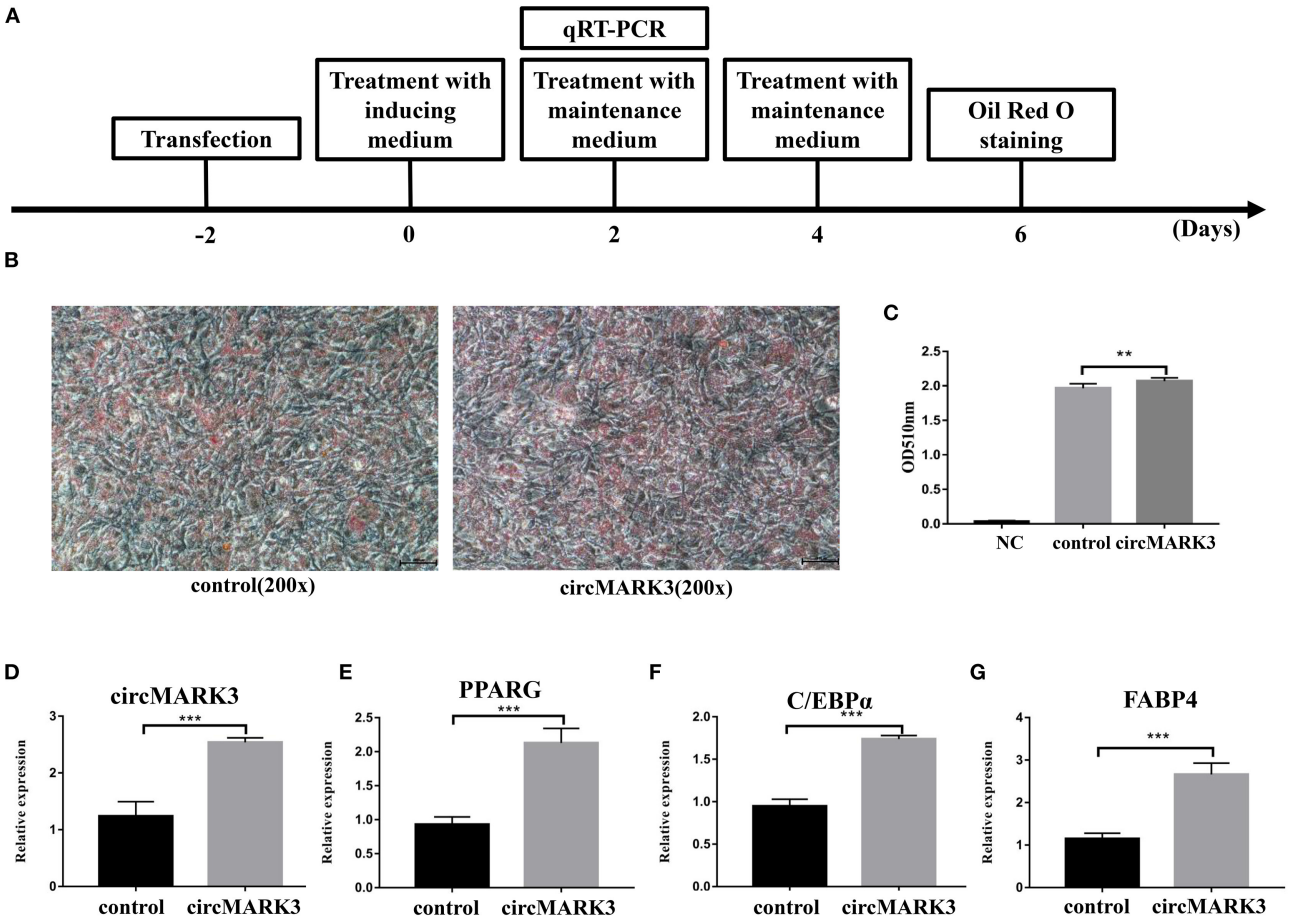

FIGURE 4 | Overexpression of mouse circMARK3 promotes adipogenic differentiation of 3T3-L1 adipocytes. **(A)** Strategy for mouse circMARK3 overexpression, adipogenic differentiation, RT-qPCR and Oil Red O staining in 3T3-L1 cells; **(B)** Oil Red O staining in 3T3-L1 cells transfected with pCD2.1-ciR and mouse pCD2.1-circMARK3 on day 6 after adipogenic differentiation. **(C)** Histogram corresponding to the quantification of Oil Red O staining by spectrophotometry; **(D–G)** RNA expression 48 h after transfection of circMARK3 **(D)**, *PPARG* **(E)**, *C/EBPα* **(F)** and *FABP4* **(G)**. In panels **(D–G)**, mouse-*β-actin* was used to normalize the expression level of the reference gene in 3T3-L1 cells. Control means the pCD2.1-ciR group, circMARK3 means the mouse pCD2.1-circMARK3 group. NC means negative control. Data are presented as the mean ± SD, $n = 3$, $^{**}P < 0.01$, $^{***}P < 0.001$.

increasingly used to discover genes and phenotype relationships (46, 47) and to provide insights into signaling networks linked to phenotypic traits of interest (46, 48). From the circRNAs obtained by RNA-seq, the top 5,000 with median absolute deviation (MAD) were used to construct the network for WGCNA, resulting in 21 modules. When the scale-free topology index was 0.9, the resulting network was closer to a power law distribution (46), but the appropriate soft threshold was not found (**Supplementary Figures S1A,B**). This may be caused by differences between samples, but they are caused by meaningful biological changes. Here, we used experience soft threshold for analysis. We found that the blue and turquoise modules were positively and negatively correlated with traits, respectively. However, since the blue module had no biological significance ($P > 0.05$), the turquoise module, containing 996 circRNAs, was the main one involved in traits of buffalo (month and weight). Taking the intersection between DE circRNAs and the turquoise modules (49), circRNA 21:6969877|69753491 was taken as a candidate factor affecting fat deposition.

The activities in living organisms are mediated by the genome (50), and gene expression is regulated by many factors. Adipocytes may include white adipocytes that store energy and brown or beige adipocytes that dissipate energy (51, 52). Transcription factor PRDM16 is a beige/brown marker (53) associated with circRNA 21:6969877|69753491 by RNA-seq analysis (31). In addition, knockout mice (MARK3$^{-/-}$) were protected against high-fat diet induced obesity and displayed attenuated weight gain (54). Both WGCNA and RNA-seq analysis indicate that circRNA 21:6969877|69753491 produced by *MARK3* gene are likely involved in fat deposition. By digestion linear RNA experiments detecting the expression of the circRNA and host genes, the expression of host genes was significantly down-regulated. Although expression of circRNA was too reduced, it was still detected. circMARK3 was highly and stably expressed in buffalo adipocytes, it may be a candidate gene for

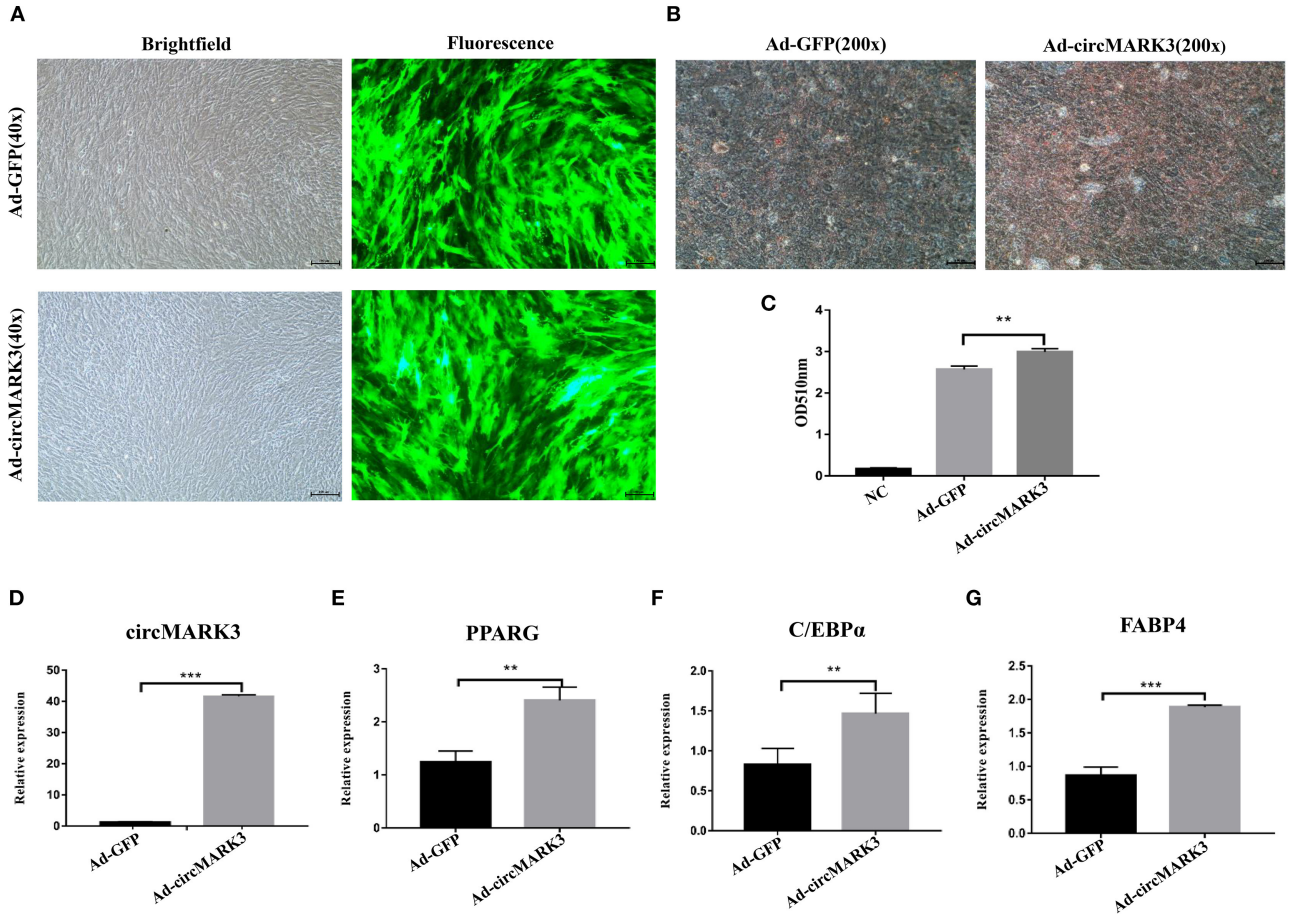

FIGURE 5 | Overexpression of buffalo circMARK3 promotes adipogenic differentiation of buffalo adipocytes. **(A)** Micrographs of GFP-positive cells in the Ad_GFP and Ad_circMARK3 groups on day 2 after cell transfection; **(B)** Oil Red O staining of buffalo adipocytes transfected with Ad_GFP and Ad_circMARK3 group on day 6 after adipogenic differentiation. **(C)** Histogram corresponding to the quantification of Oil Red O staining by spectrophotometry; **(D–G)** RNA expression two days after transfection of circMARK3 **(D)**, *PPARG* **(E)**, *C/EBPα* **(F)**, and *FABP4* **(G)**. Bovine-*GAPDH* was used to normalize the expression level of the reference gene in buffalo adipocytes. NC means negative control. Data are presented as the mean ± SD, $n = 3$, $^{**}P < 0.01$, $^{***}P < 0.001$.

influencing fat deposition in Buffalo. The function of circRNAs is determined by location (55–58), which therefore must be determined: in the nucleus, it usually participates in regulating expression of host genes (55, 56), whereas in the cytoplasm, it mainly acts as competitive endogenous RNA (ceRNA) (57, 58). Since we found that circMARK3 is mainly expressed in the cytoplasm, it may function as ceRNA. Localization is useful for future exploration of its molecular regulatory mechanism of adipose tissue development.

Since the expression patterns showed that circMARK3 is mainly expressed in adipose tissue, we speculated that it plays an important role in buffalo adipogenesis. To explore its function, we obtained buffalo adipocytes and detected circMARK3 expression during the different phases of differentiation. Adipocytes were isolated from buffalo back subcutaneous adipose tissue (36, 59) and induction of differentiation was followed by staining with Oil Red O solution. The results showed that there was a significant increase in intracellular lipid droplets after induction, which indicated that the primary adipocytes had strong differentiation activity (4). Expression of marker genes *PPARG*, *C/EBPα*, and *FABP*4 increased during adipocyte differentiation, reaching its highest level at day 10, consistent with previous studies (60, 61). These results suggested the establishment of a differentiation induction system for buffalo primary adipocytes. Adipocytes were active and could be used in subsequent experiments. During adipogenic differentiation, the expression of circMARK3 was up-regulated in the mature adipocytes of buffalo, suggesting its involvement in adipocyte differentiation.

The host gene *MARK*3 has been linked to lipid metabolism in mice (54), and we have shown that circMAK3 is conserved in mice. To confirm the effect of circMARK3 on fat deposition in mice and buffalo, overexpression of this circRNA in 3T3-L1 cells was performed using a pCD2.1-ciR overexpression vector. In buffalo adipocytes, overexpression was performed by

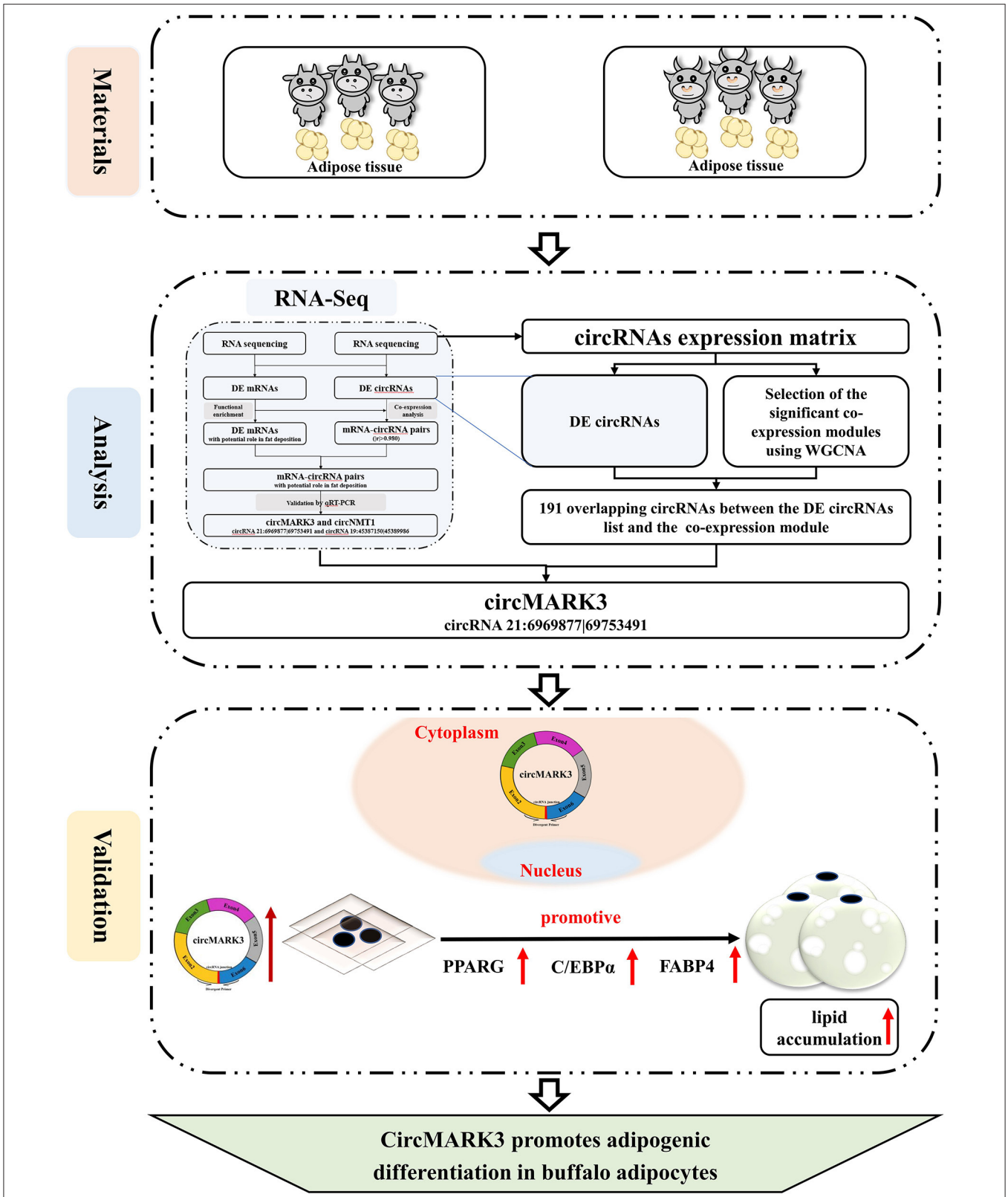

FIGURE 6 | Schematic illustration of the experimental procedure and main results. RNA-seq analysis is from a previous study (31).

an efficient adenovirus system. pCD-ciR is a more commonly used circRNAs expression vector. The linear sequence of the target circRNAs was amplified by PCR and cloned into the pCD-ciR vector, which contains the circRNAs circular expression framework. After the recombinant vector is transfected into the cells, the RNA can be sheared to form circRNAs molecules with high efficiency and stability to achieve high expression in cells. As expected, circRNAs not only significantly enhanced adipogenic differentiation of 3T3-L1, but also the accumulation of lipid droplets in buffalo adipocytes. In both systems, the expression of adipogenic marker genes *PPARG*, *C/EBPα* and *FABP4* positively correlated with the degree of the differentiation of adipocytes (4, 62) was up-regulated. These results suggest that circMARK3 promotes adipogenesis by enhancing the expression of adipogenic marker genes, but the regulatory mechanism involved in enhancing adipogenic differentiation in 3T3-L1 and buffalo adipocytes requires additional investigation.

CONCLUSIONS

The central idea and results of this research are illustrated in **Figure 6**. This study demonstrates that: (1) A candidate circRNA circMARK3 related to lipid metabolism was found by WGCNA, (2) circMARK3 is highly expressed in adipose tissue and mature adipocytes and is located in the cytoplasm, (3) circMARK3 promoted adipogenic differentiation of buffalo adipocytes and 3T3-L1 cells by up-regulating the expression levels of adipogenic marker genes *PPARG*, *C/EBPα* and *FABP4*. All in all, the study suggests that circMARK3 is a potential regulatory factor affects buffalo fat deposition, but the regulatory mechanism involved in fat production needs further exploration.

DATA AVAILABILITY STATEMENT

The original contributions presented in the study are included in the article/**Supplementary Material**, further inquiries can be directed to the corresponding author.

ETHICS STATEMENT

Ethical review and approval was not required for the animal study because all animals were bred for commercial use, rather than for experimental reasons, and they were slaughtered according to the food industry-approved halal food quality certified protocol by a Muslim cleric according to the law of Islam. Thus, no ethics approval was required by a specific committee.

AUTHOR CONTRIBUTIONS

Conceived and designed the research: YM and FL. Provided the funding: YM. Analyzed the data and wrote the paper: XF. Conducted the experiment: JZ. Modified manuscript: FL, BA, and AA. All authors contributed to the article and approved the submitted version.

FUNDING

This study was funded by the National Natural Science Foundation of China (32072720), The Leading Talents Fund in Science and Technology Innovation in Henan Province (No. 194200510022), Ningxia Hui Autonomous Region Key Research and Development Project (2019YCZX0068, 2021BEF01002, and 2021NXZD1), and the Leading Talents Fund in Science and Technology Innovation in Ningxia Hui Autonomous Region (2020GKLRLX02).

ACKNOWLEDGMENTS

The authors would like to express their gratitude to EditSprings (https://www.editsprings.cn/) for the expert linguistic services provided.

SUPPLEMENTARY MATERIAL

The Supplementary Material for this article can be found online at: https://www.frontiersin.org/articles/10.3389/fvets.2022.946447/full#supplementary-material

REFERENCES

1. Scollan N, Hocquette JF, Nuernberg K, Dannenberger D, Richardson I, Moloney A. Innovations in beef production systems that enhance the nutritional and health value of beef lipids and their relationship with meat quality. *Meat Sci.* (2006) 74:17–33. doi: 10.1016/j.meatsci.2006.05.002
2. Kandeepan G, Mendiratta S K, Shukla V, Vishnuraj M R. Processing characteristics of buffalo meat-a review. *J Meat Sci Technol.* (2013) 1:11.
3. Huang J, Feng X, Zhu R, Guo D, Wei Y, Cao X, et al. Comparative transcriptome analysis reveals that PCK1 is a potential gene affecting IMF deposition in buffalo. *BMC Genomics.* (2020) 21:710. doi: 10.1186/s12864-020-07120-w
4. Lowe CE, O'Rahilly S, Rochford JJ. Adipogenesis at a glance. *J Cell Sci.* (2011) 124:2681–6. doi: 10.1242/jcs.079699
5. Mota de Sa P, Richard AJ, Hang H, Stephens JM. Transcriptional regulation of adipogenesis. *Compr Physiol.* (2017) 7:635–74. doi: 10.1002/cphy.c160022
6. Fujiwara M, Tian L, Le PT, DeMambro VE, Becker KA, Rosen CJ, et al. The mitophagy receptor Bcl-2-like protein 13 stimulates adipogenesis by regulating mitochondrial oxidative phosphorylation and apoptosis in mice. *J Biol Chem.* (2019) 294:12683–94. doi: 10.1074/jbc.RA119.008630
7. Rosen ED. The transcriptional basis of adipocyte development. *Prostaglandins Leukot Essent Fatty Acids.* (2005) 73:31–4. doi: 10.1016/j.plefa.2005.04.004
8. Dahlman I, Arner P. Genetics of adipose tissue biology. *Prog Mol Biol Transl Sci.* (2010) 94:39–74. doi: 10.1016/B978-0-12-375003-7.00003-0
9. Moseti D, Regassa A, Kim WK. Molecular regulation of adipogenesis and potential anti-adipogenic bioactive molecules. *Int J Mol Sci.* (2016) 17:124. doi: 10.3390/ijms17010124
10. Sun C, Mao S, Chen S, Zhang W, Liu C. PPARs-orchestrated metabolic homeostasis in the adipose tissue. *Int J Mol Sci.* (2021) 22:8974. doi: 10.3390/ijms22168974
11. Lee JE, Schmidt H, Lai B, Ge K. Transcriptional and epigenomic regulation of adipogenesis. *Mol Cell Biol.* (2019) 39:e00601. doi: 10.1128/MCB.00601-18
12. Rosen ED, Hsu CH, Wang X, Sakai S, Freeman MW, Gonzalez FJ, et al. C/EBPalpha induces adipogenesis through PPARgamma: a unified pathway. *Genes Dev.* (2002) 16:22–6. doi: 10.1101/gad.948702

13. Yang J, Stack MS. Lipid regulatory proteins as potential therapeutic targets for ovarian cancer in obese women. *Cancers*. (2020) 12:3469. doi: 10.3390/cancers12113469
14. Beale EG, Hammer RE, Antoine B, Forest C. Disregulated glyceroneogenesis: PCK1 as a candidate diabetes and obesity gene. *Trends Endocrinol Metab*. (2004) 15:129–35. doi: 10.1016/j.tem.2004.02.006
15. Lei Z, Wu H, Xiong Y, Wei D, Wang X, Luoreng Z, et al. ncRNAs regulate bovine adipose tissue deposition. *Mol Cell Biochem*. (2021) 476:2837–45. doi: 10.1007/s11010-021-04132-2
16. Chen LL, Yang L. Regulation of circRNA biogenesis. *RNA Biol*. (2015) 12:381–8. doi: 10.1080/15476286.2015.1020271
17. Takaki W, Konishi H, Shoda K, Arita T, Kataoka S, Shibamoto J, et al. Significance of circular FAT1 as a prognostic factor and tumor suppressor for esophageal squamous cell carcinoma. *Ann Surg Oncol*. (2021) 28:8508–18. doi: 10.1245/s10434-021-10089-9
18. Liang WC, Wong CW, Liang PP, Shi M, Cao Y, Rao ST, et al. Translation of the circular RNA circbeta-catenin promotes liver cancer cell growth through activation of the Wnt pathway. *Genome Biol*. (2019) 20:84. doi: 10.1186/s13059-019-1685-4
19. Guarnerio J, Bezzi M, Jeong JC, Paffenholz SV, Berry K, Naldini MM, et al. Oncogenic role of fusion-circRNAs derived from cancer-associated chromosomal translocations. *Cell*. (2016) 165:289–302. doi: 10.1016/j.cell.2016.03.020
20. Papatsirou M, Artemaki PI, Karousi P, Scorilas A, Kontos CK. Circular RNAs: emerging regulators of the major signaling pathways involved in cancer progression. *Cancers*. (2021) 13:2744. doi: 10.3390/cancers13112744
21. Wei X, Li H, Yang J, Hao D, Dong D, Huang Y, et al. Circular RNA profiling reveals an abundant circLMO7 that regulates myoblasts differentiation and survival by sponging miR-378a-3p. *Cell Death Dis*. (2017) 8:e3153. doi: 10.1038/cddis.2017.541
22. Ouyang H, Chen X, Wang Z, Yu J, Jia X, Li Z, et al. Circular RNAs are abundant and dynamically expressed during embryonic muscle development in chickens. *DNA Res*. (2018) 25:71–86. doi: 10.1093/dnares/dsx039
23. Li A, Huang W, Zhang X, Xie L, Miao X. Identification and characterization of circrnas of two pig breeds as a new biomarker in metabolism-related diseases. *Cell Physiol Biochem*. (2018) 47:2458–70. doi: 10.1159/000491619
24. Liu X, Liu K, Shan B, Wei S, Li D, Han H, et al. A genome-wide landscape of mRNAs, lncRNAs, and circRNAs during subcutaneous adipogenesis in pigs. *J Anim Sci Biotechnol*. (2018) 9:76. doi: 10.1186/s40104-018-0292-7
25. Zhang Y, Guo X, Pei J, Chu M, Ding X, Wu X, et al. CircRNA expression profile during yak adipocyte differentiation and screen potential circrnas for adipocyte differentiation. Genes. (2020) 11:414. doi: 10.3390/genes11040414
26. Zhang M, Han Y, Zhai Y, Ma X, An X, Zhang S, et al. Integrative analysis of circRNAs, miRNAs, and mRNAs profiles to reveal ceRNAs networks in chicken intramuscular and abdominal adipogenesis. *BMC Genomics*. (2020) 21:594. doi: 10.1186/s12864-020-07000-3
27. Wang L, Liang W, Wang S, Wang Z, Bai H, Jiang Y, et al. Circular RNA expression profiling reveals that circ-PLXNA1 functions in duck adipocyte differentiation. *PLoS ONE*. (2020) 15:e0236069. doi: 10.1371/journal.pone.0236069
28. Wang J, Ren Q, Hua L, Chen J, Zhang J, Bai H, et al. Comprehensive analysis of differentially expressed mRNA, lncRNA and circRNA and their ceRNA networks in the longissimus dorsi muscle of two different pig breeds. *Int J Mol Sci*. (2019) 20:1107. doi: 10.3390/ijms20051107
29. Shen X, Zhang X, Ru W, Huang Y, Lan X, Lei C, et al. circINSR promotes proliferation and reduces apoptosis of embryonic myoblasts by sponging miR-34a. *Mol Ther Nucleic Acids*. (2020) 19:986–99. doi: 10.1016/j.omtn.2019.12.032
30. Shen X, Tang J, Ru W, Zhang X, Huang Y, Lei C, et al. CircINSR regulates fetal bovine muscle and fat development. *Front Cell Dev Biol*. (2020) 8:615638. doi: 10.3389/fcell.2020.615638
31. Huang J, Zhao J, Zheng Q, Wang S, Wei X, Li F, et al. Characterization of circular RNAs in Chinese buffalo (Bubalus bubalis) adipose tissue: a focus on circular RNAs involved in fat deposition. *Animals*. (2019) 9:403. doi: 10.3390/ani9070403
32. Yao Q, Song Z, Wang B, Qin Q, Zhang JA. Identifying key genes and functionally enriched pathways in sjogren's syndrome by weighted gene co-expression network analysis. *Front Genet*. (2019) 10:1142. doi: 10.3389/fgene.2019.01142
33. Langfelder P, Horvath S. WGCNA: an R package for weighted correlation network analysis. *BMC Bioinformatics*. (2008) 9:559. doi: 10.1186/1471-2105-9-559
34. Zhang XO, Wang HB, Zhang Y, Lu X, Chen LL, Yang L. Complementary sequence-mediated exon circularization. *Cell*. (2014) 159:134–47. doi: 10.1016/j.cell.2014.09.001
35. Wang C, Liu WR, Tan S, Zhou JK, Xu X, Ming Y, et al. Characterization of distinct circular RNA signatures in solid tumors. *Mol Cancer*. (2022) 21:63. doi: 10.1186/s12943-022-01546-4
36. Huang J, Zheng Q, Wang S, Wei X, Li F, Ma Y. High-Throughput RNA sequencing reveals NDUFC2-AS lncRNA promotes adipogenic differentiation in Chinese buffalo (Bubalus bubalis L). *Genes*. (2019) 10:689. doi: 10.3390/genes10090689
37. Pan C, Yang C, Ma Y, Sheng H, Lei Z, Wang S, et al. Identification of key genes associated with early calf-hood nutrition in subcutaneous and visceral adipose tissues by co-expression analysis. *Front Vet Sci*. (2022) 9:831129. doi: 10.3389/fvets.2022.831129
38. Pan C, Yang C, Wang S, Ma Y. Identifying key genes and functionally enriched pathways of diverse adipose tissue types in cattle. *Front Genet*. (2022) 13:790690. doi: 10.3389/fgene.2022.790690
39. Teng L, Shen L, Zhao W, Wang C, Feng S, Wang Y, et al. SLAMF8 Participates in acute renal transplant rejection *via* TLR4 pathway on pro-inflammatory macrophages. *Front Immunol*. (2022) 13:846695. doi: 10.3389/fimmu.2022.846695
40. Copping KJ, Callaghan MJ, Geesink GH, Gugusheff JR, McMillen IC, Rodgers RJ, et al. Periconception and first trimester diet modifies appetite, hypothalamic gene expression, and carcass traits in bulls. *Front Genet*. (2021) 12:720242. doi: 10.3389/fgene.2021.720242
41. Saleh AA, Alhotan RA, Alharthi AS, Nassef E, Kassab MA, Farrag FA, et al. Insight view on the role of in ovo feeding of clenbuterol on hatched chicks: hatchability, growth efficiency, serum metabolic profile, muscle, and lipid-related markers. *Animals*. (2021) 11:2429. doi: 10.3390/ani11082429
42. Joo ST, Hwang YH, Frank D. Characteristics of Hanwoo cattle and health implications of consuming highly marbled Hanwoo beef. *Meat Sci*. (2017) 132:45–51. doi: 10.1016/j.meatsci.2017.04.262
43. Liu L, Cao P, Zhang L, Qi M, Wang L, Li Z, et al. Comparisons of adipogenesis- and lipid metabolism-related gene expression levels in muscle, adipose tissue and liver from Wagyu-cross and Holstein steers. *PLoS ONE*. (2021) 16:e0247559. doi: 10.1371/journal.pone.0247559
44. Yamada T, Kamiya M, Higuchi M. Fat depot-specific effects of body fat distribution and adipocyte size on intramuscular fat accumulation in Wagyu cattle. *Anim Sci J*. (2020) 91:e13449. doi: 10.1111/asj.13449
45. Zhang B, Horvath S. A general framework for weighted gene co-expression network analysis. *Stat Appl Genet Mol Biol*. (2005) 4:Article17. doi: 10.2202/1544-6115.1128
46. Wang M, Wang L, Pu L, Li K, Feng T, Zheng P, et al. LncRNAs related key pathways and genes in ischemic stroke by weighted gene co-expression network analysis (WGCNA). *Genomics*. (2020) 112:2302–8. doi: 10.1016/j.ygeno.2020.01.001
47. Wei Z, Zhongqiu T, Lu S, Zhang F, Xie W, Wang Y. Gene coexpression analysis offers important modules and pathway of human lung adenocarcinomas. *J Cell Physiol*. (2020) 235:454–64. doi: 10.1002/jcp.28985
48. Wan Q, Tang J, Han Y, Wang D. Co-expression modules construction by WGCNA and identify potential prognostic markers of uveal melanoma. *Exp Eye Res*. (2018) 166:13–20. doi: 10.1016/j.exer.2017.10.007
49. Deng ZM, Dai FF, Zhou Q, Cheng YX. Hsa_circ_0000301 facilitates the progression of cervical cancer by targeting miR-1228-3p/IRF4 Axis. *BMC Cancer*. (2021) 21:583. doi: 10.1186/s12885-021-08331-4
50. Sun Y, Deng R, Zhang K, Ren X, Zhang L, Li J. Single-cell study of the extracellular matrix effect on cell growth by in situ imaging of gene expression. *Chem Sci*. (2017) 8:8019–24. doi: 10.1039/C7SC03880A
51. Cristancho AG, Lazar MA. Forming functional fat: a growing understanding of adipocyte differentiation. *Nat Rev Mol Cell Biol*. (2011) 12:722–34. doi: 10.1038/nrm3198
52. Herz CT, Kiefer FW. Adipose tissue browning in mice and humans. *J Endocrinol*. (2019) 241:R97–R109. doi: 10.1530/JOE-18-0598

53. Meyers K, Lopez M, Ho J, Wills S, Rayalam S, Taval S. Lipocalin-2 deficiency may predispose to the progression of spontaneous age-related adiposity in mice. *Sci Rep*. (2020) 10:14589. doi: 10.1038/s41598-020-71249-7
54. Lennerz JK, Hurov JB, White LS, Lewandowski KT, Prior JL, Planer GJ, et al. Loss of Par-1a/MARK3/C-TAK1 kinase leads to reduced adiposity, resistance to hepatic steatosis, and defective gluconeogenesis. *Mol Cell Biol.* (2010) 30:5043–56. doi: 10.1128/MCB.01472-09
55. Zhang Y, Zhang XO, Chen T, Xiang JF, Yin QF, Xing YH, et al. Circular intronic long noncoding RNAs. *Mol Cell.* (2013) 51:792–806. doi: 10.1016/j.molcel.2013.08.017
56. Li Z, Huang C, Bao C, Chen L, Lin M, Wang X, et al. Corrigendum: exon-intron circular RNAs regulate transcription in the nucleus. *Nat Struct Mol Biol.* (2017) 24:194. doi: 10.1038/nsmb0217-194a
57. Hansen TB, Jensen TI, Clausen BH, Bramsen JB, Finsen B, Damgaard CK, et al. Natural RNA circles function as efficient microRNA sponges. *Nature.* (2013) 495:384–8. doi: 10.1038/nature11993
58. Memczak S, Jens M, Elefsinioti A, Torti F, Krueger J, Rybak A, et al. Circular RNAs are a large class of animal RNAs with regulatory potency. *Nature.* (2013) 495:333–8. doi: 10.1038/nature11928
59. Lengi AJ, Corl BA. Factors influencing the differentiation of bovine preadipocytes in vitro. *J Anim Sci.* (2010) 88:1999–2008. doi: 10.2527/jas.2009-2439
60. Wei X, Han S, Wang S, Zheng Q, Li X, Du J, et al. ANGPTL8 regulates adipocytes differentiation and adipogenesis in bovine. *Gene.* (2019) 707:93–9. doi: 10.1016/j.gene.2019.04.048
61. Macotela Y, Emanuelli B, Mori MA, Gesta S, Schulz TJ, Tseng YH, et al. Intrinsic differences in adipocyte precursor cells from different white fat depots. *Diabetes.* (2012) 61:1691–9. doi: 10.2337/db11-1753
62. Jin X, Wang J, Hu J, Liu X, Li S, Lu Y, et al. MicroRNA-200b regulates the proliferation and differentiation of ovine preadipocytes by targeting p27 and KLF9. *Animals.* (2021) 11:2417. doi: 10.3390/ani11082417

Conflict of Interest: The authors declare that the research was conducted in the absence of any commercial or financial relationships that could be construed as a potential conflict of interest.

Publisher's Note: All claims expressed in this article are solely those of the authors and do not necessarily represent those of their affiliated organizations, or those of the publisher, the editors and the reviewers. Any product that may be evaluated in this article, or claim that may be made by its manufacturer, is not guaranteed or endorsed by the publisher.

frontiers | Frontiers in Veterinary Science

ORIGINAL RESEARCH
published: 11 July 2022
doi: 10.3389/fvets.2022.904879

FATP1 Exerts Variable Effects on Adipogenic Differentiation and Proliferation in Cells Derived From Muscle and Adipose Tissue

Jieping Huang†, Duo Guo†, Ruirui Zhu, Ye Feng, Ruirui Li, Xintong Yang and Deshun Shi**

State Key Laboratory for Conservation and Utilization of Subtropical Agro-Bioresources, Guangxi University, Nanning, China

In livestock, intramuscular adipose tissue is highly valued whereas adipose tissue in other depots is considered as waste. Thus, genetic factors that favor fat deposition in intramuscular compartments over that in other adipose depots are highly desirable in meat-producing animals. Fatty acid transport 1 (FATP1) has been demonstrated to promote cellular fatty acid uptake and metabolism; however, whether it also influences cellular lipid accumulation remains unclear. In the present study, we investigated the effects of FATP1 on the differentiation and proliferation of adipocytes in five types of cells derived from muscle and adipose tissue and estimated the effects of FATP1 on intramuscular fat (IMF) deposition. We showed that FATP1 is mainly expressed in heart and muscle tissue in buffaloes as well as cells undergoing adipogenic differentiation. Importantly, we found that FATP1 promoted the adipogenic differentiation of muscle-derived cells (buffalo myocytes and intramuscular preadipocytes and mouse C2C12 cells) but did not affect, or even inhibited, that of adipose-derived cells (buffalo subcutaneous preadipocytes and mouse 3T3-L1 cells, respectively). Correspondingly, our results further indicated that FATP1 promotes IMF deposition in mice *in vivo*. Meanwhile, FATP1 was found to enhance the proliferative activity of all the assessed cells, except murine 3T3-L1 cells. These results provide new insights into the potential effects of FATP1 on IMF deposition, especially regarding its positive effects on meat quality in buffaloes and other livestock.

Keywords: intramuscular fat deposition, FATP1, variable effects, muscle-derived cells, adipose-derived cells

OPEN ACCESS

Edited by:
Rajwali Khan,
University of Agriculture, Pakistan

Reviewed by:
Sayed Haidar Abbas Raza,
Northwest A&F University, China
Farhan Anwar Khan,
University of Agriculture, Pakistan

***Correspondence:**
Jieping Huang
huangjieping1989@126.com
Deshun Shi
ardsshi@gxu.edu.cn

†*These authors have contributed equally to this work*

Specialty section:
This article was submitted to Livestock Genomics, a section of the journal Frontiers in Veterinary Science

Received: *26 March 2022*
Accepted: *25 May 2022*
Published: *11 July 2022*

Citation:
Huang J, Guo D, Zhu R, Feng Y, Li R, Yang X and Shi D (2022) FATP1 Exerts Variable Effects on Adipogenic Differentiation and Proliferation in Cells Derived From Muscle and Adipose Tissue. Front. Vet. Sci. 9:904879. doi: 10.3389/fvets.2022.904879

INTRODUCTION

In livestock production, fat accumulated in subcutaneous and visceral depots is considered as waste. However, fat accumulated in muscle tissue (intramuscular fat [IMF]) is essential for improving the flavor and juiciness of meat, especially beef (1, 2). Therefore, strategies that enhance fat accumulation in muscle tissue while inhibit that in adipose tissue are important in animal production.

Several decades of investigation into fat deposition have revealed hundreds of genes that participate in this complex biological process (3, 4). Several of these genes, such as thyroid hormone responsive (*THRSP*) (5, 6), peroxisome proliferator-activated receptor gamma (*PPARG*) (7), and phosphoenolpyruvate carboxykinase 1 (*PCK1*) (8, 9), have been found to promote IMF deposition; however, they also favor the deposition of fat in other depots, such as subcutaneous and visceral fat depots.

Fatty acid transport 1 (FATP1), also known as solute carrier family 27 member 1 (SLC27A1), is known to enhance the transportation of fatty acids (FAs) (10) as well as their metabolism, including esterification and oxidation (11, 12). Accordingly, FATP1 has been suggested to affect lipid accumulation in cells and tissues. However, disagreements remain regarding the role of FATP1 in this process (13), with some studies supporting that FATP1 promotes lipid accumulation (14, 15) and others suggesting that FATP1 inhibits lipid accumulation (16, 17).

In this study, the effects of FATP1 on adipogenic differentiation and the proliferation of cells derived from muscle and adipose tissue were investigated in both buffaloes and mice. The results suggested that FATP1 promotes adipogenic differentiation in muscle-derived cells and enhances IMF deposition *in vivo*; in contrast, FATP1 does not affect, or even inhibits, fat deposition in adipose-derived cells. Our findings further indicated that FATP1 plays a positive role in the proliferation of all the assessed cells, except 3T3-L1 cells. These results provide a novel potential genetic factor for the improvement of meat quality in livestock and increase our knowledge of the variable effects of FATP1.

MATERIALS AND METHODS

Ethics Statement

The buffaloes used in this study were bred for commercial use. All animal-based protocols were approved by the Institutional Animal Care and Use Committee at the College of Animal Science and Technology, Guangxi University. All efforts were made to minimize the suffering of the animals.

Preparation of Buffalo Tissue Samples

Tissues from five organs—the heart, liver, spleen, lung, and kidney—as well as from the *longissimus dorsi* muscle and back fat were collected from Binlangjiang buffaloes ($n = 6$, 24 months old) (18) for gene expression profiling. All the tissues were sampled immediately after slaughter and frozen in liquid nitrogen. For primary cell isolation, *longissimus dorsi* muscle and back fat tissues were obtained from a buffalo slaughterhouse (Wufeng United Food Co., Ltd, Nanning, China). Freshly sampled tissues were kept in PBS supplemented with 1% penicillin/streptomycin and taken to the laboratory for cell isolation.

RT-qPCR Analysis

Total RNA was isolated using TRIzol Reagent (Invitrogen, Carlsbad, CA, USA) according to the manufacturer's instructions and reverse-transcribed using the PrimeScript RT Reagent Kit with gDNA Eraser (TaKaRa, Dalian, China). Two-step qPCR was performed using SYBR Green I (TaKaRa) following the manufacturer's protocol. The expression levels of target genes were normalized to that of β-actin in 3T3-L1 and C2C12 cells and those of the β-actin and *GAPDH* genes in buffalo cells and tissues, respectively. Details of the primers used are provided in **Supplementary Table 1**. The cycle threshold ($2^{-\Delta\Delta Ct}$) method was used to calculate the relative expression levels of candidate genes. Three replicates were run per sample.

Cell Preparation and Culture

Primary myocytes and primary intramuscular preadipocytes were isolated from *longissimus dorsi* muscle tissue of buffaloes using enzymatic digestion (9). Buffalo primary subcutaneous preadipocytes were isolated from back fat tissue using the tissue block method as previously described (19). 3T3-L1 and C2C12 cells were purchased from ATCC (Shanghai, China) and cultured in DMEM (Gibco) supplemented with 10% FBS (Gibco) and 1% penicillin/streptomycin (Gibco) in 5% CO_2 at 37 °C.

Adenovirus Production

The overexpression of buffalo FATP1 (Reference Sequence: XM_006057903.2) and PPARG (Reference Sequence: MN867675.1) was achieved using an adenovirus system. Adenovirus production was undertaken by Hanbio Biotechnology Co., Ltd. (Shanghai, China). Briefly, the coding sequence (CDS) of a candidate gene was inserted into the AdMax system, which included a backbone plasmid (pHBGloxΔE1, 3cre) and a shuttle plasmid (pHBAd-EF1α-MCS-CMV-EGFP). EGFP was used as a visual indicator of the efficiency of transduction.

Plasmid Construction and siRNA Oligonucleotides Synthesis

The overexpression of mouse *FATP1* (Reference Sequence: NM_011977.4) and *PPARG* (Reference Sequence: NM_011146.3) was achieved using the pcDNA3.1(+) plasmid. The CDS of each candidate gene was amplified from cDNA derived from C2C12 cells and inserted into the pcDNA3.1(+) vector (HindIII and XhoI restriction sites). Details of the primers used for plasmid construction are shown in **Supplementary Table 1**. siRNA oligonucleotides for mouse *FATP1* (GCACTGTACTAGTGCATAT) and negative control (*β-actin*) were purchased from Ruibo Biotechnology Co., Ltd, Guangzhou, China.

Transduction and Transfection

For isolated cells, including myocytes, intramuscular preadipocytes, and subcutaneous preadipocytes, the adenovirus delivery system was utilized to achieve efficient overexpression. Cells were seeded in 12-well plates at 70% density. At 80% confluence, transduction was performed at the indicated multiplicity of infection (MOI) in myocytes and intramuscular preadipocytes and at 80% of the indicated MOI in subcutaneous preadipocytes.

For 3T3-L1 and C2C12 cells, overexpression and interference were achieved using the pcDNA3.1(+) plasmid and siRNA, respectively. Cells were seeded in 12-well plates at 50% density and were transfected at 70% confluence using Lipofectamine 3000 (Invitrogen) following the manufacturer's instructions.

Induction of Adipogenic Differentiation

Two days after transduction or transfection, cells were treated with inducing medium containing 10 μg/mL insulin, 1 μ? dexamethasone, 0.5 mM IBMX, and 1 μ? rosiglitazone for 2 days and subsequently treated with maintenance medium containing 10 μg/mL insulin and 1 μM rosiglitazone until lipid droplets were clearly visible (within approximately 6–8 days). The four

agents (insulin, dexamethasone, IBMX, and rosiglitazone) were purchased from Sigma (Milwaukee, WI, USA).

Oil Red O Staining and Quantification

Following adipogenic differentiation, cells were stained with oil red O. For this, the cells were washed three times with PBS, fixed in 10% formalin first for 5 min and then for 1 h, washed with 60% isopropanol, stained with 0.3% oil red O (Sigma) for 20 min, and again washed three times with PBS. Finally, cells were observed and imaged under a microscope. For the quantitative analysis of lipid accumulation, lipid was eluted using 100% isopropanol, following which the absorbance at 510 nm was measured using a spectrophotometer.

Triglyceride Detection

The triglyceride (TG) content of cells and tissues was detected using a TG quantification kit (Applygen Technologies Inc., Beijing, China) according to the manufacturer's protocol.

EdU and CCK-8 Assays

The proliferation rate of cells was investigated using EdU and CCK-8 assays, which were, respectively performed using a Cell-Light EdU Apollo 567 *in vitro* Imaging Kit (RiboBio, Guangzhou, China) and a CCK-8 kit (Vazyme, Nanjing, China) according to the manufacturers' protocols. Both assays were performed 24 h after transduction or transfection.

In vivo Experiments

The Kunbai mice ($n = 9$, approximately 10 weeks old) were purchased from Guangxi Medical University. The mice were randomly divided into three groups, namely, a negative control group ($n = 3$, injected with the pcDNA3.1 plasmid), a positive control group ($n = 3$, injected with the pcDNA3.1_PPARG plasmid), and the experimental group ($n = 3$, injected with the pcDNA3.1_FATP1 plasmid). A total of 20 μg of plasmid was mixed with 40 μL of Entranster *in vivo* transfection reagent (Engreen, Beijing, China) and left to stand for 15 min. The mixture was then injected into the left *gastrocnemius* muscle of each mouse according to the manufacturer's instructions. After 3 weeks, 50 μL of glycerol was injected into the same anatomical location of each animal. After 2 weeks, the animals were euthanized and the *gastrocnemius* muscle was harvested for gene expression profiling (RT-qPCR) and quantification of TG content.

Statistical Analysis

Data were analyzed in SPSS software using one-way ANOVA. The Holm–Sidak method was used for correction for multiple comparisons. A p-value <0.05 was considered significant. Data are presented as means ± SD by GraphPad Prism.

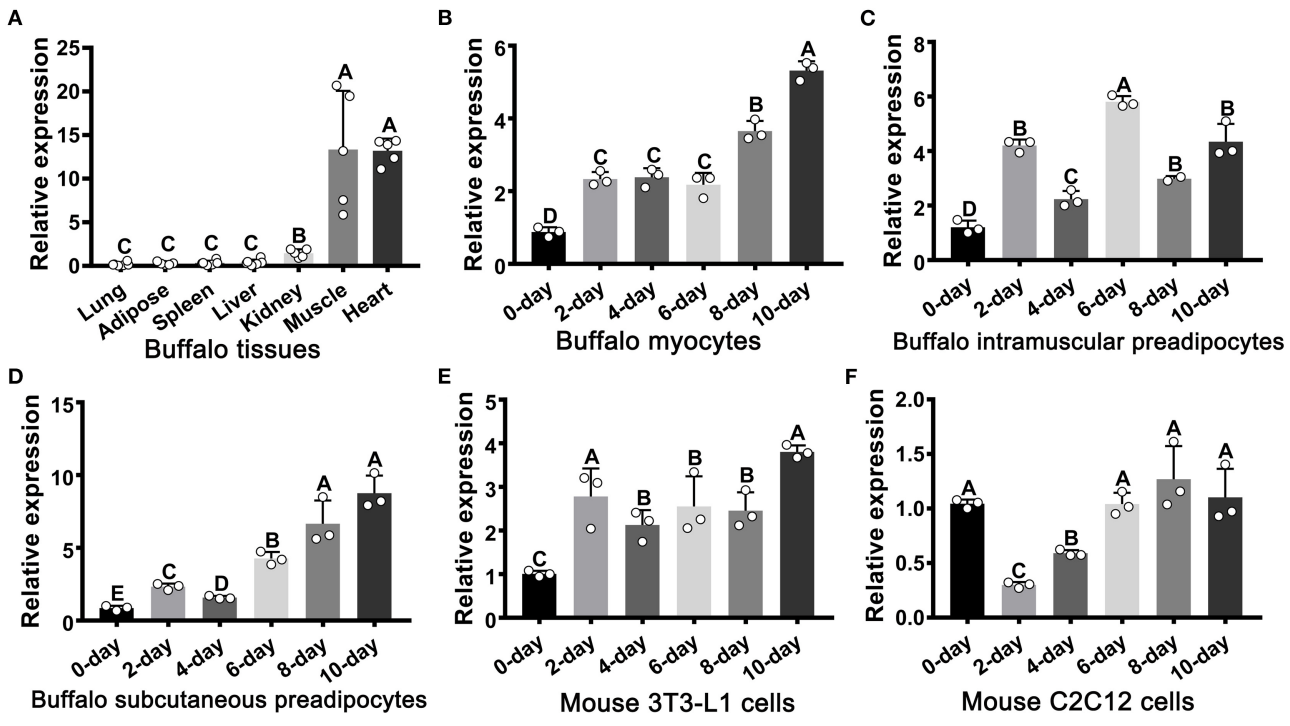

FIGURE 1 | The mRNA expression profile of FATP1 in tissues and cells as determined by RT-qPCR. **(A)** The tissue expression profile of FATP1 in the buffalo. **(B–D)** Expression dynamics of FATP1 during adipogenic differentiation in buffalo myocytes, intramuscular preadipocytes, and subcutaneous preadipocytes. **(E,F)** Expression dynamics of FATP1 during adipogenic differentiation in mouse 3T3-L1 and C2C12 cells. Data are presented as means ± SD; lowercase letters indicate a significant difference ($p < 0.05$), uppercase letters indicate a highly significant difference ($p < 0.01$).

RESULTS

The Expression Profile of FATP1 in Tissues and Cells During Adipogenic Differentiation

The expression of FATP1 was analyzed across seven tissues in the buffalo (**Figure 1A**). As expected, FATP1 was mainly expressed in cardiac and skeletal muscle (**Figure 1A**). In buffalo myocytes, FATP1 expression was markedly upregulated during adipogenic trans-differentiation (**Figure 1B**). In buffalo intramuscular and subcutaneous preadipocytes, FATP1 expression was also upregulated during adipogenic differentiation, although to a varying extent (**Figures 1C,D**), and a similar FATP1 expression profile was observed during the adipogenic differentiation of mouse 3T3-L1 preadipocytes (**Figure 1E**). However, during the adipogenic trans-differentiation of mouse C2C12 cells, the expression of FATP1 was first downregulated and then returned to the original level (**Figure 1F**). The results showed that, overall, FATP1 was highly expressed in cells during adipogenic differentiation. The adipogenic differentiation of all cell types assessed was monitored using the adipogenic markers *PPARG* and *CEBPA* (**Supplementary Figure 1**).

FATP1 Promotes Lipid Accumulation in Buffalo Myocytes

To evaluate the effects of FATP1 on lipid accumulation in buffalo myocytes, we overexpressed FATP1 by using an adenoviral system (Ad_FATP1) with EGFP serving as the indicator (Ad_EGFP). PPARG, the core regulator of adipogenesis, was employed as a positive control (Ad_PPARG). As shown in **Figure 2A**, the high intensity of green fluorescence indicated a high transduction efficiency. Both PPARG and FATP1 were significantly upregulated 2 days after transduction (on day 0 of adipogenic differentiation), with increases of ∼500- and ∼200-fold, respectively (**Figure 2B**). As expected, compared with the Ad_EGFP group, the lipid content was significantly increased in both of the Ad_PPARG and the Ad_FATP1 groups (**Figures 2C,D**). Similarly, the TG content was significantly increased in the Ad_PPARG and Ad_FATP1 groups compared with the Ad_EGFP group (**Figure 2E**). On day 2 of adipogenic differentiation, the levels of all the detected markers—the adipogenic gene *CEBPA* (**Figure 2F**), the lipogenic gene *AGPAT6* (**Figure 2G**), the FA uptake-related genes *FABP4* and *FAT*/*CD36* (**Figure 2H**), and the lipogenesis genes *HSL* and *LPL* (**Figure 2I**)—were upregulated in the Ad_PPARG group. In the Ad_FATP1 group, meanwhile, only the FA uptake-related gene *FAT*/*CD36* was upregulated, and only at a low level (**Figure 2H**). These data indicated that FATP1 promotes lipid accumulation in buffalo myocytes, although not to the same extent as PPARG.

FATP1 Promotes Adipogenic Differentiation in Buffalo Intramuscular Preadipocytes but Not in Subcutaneous Preadipocytes

Studies have indicated that the effects of FATP1 on lipid accumulation can vary according to cell type (13). Accordingly, we next investigated the effects of FATP1 on adipogenic differentiation in buffalo intramuscular and subcutaneous preadipocytes using the same strategy as that used for buffalo myocytes. As shown in **Figure 3A**, high transduction efficiency was achieved in buffalo intramuscular preadipocytes. Both PPARG and FATP1 were significantly upregulated 2 days after transduction (on day 0 of adipogenic differentiation), with increases of ∼800- and ∼400-fold, respectively (**Figure 3B**). Importantly, lipid accumulation and TG content in the Ad_PPARG and Ad_FATP1 groups were significantly higher than those in the Ad_EGFP group (**Figures 3C–E**). On day 2 of adipogenic differentiation, the levels of all the detected markers were upregulated in the Ad_PPARG group (**Figures 3F–I**), while in the Ad_FATP1 group, the adipogenic gene *CEBPA* (**Figure 3F**), the FA uptake-related gene *FABP4* (**Figure 3H**), and the lipogenesis genes *HSL* and *LPL* (**Figure 3I**) were upregulated. These results indicated that FATP1 promotes the adipogenic differentiation in buffalo intramuscular preadipocytes.

A high overexpression efficiency was obtained in subcutaneous preadipocytes as well (**Figures 4A,B**). Lipid accumulation (**Figures 4C,D**) and TG content (**Figure 4E**) were increased in the Ad_PPARG group relative to that in the Ad_EGFP group; however, no significant difference was detected between the Ad_FATP1 and Ad_EGFP groups (**Figures 4C,D**). Additionally, compared with the Ad_EGFP group, the levels of all the adipogenic markers were upregulated in the Ad_PPARG group, but not in the Ad_FATP1 group (**Figures 4F–I**). These findings suggested that FATP1 does not affect the adipogenic differentiation in buffalo subcutaneous preadipocytes.

FATP1 Promotes the Proliferation of Buffalo Myocytes, Intramuscular Preadipocytes, and Subcutaneous Preadipocytes

EdU and CCK-8 assays were employed to uncover the effects of FATP1 on the proliferative ability of buffalo myocytes, intramuscular preadipocytes, and subcutaneous preadipocytes. In myocytes, the cell proliferation rate in the Ad_FATP1 group was significantly higher than that in the control group (Ad_EGFP) as evidenced by EdU staining ($p < 0.05$; **Figures 5A,B**). Correspondingly, the results of the CCK-8 assay indicated that the cell proliferation index in the Ad_FATP1 group was significantly higher than that in the Ad_EGFP group ($p < 0.001$; **Figure 5C**). Similar results were obtained for intramuscular preadipocytes and subcutaneous preadipocytes (**Figures 5D–I**). These findings demonstrated that FATP1 enhances the proliferative capacity of buffalo myocytes, intramuscular preadipocytes, and subcutaneous preadipocytes.

FATP1 Promotes Both Adipogenic Differentiation and Proliferative Activity in C2C12 Cells

To evaluate the effects of FATP1 on lipid accumulation and proliferation in mouse C2C12 cells, the CDS of FATP1 was cloned into the pcDNA3.1(+) vector (pcDNA3.1_FATP1) and transfected into C2C12 cells. PPARG (pcDNA3.1_PPARG) was used as a positive control. High efficiency of overexpression was achieved, with ∼1500-fold and ∼100-fold increases in

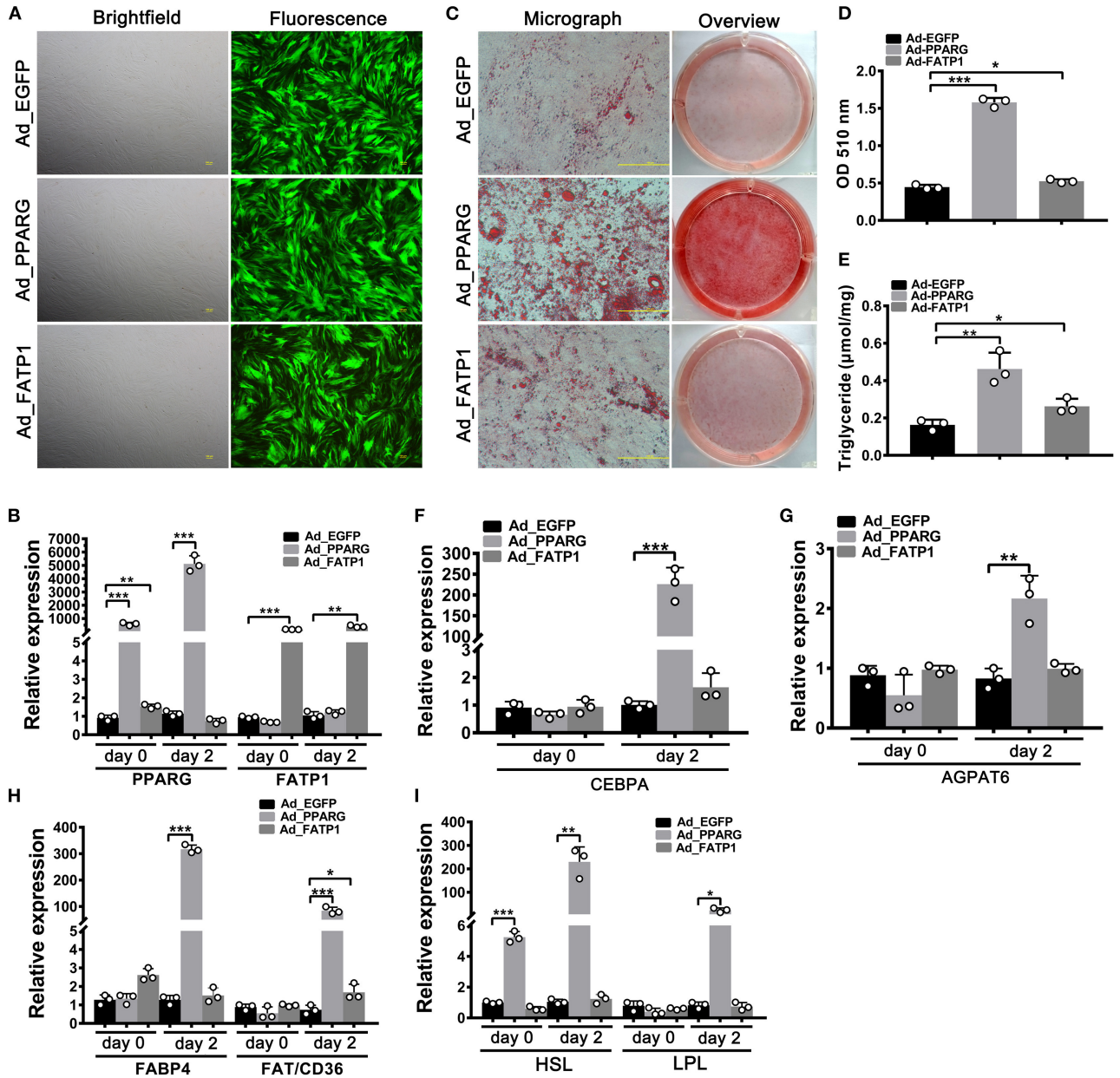

FIGURE 2 | The overexpression of FATP1 promotes lipid accumulation in buffalo myocytes. **(A)** Micrographs of buffalo myocytes 2 days after adenovirus transduction under bright and fluorescent light. Scale bar, 100 μm. The mRNA expression levels of *PPARG* and *FATP1* **(B)**, the adipogenic gene *CEBPA* **(F),** the lipogenic gene *AGPAT6* **(G)**, the fatty acid uptake-related genes *FABP4* and *FAT/CD36* **(H)**, and the lipogenesis genes *HSL* and *LPL* **(I)** in the control and experimental groups on day 0 and day 2 of adipogenic trans-differentiation (2 and 4 days after adenovirus transduction, respectively). **(C)** Oil red O staining of "myocytes" on day 8 of adipogenic trans-differentiation. Scale bar, 100 μm. **(D,E)** Quantification of lipid accumulation and triglyceride content in "myocytes" on day 8 of adipogenic trans-differentiation. EGFP overexpression (Ad_EGFP) served as a negative control; PPARG+EGFP overexpression (Ad_PPARG) served as a positive control; FATP1+EGFP overexpression (Ad_FATP1) served as the experimental group. Data are presented as means ± SD, * $p < 0.05$, ** $p < 0.01$, *** $p < 0.001$.

expression for PPARG and FATP1, respectively, being observed (**Figure 6A**). Importantly, both lipid accumulation ($p < 0.05$; **Figure 6B**) and TG content ($p < 0.05$; **Figure 6C**) were increased in both of the PPARG and FATP1 groups compared with that in the negative control group. The cell proliferation rate was significantly increased in the FATP1 group compared with that in the negative control group ($p < 0.05$; **Figures 6D–F**).

FATP1 Inhibits Both Adipogenic Differentiation and Proliferative Ability in 3T3-L1 Cells

To test whether the effects of FATP1 on adipogenic differentiation and proliferation differed between C2C12 and 3T3-L1 cells, we overexpressed FATP1 and PPARG in 3T3-L1 cells using

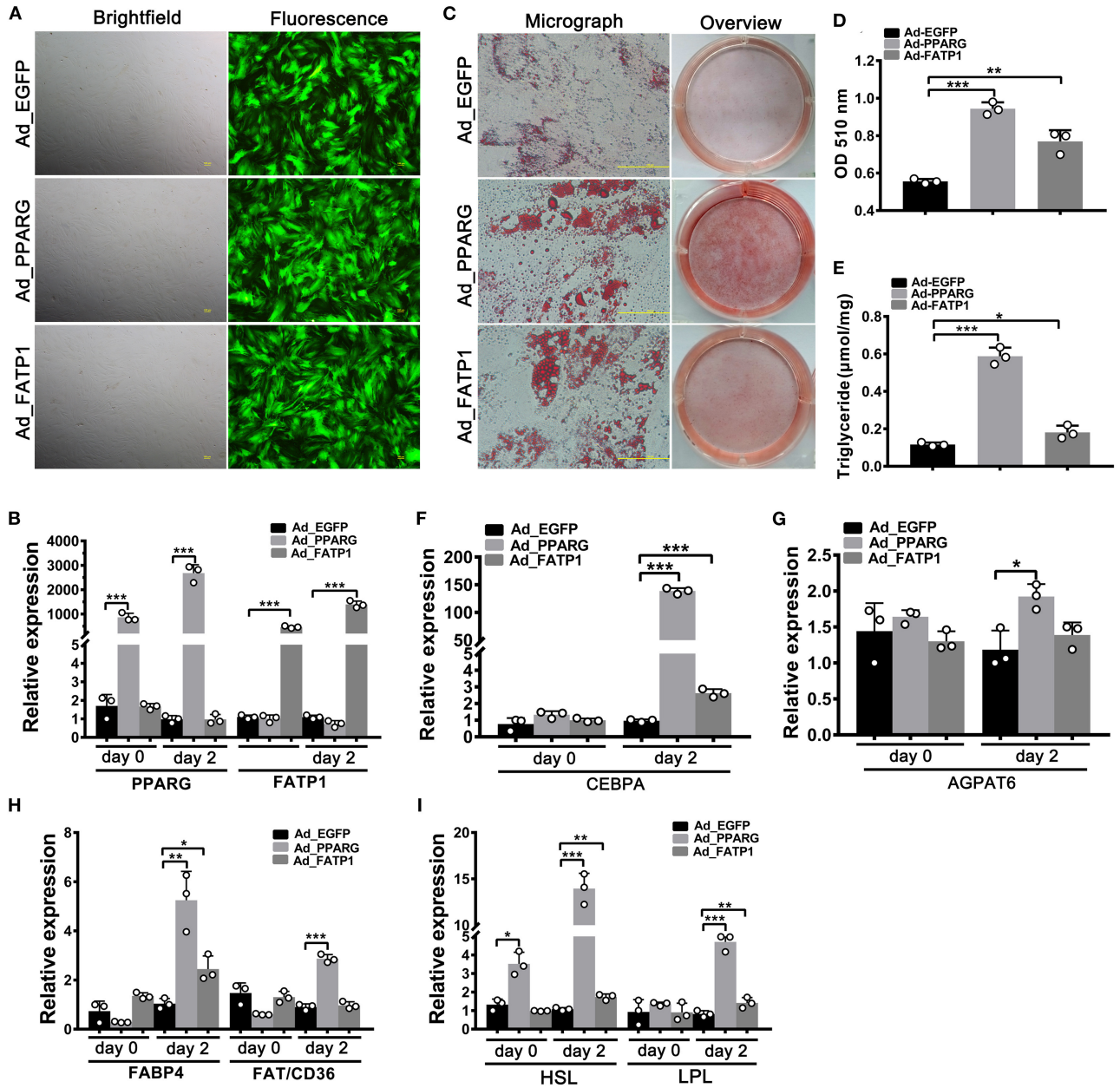

FIGURE 3 | The overexpression of FATP1 promotes adipogenic differentiation in buffalo intramuscular preadipocytes. **(A)** Micrographs of buffalo myocytes on day 2 of adenovirus transduction under bright and fluorescent light. Scale bar, 100 μm. The mRNA expression levels of *PPARG* and *FATP1* **(B),** the adipogenic gene *CEBPA* **(F),** the lipogenic gene *AGPAT6* **(G)**, the fatty acid uptake-related genes *FABP4* and *FAT/CD36* **(H),** and the lipogenesis genes *HSL* and *LPL* **(I)** in the control and experimental groups on day 0 and day 2 of adipogenic trans-differentiation (2 and 4 days after adenovirus transduction, respectively). **(C)** Oil red O staining of "myocytes" on day 8 of adipogenic trans-differentiation. Scale bar, 100 μm. **(D,E)** Quantification of lipid accumulation and triglyceride content in "myocytes" on day 8 of adipogenic trans-differentiation. EGFP overexpression (Ad_EGFP) served as a negative control; PPARG+EGFP overexpression (Ad_PPARG) served as a positive control; FATP1+EGFP overexpression (Ad_FATP1) served as the experimental group. Data are presented as means ± SD, * $p < 0.05$, ** $p < 0.01$, *** $p < 0.001$.

the same system as that used for C2C12 cells. We found that PPARG and FATP1 levels were increased by only ∼10- and ∼15-fold, respectively, compared with the controls (**Figure 7A**). Moreover, relative to that in the control group, lipid accumulation was significantly decreased in the FATP1 overexpression group and significantly increased in the PPARG overexpression group ($p < 0.05$; **Figure 7B**). Similar results were obtained for TG content ($p < 0.05$; **Figure 7C**). However, cell proliferation was inhibited in the FATP1 overexpression group (**Figures 7D–F**), which was not consistent with that in buffalo

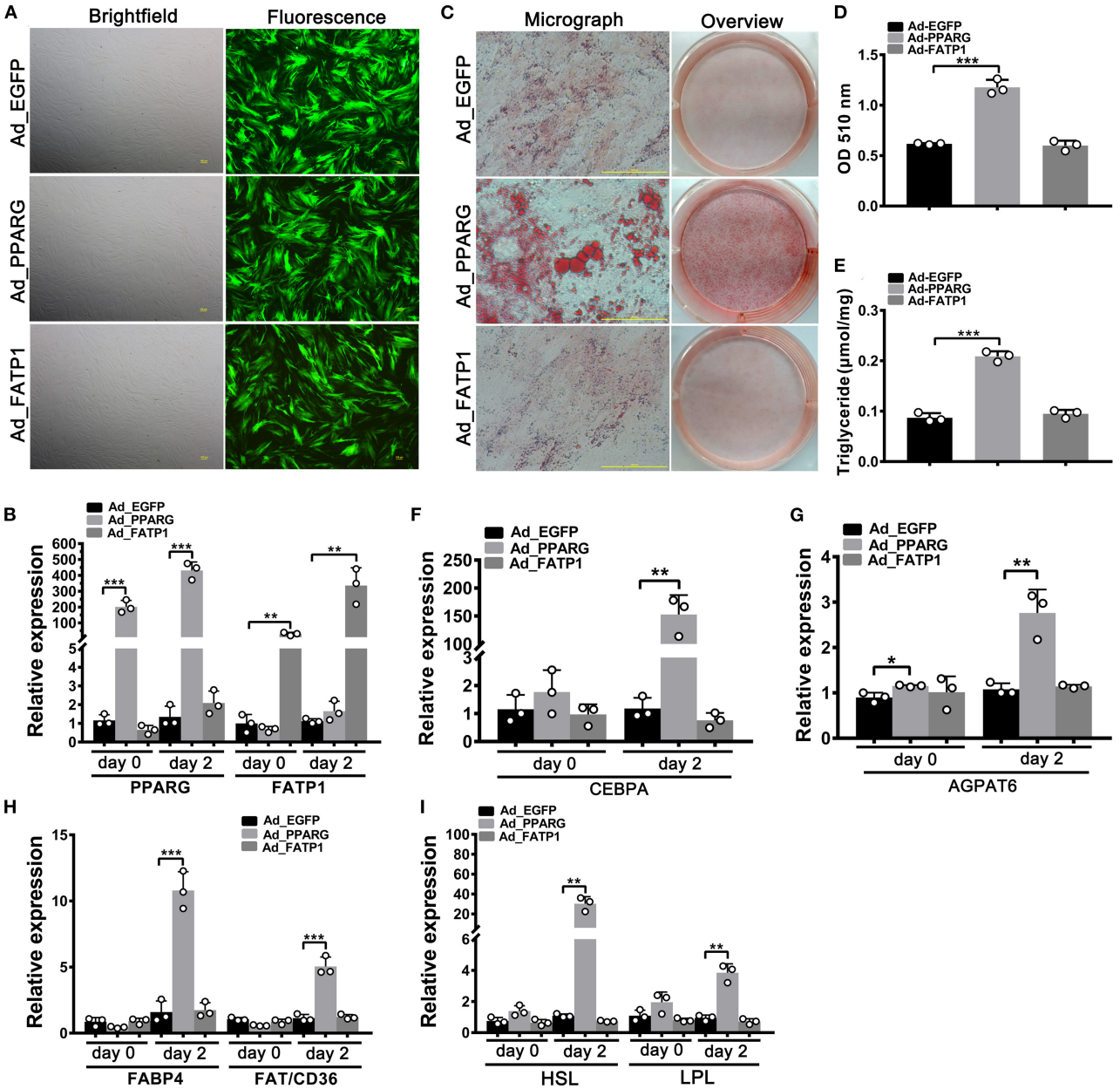

FIGURE 4 | The overexpression of FATP1 does not affect adipogenic differentiation in buffalo subcutaneous preadipocytes. **(A)** Micrographs of buffalo myocytes on day 2 of adenovirus transduction under bright and fluorescent light. Scale bar, 100 μm. The mRNA expression levels of *PPARG* and *FATP1* **(B)**, the adipogenic gene *CEBPA* **(F)**, the lipogenic gene *AGPAT6* **(G)**, the fatty acid uptake-related genes *FABP4* and *FAT/CD36* **(H)**, and the lipogenesis genes *HSL* and *LPL* **(I)** in the control and experimental groups on day 0 and day 2 of adipogenic trans-differentiation (2 and 4 days after adenovirus transduction, respectively). **(C)** Oil red O staining of "myocytes" on day 8 of adipogenic trans-differentiation. Scale bar, 100 μm. **(D,E)** Quantification of lipid accumulation and triglyceride content in "myocytes" on day 8 of adipogenic trans-differentiation. EGFP overexpression (Ad_EGFP) served as a negative control; PPARG+EGFP overexpression (Ad_PPARG) served as a positive control; FATP1+EGFP overexpression (Ad_FATP1) served as the experimental group. Data are presented as means ± SD, * $p < 0.05$, ** $p < 0.01$, *** $p < 0.001$.

subcutaneous preadipocytes. Thus, further interference of FATP1 was accomplished by siRNA to confirm the effects of FATP1 on lipid accumulation and proliferation in mouse 3T3-L1 cells. As shown in **Figures 7G–I**, interference of FATP1 enhanced lipid accumulation and TG synthesis. Besides, interference of FATP1 promoted the proliferation of 3T3-L1 cells as well (**Figures 7J–L**). Therefore, the results of overexpression of FATP1 were consistent well with those of interference. FATP1 inhibited both adipogenic differentiation and proliferative ability in 3T3-L1 cells.

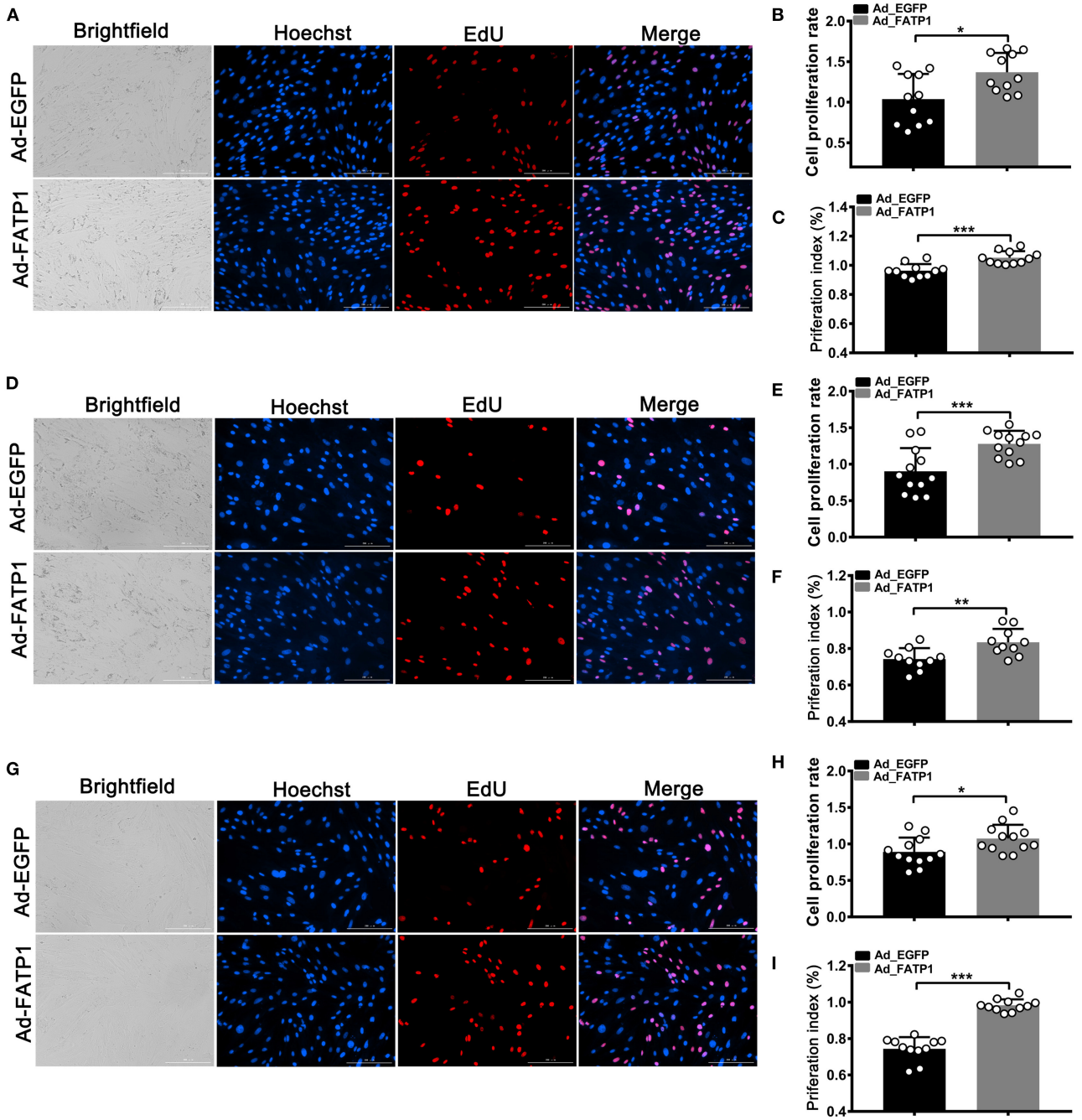

FIGURE 5 | FATP1 promotes the proliferation of buffalo myocytes, intramuscular preadipocytes, and subcutaneous preadipocytes. **(A,D,G)** Micrographs of EdU assays for buffalo myocytes, intramuscular preadipocytes, and subcutaneous preadipocytes, respectively. Blue indicates the nuclei of all the cells; EdU-stained nuclei are shown in red. Scale bar, 200 μm. **(B,E,H)** Statistical analysis of EdU assays for buffalo myocytes, intramuscular preadipocytes, and subcutaneous preadipocytes, respectively. **(C,F,I)** Statistical analysis of CCK-8 assays for buffalo myocytes, intramuscular preadipocytes, and subcutaneous preadipocytes, respectively. Data are presented as means ± SD; * $p < 0.05$, ** $p < 0.01$, *** $p < 0.001$.

FATP1 Increases Intramuscular Fat Content *in vivo*

The above evaluation in cellular level indicated that FATP1 is functional conservative in cell adipogenic differentiation between buffaloes and mice. To demonstrate the effects of FATP1 on IMF *in vivo*, we utilized the glycerol model of muscle regeneration in which IMF deposition is more easily observed (20). We injected the FATP1_expressing plasmid (pcDNA3.1_FATP1)

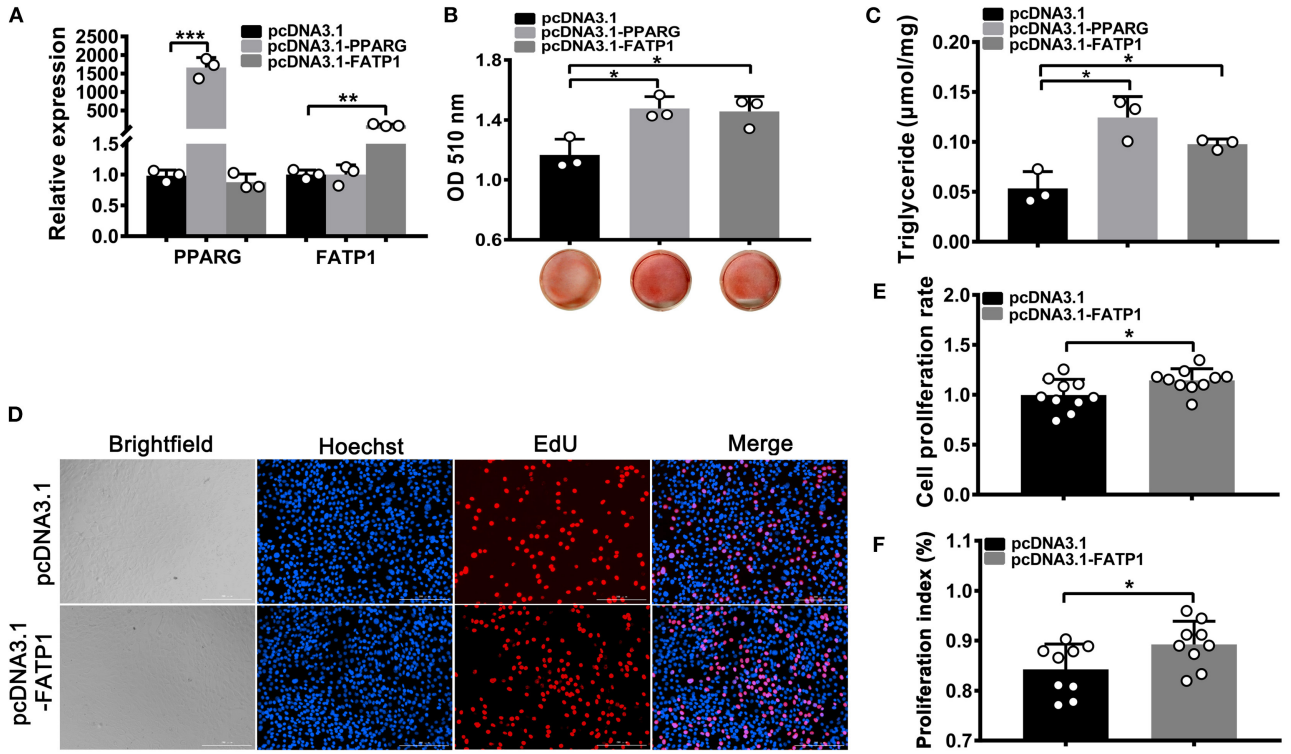

FIGURE 6 | FATP1 enhances the proliferation and promotes the adipogenic trans-differentiation of C2C12 cells. **(A)** The mRNA expression levels of PPARG and FATP1 as determined by RT-qPCR. **(B)** Histogram showing the quantitation of oil red O staining. **(C)** The triglyceride levels of C2C12 cells on day 8 of adipogenic trans-differentiation. **(D)** Micrographs of the EdU assay in C2C12 cells. Scale bar, 200 μm. **(E)** Statistical analysis of EdU assays in C2C12 cells. **(F)** Statistical analysis of CCK-8 assays in C2C12 cells. Data are presented as means ± SD, * $p < 0.05$, ** $p < 0.01$, *** $p < 0.001$.

and the PPARG_expressing plasmid (pcDNA3.1_PPARG) into the *gastrocnemius* muscle of mice using Entranster *in vivo* transfection reagent (21). The *in vivo* overexpression strategy *is* presented in **Figure 8A**. Both PPARG (positive control) and FATP1 were significantly overexpressed (**Figures 8B,C**). Importantly, the TG content was significantly increased in FATP1_ and PPARG_overexpressing mice compared with that in mice administered the control plasmid ($p < 0.05$; **Figure 8D**). Correspondingly, at the molecular level, the levels of the adipogenic marker genes *CEBPA* and *FABP4*, the fat synthesis-related gene *AGPAT6*, and the lipolysis gene *LPL* were significantly upregulated in animals overexpressing either FATP1 or PPARG (**Figures 8E–H**). These results indicated that FATP1 increases IMF deposition *in vivo* in mice.

DISCUSSION

In this study, we found that FATP1 exerts variable effects on adipogenic and proliferative potential of cells derived from muscle and adipose tissue as well as IMF deposition. The main results of the present study indicated that (1) in buffaloes, FATP1 is mainly expressed in cardiac and skeletal muscle and is highly expressed in cells undergoing adipogenic differentiation; (2) FATP1 promotes adipogenic differentiation in cells derived from muscle tissue but does not affect, or even inhibits, adipogenic differentiation in adipose tissue-derived cells; (3) FATP1 enhances the proliferative capacity of buffalo myocytes, intramuscular preadipocytes, and subcutaneous preadipocytes as well as that of murine C2C12 cells, but inhibits the proliferation of 3T3-L1 cells; (4) FATP1 enhances IMF deposition in the mouse *in vivo*.

FATP1 is a key transporter in cellular FA uptake (22, 23). Tissues such as heart, skeletal muscle, and adipose tissue display rapid FA uptake and metabolism. In mice, FATP1 mRNA is abundantly detected in the heart, skeletal muscle, and adipose tissue (24), while in humans, FATP1 mRNA is highly expressed in skeletal muscle and adipose tissue (25). Recently, it was reported that bovine FATP1 mRNA is mainly detected in the heart, skeletal muscle, and adipose tissues (26). In the present study, FATP1 mRNA was mainly detected in heart and skeletal muscle, whereas its expression level was relatively low in adipose tissue (**Figure 1A**). Indeed, it has been reported that bovine FATP1 mRNA was abundantly expressed in heart and skeletal muscle but not in adipose tissue (10). Thus, results from different studies can vary, likely due to individual differences in metabolic rates, which can be affected by both genetic and environmental factors. This idea is supported by the variable FATP1 expression profile observed during the adipogenic differentiation process in cells with different origins (**Figures 1B–F**). Nevertheless, our data showed that FATP1 mRNA was mainly upregulated and

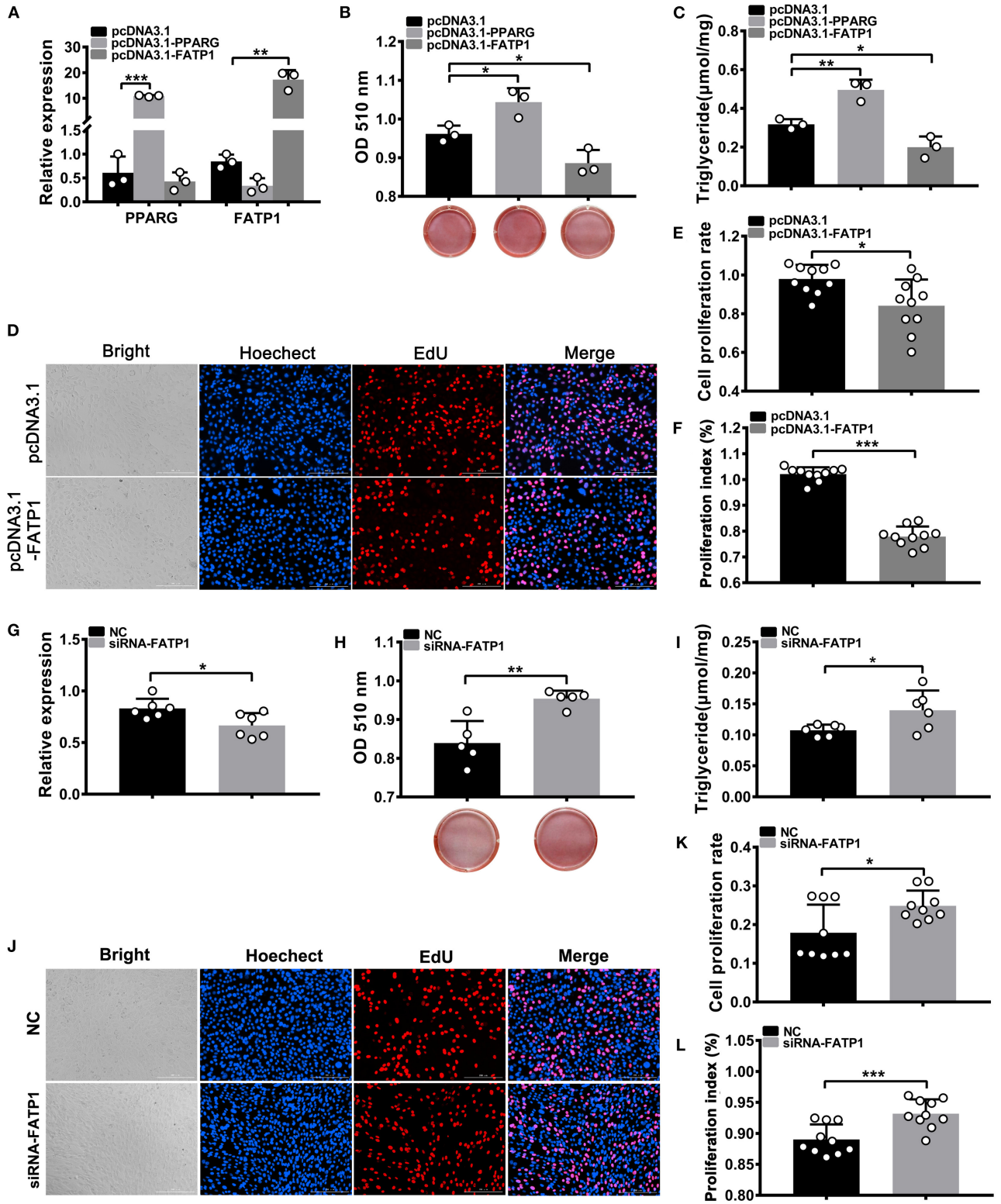

FIGURE 7 | FATP1 inhibits both the proliferation and adipogenic differentiation of 3T3-L1 cells. **(A)** The overexpression efficiency of PPARG and FATP1 and **(G)** the interference efficiency in 3T3-L1 cells determined by RT-qPCR. Histogram showing the quantitation of oil red O staining after FATP1 overexpression **(B)** and FATP1 interference **(H)**. The triglyceride levels on day 8 of adipogenic differentiation in 3T3-L1 cells after FATP1 overexpression **(C)** and FATPT interference **(I)**. Micrographs of EdU assays in 3T3-L1 cells after FATP1 overexpression **(D)** and FATP1 interference **(J)**. Scale bar, 200 μm. Statistical analysis of EdU assays in 3T3-L1 cells after FATP1 overexpression **(E)** and FATP1 interference **(K)**. Statistical analysis of CCK-8 assays in 3T3-L1 cells after FATP1 overexpression **(F)** and FATP1 interference **(L)**. Data are presented as means ± SD, * $p < 0.05$, ** $p < 0.01$, *** $p < 0.001$.

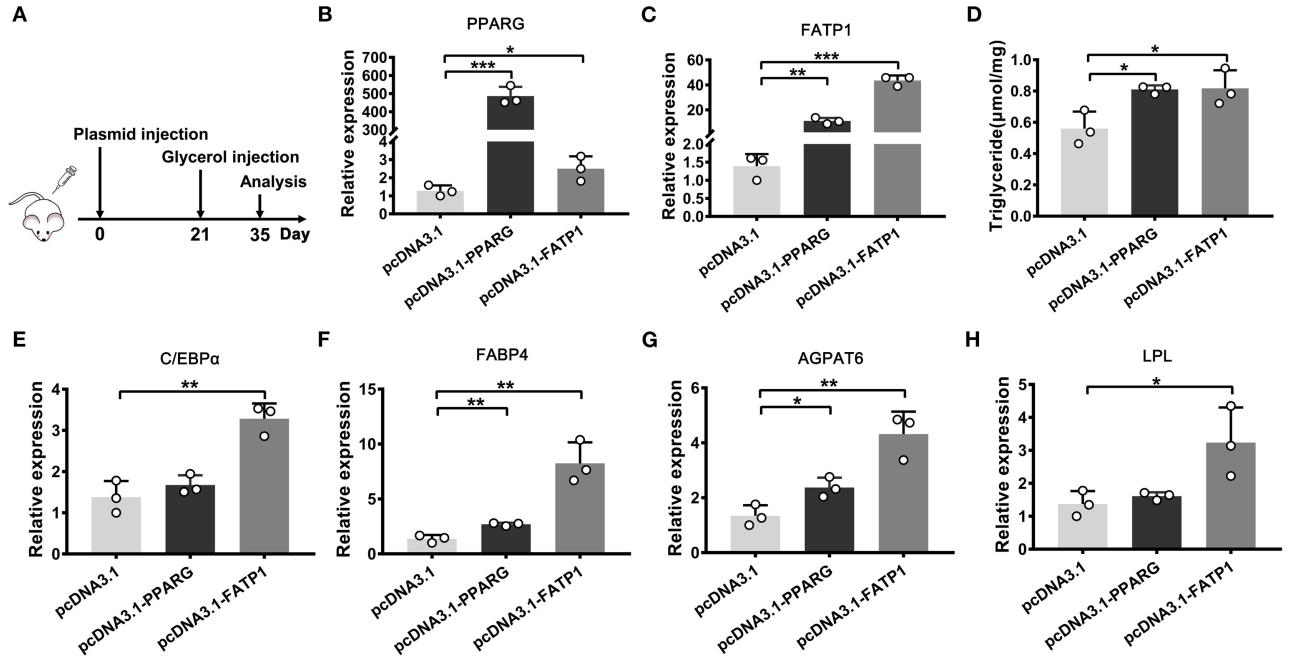

FIGURE 8 | The overexpression of FATP1 increases the intramuscular fat content in the mouse. **(A)** The strategy employed for intramuscular plasmid injection. The expression of *PPARG* **(B)**, *FATP1* **(C)**, *CEBPA* **(E)**, *FABP4* **(F),** *AGPAT6* **(G)**, and *LPL* **(H,D)** triglyceride levels in the *gastrocnemius* muscle injected with the indicated plasmid 2 weeks after glycerol injection. Data are presented as means ± SD, * $p < 0.05$, ** $p < 0.01$, *** $p < 0.001$.

exhibited high levels of expression in cells undergoing adipogenic differentiation (**Figures 1B–F**). These results support that FATP1 is vital for cellular FA uptake and metabolism.

Given its important role in uptake, esterification, and oxidation of FAs, FATP1 has been proposed to function as a regulator of lipid accumulation in cells. However, the effects of FATP1 on cellular lipid accumulation remains unclear. While some studies have demonstrated that FATP1 promotes lipid accumulation in muscle-derived cells such as quail QM-7 muscle cells (17), human muscle cells (27), and porcine intramuscular preadipocytes (15), others have reported that FATP1 does not affect, or even inhibits, lipid accumulation in muscle tissue (16, 28, 29). Here, our data support that FATP1 promotes lipid accumulation in muscle-derived cells, including mouse C2C12 cells (**Figures 6A–C**), buffalo myocytes (**Figure 2**), and buffalo intramuscular preadipocytes (**Figure 3**), and that FATP1 enhances IMF deposition in the mouse *in vivo* (**Figure 8**). We further found that FATP1 inhibits adipogenic differentiation in 3T3-L1 cells (**Figure 7**), which is consistent with previously reported results (30); however, FATP1 did not affect adipogenic differentiation in buffalo subcutaneous preadipocytes (**Figure 4**). In summary, FATP1 promotes adipogenesis in muscle tissue and muscle tissue-derived cells, but does not influence, and may even inhibit, adipogenesis in cells derived from adipose tissue.

Results of several studies have indicated that specific molecules or genes can exert differential effects on adipogenesis in intramuscular and subcutaneous adipocytes (31–33). Indeed, IMF is significantly different from subcutaneous and visceral fat (34, 35). Muscle cells and mature adipocytes secrete specific factors to further regulate fat deposition (36). Accordingly, the gene regulatory networks involved in the development of intramuscular and subcutaneous adipocytes are different (37, 38). In livestock, especially bovines, IMF is highly appreciated for its significant positive effect on meat quality, while fat deposition in other compartments, such as subcutaneous or visceral depots, is considered as waste (39). Regulatory factors that favor IMF deposition over subcutaneous or visceral fat deposition are highly desirable in the production of livestock animals. Our results indicate that FATP1 may fulfill this criterion. We demonstrate that FATP1 promotes IMF deposition in the mouse *in vivo* (**Figure 8**). As previous mentioned, FATP1 is a key transporter in cellular FAs uptake (22, 23). Overexpression of FATP1 significantly enhances FAs uptake in muscle. The excess FAs can be used for TG synthesis in the cytoplasm or delivered into mitochondria for ATP produce (40). When the efficiency of TG synthesis higher than that of ATP produce, lipid droplets can be accumulated in muscle tissue. On the other hand, though FATP1 has been demonstrated to be with no effect or negative effect on lipid accumulation in adipose tissue-derived cells, further *in vivo* experiment is necessary.

Cell proliferation underlies tissue development. Both proliferation and adipogenic differentiation require a large amount of energy. Since FATP1 plays an important role in adipogenic differentiation, it could also affect the proliferation of cells. Our data demonstrated that FATP1 promotes the proliferation of cells derived from muscle and adipose tissues in buffalo (**Figure 5**). Thus, FATP1 promotes the development of muscle and adipose tissues by enhancing cell proliferation. In livestock, the development of muscle and adipose tissue comprises two main stages, namely, cell proliferation in the early

stage and differentiation in the adult stage (39, 41, 42). Thus, in the early stages, high levels of FATP1 in muscle benefits muscle development; concomitantly, low levels of FATP1 in adipose tissue will reduce waste in buffalo production. Our data also showed that FATP1 promotes the proliferation of C2C12 cells but inhibits that in 3T3-L1 preadipocytes (**Figures 7D–F**), indicating that the effects of FATP1 on the cell proliferation are different between buffaloes and mice. Therefore, using mice as animal models to evaluate the effects of FATP1 on cell proliferation may need further consideration.

In conclusion, our findings support that FATP1 enhances fat deposition in intramuscular compartments but does not affect, or even inhibits, that in other depots. Our data further indicate that FATP1 enhances the proliferative ability of both muscle- and adipose-derived cells, except 3T3-L1 cells. These results provide new insights into the potential effects of FATP1 on animal production, especially regarding its role in improving meat quality in buffaloes and other livestock.

DATA AVAILABILITY STATEMENT

The datasets presented in this study can be found in online repositories. The names of the repository/repositories and accession number(s) can be found in the article/supplementary materials. The datasets have been deposited in figshare and the accession number (DOI) is 10.6084/m9.figshare.20174003.

ETHICS STATEMENT

The animal study was reviewed and approved by Institutional Animal Care and Use Committee at the College of Animal Science and Technology, Guangxi University. Written informed consent was obtained from the owners for the participation of their animals in this study.

AUTHOR CONTRIBUTIONS

JH designed the study, analyzed the data, and drafted the manuscript. DG performed the experiments and analyzed the data. RZ, YF, RL, and XY helped to carry out the experiments and collected tissue samples. DS provided technical guidance and the experimental platform. All authors read and approved the final version of the manuscript.

FUNDING

This work was supported by the National Natural Science Foundation of China (32060747 and U20A2051) and the Guangxi Natural Science Foundation (2020JJA130143 and 2021AC19014).

ACKNOWLEDGMENTS

We would like to thank the Bama County Program for Talents in Science and Technology, Guangxi, China.

SUPPLEMENTARY MATERIAL

The Supplementary Material for this article can be found online at: https://www.frontiersin.org/articles/10.3389/fvets.2022.904879/full#supplementary-material

REFERENCES

1. Khan R, Raza S, Junjvlieke Z, Wang X, Garcia M, Elsaeid Elnour I, et al. Function and transcriptional regulation of bovine torc2 gene in adipocytes: roles of c/ebpγ, xbp1, insm1 and znf263. *Int J Mol Sci.* (2019) 20:4338. doi: 10.3390/ijms20184338
2. Khan R, Raza S, Junjvlieke Z, Wang X, Wang H, Cheng G, et al. Bta-miR-149-5p inhibits proliferation and differentiation of bovine adipocytes through targeting CRTCs at both transcriptional and posttranscriptional levels. *J Cell Physiol.* (2020) 235:5796–810. doi: 10.1002/jcp.29513
3. Lowe CE, O'Rahilly S. Adipogenesis at a glance. *J Cell Sci.* (2011) 124:2681–6. doi: 10.1242/jcs.079699
4. de Sá PM, Richard AJ, Hang H, Stephens JM. Transcriptional regulation of adipogenesis. *Compr Physiol.* (2017) 7:635–74. doi: 10.1002/cphy.c160022
5. Hudson NJ, Reverter A, Greenwood PL, Guo B, Cafe LM. Longitudinal muscle gene expression patterns associated with differential intramuscular fat in cattle. *Animal.* (2015) 9:650–9. doi: 10.1017/S1751731114002754
6. López-Pedrouso M, Franco D, Serrano MP, Maggiolino A, Landete-Castillejos T, Palo D, et al. A proteomic-based approach for the search of biomarkers in Iberian wild deer (Cervus elaphus) as indicators of meat quality. *J Proteomics.* (2019) 205:103422. doi: 10.1016/j.jprot.2019.103422
7. De Jager N, Hudson NJ, Reverter A, Barnard R, Cafe LM, Greenwood PL, et al. Gene expression phenotypes for lipid metabolism and intramuscular fat in skeletal muscle of cattle. *J Anim Sci.* (2013) 91:1112–28. doi: 10.2527/jas.2012-5409
8. Ren Z, Wang Y, Ren Y, Zhang Z, Gu W, Wu Z, et al. Enhancement of porcine intramuscular fat content by overexpression of the cytosolic form of phosphoenolpyruvate carboxykinase in skeletal muscle. *Sci Rep.* (2017) 7:43746. doi: 10.1038/srep43746
9. Huang J, Feng X, Zhu R, Guo D, Wei Y, Cao X, et al. Comparative transcriptome analysis reveals that PCK1 is a potential gene affecting IMF deposition in buffalo. *BMC Genomics.* (2020) 21:710. doi: 10.1186/s12864-020-07120-w
10. Ordovás L, Roy R, Zaragoza P. Structural and functional characterization of the bovine solute carrier family 27 member 1 (SLC27A1) gene. *Cytogenet Genome Res.* (2006) 115:115–22. doi: 10.1159/000095230
11. Nickerson JG, Alkhateeb H, Benton CR, Lally J, Nickerson J, Han XX, et al. Greater transport efficiencies of the membrane fatty acid transporters FAT/CD36 and FATP4 compared with FABPpm and FATP1 and differential effects on fatty acid esterification and oxidation in rat skeletal muscle. *J Biol Chem.* (2009) 284:16522–30. doi: 10.1074/jbc.M109.004788
12. Sebastián D, Guitart M, García-Martínez C, Mauvezin C, Orellana-Gavaldà JM, et al. Novel role of FATP1 in mitochondrial fatty acid oxidation in skeletal muscle cells. *J Lipid Res.* (2009) 50:1789–99. doi: 10.1194/jlr.M800535-JLR200
13. Huang J, Zhu R. The role of FATP1 in lipid accumulation: a review. *Mol Cell Biochem.* (2021) 476:1897–903. doi: 10.1007/s11010-021-04057-w
14. Qi R, Long D, Wang J, Wang Q, Huang X, Cao C, et al. MicroRNA-199a Targets the Fatty Acid Transport Protein 1 Gene and Inhibits the Adipogenic Trans-Differentiation of C2C12 Myoblasts. *Cell Physiol Biochem.* (2016) 39:1087–97. doi: 10.1159/000447817
15. Chen X, Luo Y, Wang R, Zhou B, Huang Z, Jia G, et al. Effects of fatty acid transport protein 1 on proliferation and differentiation of porcine intramuscular preadipocytes. *Anim Sci J.* (2017) 88:731–8. doi: 10.1111/asj.12701

16. Guitart M, Osorio-Conles Ó, Pentinat T, Cebrià J, García-Villoria J, Sala D, et al. Fatty acid transport protein 1 (FATP1) localizes in mitochondria in mouse skeletal muscle and regulates lipid and ketone body disposal. *PLoS ONE.* (2014) 9:e98109. doi: 10.1371/journal.pone.0098109
17. Qiu F, Xie L, Ma JE, Luo W, Zhang L, Chao Z, et al. Lower Expression of SLC27A1 enhances intramuscular fat deposition in chicken via down-regulated fatty acid oxidation mediated by CPT1A. *Front Physiol.* (2017) 8:449. doi: 10.3389/fphys.2017.00449
18. Huang J, Liu X, Feng X, Zhang M, Qu K, Liu J, et al. Characterization of different adipose depots in fattened buffalo: histological features and expression profiling of adipocyte markers. *Arch Anim Breed.* (2020) 63:61–7. doi: 10.5194/aab-63-61-2020
19. Huang J, Zheng Q, Wang S, Wei X, Li F. High-throughput RNA sequencing reveals NDUFC2-AS lncRNA promotes adipogenic differentiation in Chinese buffalo (*Bubalus bubalis* L). *Genes*. (2019) 10:689. doi: 10.3390/genes10090689
20. Mathes S, Fahrner A, Ghoshdastider U, Rüdiger HA, Leunig M, Wolfrum C, et al. FGF-2-dependent signaling activated in aged human skeletal muscle promotes intramuscular. *Adipogenesis*. (2021) 118: e2021013118. doi: 10.1073/pnas.2021013118
21. Chen M, Wei X, Song M, Jiang R, Huang K, Deng Y, et al. Circular RNA circMYBPC1 promotes skeletal muscle differentiation by targeting MyHC. *Mol Ther Nucleic Acids.* (2021) 24:352–68. doi: 10.1016/j.omtn.2021.03.004
22. Pohl J, Ring A, Hermann T. Role of FATP in parenchymal cell fatty acid uptake. *Biochim Biophys Acta.* (2004) 1686:1–6. doi: 10.1016/j.bbalip.2004.06.004
23. Bonen A, Chabowski A, Luiken JA, Glatz JF. Is membrane transport of FFA mediated by lipid, protein, or both? Mechanisms and regulation of protein-mediated cellular fatty acid uptake: molecular, biochemical, and physiological evidence. *Physiology.* (2007) 22:15–29. doi: 10.1152/physiologyonline.2007.22.1.15
24. Schaffer JE. Expression cloning and characterization of a novel adipocyte long chain fatty acid transport protein. *Cell.* (1994) 79:427–36. doi: 10.1016/0092-8674(94)90252-6
25. Martin G, Nemoto M, Gelman L, Geffroy S, Najib J, Fruchart JC, et al. The human fatty acid transport protein-1 (SLC27A1; FATP-1) cDNA and gene: organization, chromosomal localization, and expression. *Genomics.* (2000) 66:296–304. doi: 10.1006/geno.2000.6191
26. Zhao Z, Tian H, Shi B, Jiang Y, Liu X. Transcriptional Regulation of the Bovine Fatty Acid Transport Protein 1 Gene by Krüppel-Like Factors 15. *Animals.* (2019) 9:654. doi: 10.3390/ani9090654
27. García-Martínez C, Marotta M, Moore-Carrasco R, Guitart M, Camps M, Busquets S, et al. Impact on fatty acid metabolism and differential localization of FATP1 and FAT/CD36 proteins delivered in cultured human muscle cells. *Am J Physiol Cell Physiol.* (2005) 288:C1264–72. doi: 10.1152/ajpcell.00271.2004
28. Chiu HC, Kovacs A, Blanton RM, Han X, Courtois M, Weinheimer CJ, et al. Transgenic expression of fatty acid transport protein 1 in the heart causes lipotoxic cardiomyopathy. *Circ Res.* (2005) 96:225–33. doi: 10.1161/01.RES.0000154079.20681.B9
29. Holloway GP, Chou CJ, Lally J, Stellingwerff T, Maher AC, Gavrilova O, et al. Increasing skeletal muscle fatty acid transport protein 1 (FATP1) targets fatty acids to oxidation and does not predispose mice to diet-induced insulin resistance. *Diabetologia.* (2011) 54:1457–67. doi: 10.1007/s00125-011-2114-8
30. Lobo S, Wiczer BM, Smith AJ, Hall AM. Fatty acid metabolism in adipocytes: functional analysis of fatty acid transport proteins 1 and 4. *J Lipid Res.* (2007) 48:609–20. doi: 10.1194/jlr.M600441-JLR200
31. Chung KY, Smith SB, Choi SH. Oleic acid enhances G protein coupled receptor 43 expression in bovine intramuscular adipocytes but not in subcutaneous adipocytes. *J Anim Sci.* (2016) 94:1875–83. doi: 10.2527/jas.2015-0010
32. Liu X, You W, Cheng H, Zhang Q, Song E, Wan F, et al. Effect of mevalonic acid on cholesterol synthesis in bovine intramuscular and subcutaneous adipocytes. *J Appl Genet.* (2016) 57:113–8. doi: 10.1007/s13353-015-0300-y
33. Wu W, Zhang D, Yin Y, Ji M, Xu K, Huang X, et al. Comprehensive transcriptomic view of the role of the LGALS12 gene in porcine subcutaneous and intramuscular adipocytes. *BMC Genomics.* (2019) 20:509. doi: 10.1186/s12864-019-5891-y
34. Bong JJ, Cho KK. Comparison of gene expression profiling between bovine subcutaneous and intramuscular adipose tissues by serial analysis of gene expression. *Cell Biol Int.* (2009) 34:125–33. doi: 10.1042/CBI20090046
35. Ortiz-Colón G, Grant AC, Doumit ME. Bovine intramuscular, subcutaneous, and perirenal stromal-vascular cells express similar glucocorticoid receptor isoforms, but exhibit different adipogenic capacity. *J Anim Sci.* (2009) 87:1913–20. doi: 10.2527/jas.2008-1350
36. Komolka K, Albrecht E, Wimmers K, Michal JJ. Molecular heterogeneities of adipose depots - potential effects on adipose-muscle cross-talk in humans, mice and farm animals. *J Genomics.* (2014) 2:31–44. doi: 10.7150/jgen.5260
37. Rajesh RV, Heo GN, Park MR, Nam JS, Kim NK, Yoon D, et al. Proteomic analysis of bovine omental, subcutaneous and intramuscular preadipocytes during in vitro adipogenic differentiation. *Comp Biochem Physiol Part D Genomics Proteomics.* (2010) 5:234–44. doi: 10.1016/j.cbd.2010.06.004
38. Xu K, Ji M, Huang X, Peng Y, Wu W, Zhang J. Differential Regulatory Roles of MicroRNAs in Porcine Intramuscular and Subcutaneous. *Adipocytes.* (2020) 68:3954–62. doi: 10.1021/acs.jafc.9b08191
39. Li X, Fu X, Yang G, Du M. Review: enhancing intramuscular fat development via targeting fibro-adipogenic progenitor cells in meat animals. *Animal.* (2020) 14:312–21. doi: 10.1017/S175173111900209X
40. Sleeth ML, Thompson EL, Ford HE, Zac-Varghese S. Free fatty acid receptor 2 and nutrient sensing: a proposed role for fibre, fermentable carbohydrates and short-chain fatty acids in appetite regulation. *Nutr Res Rev.* (2010) 23:135–45. doi: 10.1017/S0954422410000089
41. Huang K, Chen M, Zhong D, Luo X, Feng T, Song M, et al. Circular RNA Profiling Reveals an Abundant circEch1 That Promotes Myogenesis and Differentiation of Bovine Skeletal Muscle. *J Agric Food Chem.* (2021) 69:592–601. doi: 10.1021/acs.jafc.0c06400
42. Yang Y, Yan J, Fan X. The genome variation and developmental transcriptome maps reveal genetic differentiation of skeletal muscle in *pigs. 17*. (2021) e1009910. doi: 10.1371/journal.pgen.1009910

Conflict of Interest: The authors declare that the research was conducted in the absence of any commercial or financial relationships that could be construed as a potential conflict of interest.

Publisher's Note: All claims expressed in this article are solely those of the authors and do not necessarily represent those of their affiliated organizations, or those of the publisher, the editors and the reviewers. Any product that may be evaluated in this article, or claim that may be made by its manufacturer, is not guaranteed or endorsed by the publisher.

frontiers | Frontiers in Veterinary Science

TYPE Original Research
PUBLISHED 27 July 2022
DOI 10.3389/fvets.2022.951168

OPEN ACCESS

EDITED BY
Anning Li,
Northwest A&F University, China

REVIEWED BY
Xing Du,
Nanjing Agricultural University, China
Linjie Wang,
Sichuan Agricultural University, China

*CORRESPONDENCE
Bojiang Li
bojiangli@syau.edu.cn
Shuyi Zhang
szhang@syau.edu.cn

SPECIALTY SECTION
This article was submitted to Livestock Genomics, a section of the journal Frontiers in Veterinary Science

RECEIVED 23 May 2022
ACCEPTED 05 July 2022
PUBLISHED 27 July 2022

CITATION
Tan X, He Y, Qin Y, Yan Z, Chen J, Zhao R, Zhou S, Irwin DM, Li B and Zhang S (2022) Comparative analysis of differentially abundant proteins between high and low intramuscular fat content groups in donkeys. *Front. Vet. Sci.* 9:951168. doi: 10.3389/fvets.2022.951168

Comparative analysis of differentially abundant proteins between high and low intramuscular fat content groups in donkeys

Xiaofan Tan[1], Yu He[1], Yanchun Qin[1], Zhiwei Yan[1], Jing Chen[1], Ruixue Zhao[1], Shenglan Zhou[1], David M. Irwin[2], Bojiang Li[1]* and Shuyi Zhang[1]*

[1]Department of Animal Genetics, Breeding and Reproduction, College of Animal Science and Veterinary Medicine, Shenyang Agricultural University, Shenyang, China, [2]Department of Laboratory Medicine and Pathobiology, University of Toronto, Toronto, ON, Canada

Intramuscular fat (IMF) is an important regulator that determines meat quality, and its content is closely related to flavor, tenderness, and juiciness. Many studies have used quantitative proteomic analysis to identify proteins associated with meat quality traits in livestock, however, the potential candidate proteins that influence IMF in donkey muscle are not fully understood. In this study, we performed quantitative proteomic analysis, with tandem-mass-tagged (TMT) labeling, with samples from the longissimus dorsi (LD) muscle of the donkey. A total of 585,555 spectra were identified from the six muscle samples used in this study. In total, 20,583 peptides were detected, including 15,279 unique peptides, and 2,540 proteins were identified. We analyzed differentially abundant proteins (DAPs) between LD muscles of donkeys with high (H) and low (L) IMF content. We identified 30 DAPs between the H and L IMF content groups, of which 17 were upregulated and 13 downregulated in the H IMF group. Gene Ontology (GO) and Kyoto Encyclopedia of Genes and Genomes (KEGG) functional enrichment analysis of these DAPs revealed many GO terms (e.g., bone morphogenetic protein (BMP) receptor binding) and pathways (e.g., Wnt signaling pathway and Hippo signaling pathway) involved in lipid metabolism and adipogenesis. The construction of protein–protein interaction networks identified 16 DAPs involved in these networks. Our data provide a basis for future investigations into candidate proteins involved in IMF deposition and potential new approaches to improve meat quality in the donkey.

KEYWORDS

donkey, IMF, proteomics, differentially abundant proteins, functional analysis

Introduction

Donkeys are domesticated animals that belong to the horse family (1). They are one of the most important livestock animals in many countries in Africa and the Middle East, which are mainly used for farming or other work on large farms (2, 3). With the increase of interest in donkey breeding, it is increasingly being used as a milk and meat-producing animal (4, 5). Donkey milk has been shown to be the best substitute for human milk for children who are allergic to milk proteins (6). Donkey meat is characterized by high-quality protein, vitamins, and minerals, which is the preferred meat for many consumers due to its high protein content (5, 7, 8). According to a previous study, 100 g of donkey meat contains 22.8 g of protein and 2.02 g of fat (2, 9, 10). With improvements in living standards, consumers are becoming more concerned about the quality of livestock meat. In recent years, donkey meat consumption has increased in many countries, including China and Italy, and has undoubtedly become one of the livestock meat choices (6, 11, 12).

Intramuscular fat (IMF), also referred to as marbling, is the amount of fat that accumulates between muscle fibers or inside muscle cells (13). Its main components are phospholipids and triglycerides (14, 15). A previous study reported that IMF content is mainly determined by the number and size of intramuscular adipocytes (16). Furthermore, IMF is a complex quantitative trait, which is influenced by a variety of regulatory factors, such as gene regulation (17), sex (18), age, or body weight (19), as well as environmental conditions, cell signals, and diet (20). A previous study has shown that IMF plays a key role in many meat quality characteristics and quality (21). For example, IMF can improve meat quality by improving flavor, juiciness, and tenderness (22, 23). Therefore, IMF not only plays a very important role in animal husbandry production but also is closely related to a healthy and desirous human food supply. In recent years, the identification of candidate genes for IMF to improve meat quality has become an important research topic in livestock breeding. A large number of studies have investigated candidate genes affecting IMF content in many species, including cattle (24), pigs (25), sheep (26), and goats (27). Genes, such as PHKG1 (28), MYH3 (20), and PLIN1 (29), have been identified as candidates for regulating IMF content in pigs. However, candidate genes and regulatory mechanisms for IMF content in donkeys are not fully resolved.

With recent developments in proteomic technologies, it has become an increasingly important approach to identify candidate proteins related to meat quality in livestock. A previous study identified 127 proteins with differential abundance associated with IMF in the longissimus dorsi (LD) muscle of pigs between days 120 d and 240 of growth (30). Hou et al. (31) identified proteins from the pig related to postmortem meat quality using a TMT (tandem-mass-tagged)-labeled quantitative proteomic. Similarly, proteomics was used to detect proteins associated with meat quality traits in other species including sheep (32), cattle (33), and chickens (34). Current proteomic studies on the donkey have mainly focused on the identification of proteins associated with donkey milk (35, 36). Few studies on proteins related to the regulation of donkey meat quality have been reported.

In this study, expression profiling of proteins was performed using LD muscle samples with divergent IMF content phenotypes (H and L IMF content groups). We used bioinformatic methods to identify the differentially abundant proteins (DAPs) between the H and L IMF groups. Gene Ontology (GO) and Kyoto Encyclopedia of Genes and Genomes (KEGG) enrichment analysis of the DAPs was conducted. The aim of this study was to identify candidate proteins that influence IMF content in donkeys and to provide a basis for improving the quality of donkey meat.

Materials and methods

Ethics statement

All animal procedures described in this study were conducted according to the animal husbandry guidelines of the Shenyang Agricultural University. The studies on these animals were reviewed and approved by the Ethics Committee and Experimental Animal Committee of Shenyang Agriculture University (No. 202006032).

Sample preparation

All animals used in this study were derived from a population of 30 donkeys described in a previous study (37). These animals were raised under the same environmental conditions. At about 15 months of age, all donkeys are slaughtered in the same abattoir and LD muscle tissue samples were collected for IMF determination and protein extraction. Samples for protein extraction were immediately frozen in liquid nitrogen and then stored at−80°C until use. The Soxhlet extraction method (37) was used to determine the IMF content of the samples.

Protein extraction and digestion

Protein in the samples was isolated after disruption of the tissue in SDT [4% sodium dodecyl sulfate (SDS), 100 mM Tris-HCl,1 mM DTT, pH 7.6] buffer, with the protein concentration quantified with the bicinchoninic acid (BCA) Protein Assay Kit (Bio-Rad, USA). Protein digestion was performed using trypsin according to the filter-aided sample

preparation (FASP) method previously described by Matthias Mann (38). Briefly, protein from each sample was incorporated into SDT [4% SDS, 100 mM dithiothreitol (DTT), 150 mM Tris-HCl pH 8.0] buffer. The detergent, DTT, and other low-molecular-weight components were removed using UA buffer (8 M urea, 150 mM Tris-HCl pH 8.0). Iodoacetamide (IAA), 100 µl of 100 mM IAA in UA buffer, was added to block reduced cysteine residues and incubated in the dark for 30 min. The filter was then washed three times with 100 µl UA buffer and then twice with 100 µl 25 mM NH_4HCO_3 buffer. The eluted protein suspension was then digested overnight at 37°C with 4 µg trypsin (Promega) in 40 µl of 25 mM NH_4HCO_3 buffer and the resulting peptides were collected as filtrate. Digested peptides for each sample were desalted on C_{18} cartridges, concentrated by vacuum centrifugation, and reconstituted in 40 µl of 0.1% (v/v) formic acid.

Tandem-mass-tag labeling

Peptides from the three high (H1, H2, and H3) and three low (L1, L2, and L3) IMF content donkey samples were labeled with 126, 127, 128, 129, 130, and 131 isotope tags, respectively, using TMT reagents according to the manufacturer's instructions (Thermo Scientific, Waltham, USA).

Liquid chromatography–mass spectrometry analysis

Liquid chromatography–mass spectrometry (LC–MS/MS) analysis was conducted on a Q Exactive mass spectrometer (Thermo Scientific, Waltham, USA). MS data were obtained using a data-dependent top 10 method dynamically choosing the most abundant precursor ions from the survey scan (300–1,800 m/z) for high-energy collisional dissociation (HCD) fragmentation. The automatic gain control (AGC) target was 3×10^6 and the maximum injection time was 10 ms. The dynamic exclusion duration was 40.0 s. Survey scans were obtained at a resolution of 70,000 at m/z 200 and resolution for HCD spectra was set to 17,500 at m/z 200, and isolation width was 2 m/z. The normalized collision energy was 30 eV and the underfill ratio was 0.1%.

Identification and quantitation of proteins

The MS raw data for each sample were searched against the donkey UniProt database using the MASCOT engine (Matrix Science, London, UK; version 2.2) embedded into Proteome Discoverer 1.4 software for protein identification and quantitation. Proteins with fold change (FC) >1.2 or <0.833 and $p < 0.05$ were considered to be significantly DAPs.

Gene ontology and KEGG pathway enrichment analysis of DAPs

The gene ontology (GO) term annotation of selected DAPs was performed using Blast2GO software (39, 40). The DAPs were blasted against the Kyoto Encyclopedia of Genes and Genomes (KEGG) database (http://geneontology.org/) to retrieve their KEGG orthology identifications, which were subsequently mapped to the pathways in KEGG (41). GO and KEGG enrichment was analyzed using the Fisher's exact test. GO and KEGG terms with $p < 0.05$ were considered significantly enriched.

Protein–protein interactions analysis

For protein–protein interactions, we used STRING v11.5 (42) to predict and visualize networks according to default parameters. Protein interactions were illustrated using Cytoscape software (43).

Results

Characterization of identified proteins

We selected three LD muscle samples with high (H1, H2, and H3) and three with low (L1, L2, and L3) IMF content from a population of 30 individuals. Statistical analysis of the data showed that IMF content was significantly different between H and L samples (3.04 ± 0.12%, 6.39 ± 0.47%; $p < 0.01$). We further characterized the protein abundance profiles of the six samples using the TMT-labeled proteomic approach. The entire proteomic experimental flow for this study is shown in Figure 1. A total of 585,555 spectra were detected from the six LD muscle samples by LC–MS/MS analysis (Figure 2A). From this, we identified a total of 20,583 peptides, of which 15,279 were unique, corresponding to 2,540 distinct proteins (Figure 2A; Supplementary Table S1). A statistical analysis of the lengths of the identified peptide was conducted, which showed that the peptides were mainly between 5 and 15 amino acids with peptides of 7 and 9 amino acids in length being the highest (Figure 2B). Further analyses of the numbers of peptides identified in the proteins showed that about 50% of the proteins contained 1–3 identified peptides (Figure 2C). The molecular weights of the identified proteins indicated that most of these proteins have molecular weights between 10 and 70 kDa (Figure 2D).

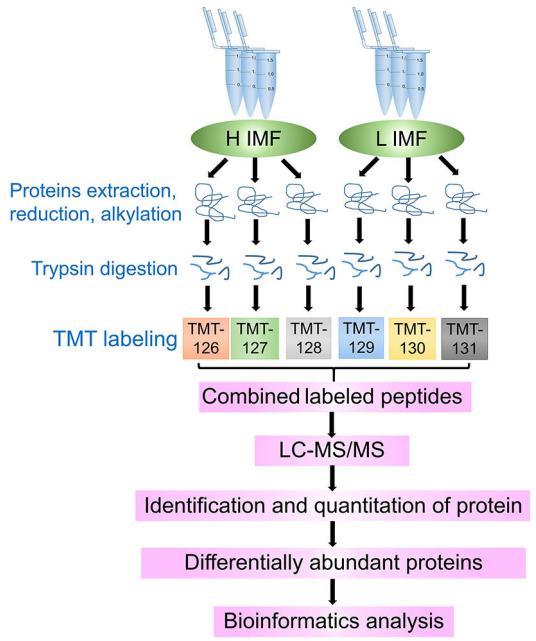

FIGURE 1
Schematic protocol for the identification of longissimus dorsi muscle proteins from tissue samples with high (H) and low (L) intramuscular fat (IMF) content using tandem-mass-tagged (TMT)-labeled quantitative proteomics. The H and L IMF samples were in triplicate, and each sample used a different TMT label.

Identification of DAPs between high and low IMF groups

To further explore candidate proteins associated with IMF deposition in donkeys, we analyzed the differentially abundant proteins in the high and low IMF content groups. A total of 30 DAPs were identified between the H and L IMF groups, with 13 upregulated and 17 downregulated in the H IMF group (Figure 3A). Summary information on these proteins is listed in Supplementary Table S2. The top upregulated DAP is MAP4K4, while the top downregulated DAP is Rho-associated protein kinase 2 (ROCK2) (Supplementary Table S2). We also examined the abundance patterns of these DAPs in the six samples, which showed clear abundance differences between the high and low IMF group samples (Figure 3B).

Gene ontology and KEGG enrichment analysis of DAPs

To explore the potential biological functions of the DAPs in IMF deposition, we performed GO and KEGG functional enrichment analyses of the DAPs. Here, 227, 27, and 24 GO terms were found to be significantly enriched in biological process, cellular component, and molecular function, respectively (Supplementary Table S3). The top 30 significantly enriched GO terms are shown in Figure 4A. This data suggests that the DAPs are primarily involved in bone morphogenetic protein (BMP) receptor binding, which is associated with lipid metabolism. The KEGG enrichment analysis suggested that the DAPs are significantly enriched in 19 pathways (Figure 4B). Interestingly, some of these KEGG participate in the lipogenic processes, for instance, the Wnt signaling and Hippo signaling pathways. Further, a DAP, ROCK2, is significantly enriched in the Wnt signaling pathway. These results suggest that the enrichment of DAPs in these pathways may be closely related to the lipogenic process.

Protein–protein interactions analysis for DAPs

Next, we examined protein–protein interactions of the 30 DAPs to better understand IMF deposition. A protein–protein interaction analysis of the DAPs was conducted based on the STRING database, which contains details functional relationships between proteins, thus allowing predictions on the functional impact of changing protein abundance (44). The results of this analysis showed that 16 DAPs are involved in a protein–protein interaction network (Figure 5). For example, a DAP, ROCK2, interacts with UBR4, TJP1, MBP, and PTEN. In addition, the ADGRV1 and USH2A proteins interact with each other.

Discussion

In recent years, consumers have become increasingly interested in donkey meat, with China becoming the world's largest consumer of this meat (45). IMF plays a vital role in the quality of livestock meat, therefore, the identification of candidate proteins affecting IMF is essential for improving meat quality. Previous studies have applied proteomics to identify DAPs of IMF in other species including pigs (30) and goats (46). However, there is a paucity of research on candidate proteins for quality traits in donkey meat. In this study, we identified 30 proteins that were differentially abundant between LD muscle samples with high and low IMF content based on proteomic techniques. Our results suggest that the identified DAPs are candidates for influencing IMF content in donkey meat.

Further, of these DAPs, many are associated with the adipogenic processes. For example, ROCK2, a downregulated protein, inhibits adipogenesis based on knockdown experiments (47). Protein interaction analysis revealed that ROCK2 potentially binds UBR4, TJP1, MBP, and PTEN proteins. These results suggest that the ROCK2 protein might act as a suppressor of IMF deposition in the donkey by binding these proteins.

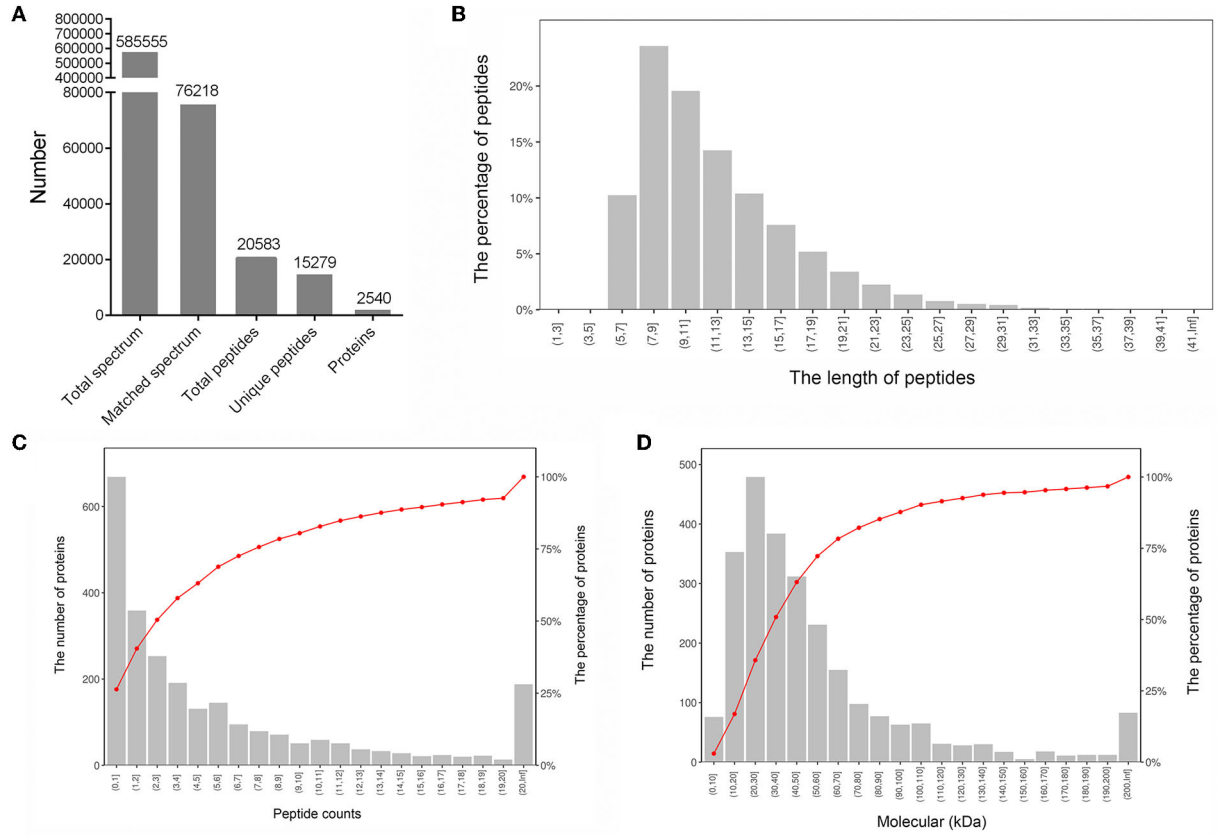

FIGURE 2
Characterization of proteins from six longissimus dorsi muscle samples. **(A)** Overview information of identified proteins in this study. **(B)** Distribution of the lengths of the identified peptides. **(C)** Distribution of the numbers of identified proteins containing different numbers of peptides. **(D)** Distribution of the molecular weights of the identified proteins.

Ahbara et al. (48) revealed the SPAG8 gene is a candidate for growth traits and adipogenesis in sheep. A previous study identified the RPL27A gene as a candidate gene for bovine marbling, with an single nucleotide polymorphism (SNP) in its promoter used as a molecular marker for bovine marbling (49). Tu et al. (50) found that a high-fat diet increases the expression level of TPM1. Another interesting finding is that PRMT3 acts as a co-transcription factor by translocating into the nucleus and binding to LXRα to regulate downstream gene expression, thereby promoting lipogenesis (51). These proteins (i.e., SPAG8, RPL27A, TPM1, MBP, and PRMT3) were identified as DAPs between the H and L IMF groups in this study, suggesting that they are important regulators of IMF. However, the mechanism of action of these DAPs in IMF deposition in donkeys needs to be further demonstrated.

Our study identified a number of GO terms related to the lipogenic process based on enrichment analysis of the DAPs, including tRNA methylation and BMP receptor binding. Zhao et al. (52) showed that RNA methylation has a crucial role and is required for adipose differentiation. In addition, it has been shown that tRNA methylation levels regulate the translation initiation of genes and thus affect protein synthesis (53). These data suggest that some DAPs may regulate IMF deposition by affecting tRNA methylation. BMP signaling is essential for the differentiation of mesenchymal stem cells (MSCs) into the adipocyte lineage (54). Jung et al. (55) found that plasma BMP2 levels were positively correlated with IMF content in steers, suggesting that BMP signaling contributes to meat quality. In addition, a GO term, positive regulation of c-Jun N-terminal kinase (JNK) cascade, was significantly enriched in this study. A previous study demonstrated that JNK signaling inhibits adipose differentiation by suppressing peroxisome proliferator-activated receptor-gamma (PPARγ) and fatty acid binding protein 4 (AP2) expression (56). Taken together, these DAPs may regulate the deposition of IMF through an association with adipogenesis.

In addition, DAPs were enriched in many key signaling pathways (e.g., Wnt and Hippo signaling pathways) involved in the adipogenic process. The Wnt signaling pathway is a highly conserved critical factor in animals that negatively regulates adipose differentiation (57). Mechanistically, Wnt signaling

10.3389/fvets.2022.951168

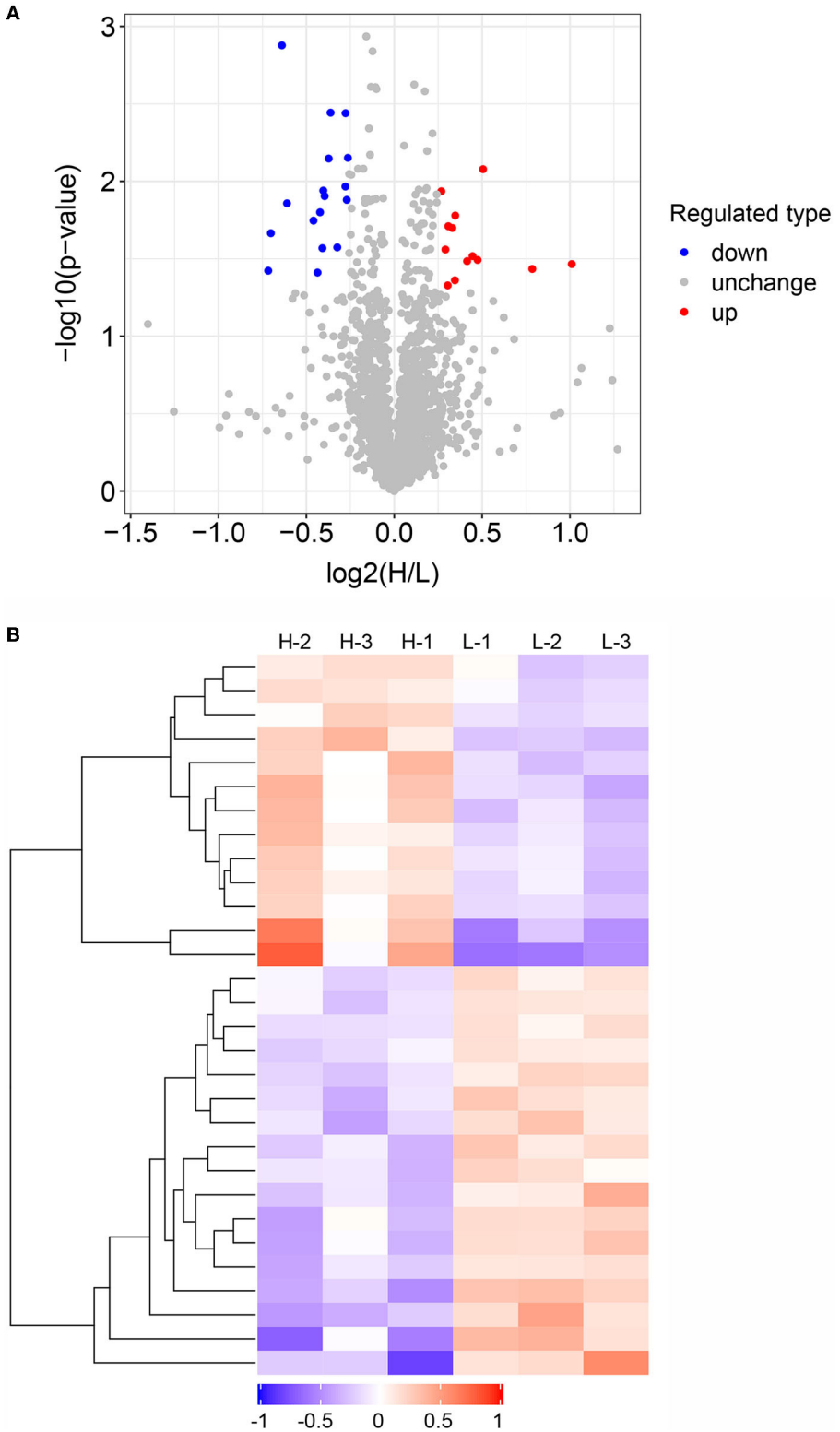

FIGURE 3
Analysis of differentially abundant proteins (DAPs) between high and low intramuscular fat (IMF) groups. **(A)** Volcano plot showing DAPs between high and low IMF groups. Red, gray, and blue dots represent upregulated, unchanged, and downregulated proteins, respectively. **(B)** Heatmap showing the abundance patterns of the DAPs between the three high and three low IMF samples.

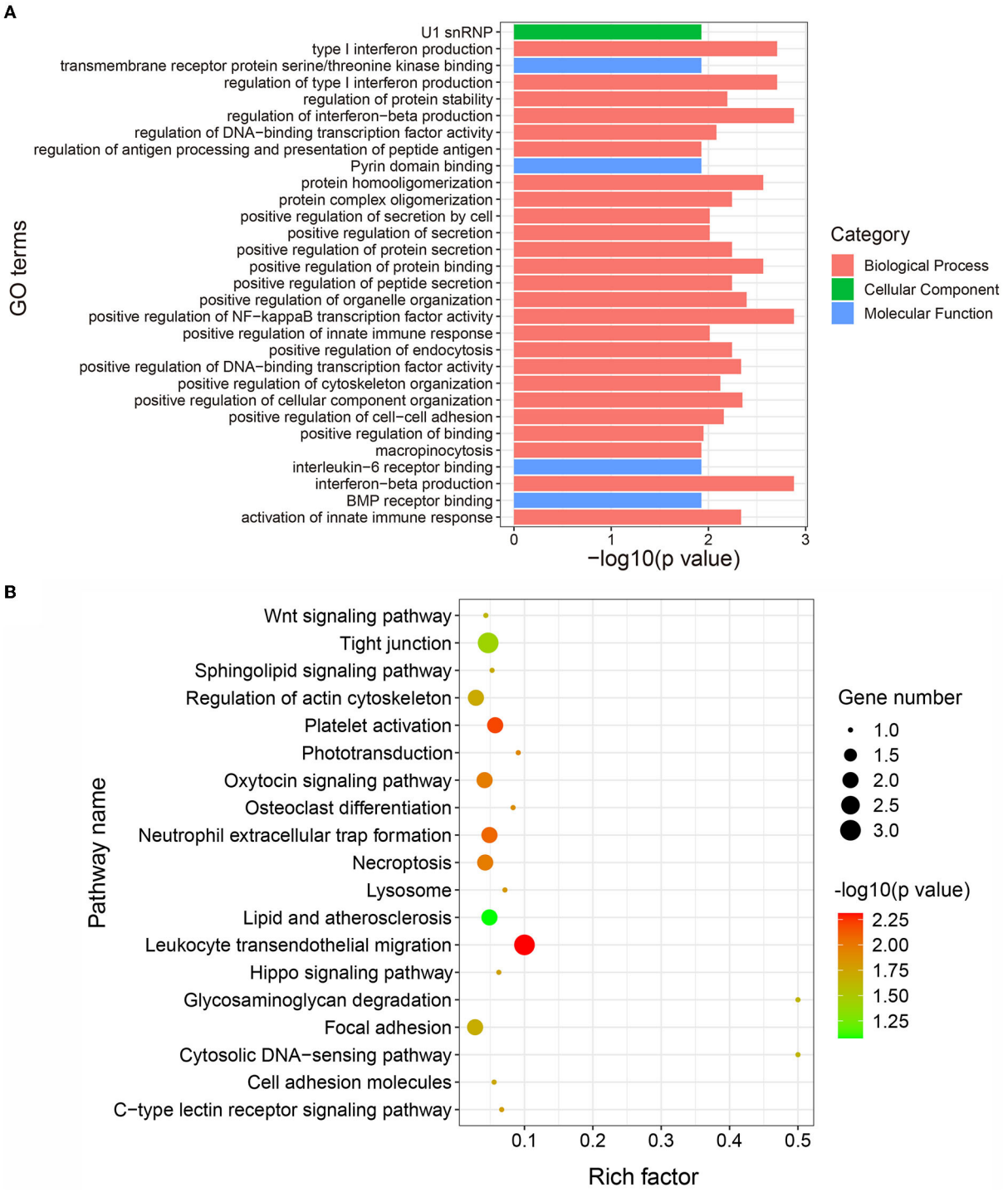

FIGURE 4
Gene ontology (GO) and Kyoto Encyclopedia of Genes and Genomes (KEGG) functional enrichment analysis of differentially abundant proteins (DAPs). **(A)** Top 30 significantly enriched GO terms. The X-axis represents the −log10 (*p* value) value of the GO terms and the Y-axis represents the GO term name. **(B)** Significantly enriched pathways of DAPs. The X-axis represents the rich factor and the Y-axis represents the pathway. The size and color of the bubbles represent the number of proteins enriched in the pathway and enrichment significance, respectively.

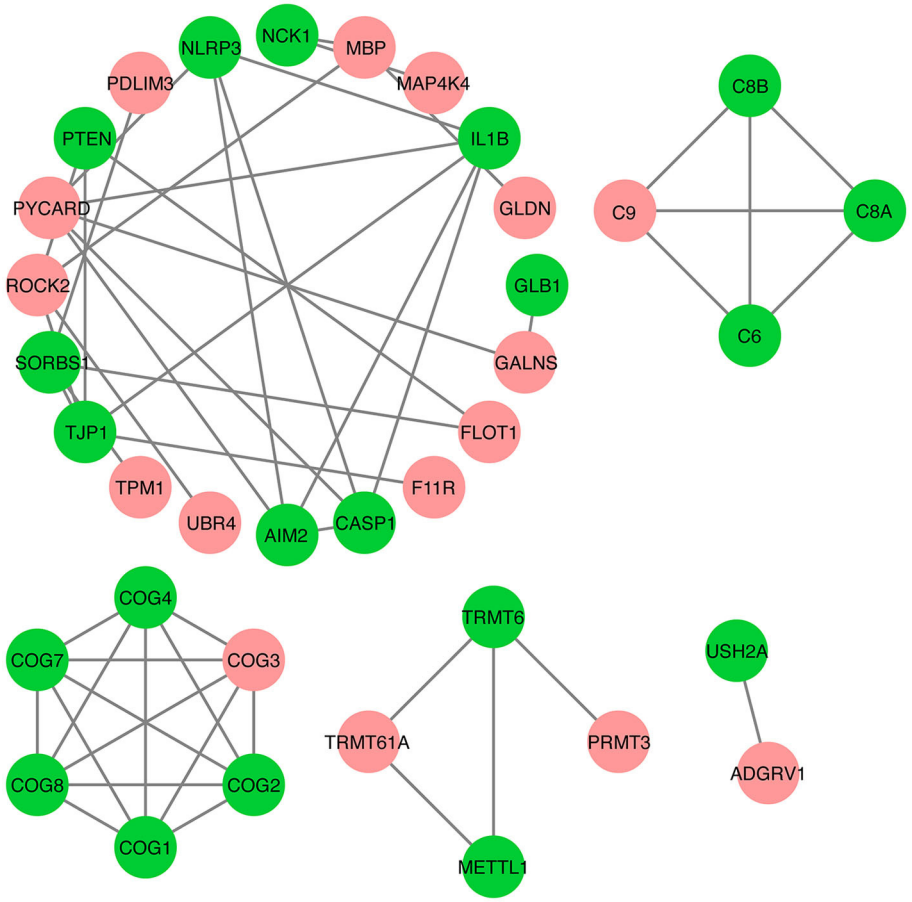

FIGURE 5
Protein–protein interactions analysis for differentially abundant proteins (DAPs). The red nodes represent DAPs, while the green nodes represent other proteins that interact with DAPs. The edge represents interactions between proteins.

inhibits adipogenesis by suppressing the expression of PPARγ and CCAAT/enhancer-binding protein alpha (C/EBP)α (58). Activation of Wnt signaling, by transgenic overexpression of Wnt10, in mice leads to significantly reduced adipose tissue weight (59). A downregulated protein identified in our study, ROCK2, is significantly enriched in the Wnt signaling pathway, suggesting that it inhibits IMF deposition by mediating the Wnt signaling pathway. The Hippo signaling pathway was also enriched, and it has been shown to be involved in adipocyte proliferation and differentiation in animals (60, 61). In Hippo signaling pathway, serine/threonine kinase 24 (Ste20) family kinases mammalian STE20-like kinase (MST1/2) activate large tumor suppressor (LATS) kinases through phosphorylation, which in turn allows phosphorylation of yes-associated protein (YAP) protein and facilitates the binding of YAP to 14-3-3 proteins (62). Park et al. (63) found that MST1/2 promotes the differentiation of 3T3-L1 cells through the activation of PPARγ. Deng et al. (61) demonstrated that YAP1 inhibits the differentiation of ovine adipocytes by affecting PPARG and RXR alpha levels. These results suggest that the Hippo signaling pathway is implicated in the deposition of IMF in the donkey. However, how DAPs involved in Hippo signaling regulate the deposition of IMF in donkeys still needs to be further explored.

Conclusion

In summary, we identified 30 candidate proteins that might affect IMF content in the LD muscle of donkeys. We provide evidence that some of the DAPs affect IMF deposition as they are involved in adipogenic functions or signaling pathways in other animals. Our data provide evidence for the role of these proteins in IMF content in the donkey and provide new insights into the molecular mechanisms of the regulation of IMF deposition.

Data availability statement

The original contributions presented in the study are included in the article/Supplementary material, further inquiries can be directed to the corresponding author/s.

Ethics statement

The animal study was reviewed and approved by the Ethics Committee and Experimental Animal Committee of Shenyang Agriculture University. Written informed consent was obtained from the owners for the participation of their animals in this study.

Author contributions

BL and SZha conceived and designed this study. YH, YQ, and XT performed the experiments. ZY, JC, SZho, and RZ analyzed the data. XT and BL drafted the manuscript. DI and BL revised the manuscript.

Funding

This research was supported by grants from the National Natural Science Foundation of China (No. 32002147), the China Postdoctoral Science Foundation (No. 2021MD703855), the Educational Department of Liaoning Province (No. LJKZ0671), the Natural Science Foundation of Liaoning Province (No. 2021-BS-140), the Science and Technology Plan Project of Shenyang City (Nos. 21-116-3-40 and 21-110-3-10), the Organization Department of Liaoning Provincial Committee of China (No. XLYC1907018), and the Shenyang Agricultural University Research Start-up Funding (No. 880418062).

Conflict of interest

The authors declare that the research was conducted in the absence of any commercial or financial relationships that could be construed as a potential conflict of interest.

Publisher's note

All claims expressed in this article are solely those of the authors and do not necessarily represent those of their affiliated organizations, or those of the publisher, the editors and the reviewers. Any product that may be evaluated in this article, or claim that may be made by its manufacturer, is not guaranteed or endorsed by the publisher.

Supplementary material

The Supplementary Material for this article can be found online at: https://www.frontiersin.org/articles/10.3389/fvets.2022.951168/full#supplementary-material

References

1. Orlando L. Equids. *Curr Biol.* (2015) 25:R973–978. doi: 10.1016/j.cub.2015.09.005

2. Shi T, Hu W, Hou H, Zhao Z, Shang M, Zhang L. Identification and comparative analysis of long non-coding RNA in the skeletal muscle of two Dezhou Donkey strains. *Genes (Basel).* (2020) 11:508. doi: 10.3390/genes11050508

3. Polidori P, Vincenzetti S, Cavallucci C, Beghelli D. Quality of donkey meat and carcass characteristics. *Meat Sci.* (2008) 80:1222–4. doi: 10.1016/j.meatsci.2008.05.027

4. De Palo P, Maggiolino A, Milella P, Centoducati N, Papaleo A, Tateo A. Artificial suckling in Martina Franca donkey foals: effect on in vivo performances and carcass composition. *Trop Anim Health Prod.* (2016) 48:167–73. doi: 10.1007/s11250-015-0940-2

5. De Palo P, Tateo A, Maggiolino A, Marino R, Ceci E, Nisi A, et al. Martina Franca donkey meat quality: influence of slaughter age and suckling technique. *Meat Sci.* (2017) 134:128–34. doi: 10.1016/j.meatsci.2017.07.025

6. Polidori P, Pucciarelli S, Ariani A, Polzonetti V, Vincenzetti S A. comparison of the carcass and meat quality of Martina Franca donkey foals aged 8 or 12 months. *Meat Sci.* (2015) 106:6–10. doi: 10.1016/j.meatsci.2015.03.018

7. Trinchese G, Cavaliere G, De Filippo C, Aceto S, Prisco M, Chun JT, et al. Human milk and donkey milk, compared to cow milk, reduce inflammatory mediators and modulate glucose and lipid metabolism, acting on mitochondrial function and oleylethanolamide levels in rat skeletal muscle. *Front Physiol.* (2018) 9:32. doi: 10.3389/fphys.2018.00032

8. Zhang X, Li H, Yu J, Zhou X, Ji C, Wu S, et al. Label-free based comparative proteomic analysis of whey proteins between different milk yields of Dezhou donkey. *Biochem Biophys Res Commun.* (2019) 508:237–42. doi: 10.1016/j.bbrc.2018.11.130

9. Lanza M, Landi C, Scerra M, Galofaro V, Pennisi P. Meat quality and intramuscular fatty acid composition of Sanfratellano and Haflinger foals. *Meat Sci.* (2009) 81:142–7. doi: 10.1016/j.meatsci.2008.07.008

10. Lorenzo JM, Sarries MV, Tateo A, Polidori P, Franco D, Lanza M. Carcass characteristics, meat quality and nutritional value of horsemeat: a review. *Meat Sci.* (2014) 96:1478–88. doi: 10.1016/j.meatsci.2013.12.006

11. Seyiti S, Kelimu A. Donkey industry in China: current aspects, suggestions and future challenges. *J Equine Vet Sci.* (2021) 102:103642. doi: 10.1016/j.jevs.2021.103642

12. Polidori P, Vincenzetti S, Pucciarelli S, Polzonetti V. Comparison of carcass and meat quality obtained from mule and donkey. *Animals-Basel.* (2020) 10:1620. doi: 10.3390/ani10091620

13. Listrat A, Lebret B, Louveau I, Astruc T, Bonnet M, Lefaucheur L, et al. How muscle structure and composition influence meat and flesh quality. *ScientificWorldJournal.* (2016) 2016:3182746. doi: 10.1155/2016/3182746

14. da Costa AS, Pires VM, Fontes CM, Mestre Prates JA. Expression of genes controlling fat deposition in two genetically diverse beef cattle breeds fed high or low silage diets. *BMC Vet Res.* (2013) 9:118. doi: 10.1186/1746-6148-9-118

15. Silva DBD, Fonseca LFS, Pinheiro DG, Muniz MMM, Magalhaes AFB, Baldi F, et al. Prediction of hub genes associated with intramuscular fat content in Nelore cattle. *BMC Genom.* (2019) 20:1–12. doi: 10.1186/s12864-019-5904-x

16. Li X, Fu X, Yang G, Du M. Review: Enhancing intramuscular fat development via targeting fibro-adipogenic progenitor cells in meat animals. *Animal.* (2020) 14:312–21. doi: 10.1017/S175173111900209X

17. Plastow GS, Carrion D, Gil M, Garcia-Regueiro JA, Gispert M, Oliver MA, et al. Quality pork genes and meat production. *Meat Sci.* (2005) 70:409–21. doi: 10.1016/j.meatsci.2004.06.025

18. Skrlep M, Batorek N, Bonneau M, Prevolnik M, Kubale V, Candek-Potokar M. Effect of immunocastration in group-housed commercial fattening pigs on reproductive organs, malodorous compounds, carcass and meat quality. *Czech J Anim Sci.* (2012) 57:290–9. doi: 10.17221/5964-CJAS

19. Tyra M, Ropka-Molik K, Terman A, Piorkowska K, Oczkowicz M, Bereta A. Association between subcutaneous and intramuscular fat content in porcine ham and loin depending on age, breed and FABP3 and LEPR genes transcript abundance. *Mol Biol Rep.* (2013) 40:2301–8. doi: 10.1007/s11033-012-2311-7

20. Cho IC, Park HB, Ahn JS, Han SH, Lee JB, Lim HT, et al. A functional regulatory variant of MYH3 influences muscle fiber-type composition and intramuscular fat content in pigs. *PLoS Genet.* (2019) 15:e1008279. doi: 10.1371/journal.pgen.1008279

21. Gao SZ, Zhao SM. Physiology, affecting factors and strategies for control of pig meat intramuscular fat. *Recent Pat Food Nutr Agric.* (2009) 1:59–74. doi: 10.2174/2212798410901010059

22. Hausman GJ, Dodson MV, Ajuwon K, Azain M, Barnes KM, Guan LL, et al. Board-invited review: the biology and regulation of preadipocytes and adipocytes in meat animals. *J Anim Sci.* (2009) 87:1218–46. doi: 10.2527/jas.2008-1427

23. Li QQ, Huang ZY, Zhao WJ, Li MX, Li CC. Transcriptome analysis reveals long intergenic non-coding RNAs contributed to intramuscular fat content differences between Yorkshire and Wei pigs. *Int J Mol Sci.* (2020) 21:1732. doi: 10.3390/ijms21051732

24. Ochsner KP, MacNeil MD, Lewis RM, Spangler ML. Economic selection index development for Beefmaster cattle I: terminal breeding objective. *J Anim Sci.* (2017) 95:1063–70. doi: 10.2527/jas.2016.1231

25. Gao Y, Zhang R, Hu X, Li N. Application of genomic technologies to the improvement of meat quality of farm animals. *Meat Sci.* (2007) 77:36–45. doi: 10.1016/j.meatsci.2007.03.026

26. Mortimer SI, van der Werf JHJ, Jacob RH, Hopkins DL, Pannier L, Pearce KL, et al. Genetic parameters for meat quality traits of Australian lamb meat. *Meat Sci.* (2014) 96:1016–24. doi: 10.1016/j.meatsci.2013.09.007

27. Pena F, Juarez M, Bonvillani A, Garcia P, Polvillo O, Domenech V. Muscle and genotype effects on fatty acid composition of goat kid intramuscular fat. *Ital J Anim Sci.* (2011) 10:212–6. doi: 10.4081/ijas.2011.e40

28. Ma JW, Yang J, Zhou LS, Ren J, Liu XX, Zhang H, et al. A splice mutation in the PHKG1 gene causes high glycogen content and low meat quality in pig skeletal muscle. *PLoS Genet.* (2014) 10:e1004710. doi: 10.1371/journal.pgen.1004710

29. Li BJ, Weng QN, Dong C, Zhang ZK, Li RY, Liu JG, et al. A key gene, PLIN1, can affect porcine intramuscular fat content based on transcriptome analysis. *Genes*. (2018) 9:194. doi: 10.3390/genes9040194

30. Ma C, Wang WW, Wang YD, Sun Y, Kang L, Zhang Q, et al. TMT-labeled quantitative proteomic analyses on the longissimus dorsi to identify the proteins underlying intramuscular fat content in pigs. *J Proteomics*. (2020) 213:103630. doi: 10.1016/j.jprot.2019.103630

31. Hou XH, Liu QF, Meng QS, Wang LG, Yan H, Zhang LC, et al. TMT-based quantitative proteomic analysis of porcine muscle associated with postmortem meat quality. *Food Chem.* (2020) 328:127133. doi: 10.1016/j.foodchem.2020.127133

32. Ma DY, Yu QQ, Hedrick VE, Cooper BR, Sobreira TJP, Oh JH, et al. Proteomic and metabolomic profiling reveals the involvement of apoptosis in meat quality characteristics of ovine M. longissimus from different callipyge genotypes. *Meat Sci.* (2020) 166:108140. doi: 10.1016/j.meatsci.2020.108140

33. Poleti MD, Regitano LCA, Souza G, Cesar ASM, Simas RC, Silva-Vignato B, et al. Longissimus dorsi muscle label-free quantitative proteomic reveals biological mechanisms associated with intramuscular fat deposition. *J Proteomics.* (2018) 179:30–41. doi: 10.1016/j.jprot.2018.02.028

34. Zhang J, Cao J, Geng A, Wang H, Chu Q, Yang L, et al. Comprehensive proteomic characterization of the pectoralis major at three chronological ages in Beijing-you chicken. *Front Physiol.* (2021) 12:658711. doi: 10.3389/fphys.2021.658711

35. Li W, Li M, Cao X, Han H, Kong F, Yue X. Comparative analysis of whey proteins in donkey colostrum and mature milk using quantitative proteomics. *Food Res Int.* (2020) 127:108741. doi: 10.1016/j.foodres.2019.108741

36. Zhang X, Jiang B, Ji C, Li H, Yang L, Jiang G, et al. Quantitative label-free proteomic analysis of milk fat globule membrane in donkey and human milk. *Front Nutr.* (2021) 8:670099. doi: 10.3389/fnut.2021.670099

37. Li B, Feng C, Zhu S, Zhang J, Irwin DM, Zhang X, et al. Identification of candidate circular RNAs underlying intramuscular fat content in the donkey. *Front Genet.* (2020) 11:587559. doi: 10.3389/fgene.2020.587559

38. Wisniewski JR, Zougman A, Nagaraj N, Mann M. Universal sample preparation method for proteome analysis. *Nat Methods.* (2009) 6:359–62. doi: 10.1038/nmeth.1322

39. Ashburner M, Ball CA, Blake JA, Botstein D, Butler H, Cherry JM, et al. Gene ontology: tool for the unification of biology. *Gene Ontol Consortium Nat Genet.* (2000) 25:25–9. doi: 10.1038/75556

40. Gotz S, Garcia-Gomez JM, Terol J, Williams TD, Nagaraj SH, Nueda MJ, et al. High-throughput functional annotation and data mining with the Blast2GO suite. *Nucleic Acids Res.* (2008) 36:3420–35. doi: 10.1093/nar/gkn176

41. Kanehisa M, Goto S, Sato Y, Furumichi M, Tanabe M KEGG. for integration and interpretation of large-scale molecular data sets. *Nucleic Acids Res.* (2012) 40:D109–114. doi: 10.1093/nar/gkr988

42. Szklarczyk D, Gable AL, Lyon D, Junge A, Wyder S, Huerta-Cepas J, et al. STRING v11: protein-protein association networks with increased coverage, supporting functional discovery in genome-wide experimental datasets. *Nucleic Acids Res.* (2019) 47:D607–13. doi: 10.1093/nar/gky1131

43. Shannon P, Markiel A, Ozier O, Baliga NS, Wang JT, Ramage D, et al. Cytoscape: a software environment for integrated models of biomolecular interaction networks. *Genome Res.* (2003) 13:2498–504. doi: 10.1101/gr.1239303

44. Liu G, Wong L, Chua HN. Complex discovery from weighted PPI networks. *Bioinformatics.* (2009) 25:1891–7. doi: 10.1093/bioinformatics/btp311

45. Polidori P, Cammertoni N, Santini G, Klimanova Y, Zhang JJ, Vincenzetti S. Effects of donkeys rearing system on performance indices, carcass, and meat quality. *Foods*. (2021) 10:3119. doi: 10.3390/foods10123119

46. Du Y, Wang Y, Xu Q, Zhu J, Lin Y. TMT-based quantitative proteomics analysis reveals the key proteins related with the differentiation process of goat intramuscular adipocytes. *BMC Genom.* (2021) 22:417. doi: 10.1186/s12864-021-07730-y

47. Noguchi M, Hosoda K, Fujikura J, Fujimoto M, Iwakura H, Tomita T, et al. Genetic and pharmacological inhibition of Rho-associated kinase II enhances adipogenesis. *J Biol Chem.* (2007) 282:29574. doi: 10.1074/jbc.M705972200

48. Ahbara A, Bahbahani H, Almathen F, Al Abri M, Agoub MO, Abeba A, et al. Genome-wide variation, candidate regions and genes associated with fat deposition and tail morphology in Ethiopian indigenous sheep. *Front Genet.* (2018) 9:699. doi: 10.3389/fgene.2018.00699

49. Yamada T, Sasaki S, Sukegawa S, Miyake T, Fujita T, Kose H, et al. Association of a single nucleotide polymorphism in ribosomal protein L27a gene with marbling in Japanese Black beef cattle. *Anim Sci J.* (2009) 80:631–5. doi: 10.1111/j.1740-0929.2009.00688.x

50. Tu ZL Yu B, Huang DY, Ojha R, Zhou SK, An HD, et al. Proteomic analysis and comparison of intra and extracranial cerebral atherosclerosis responses to hyperlipidemia in rabbits. *Mol Med Rep.* (2017) 16:2347–54. doi: 10.3892/mmr.2017.6869

51. Kim DI, Park MJ, Lim SK, Park JI, Yoon KC, Han HJ, et al. PRMT3 regulates hepatic lipogenesis through direct interaction with LXRα. *Diabetes*. (2015) 64:60. doi: 10.2337/db13-1394

52. Zhao X, Yang Y, Sun BF, Yue S, Xin Y, Xiao W, et al. FTO-dependent demethylation of N6-methyladenosine regulates mRNA splicing and is required for adipogenesis. *Cell Res.* 24:1403–19. doi: 10.1038/cr.2014.151

53. Liu F, Clark W, Luo G, Wang X, He CJC. ALKBH1-mediated tRNA demethylation regulates translation. (2016) 167:233–47. doi: 10.1016/j.cell.2016.11.045

54. Huang H, Song TJ Li X, Hu L, He Q, Liu M, et al. BMP signaling pathway is required for commitment of C3H10T1/2 pluripotent stem cells

to the adipocyte lineage. *Proc Natl Acad Sci USA*. (2009) 106:12670–5. doi: 10.1073/pnas.0906266106

55. Jung DS, Baik M Up-regulation of bone morphogenetic protein and its signaling molecules following castration of bulls and their association with intramuscular fat content in Korean cattle. *Sci Rep-UK*. (2019) 9:1–7. doi: 10.1038/s41598-019-56439-2

56. Sanyal A, Naumann J, Hoffmann LS, Chabowska-Kita A, Ehrlund A, Schlitzer A, et al. Interplay between obesity-induced inflammation and cGMP signaling in white adipose tissue. *Cell Rep*. (2017) 18:225. doi: 10.1016/j.celrep.2016.12.028

57. Ross SE, Hemati N, Longo KA, Bennett CN, Lucas PC, Erickson RL, et al. Inhibition of adipogenesis by Wnt signaling. *Science*. (2000) 289:950–3. doi: 10.1126/science.289.5481.950

58. Rosen ED, MacDougald OA. Adipocyte differentiation from the inside out. *Nat Rev Mol Cell Biol*. (2006) 7:885–96. doi: 10.1038/nrm2066

59. Wright WS, Longo KA, Dolinsky VW, Gerin I, Kang S, Bennett CN, et al. Wnt10b inhibits obesity in ob/ob and agouti mice. *Diabetes*. (2007) 56:295–303. doi: 10.2337/db06-1339

60. Hong JH, Hwang ES, McManus MT, Amsterdam A, Tian Y, Kalmukova RTAZ, a transcriptional modulator of mesenchymal stem cell differentiation. *J Sci*. (2005) 309:1074–8. doi: 10.1126/science.1110955

61. Deng K, Ren C, Fan Y, Pang J, Zhang G, Zhang Y, et al. YAP1 regulates PPARG and RXR alpha expression to affect the proliferation and differentiation of ovine preadipocyte. *J Cell Biochem*. (2019) 120:19578–89. doi: 10.1002/jcb.29265

62. Ibar C, Irvine KD. DC integration of hippo-YAP signaling with metabolism. *Dev Cell*. (2020) 54:256–67. doi: 10.1016/j.devcel.2020.06.025

63. Park BH, Kim DS, Won GW, Jeon HJ, Oh BC, Lee Y, et al. Mammalian Ste20-like kinase and SAV1 promote 3T3-L1 adipocyte differentiation by activation of PPARγ. *PLoS ONE*. (2012) 7:e30983. doi: 10.1371/journal.pone.0030983

frontiers | Frontiers in Veterinary Science

TYPE Original Research
PUBLISHED 08 August 2022
DOI 10.3389/fvets.2022.982258

OPEN ACCESS

EDITED BY
Rajwali Khan,
University of Agriculture, Pakistan

REVIEWED BY
Xiao Li,
Northwest A&F University, China
Shuting Xiong,
Hunan Agricultural University, China
Longchao Zhang,
Institute of Animal Sciences (CAAS), China

*CORRESPONDENCE
Di Liu
liudi1963@163.com
Xiuqin Yang
xiuqinyang@neau.edu.cn

†These authors have contributed equally to this work

SPECIALTY SECTION
This article was submitted to Livestock Genomics, a section of the journal Frontiers in Veterinary Science

RECEIVED 30 June 2022
ACCEPTED 18 July 2022
PUBLISHED 08 August 2022

CITATION
Sun Y, Lin X, Zhang Q, Pang Y, Zhang X, Zhao X, Liu D and Yang X (2022) Genome-wide characterization of lncRNAs and mRNAs in muscles with differential intramuscular fat contents. *Front. Vet. Sci.* 9:982258. doi: 10.3389/fvets.2022.982258

Genome-wide characterization of lncRNAs and mRNAs in muscles with differential intramuscular fat contents

Yuanlu Sun[1†], Xu Lin[1†], Qian Zhang[1], Yu Pang[1], Xiaohan Zhang[1], Xuelian Zhao[1], Di Liu[2*] and Xiuqin Yang[1*]

[1]College of Animal Science and Technology, Northeast Agricultural University, Harbin, China, [2]Heilongjiang Academy of Agricultural Sciences, Harbin, China

Meat quality is one of the most important traits in pig production. Long non-coding RNAs (lncRNAs) have been involved in diverse biological processes such as muscle development through regulating gene expression. However, studies on lncRNAs lag behind and a comparatively small number of lncRNAs have been identified in pigs. Also, the effects of lncRNAs on meat quality remain to be characterized. Here, we analyzed lncRNAs in longissimus thoracis (LT) and semitendinosus (ST) muscles, being different in meat quality, with RNA-sequencing technology. A total of 500 differentially expressed lncRNAs (DELs) and 2,094 protein-coding genes (DEGs) were identified. Through KEGG analysis on DELs, we first made clear that fat deposition might be the main reason resulting in the differential phenotype of LT and ST, for which cGMP–PKG and VEGF signaling pathways were the most important ones. In total, forty-one key DELs and 50 DEGs involved in the differential fat deposition were then characterized. One of the key genes, cAMP-response element binding protein 1, was selected to confirm its role in porcine adipogenesis with molecular biology methods and found that it promotes the differentiation of porcine preadipocytes, consistent with its higher expression level and intramuscular fat contents in LT than that in ST muscle. Furthermore, through integrated analysis of DELs and DEGs, transcription factors important for differential fat deposition were characterized among which BCL6 has the most target DEGs while MEF2A was targeted by the most DELs. The results provide candidate genes crucial for meat quality, which will contribute to improving meat quality with molecular-breeding strategies.

KEYWORDS

meat quality, lncRNA, fat deposition, CREB1, adipogenesis

Introduction

Meat quality is one of the most important economic traits in pig breeding. With the improvement of living standards, people have paid more and more attention to meat quality. Meat quality parameters determining the visual appearance of meat, such as color, tender, water holding capacity, etc., have become crucial for consumer acceptability, which is an incentive for pig breeders and farmers to improve meat quality. However, meat quality is a comprehensive indicator and most of the traits

have low-to-moderate heritability (1, 2). In addition, some items of meat quality are negatively correlated with lean meat percentage and growth traits. Thus, it is difficult to improve meat quality through traditional methods. Molecular-breeding strategies such as marker-assisted selection, gene modification, etc., should be preferred means for which revealing the mechanisms underlying meat quality is the prerequisite.

Numerous efforts have focused on meat quality. It has been shown that *RN*, *RYR1*, *PHKG1*, *IGF2*, and *RAKG3* are major genes controlling meat-quality traits (2–6) and various candidate genes were identified as well (7–9). The development of next-generation sequencing technology made it convenient and efficient to identify candidate genes, especially novel and/or low-abundance transcripts such as long non-coding RNAs (lncRNAs), at the genome-wide level.

Long non-coding RNAs are a class of RNAs with more than 200 nucleotides in length. It was initially identified as mRNA-like transcripts with no protein-coding capability (10). LncRNAs engage in diverse biological processes through regulating gene expression at transcriptional, translational, and post-translational levels (11). LncRNA profiling has been made at a genome-wide level in skeletal muscles and differentially expressed lncRNAs (DELs) were identified with RNA-sequencing (RNA-seq) technology (12–14). But compared to that in humans and mice, studies on lncRNAs lag behind and there are numerous classes of lncRNAs to be identified in pigs. Also, the effects of lncRNAs on meat quality remain to be characterized.

Min pig is a Chinese indigenous breed and excellent in meat quality. Longissimus thoracis (LT) and semitendinosus (ST) exhibit differences in many parameters of meat quality such as tenderness and lightness value (15). Intramuscular fat (IMF) content, correlated positively with meat quality, is also different between LT and ST muscles (16). In addition, LT and ST samples from the same pig can avoid the influence of individual differences and be compared stringently to reveal mechanisms underlying their differential phenotype. Thus LT and ST muscles are good materials for clarification of mechanisms underlying meat quality. To the best of our knowledge, no studies were found aimed at identifying candidate lncRNAs for meat quality in LT and ST muscles. Here, lncRNA profiling was made in LT and ST muscles to characterize DELs with RNA-seq technology, and key lncRNAs and protein-coding genes involved in the formation of fat deposition were found. The results will contribute to further revealing mechanisms underlying meat quality.

Materials and methods

Animals, samples, and RNA isolation

Min pigs, a Chinese local pig breeds, were used here and obtained from the Institute of Animal Husbandry, Heilongjiang Academy of Agricultural Sciences, Harbin, China. LT and ST muscles were sampled from three 210-day-old individuals for RNA-seq analysis. Fat tissues were collected from new born piglets for isolating preadipocytes. Total RNA was isolated with TRIzol reagent (Invitrogen, CA, USA), assessed with agarose gel electrophoresis, and quantified with a Nanodrop 2000 (IMPLEN, CA, USA). All the procedures of animal treatment were strictly based on the protocol of the Animal Care Committee of Northeast Agricultural University.

Library construction and sequencing

Library preparation and RNA-sequencing were performed by Frasergen Inc. (Wuhan, China). In brief, three μg total RNA per sample was used for library construction. rRNA was first removed with Epicentre Ribo-zeroTM rRNA Removal Kit (Epicentre, Madison, WI, USA), and purified with ethanol precipitation. Next, sequencing libraries were constructed with NEBNext® UltraTM Directional RNA Library Prep Kit for Illumina® (NEB, Ipswich, MA, USA) according to the manufacturer's instructions. Then, 150–200 bp long cDNA fragments were selected with the AMPure XP system (Beckman Coulter, Brea, CA, USA). After being treated with USER Enzyme (NEB), PCR was performed with High-Fidelity DNA polymerase, and the products were purified with the AMPure XP system (Beckman Coulter). Afterward, the index-coded samples were clustered on a cBot Cluster Generation System with TrueSeq PE Cluster Kit v3-cBot-Hs (Illumina) based on the manufacturer's instructions. At last, the libraries were sequenced on an Illumina Noveseq platform.

Raw data processing

Raw reads were first filtered and trimmed using SOAPnuke with –lowQual = 20, –nRate = 0.005, and –qualRate = 0.5 to obtain clean reads. Q20, Q30, and GC contents of the clean reads were calculated by SOAPnuke. Paired-end clean reads were mapped to the reference genome (Sus scrofa 11.1, http://asia.ensembl.org/Sus_scrofa/Info/Index) using HISAT2 (2.1.0) and the coverage of RNA-seq reads was calculated by geneBody_coverage.py script of RSeQC software. Then, mapped reads were assembled using StringTie software in a reference-based approach. The expression level of transcripts was measured with fragments per kilobase of transcript per million fragments (FPKM) mapped, and those with FPKM > 0.1 in at least one sample were used for further analysis.

LncRNA characterization

Novel lncRNAs were identified by using CNCI (parameters: –m –p 1), CPC2 (default parameter), and

PLEK (parameters: –thread 4 –min length 200) softwares simultaneously, and those without coding potential by all of the three tools were considered as candidate lncRNAs. Differentially expressed lncRNAs (DELs) were screened with criteria: the absolute log2(fold change) > 1 and p-value < 0.05. Heatmap was plotted by online tools (https://www.bioinformatics.com.cn). To explore the function of lncRNAs, *cis*-target protein-coding genes were predicted within 100,000 bp upstream and downstream of lncRNAs, and they were subjected to Gene Ontology (GO) and Kyoto Encyclopedia of Genes and Genomes (KEGG) pathway analysis.

mRNA characterization

Differentially expressed mRNAs (DEmRs) were characterized with the same criteria as that for DELs, that is, | log2(fold change) | > 1 and p-value < 0.05. Search Tool for the Retrieval of InteractingGenes/Proteins (STRING) was used to reveal the interaction among the differentially expressed protein-coding genes (DEGs), and Cytoscape (Version 3.7.1) was used to visualize the relationship. Based on the minimum required interaction score of 0.7, the network was constructed, of which the core subnetwork was characterized by the radiality analysis. Radiality calculates the correlation between target genes and all nodes, namely, directly and indirectly related nodes, the rank of genes represents the degree of importance of genes in the protein–protein interaction (PPI) network more comprehensively. Parameter as follow: Crad (V)=[$\sum$wϵv ΔG+1-dist(v,w)]/ n-1 (ΔG represents diameter, dist(v,w) represents distance from any node to V, and n means total nodes). Transcription factors (TFs) were identified through searching the AnimalTFDB database (http://bioinfo.life.hust.edu.cn/ AnimalTFDB/, version 3.0) with hmmscan program. Target genes of TFs were predicted with Cistrome DB program (http://cistrome.org/db, accessed on 15 April 2022) with a score > 3, and TF-DEG pairs with a Pearson correlation coefficient in expression level > 0.8 were selected for further analysis.

Real-time quantitative PCR

Reverse transcription (RT) was performed with the PrimeScript^{TM} RT Reagent Kit (TaKaRa, Dalian, China) to synthesize cDNA according to the manufacturer's instructions. Real-time quantitative PCR (qPCR) was conducted with ChamQ Universal SYBR qPCR Master Mix (Vazyme, Nanjing, China) according to the manufacturer's instructions, each with three replicates. β-actin gene was used as a reference and 2–ΔΔCt (17) method was used to calculate the relative expression level of target genes. Primers used in qPCR was given in Supplementary Table S1.

Preadipocyte culture, differentiation, and oil red O staining

Primary preadipocytes culture and differentiation induction were described previously (18). Briefly, subcutaneous fat tissues were sampled from the newborn Min pigs and digested with 0.1% type I collagenase (Invitrogen), and then filtered through 400-mesh filters. The cells obtained were cultured in DMEM/F12 medium (Dulbecco's modified Eagle's medium/Nutrient Mixture F-12) containing 10% fetal bovine serum (FBS) and 1% penicillin–streptomycin. The medium was changed every 2 days.

For differentiation induction, cells were first cultured in DMEM/F12 medium supplemented with 10% FBS, 0.5 mmol/L 3-isobutyl−1-methylxanthine, 1 μmol/L dexamethasone and 5 μg/ml insulin for 2 days and then transferred into DMEM/F12 medium containing 10% FBS and 5 μg/ml insulin to maintain the differentiation.

The adipocytes were stained with an Oil Red O kit (Leagene, Beijing, China), and then viewed under a light microscope and photographed (Carl Zeiss AG, Jena, Germany). Cellular Oil Red O was then isolated with isopropanol and quantified with optical absorbance at 510 nm.

Transiently transfection

The coding sequence of the porcine cAMP-response element-binding protein 1 (CREB1) gene was amplified and subcloned into the pCMV-HA vector at enzyme sites EcoRI and XhoI to construct overexpression plasmids. SiRNA sequences were designed and synthesized by General Biol (Anhui, China) to knock down the expression of *CREB1* in preadipocytes. The optimal siRNA sequence, selected through preliminary experiments, was given in Supplementary Table S1. In total, 30 nmol/μl of siRNA or 0.5 μg of overexpression plasmids were transiently transfected into preadipocytes with Lipofectamine 2000 reagent (Invitrogen) according to the manufacturer's instructions. At 24 h after transfection, the cells were induced to differentiation. The cell culture medium was changed every 2 days and at 8 days post-induction, cells were stained with Oil Red O or collected to measure the expression of the adipogenic marker gene, peroxisome proliferator-activated receptor (PPAR)γ and CCAAT/enhancer-binding protein (C/EBP)α, with the qPCR method.

Statistical analysis

All the experiments were repeated at least three times independently, each with triplicate. Data were given as mean ± standard error. SPSS 19.0 software was used to analyze the data. The Student's t-test was performed to compare the difference

between the two groups. A $p < 0.05$ was considered to be statistically significant. Significant difference was indicated with * ($p < 0.05$) and ** ($p < 0.01$).

Results

Overview of lncRNA sequencing

After filtering out redundant and low quality reads, 65.36 and 68.66 million clean read pairs were obtained in LT and ST muscles on average, respectively, comprising at least 98% of Quality 20 (Q20) reads and 94.4% of Q30 reads. In each sample more than 94.9% clean reads were mapped to reference genome (Sus scrofa 11.1) (Supplementary Table S2-1).

A total of 13,635 lncRNAs and 38,468 mRNAs were obtained. Among them, 12,437 lncRNAs were novel as identified by CNCI, CPC, and PLEK programs, and 9473 mRNAs were novel, accounting for 91.21 and 24.63% of total lncRNAs and mRNAs, respectively (Supplementary Table S2-2). The majority of the novel lncRNAs were intronic, and antisense lncRNAs were the least (Figure 1A). The novel lncRNAs ranged from 201 to 31,717 bp in length with an average of 1,168 bp, and were composed of 2–66 exons with an average number of 4.5 (Supplementary Table S2-3). In general, lncRNAs are shorter than mRNAs in length and composed of fewer exons. The distributions of exon number and length of lncRNAs and mRNAs were shown in Figures 1B,C. The expression level of lncRNAs is lower than that of the mRNAs (Figure 1D). Although the abundance of unique lncRNAs is much lower than that of mRNAs in chromosomes, they have similar distribution: both the lncRNAs and mRNAs were mainly distributed on chromosomes 1 and 6 (Figure 1E).

Differentially expressed lncRNAs and their functions

To identify lncRNAs involved in the differential phenotype of two muscles, RNA-seq was performed and a total of 500 DELs were obtained with 245 upregulated and 255 downregulated in ST compared with LT muscle (Supplementary Table S3-1). Among the DELs, 108 were specific to ST tissue and 100 were specific to LT tissue (Figures 2A,B). Heatmap of top DELs were shown in Figure 2C. The differential expression of five DELs was validated by real-time quantitative PCR (qPCR) and consistent results were obtained except for one lncRNA, ENSSSCT00000080343.

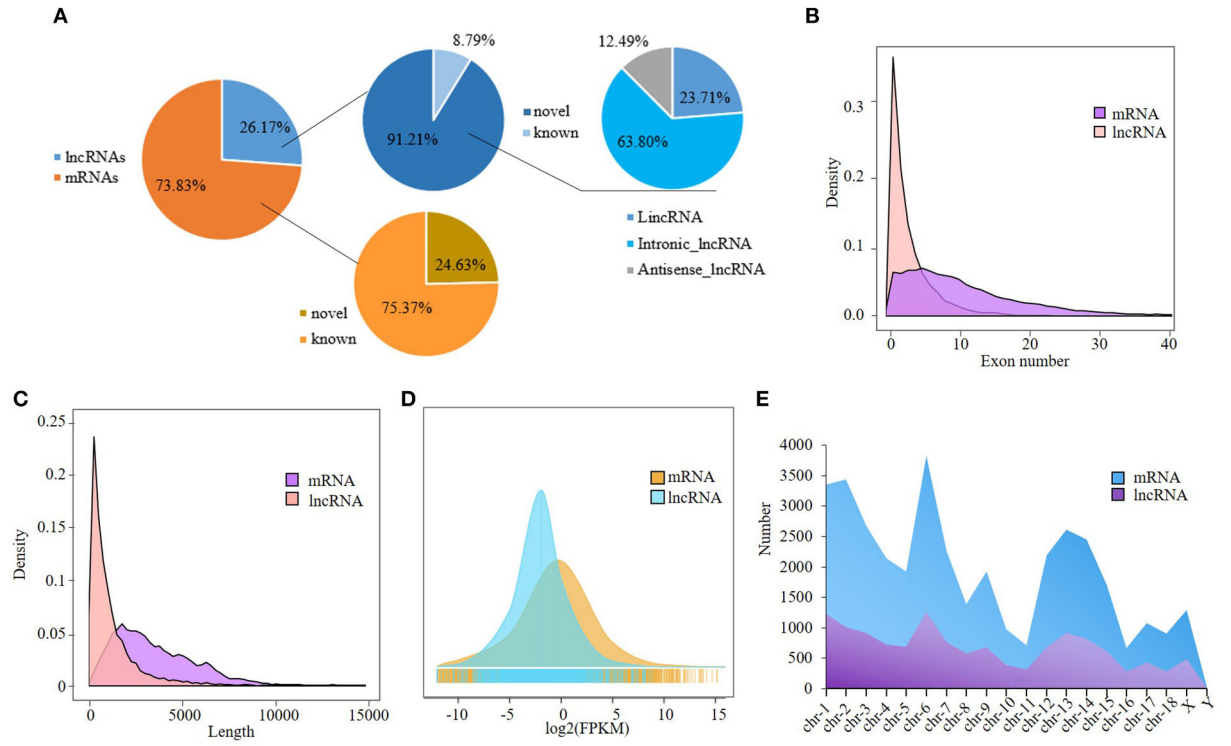

FIGURE 1
Analysis of RNA-seq data. **(A)** Classification of lncRNAs and mRNAs; **(B,C)** Transcript length and exon number distribution of the lncRNAs and mRNAs; **(D)** Distribution of the lncRNAs and mRNAs in chromosomes; **(E)** Expression level distribution of the lncRNAs and mRNAs.

It has a tendency to increase in ST compared with LT, but the difference was not as obvious as that in RNA-seq (Figure 2D). The results indicate that RNA-seq data was reliable.

Gene ontology and KEGG analyses were applied on the target genes of DELs. A total of 2,401 GO terms involved in categories of cellular component (CC), biological process (BP), and molecular function (MF) were enriched

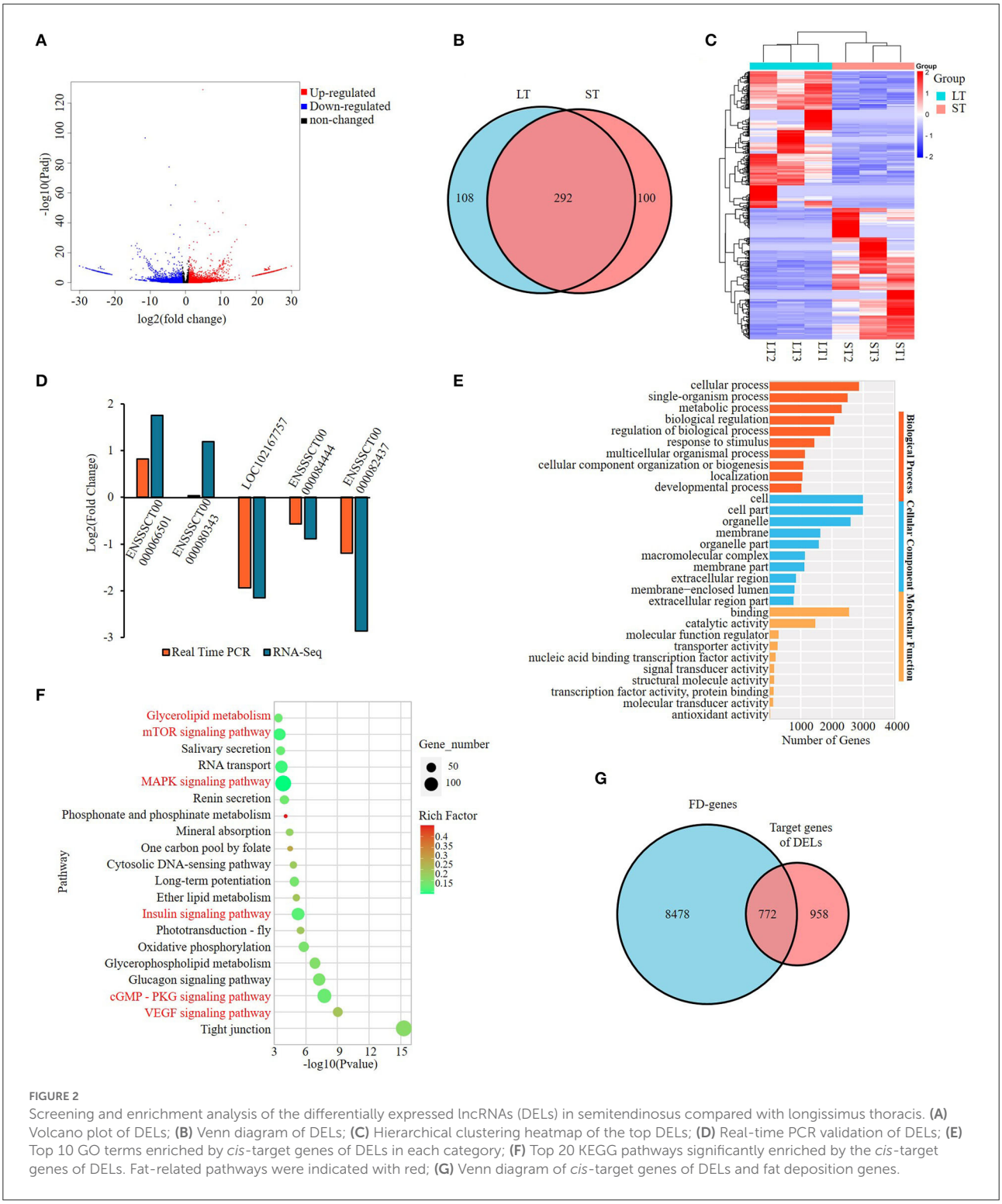

FIGURE 2
Screening and enrichment analysis of the differentially expressed lncRNAs (DELs) in semitendinosus compared with longissimus thoracis. **(A)** Volcano plot of DELs; **(B)** Venn diagram of DELs; **(C)** Hierarchical clustering heatmap of the top DELs; **(D)** Real-time PCR validation of DELs; **(E)** Top 10 GO terms enriched by *cis*-target genes of DELs in each category; **(F)** Top 20 KEGG pathways significantly enriched by the *cis*-target genes of DELs. Fat-related pathways were indicated with red; **(G)** Venn diagram of *cis*-target genes of DELs and fat deposition genes.

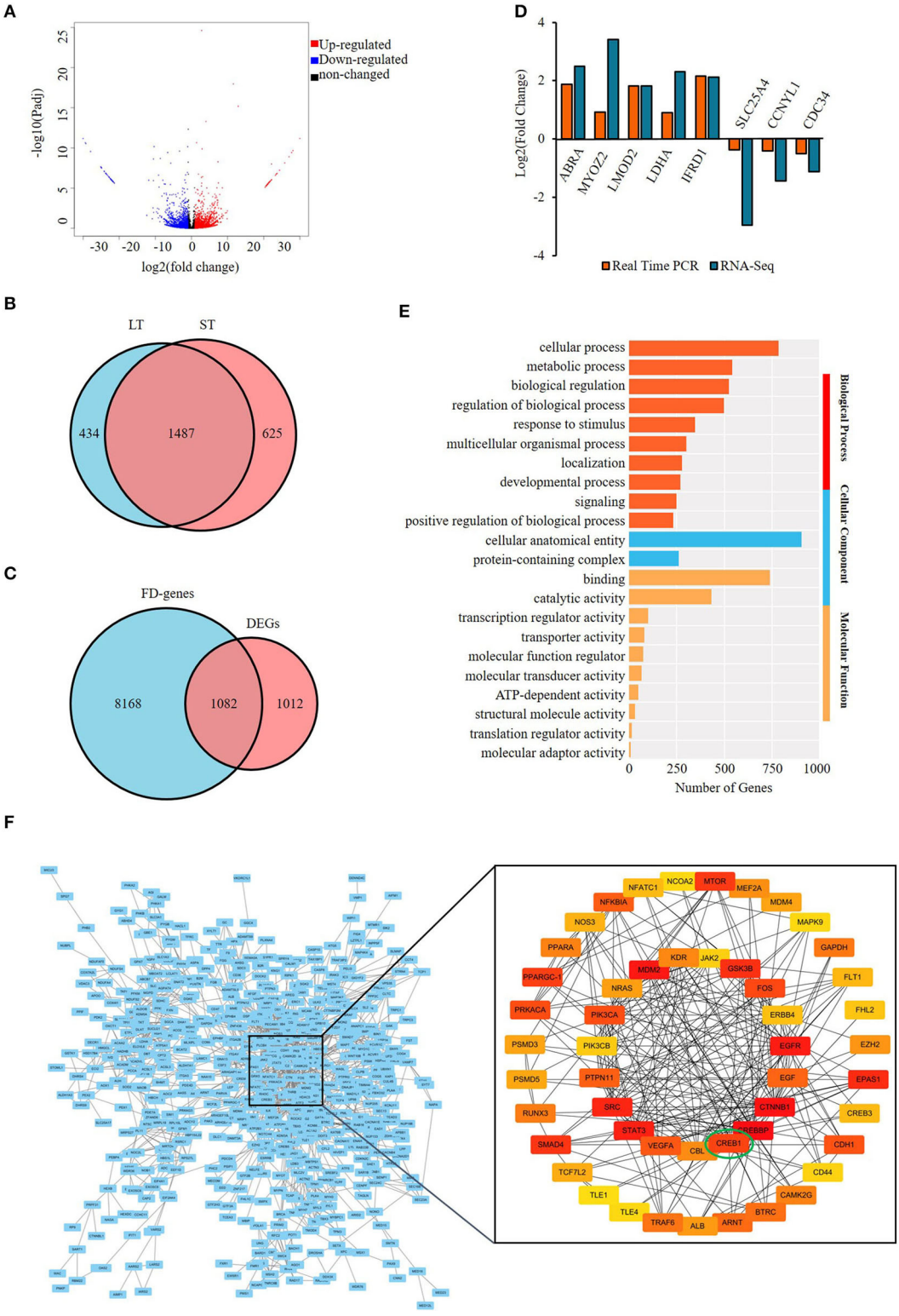

FIGURE 3
Screening and enrichment analysis of the differentially expressed genes (DEGs) in semitendinosus compared with longissimus thoracis. **(A)** Volcano plot of DEGs; **(B)** Venn diagram of differentially expressed mRNAs; **(C)** Venn diagram of DEGs and fat deposition genes; **(D)** real-time PCR validation of DE mRNA; **(E)** Top 10 GO terms enriched by FD–DEGs in each category.; **(F)** Protein–protein analysis of FD–DEGs. The minimum interaction score was set as 0.7. The color of the circle represents the degree of importance.

(Supplementary Table S3-2). Cell and cell part were the GO terms enriched with the most genes among all three categories, while in BP category metabolic process is the most highly enriched GO terms with over 2,000 genes (Figure 2E). The KEGG analysis showed that DELs were mainly enriched in fat-related pathways significantly ($p < 0.05$) (Supplementary Table S3-3). Of the top 20 pathways, six were involved in adipogenesis, namely, VEGF signaling pathway, cGMP-PKG signaling pathway, Insulin signaling pathway, MAPK signaling pathway, mTOR signaling pathway, and Glycerolipid metabolism, among which VEGF and cGMP–PKG ranked top 2 and 3, respectively (Figure 2F).

To further identify the role of DELs, we downloaded 9,250 fat deposition (FD) genes from GeneCards database (https://www.genecards.org/, accessed on 15 Apr 2022) and found that 772 target genes of DELs were included in the FD gene list, representing 44.6% of all target genes of DELs (Figure 2G; Supplementary Table S3-4). Of the 500 DELs identified, 71.6% (358) have target genes belonging to the list and were named FD–DELs here (Supplementary Table S3-5). In addition, 59.5% of target genes involved in the top 20 significantly enriched pathways were FD genes (Supplementary Table S3-6). These results suggest that fat deposition might be the main reason resulting in the differential phenotype of two muscles. Thereafter, we will focus on FD-genes to reveal the difference between the two muscles in the following analysis.

Analysis of differentially expressed protein-coding genes and their functions

A total of 2,094 differentially expressed protein-coding genes (DEGs), covering 2,546 DEmRs were identified. Among the DEmRs, 1,495 were upregulated and 1,051 downregulated in the ST compared with LT (Figure 3A) (Supplementary Table S4-1); 625 and 434 were specifically expressed in ST and LT, respectively (Figure 3B). The intersection of DEGs and FD genes showed that 1,082 were FD–DEGs, accounting for 51.2% of total DEGs (Figure 3C; Supplementary Table S4-2). The differential expression of eight DEGs was validated with qPCR, and consistent results were obtained (Figure 3D).

The FD–DEGs were enriched in various GO terms involved in BP, MF, and CC (Supplementary Table S4-3). In the BP category, cellular process is the most highly enriched terms with 786 genes (Figure 3E). To explore the interaction among the FD–DEGs identified, PPI analysis was performed and genes with a score > 0.7 were visualized with cytoscape (Version 3.7.1) (Figure 3F). The subnetwork constructed consists of 50 nodes and 230 edges. The number of edges in each node is ranged from 2 to 30. Epidermis growth factor (EGF) receptor (EGFR), signal transducer, and activator of transcription 3 (STAT3), cAMP-response element binding protein 1 (*CREB1*)-binding protein (CREBBP) and catenin beta 1 have the most edges. *CREB1* has 12 edges and is ranked 12 among all the genes. These 50 genes, namely, PPARα, PPARγ coactivator-1 (PPARGC-1), EGF, vascular endothelial growth factor A, and *CREB1* should be the key protein-coding genes engaged in the differential deposition of fat between two muscles (Supplementary Table S4-4).

Effects of CREB1 on porcine adipogenesis

Among the 50 key DEGs, *CREB1* was only expressed in LT muscle which has more intramuscular fat (IMF) content

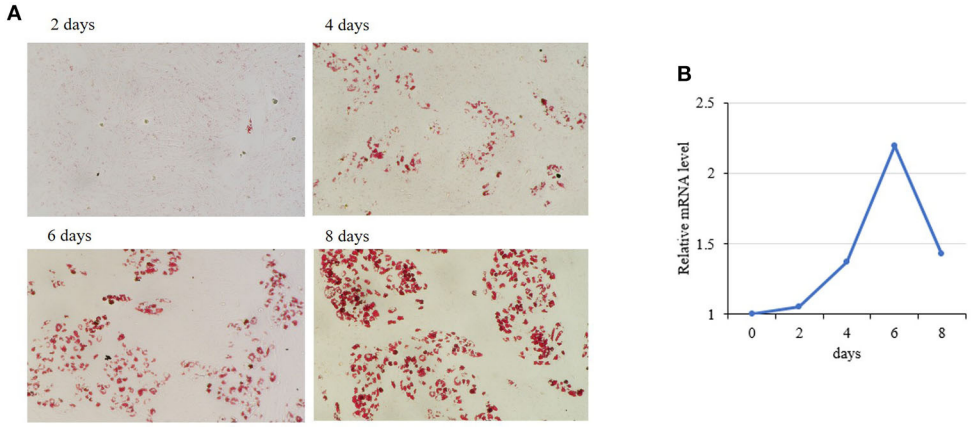

FIGURE 4
Expression of porcine *CREB1* during differentiation of preadipocytes. **(A)** Oil Red O staining of preadipocytes during differentiation induction; **(B)** relative mRNA level of *CREB1* during differentiation of preadipocytes.

than that of ST. To confirm the role of these key DEGs in the differential fat deposition between two muscles, we analyzed *CREB1* in primary cultured porcine preadipocytes. Oil Red O staining showed that the preadipocytes were induced to differentiation successfully (Figure 4A). During the preadipocyte differentiation, the expression of *CREB1* increased gradually with the highest level at 6-days post-induction (Figure 4B). Overexpression and knockdown of *CREB1* were used to explore the functions and transfection efficiency was shown in Supplementary Figure S1. Overexpression of *CREB1* promotes the differentiation of preadipocytes as revealed by Oil Red O staining at 8 days post-induction (Figure 5A), which was confirmed with quantification assay (Figure 5B). Furthermore, the relative mRNA level of the adipogenic marker, PPARγ, and C/EBPα, increased significantly ($p < 0.01$) (Figure 5C). Consistently, knockdown of *CREB1* by siRNA inhibits the differentiation of preadipocytes as revealed by both Oil Red O staining and quantification assay (Figures 5D,E), and the relative mRNA level of PPARγ was decreased significantly ($p < 0.01$) (Figure 5F). Thus, *CREB1* promotes the differentiation of porcine preadipocytes, that is, promotes adipogenesis, which is consistent with its higher expression level and fat contents in LT than that in ST muscle.

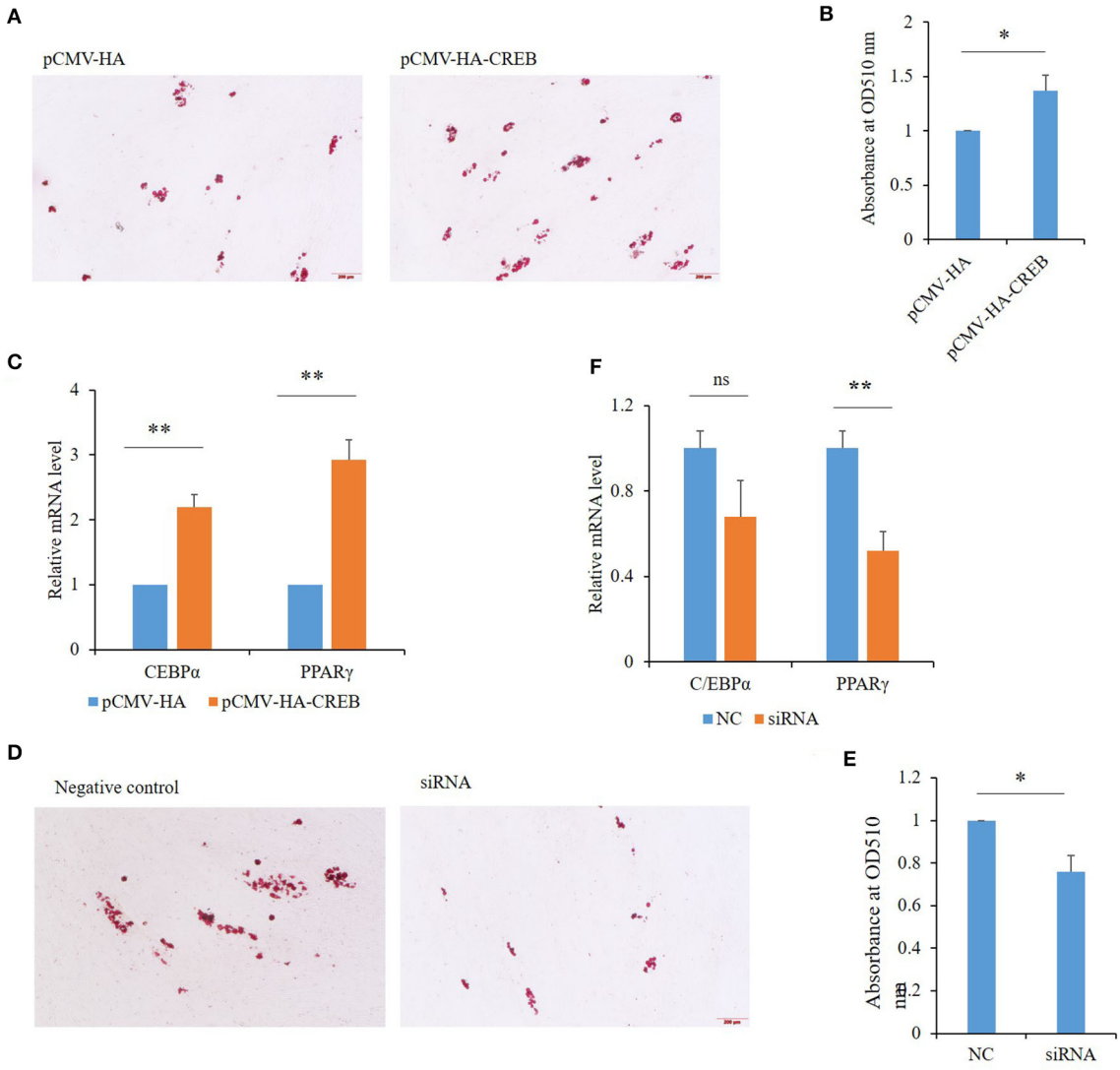

FIGURE 5
Effects of *CREB1* on porcine preadipocyte differentiation. **(A)** Oil Red O staining of preadipocytes overexpressing *CREB1* gene at 8 days post-induction; **(B)** quantitative analysis of triglyceride contents in preadipocytes overexpressing *CREB1* gene with optical absorbance; **(C)** expression of C/EBPα and PPARγ in preadipocytes overexpressing *CREB1* gene; **(D)** Oil Red O staining of preadipocytes knocked down for *CREB1* gene at 8 days post-induction; **(E)** quantitative analysis of triglyceride contents in preadipocytes knocked down for *CREB1* gene with optical absorbance; **(F)** expression of C/EBPα and PPARγ in preadipocytes knocked down for *CREB1* gene. *$p < 0.05$, **$p < 0.01$.

Integrated analysis of DELs and DEGs

Characterization of key lncRNAs

Through integrated analysis of FD–DELs and FD–DEGs, we found that 142 FD–DELs have *cis*-target genes covered by FD–DEGs. Coexpression analysis showed that 41 of 142 FD–DELs have a correlation coefficient > 0.9 with target genes. These 41 FD–DELs were expressed stably among samples, and thereafter, can be used as key lncRNAs in future studies revealing the mechanisms underlying the differential fat contents between two muscles (Figure 6).

Transcription factor characterization

In total, 265 out of the FD–DEGs were characterized as TFs, that is, FD–DETFs, through searching the AnimalTFDB database with hmmscan program (Supplementary Table S5-1). Among the FD–DETFs, 26 were *cis*-targets of FD–DELs, corresponding to 33 FD–DELs (Supplementary Table S5-2). In addition, target genes of the 26 FD–DETFs were characterized by Cistrome DB program with a score of > 3 and DETF-DEG pairs with a Pearson correlation coefficient of > 0.8 were selected (Supplementary Table S5-3). To reveal the relationship between these FD–DETFs, FD–DELs, and FD–DEGs, a network was constructed. A total of five FD–DETFs, eight FD–DELs and 95 FD–DEGs were included in the network in which BCL6 has the most target FD–DEGs, while MEF2A was targeted by the most FD–DELs (Figure 7).

Discussion

Intramuscular fat deposition is crucial for improving meat quality as its content is positively correlated with tenderness, juiciness, flavor, etc. (19). Meat marbling, a continuing demand for livestock production, is determined by IMF content. There is an obvious difference between LT and ST muscles in IMF content and lipid deposition: LT has higher IMF content and earlier deposition of lipid than ST in pigs (16). Here, through genome-wide analysis of lncRNAs involved in the differential phenotype of LT and ST, we first made clear that fat deposition in them, that is, IMF, might be the main reason leading to the difference, and that cGMP–PKG and VEGF signaling pathways were the most important pathways regulating the difference. The key DELs and DEGs related to fat deposition were then identified, and the involvement of these key genes in adipogenesis in pigs was validated with molecular biological methods in which *CREB1* was taken as an example and consistent results were obtained. In addition, TFs important for differential fat deposition were characterized. All in all, we provide candidate genes for further clarifying the mechanisms underlying meat quality.

Owing to its importance in improving meat quality, many studies have focused on revealing the mechanisms underlying IMF content, and some lncRNAs have been implicated in IMF content in recent years, namely, LncIMF4 (20), IMFNCR (21), IRLnc (22), IMFlnc1 (23), etc. Efforts were also made to characterize lncRNAs involved in IMF deposition at the

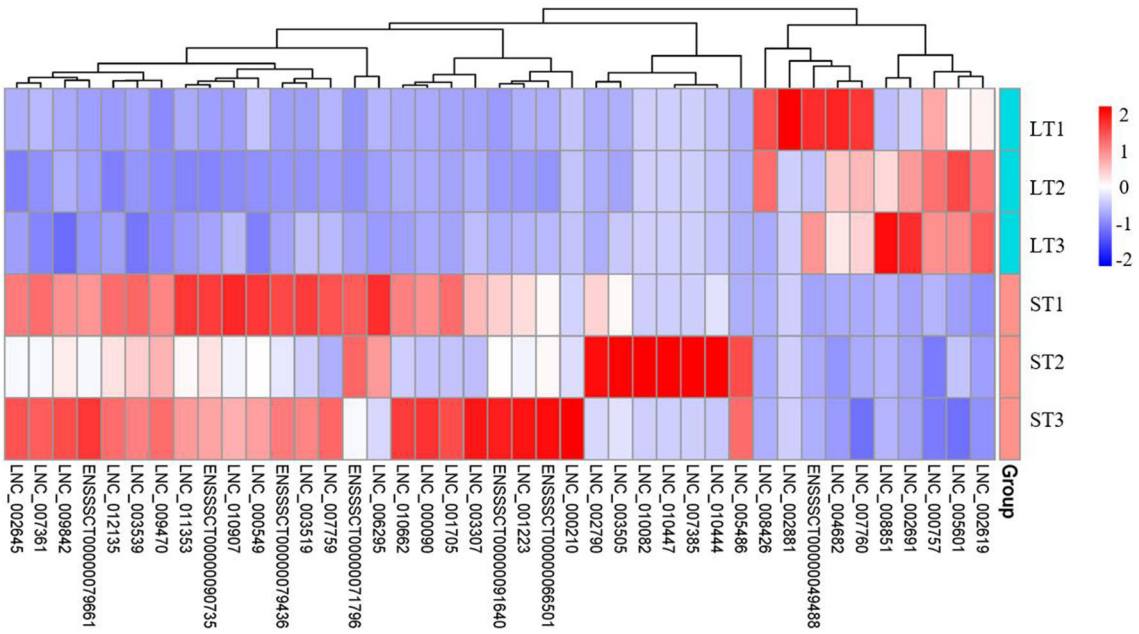

FIGURE 6
Hierarchical clustering heatmap of key lncRNAs.

genome-wide level in pigs (24–26). However, IMF is a highly complicated and metabolically active trait in which genetic factors involved are distinctive and diverse. There are often differences in the genetic cause of IMF accumulation, and the association between genetic markers and IMF content is not always consistent between breeds. Thereafter, it is necessary to identify lncRNAs related to the IMF content in pig breeds such as Min that have not been studied. To the best of our knowledge, no studies focused on revealing lncRNAs involved in differential IMF contents between LT and ST muscles yet. We identified 12,437 novel lncRNAs in the skeletal muscles of Min pigs further indicating the heterogeneous and diverse of lncRNAs. LncRNAs in Min pigs share similarities in structure and classification with their counterparts in mammals (27–29). The number of lncRNAs identified here is somewhat higher than that in other pig breeds such as Duroc, Landrace, and Guizhou miniature pigs (30–33), which might be caused by the rich genetic resource in Min pigs, and also by the different screening criteria used for lncRNA characterization.

A total of 500 DELs were identified between LT and ST muscles in Min pigs. Through integrated analysis of DELs and DEGs, 41 key lncRNAs related to differential IMF content between LT and ST muscles were characterized. Only seven of the key lncRNAs were known, indicating enormous genetic information involved in IMF deposition remains to be identified. These key lncRNAs will be the emphasis in clarifying the differential IMF content between LT and ST muscles in the future study. In addition, 50 key DEGs engaged in differential fat deposition between the two muscles were characterized including widely known fat-related genes such as PPARα (34), PPARGC-1 (35), mTOR (36), EGF and its receptor, EGFR (37).

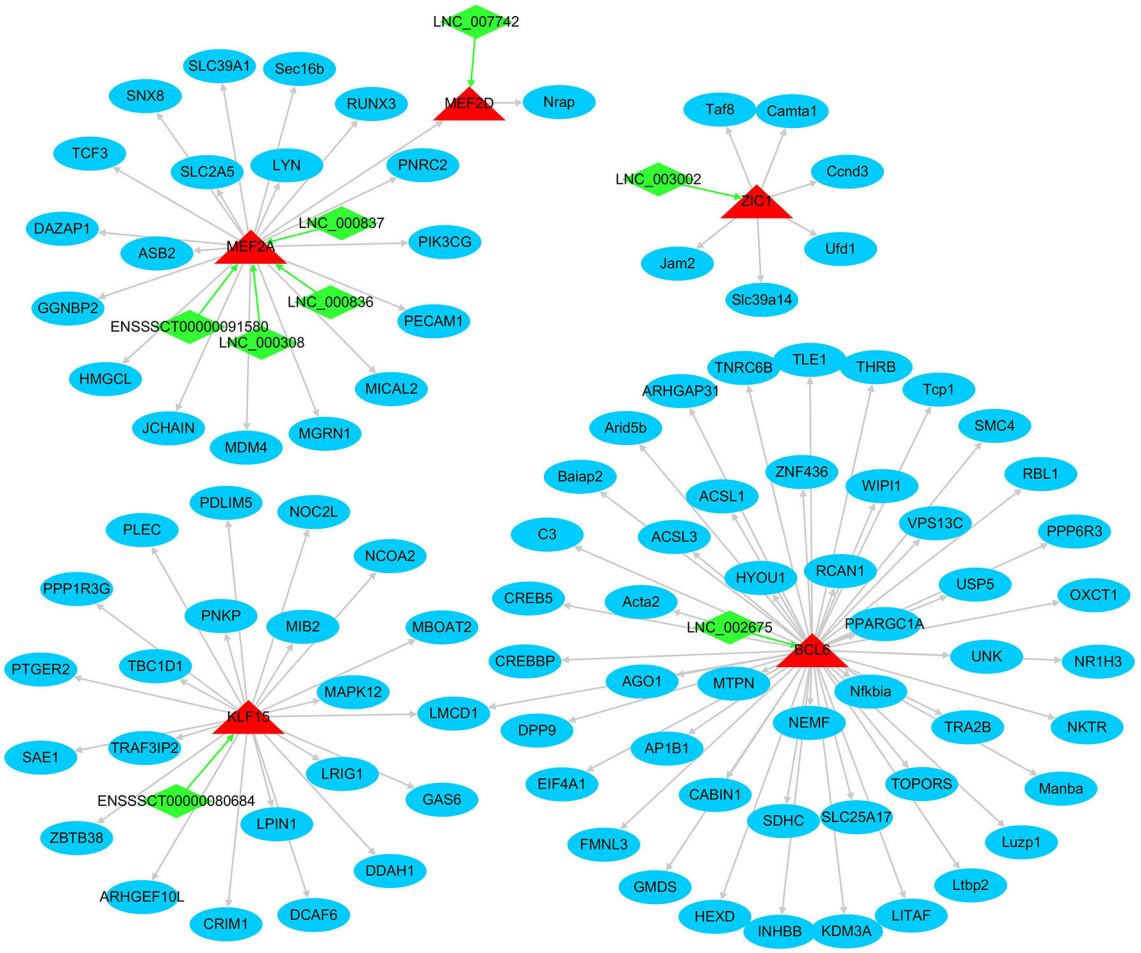

FIGURE 7
The network formed by fat deposition (FD)-differentially expressed transcription factors, FD-differentially expressed lncRNAs, and FD-differentially expressed genes. Arrows indicate the target direction. The green quadrilateral represents lncRNA, the red triangle represents TF, and the blue circle represents mRNA.

CREB1 and the binding protein, CREBBP, genes were also identified as key factors influencing the fat deposition in LT and ST muscles. *CREB1*, also named CREB, has been involved in adipogenesis in mice (38–40). Expression of constitutively active CREB alone in 3T3-L1 cells was sufficient to induce adipogenesis, while ectopic expression of a dominant-negative CREB protein blocked adipogenesis effectively in cells treated with differentiation-inducing agents (38). Depletion of *CREB1* inhibits the adipogenic conversion of 3T3-L1 cells overexpressing C/EBPα, C/EBPβ, or PPARγ2 (39). *CREB1* drives the expression of several adipocyte-specific genes such as fatty acid binding protein and fatty acid synthetase through binding to the putative cAMP response elements in the promoter (38, 41). However, all the aforementioned studies were performed in cell lines, 3T3-L1, and little was known about pig *CREB1*. Here, in primary-cultured porcine preadipocytes, we showed that porcine *CREB1* promotes adipogenesis. The results not only confirmed the reliability of data characterized by bioinformatic approaches here but contribute to further revealing the role of CREB1 in adipogenesis.

Adipogenesis is a highly orchestrated process of cell differentiation from preadipocytes to mature adipocytes in which TFs are the best-understood regulators (42). It is an elegant progression controlled by the TF cascade which is followed by the expression of adipocyte genes. The sequential activation of TFs is the prerequisite for adipogenesis. To date, many TFs such as PPARγ, C/EBP, and Krüppel-like factors, etc., have been found to play important roles in preadipocyte differentiation. These TFs come from a large variety of families and have many different DNA-binding domains, which provide the basis for transcriptionally activating the expression of a large number of adipocyte genes. Although substantial ongoing progress has been made in our understanding of adipogenesis, more regulators of adipocyte development including TFs remain to be identified (42). Here, through integrated analysis of DELs and DEGs, we characterized important TFs, and their interactive genes and lncRNAs involved in the differential fat deposition between LT and ST muscles. It is worth revealing their role in IMF deposition with molecular biology approaches.

Data availability statement

The datasets presented in this study are deposited in the NCBI GEO repository, accession number: GSE207449.

Ethics statement

The animal study was reviewed and approved by Laboratory Animal Welfare and Ethics Committee of Northeast Agricultural University.

Author contributions

XY and DL: funding acquisition and writing–reviewing. XY: conceptualization. YS, XL, QZ, XZhan, and XZhao: investigation. YP and XL: data analysis. XY and YS: writing. All authors contributed to the article and approved the submitted version.

Funding

This research was funded by the National Natural Science Foundation of China (32172696) and the China Postdoctoral Science Foundation (2020M670876). Heilongjiang operation expenses for scientific research (CZKYF2020A004).

Conflict of interest

The authors declare that the research was conducted in the absence of any commercial or financial relationships that could be construed as a potential conflict of interest.

Publisher's note

Supplementary material

The Supplementary Material for this article can be found online at: https://www.frontiersin.org/articles/10.3389/fvets.2022.982258/full#supplementary-material

SUPPLEMENTARY FIGURE S1
Efficiency of overexpressing or knockdown of *CREB1* in preadipocytes.

SUPPLEMENTARY TABLE S1
Primers used for real-time quantitative PCR.

SUPPLEMENTARY TABLE S2
Overview of RNA-seq data.

SUPPLEMENTARY TABLE S2-1
Quality of RNA-seq results.

SUPPLEMENTARY TABLE S2-2
Novel lncRNAs identified.

SUPPLEMENTARY TABLE S3
Analysis of differentially expressed lncRNAs.

SUPPLEMENTARY TABLE S3-1
Differentially expressed lncRNAs identified.

SUPPLEMENTARY TABLE S3-2
GO terms enrichment by differentially expressed lncRNAs.

SUPPLEMENTARY TABLE S3-3
KEGG pathways enriched by differentially expressed lncRNAs.

SUPPLEMENTARY TABLE S3-4
Target genes of differentially expressed lncRNA.

SUPPLEMENTARY TABLE S3-5
Differentially expressed lncRNAs involved in fat deposition.

SUPPLEMENTARY TABLE S3-6
Target genes involved in top 20 KEGG pathways.

SUPPLEMENTARY TABLE S4
Analysis of differentially expressed mRNAs.

SUPPLEMENTARY TABLE S4-1
Differentially expressed mRNAs identified.

SUPPLEMENTARY TABLE S4-2
Differentially expressed genes involved in fat deposition.

SUPPLEMENTARY TABLE S4-3
GO terms enriched by FD-DEGs.

SUPPLEMENTARY TABLE S4-4
Key protein-coding genes identified.

SUPPLEMENTARY TABLE S5
Characterization of transcription factors.

SUPPLEMENTARY TABLE S5-1
Differentially expressed transcription factors involved in fat deposition.

SUPPLEMENTARY TABLE S5-2
FD-DETFs belonging to cis-targets of FD-DELs.

SUPPLEMENTARY TABLE S5-3
Important DEGs targeted by FD-DETFs.

References

1. Miar Y, Plastow GS, Moore SS, Manafiazar G, Charagu P, Kemp RA, et al. Genetic and phenotypic parameters for carcass and meat quality traits in commercial crossbred pigs. *J Anim Sci.* (2014) 92:2869–84. doi: 10.2527/jas.2014-7685

2. Van Wijk HJ, Arts DJ, Matthews JO, Webster M, Ducro BJ, Knol EF. Genetic parameters for carcass composition and pork quality estimated in a commercial production chain. *J Anim Sci.* (2005) 83:324–33. doi: 10.2527/2005.832324x

3. Barbut S, Sosnicki AA, Lonergan SM, Knapp T, Ciobanu DC, Gatcliffe LJ, et al. Progress in reducing the pale, soft and exudative (PSE) problem in pork and poultry meat. *Meat Sci.* (2008) 79:46–63. doi: 10.1016/j.meatsci.2007.07.031

4. Heuven HC, van Wijk RH, Dibbits B, Van Kampen TA, Knol EF, Bovenhuis H, et al. Mapping carcass and meat quality QTL on Sus Scrofa chromosome 2 in commercial finishing pigs. *Genet Sel Evol.* (2009) 41:4. doi: 10.1186/1297-9686-41-4

5. Ryan MT, Hamill RM, O'Halloran AM, Davey GC, McBryan J, Mullen AM, et al. variation in the promoter of the PRKAG3 gene and association with meat quality traits in pig. *BMC Genet.* (2012) 13:66. doi: 10.1186/1471-2156-13-66

6. Ma J, Yang J, Zhou L, Ren J, Liu X, Zhang H, et al. splice mutation in the PHKG1 gene causes high glycogen content and low meat quality in pig skeletal muscle. *PLoS Genet.* (2014) 10:e1004710. doi: 10.1371/journal.pgen.1004710

7. Corominas J, Marchesi JA, Puig-Oliveras A, Revilla M, Estelle J, Alves E, et al. Epigenetic regulation of the ELOVL6 gene is associated with a major QTL effect on fatty acid composition in pigs. *Genet Sel Evol.* (2015) 47:20. doi: 10.1186/s12711-015-0111-y

8. Dong C, Zhang X, Liu K, Li B, Chao Z, Jiang A, et al. Comprehensive analysis of porcine prox1 gene and its relationship with meat quality traits. *Animals.* (2019) 9:744. doi: 10.3390/ani9100744

9. Oyelami FO, Zhao Q, Xu Z, Zhang Z, Sun H, Zhang Z, et al. Haplotype block analysis reveals candidate genes and QTLs for meat quality and disease resistance in Chinese Jiangquhai Pig Breed. *Front Genet.* (2020) 11:752. doi: 10.3389/fgene.2020.00752

10. Wang S, Jin J, Xu Z, Zuo B. Functions and regulatory mechanisms of lncRNAs in skeletal myogenesis, muscle disease and meat production. *Cells.* (2019) 8:1107. doi: 10.3390/cells8091107

11. Kosinska-Selbi B, Mielczarek M, Szyda J. Review: long non-coding RNA in livestock. *Animal.* (2020) 14:2003–13. doi: 10.1017/S1751731120000841

12. Munoz M, Garcia-Casco JM, Caraballo C, Fernandez-Barroso MA, Sanchez-Esquiliche F, Gomez F, et al. Identification of candidate genes and regulatory factors underlying intramuscular fat content through longissimus dorsi transcriptome analyses in heavy Iberian Pigs. *Front Genet.* (2018) 9:608. doi: 10.3389/fgene.2018.00608

13. Zhao W, Li Z, Liu Q, Xie S, Li M, Wang Y, et al. Analysis of long intergenic non-coding RNAs transcriptomic profiling in skeletal muscle growth during porcine embryonic development. *Sci Rep.* (2021) 11:15240. doi: 10.1038/s41598-021-94014-w

14. Li R, Li B, Jiang A, Cao Y, Hou L, Zhang Z, et al. Exploring the lncRNAs related to skeletal muscle fiber types and meat quality traits in pigs. *Genes.* (2020) 11:883. doi: 10.3390/genes11080883

15. Listrat A, Gagaoua M, Normand J, Gruffat D, Andueza D, Mairesse G, et al. Contribution of connective tissue components, muscle fibres and marbling to beef tenderness variability in longissimus thoracis, rectus abdominis, semimembranosus and semitendinosus muscles. *J Sci Food Agric.* (2020) 100:2502–11. doi: 10.1002/jsfa.10275

16. Chen FF, Wang YQ, Tang GR, Liu SG, Cai R, Gao Y, et al. Differences between porcine longissimus thoracis and semitendinosus intramuscular fat content and the regulation of their preadipocytes during adipogenic differentiation. *Meat Sci.* (2019) 147:116–26. doi: 10.1016/j.meatsci.2018.09.002

17. Livak KJ, Schmittgen TD. Analysis of relative gene expression data using real-time quantitative PCR and the 2(-Delta Delta C(T)) Method. *Methods.* (2001) 25:402–8. doi: 10.1006/meth.2001.1262

18. Zhu J, Yang Z, Hao W, Li J, Wang L, Xia J, et al. Characterization of a read-through fusion transcript, BCL2L2-PABPN1, involved in porcine adipogenesis. *Genes.* (2022) 13:445. doi: 10.3390/genes13030445

19. Fernande X, Monin G, Talmant A, Mourot J, Lebret B. Influence of intramuscular fat content on the quality of pig meat - 2. Consumer acceptability of m longissimus lumborum. *Meat Sci.* (1999) 53:67–72. doi: 10.1016/S0309-1740(99)00038-8

20. Sun Y, Cai R, Wang Y, Zhao R, Qin J, Pang WA, et al. Newly identified LncRNA LncIMF4 controls adipogenesis of porcine intramuscular preadipocyte through attenuating autophagy to inhibit lipolysis. *Animals.* (2020) 10:926. doi: 10.3390/ani10060926

21. Zhang M, Li F, Sun JW, Li DH, Li WT, Jiang RR, et al. LncRNA IMFNCR promotes intramuscular adipocyte differentiation by sponging miR-128-3p and miR-27b-3p. *Front Genet.* (2019) 10:42. doi: 10.3389/fgene.2019.00042

22. Wang L, Zhou ZY, Zhang T, Zhang L, Hou X, Yan H, et al. IRLnc: a novel functional noncoding RNA contributes to intramuscular fat deposition. *BMC Genomics.* (2021) 22:95. doi: 10.1186/s12864-020-07349-5

23. Wang J, Chen MY, Chen JF, Ren QL, Zhang JQ, Cao H, et al. LncRNA IMFlnc1 promotes porcine intramuscular adipocyte adipogenesis by sponging miR-199a-5p to up-regulate CAV-1. *BMC Mol Cell Biol.* (2020) 21:77. doi: 10.1186/s12860-020-00324-8

24. Cui JX, Zeng QF, Chen W, Zhang H, Zeng YQ. Analysis and preliminary validation of the molecular mechanism of fat deposition in fatty and lean pigs by high-throughput sequencing. *Mamm Genome.* (2019) 30:71–80. doi: 10.1007/s00335-019-09795-3

25. Cheng F, Liang J, Yang L, Lan G, Wang L, Wang L, et al. Systematic identification and comparison of the expressed profiles of lncRNAs, miRNAs,

circRNAs, and mRNAs with associated co-expression networks in pigs with low and high intramuscular fat. *Animals.* (2021) 11:3212. doi: 10.3390/ani11113212

26. Li Q, Huang Z, Zhao W, Li M, Li C. Transcriptome analysis reveals long intergenic non-coding RNAs contributed to intramuscular fat content differences between Yorkshire and Wei Pigs. *Int J Mol Sci.* (2020) 21:1732. doi: 10.3390/ijms21051732

27. Derrien T, Johnson R, Bussotti G, Tanzer A, Djebali S, Tilgner H. The GENCODE v7 cat-alog of human long noncoding RNAs: analysis of their gene structure, evolution, and expression. *Genome Res.* (2012) 22:1775–89. doi: 10.1101/gr.132159.111

28. Zhang K, Huang K, Luo Y, Li S. Identification and functional analysis of long non-coding RNAs in mouse cleavage stage embryonic development based on single cell transcriptome data. *BMC Genom.* (2014) 15:845. doi: 10.1186/1471-2164-15-845

29. Liu X, Wei S, Deng S, Li D, Liu K, Shan B, et al. Genome-wide identification and comparison of mRNAs, lncRNAs and circRNAs in porcine intramuscular, subcutaneous, retroperitoneal and mesenteric adipose tissues. *Anim Genet.* (2019) 50:228–41. doi: 10.1111/age.12781

30. Miao Z, Wang S, Zhang J, Wei P, Guo L, Liu D, et al. Identification and comparison of long non-conding RNA in Jinhua and Landrace pigs. *Biochem Biophys Res Commun.* (2018) 506:765–71. doi: 10.1016/j.bbrc.2018.06.028

31. Xing K, Wang K, Ao H, Chen S, Tan Z, Wang Y, et al. Comparative adipose transcriptome analysis digs out genes related to fat deposition in two pig breeds. *Sci Rep.* (2019) 9:12925. doi: 10.1038/s41598-019-49548-5

32. Li M, Liu Y, Xie S, Ma L, Zhao Z, Gong H, et al. Transcriptome analysis reveals that long noncoding RNAs contribute to developmental differences between medium-sized ovarian follicles of Meishan and Duroc sows. *Sci Rep.* (2021) 11:22510. doi: 10.1038/s41598-021-01817-y

33. Zhang B, Yan Z, Wang P, Yang Q, Huang X, Shi H, et al. Identification and Characterization of lncRNA and mRNA in Testes of Landrace and Hezuo Boars. *Animals.* (2021) 11:2263. doi: 10.3390/ani11082263

34. Hinds TD Jr, Kipp ZA, Xu M, Yiannikouris FB, Morris AJ, Stec DF, et al. Adipose-specific PPARalpha knockout mice have increased lipogenesis by PASK-SREBP1 signaling and a polarity shift to inflammatory macrophages in white adipose tissue. *Cells.* (2021) 11:4. doi: 10.3390/cells11010004

35. Kong S, Cai B, Nie Q. PGC-1α affects skeletal muscle and adipose tissue development by regulating mitochondrial biogenesis. *Mol Genet Genom.* (2022) 297:621–33. doi: 10.1007/s00438-022-01878-2

36. Cai H, Dong LQ, Liu F. Recent advances in adipose mTOR signaling and function: therapeutic prospects. *Trends Pharmacol Sci.* (2016) 37:303–17. doi: 10.1016/j.tips.2015.11.011

37. Harrington M, Pond-Tor S, Boney CM. Role of epidermal growth factor and ErbB2 receptors in 3T3-L1 adipogenesis. *Obesity.* (2007) 15:563–71. doi: 10.1038/oby.2007.562

38. Reusch JE, Colton LA, Klemm DJ. activation induces adipogenesis in 3T3-L1 cells. *Mol Cell Biol.* (2000) 20:1008–20. doi: 10.1128/MCB.20.3.1008-1020.2000

39. Fox KE, Fankell DM, Erickson PF, Majka SM, Crossno JT Jr, Klemm DJ. Depletion of cAMP-response element-binding protein/ATF1 inhibits adipogenic conversion of 3T3-L1 cells ectopically expressing CCAAT/enhancer-binding protein (C/EBP) alpha, C/EBP beta, or PPAR gamma 2. *J Biol Chem.* (2006) 281:40341–53. doi: 10.1074/jbc.M605077200

40. Ma X, Zhang H, Yuan L, Jing H, Thacker P, Li D, et al. CREBL2, interacting with CREB, induces adipogenesis in 3T3-L1 adipocytes. *Biochem J.* (2011) 439:27–38. doi: 10.1042/BJ20101475

41. Klemm DJ, Leitner JW, Watson P, Nesterova A, Reusch JE, Goalstone ML, et al. Insulin-induced adipocyte differentiation. Activation of CREB rescues adipogenesis from the arrest caused by inhibition of prenylation. *J Biol Chem.* (2001) 276:28430–5. doi: 10.1074/jbc.M103382200

42. de Sá PM, Richard AJ, Hang H, Stephens JM. Transcriptional regulation of adipogenesis. *Compr Physiol.* (2017) 7:635–74. doi: 10.1002/cphy.c160022

frontiers | Frontiers in Genetics

TYPE Original Research
PUBLISHED 30 August 2022
DOI 10.3389/fgene.2022.988756

OPEN ACCESS

EDITED BY
Rajwali Khan,
University of Agriculture, Peshawar, Pakistan

REVIEWED BY
Hamayun Khan,
University of Agriculture, Peshawar, Pakistan
Yinghui Ling,
Anhui Agricultural University, China
M. Subhan Qureshi,
University of Agriculture, Peshawar, Pakistan

*CORRESPONDENCE
S. K. Duckett,
sducket@clemson.edu

SPECIALTY SECTION
This article was submitted to Livestock Genomics, a section of the journal Frontiers in Genetics

RECEIVED 07 July 2022
ACCEPTED 25 July 2022
PUBLISHED 30 August 2022

CITATION
Greene MA, Powell R, Bruce T, Bridges WC and Duckett SK (2022), miRNA transcriptome and myofiber characteristics of lamb skeletal muscle during hypertrophic growth[1]. *Front. Genet.* 13:988756. doi: 10.3389/fgene.2022.988756

miRNA transcriptome and myofiber characteristics of lamb skeletal muscle during hypertrophic growth[1]

M. A. Greene[1], R. Powell[2], T. Bruce[2,3], W. C. Bridges[4] and S. K. Duckett[1]*

[1]Department of Animal and Veterinary Sciences, Clemson University, Clemson, SC, United States, [2]Clemson Light Imaging Facility, Clemson University, Clemson, SC, United States, [3]Department of Bioengineering, Clemson University, Clemson, SC, United States, [4]School of Mathematical and Statistical Sciences, Clemson University, Clemson, SC, United States

Postnatal muscle growth is achieved through hypertrophy of the muscle fibers and is impacted by the activity of satellite cells, the quiescent muscle stem cell. Several miRNAs are preferentially expressed in skeletal muscle and could provide a mechanism for increasing muscle hypertrophy through satellite cell proliferation and/or differentiation. The objectives of this study were to: 1) Characterize the miRNA transcriptome of the longissimus thoracis et lumborum muscle at several developmental timepoints [gestational d 85 (PN1), 110 (PN2), 133 (PN3), postnatal d 42 (PW1), 65 (PW2), 243 (MAT)] during muscle hypertrophy in lambs, and 2) examine miR-29a, identified in sequencing to be differentially regulated across development, loss of function on satellite cell proliferation and differentiation. Muscle fiber characteristics showed drastic increases ($p < 0.0001$) in fiber size and alterations in muscle fiber type occur during pre and postnatal development. miRNA sequencing comparisons were performed in developmental order (PN1 vs. PN2, PN2 vs. PN3, PN3 vs. PW1, PW1 vs. PW2, PW2 vs. MAT). There were 184 differentially expressed ($P_{adj} < 0.05$) miRNA, 142 unique miRNA, from all 5 comparisons made. The transitional stage (PN3 vs. PW1) had the largest number (115) of differentially expressed miRNA. Inhibition of miR-29a in satellite cell culture increased ($p < 0.05$) cell proliferation and differentiation capacity. Characterization of the miRNA transcriptome provides valuable insights into the miRNA involved in muscle fiber hypertrophy and the potential importance of the transitional period.

KEYWORDS

miRNA, skeletal muscle, transcriptome (RNA-seq), hypertrophy, sheep—lamb

Introduction

Adult muscle tissue is composed of multinucleated myofibers, or muscle fibers, that originate from mesenchymal stems cells and the mesodermal layer of the embryo (Houba and Te Pas, 2004). Muscle fiber development for sheep consists of a prenatal hyperplasia stage, complete between gestational d (gd) 78 (Zhu et al., 2004) and gd85 (Fahey et al., 2005) in the sheep, at which point muscle growth occurs *via* hypertrophy. Postnatal muscle growth is achieved through hypertrophy of the muscle fibers and is impacted by the activity of satellite cells, the quiescent muscle stem cell (Mauro, 1961; Rehfeldt et al., 2011; Chal and Pourquié, 2017). Satellite cells, when activated, will proliferate and differentiate to fuse with existing myofibers to promote hypertrophy, replace nuclei that are no longer functional, or repair damage to the muscle fiber (Cardasis and Cooper, 1975). During neonatal growth, there is a rapid accumulation of protein and myonuclei in skeletal muscle related to greater satellite cell numbers during this time period that decline with age (Davis and Fiorotto, 2009). Several molecular pathways that regulate the hypertrophy process in skeletal muscle have been documented and include IGF1, myostatin, androgens, B-agonists and osteocalcin (Schiaffino et al., 2021). However, many factors appear involved in skeletal muscle hypertrophy but little is known about the role of non-coding RNAs in this process.

miRNA are small noncoding RNA that regulate 60% of protein coding gene expression post transcriptionally in the human genome (Friedman et al., 2009). miRNA usually repress gene expression through complementary binding with target mRNA 3' untranslated regions (Hu and Coller, 2012). Hundreds of miRNA have been characterized across numerous cell lines, the majority of which focus on cancer and tumor formation/progression, or in other words cellular proliferation (Forterre et al., 2020). Several miRNAs are preferentially expressed in skeletal muscle and are involved in muscle development (Horak et al., 2016). miRNAs could provide a mechanism for increasing muscle hypertrophy through satellite cell proliferation and/or differentiation (Rupaimoole and Slack, 2017). Several *in vitro* studies have shown that certain miRNA can alter myocyte proliferation and differentiation through the targeting of mRNA (Anderson et al., 2006; Chen et al., 2006; Crist et al., 2012; Antoniou et al., 2014; Qadir et al., 2014). The use of miRNA mimics or inhibitors has been shown to alter satellite cell proliferation *in vitro* with miR-27b in sheep (Zhang et al., 2018), with miR-192 (Zhao et al., 2016) and miR-199b in pigs (Zhu et al., 2019), and with miR-92a in mice (Verma et al., 2019), which indicate that miRNA may play a role in skeletal muscle hypertrophy. The objectives of this study were to: 1) Characterize the miRNA transcriptome of the longissimus thoracis et lumborum muscle at several developmental timepoints (gd 85, 110, 133, postnatal d 42, 65, 243) during muscle hypertrophy in lambs, and 2) examine miR-29a, identified in sequencing to be differentially regulated across development, loss of function on satellite cell proliferation and differentiation.

Materials and methods

All animal experimental procedures were reviewed and approved by the Clemson University Institutional Animal Care and Use Committee (AUP-2018-055 and AUP-2018-049).

Experimental design

Suffolk ewes ($n = 22$) were mated to a single Texel ram (Texel Muscled; GeneSeek). Ewes were confirmed pregnant at gd 65 by transabdominal ultrasound (BCF Easi-Scan Curve; MIV Imaging, Rochester MN). At gd 85 (PN1), 110 (PN2), and 133 (PN3) of gestation, terminal surgeries (n = 3/time) were performed, and fetuses collected. Fetuses were towel dried and weighed and the right-side longissimus muscle was extracted and weighed. Samples of the left-side longissimus muscle were collected on male fetuses and immediately frozen in liquid nitrogen before storing at −80°C. Another group of ewes ($n = 10$) went to term. Wether lambs ($n = 3$) were weighed prior to a longissimus muscle biopsy being performed using a punch biopsy on 42-d (left side at 12th rib; PW1) and 65-d (right side at 12th rib; PW2) of age prior to weaning at d 75. Wether ($n = 3$) lambs that were biopsied at 42 and 65 d of age were finished on forages to 243-d of age (MAT) and slaughtered at the Clemson University Meat Lab. A live weight was collected prior to transport and longissimus muscle samples were collected from the left side at the 13th rib at slaughter. Longissimus muscle samples were snap frozen in liquid nitrogen and stored at −80°C for subsequent RNA extraction. After slaughter, carcasses were allowed to chill overnight at 4°C and then the right-side longissimus muscle was excised and weighed.

Sample preparation for miRNA sequencing

Total RNA was extracted from longissimus muscle tissue using Trizol reagent (Invitrogen, Thermo Fisher Scientific, Waltham, MA) according to the manufacturer. Any genomic DNA contamination was removed from the RNA with a DNA-free Kit (Ambion, Carlsbad, CA) according to the manufacturer. A Nanodrop 1 spectrophotometer (Thermo Fisher) was used to quantify total RNA. RNA integrity numbers (RIN) were generated using an Agilent 2,100 Bioanalyzer (Agilent Technologies, Santa Clara, CA) according to the manufacturer and all RIN values were above 7. Total RNA samples were stored

at −80°C until being shipped on dry ice to Novogene (Durham, NC) for library preparation and sequencing.

Library preparation and sequencing data analysis

Three μg of total RNA per sample was used to construct a small RNA library and index codes were added using NEBNext® Multiplex Small RNA Library Prep Set for Illumina® (NEB, United States) according to the manufacturer's recommendations. Library quality was evaluated with an Agilent Bioanalyzer 2,100 using DNA High Sensitivity Chips. Clustering of index-coded samples was done using a cBot Cluster Generation System and a TruSeq SR Cluster Kit v3-cBot-HS (Illumina) according to the manufacturer's instructions. Library preparations were sequenced using an Illumina platform and 50bp single-end reads were generated.

Bowtie was used to map reads to the reference genome (Langmead et al., 2009). miRBase20.0 was used as a reference and known miRNA were identified with mirdeep2 (Friedländer et al., 2012) and srna-tools-cli. Reads from protein-coding genes, repeat sequences, rRNA, tRNA, snRNA, and snoRNA were removed with RepeatMasker. Unmapped reads were predicted using miREvo (Wen et al., 2012) and mirdeep2 based on characteristics of a hairpin structure: the secondary structure, Dicer cleavage site and minimum free energy of the small RNA. miRNA expression was estimated by transcripts per million and normalized (Zhou et al., 2010). Prediction of target genes of miRNA was performed by miRanda (Enright et al., 2003). Gene Ontology (GO) enrichment analysis was performed on target mRNA of differentially expressed miRNAs using GOseq based Wallenius non-central hyper-geometric distribution (Young et al., 2010) to adjust for gene length bias. Target gene candidates were enriched in KEGG pathways using KOBAS software (Mao et al., 2005; Kanehisa et al., 2008).

Muscle fiber histology

At harvest, longissimus muscle samples at the 12/13th rib were collected, placed in a form with optimal cutting temperature compound (OCT; ThermoFisher), and immediately frozen in liquid nitrogen. Muscle samples were stored at −80°C until subsequent muscle histology was performed. Muscle samples were cryosectioned at a thickness of 10 μm, fixed for 2 min in ice cold acetone, and stained according to Greene et al. (2019) with modifications. Two tissue sections per animal were used for Type I/II and Type IIa/IIx myofiber typing. Cryosections of muscle samples were stained to determine Type I and Type II myofibers using primary antibodies (MHC-fast mouse IgG1, My-32, Abcam, ab51263, RRID:AB_2297993; MHC-slow mouse IgG2b, Developmental Studies Hybridoma Bank [DHSB], BA-F8, RRID:AB_10572253) and secondary antibodies (Alex Fluor 546 goat anti-mouse IgG1, Thermo Fisher, A-21123, RRID: AB_2535765) and Alexa Fluor 488 goat anti-mouse IgG2b, Thermo Fisher, A-21141, RRID:AB_2535778). Additional cryosections were stained to determine Type IIa or Type IIx myofibers using primary antibodies (MHC-Type IIa mouse IgG1, DSHB, SC-71, RRID:AB_2147165; MHC-Type IIx mouse IgM, DHSB, 6H1, RRID:AB_1157897) and secondary antibodies (Alex Fluor 546 goat anti-mouse IgG1, Thermo Fisher, A-21123, RRID:AB_2535765; Alex Fluor 488 goat anti-mouse IgM, Thermo Fisher, A-21042, RRID:AB_2535711). Sections were also counterstained with Alexa Fluor 633 wheat germ agglutinin at 10 μg/ml (Invitrogen, W21404) to outline muscle fiber membranes (Kostrominova, 2011). Stained muscle sections were mounted in Prolong Gold (P36939, Invitrogen) and samples were imaged using a Leica DMi8 widefield microscope system equipped with a Nikon ×20 objective (N.A. = 0.40) and a Leica DFC 9000 GTC Camera (Leica Microsystems, Buffalo Grove, IL). Camera exposure times were kept constant for all samples within each antibody group. At least ten unique sample regions (each measuring 670.15 μm × 670.15 μm) were imaged per section. To image samples stained with Alex Fluor 488 (depicted in green), we used a GFP filter cube (Ex/Em 455-495/505-555 nm). A Cherry filter (Ex/Em 540-580/592-668 nm) was used to image samples stained with Alexa Fluor 546 (depicted in red). For Alexa Fluor 633 (depicted in magenta), a Y5 filter cube (Ex/Em 600-660/662-738 nm) was used for imaging. Images were collected and exported as. TIF for analyses using Leica LAS-X software (version 3.6.0.20104, Leica Microsystems). Number and cross-sectional area of Type I/II myofibers and Type IIa/IIx myofibers were counted on four images per animal using ImageJ software (NIH, https://imagej.nih.gov/ij/docs/guide/146-1.html) by a single trained individual. Results were averaged by image and subjected to statistical analyses as described below.

In vitro cell culture

Satellite cells were isolated according to Li et al. 2009 and Danoviz and Yablonka-Reuveni (2012). In brief, muscle tissue was be stripped of connective tissue and any fat, then further processed with a sterile food processor. The tissue was then enzymatically digested for 60 min in a 37°C water bath with 1.5 mg/ml pronase in PBS to facilitate satellite cell liberation. Tissue slurry was shaken vigorously every 10 min during the digestion. Following digestion, the tissue slurry was centrifuged at 800 × g for 10 min to separate the digested tissue from the pronase, which was discarded as supernatant. From this point the tissue slurry was resuspended in PBS 1:1 with the volume of the tissue pellet. Then the tissue slurry was triturated until sufficiently homogenized to liberate the satellite cells. The tube was then centrifuged at 400 × g for 10 min. Supernatant was

decanted and retained. This process was completed 2 times to allow for complete liberation of satellite cells from the basal lamina. Following the 2nd centrifugation the supernatant was filtered through a 250 μm and a 70 μm cell strainer and cells were pelleted at 800 x g for 10 min. Cells were resuspended for 2 h to allow for debris removal in a preplating media [Dulbecco's modified eagle's medium (DMEM; Gibco, Thermo Fisher) + 10% fetal bovine serum (FBS; Avantor, VWR, Radnor, PA) + 1% penicillin/streptomycin (Corning, VWR)]. After 2 h, cells were transferred to a new flask for selective adhesion to increase satellite cell population purity for an additional 24 h (Gharaibeh et al., 2008). Cells were pelleted following the preplating, counted with a hemocytometer, and frozen (DMEM + 20% FBS + 10% DMSO) for later experiments.

Satellite cells were cultured to assess the impact of miR-29a inhibition by AntogmiR-29a (Creative Biogene, Shirley, NY) during the proliferation or differentiation stages of cell development. Experiments were run in duplicate. Satellite cells were plated in 0.1% gelatin coated 24 well plates at 20,000 cells/well and 0.1% gelatin coated 96 well plates at 5,000 cells/well for imaging. Cultures were seeded and incubated for 48 h to reach ~60% confluence prior to AntagomiR-29a transfection. Following treatment, cultures were grown for 4 d (the proliferation phase) in growth media [DMEM high glucose, 20% FBS, 1% penicillin/streptomycin, and 0.1% gentamicin (VWR)]. Cultures were differentiated for 4 d (the differentiation phase) in differentiation media (DMEM low glucose, 2% FBS, 1% penicillin/streptomycin, and 0.1% gentamicin). Cell media was changed every 2 d.

Cell transfection

Satellite cell cultures were transfected using RNAiMAX lipofectamine (ThermoFisher) according to manufacturer recommendations. AntagomiR-29a was synthesized by Creative Biogene and administered at two levels 100 and 300 nM. Cells were transfected either on d 0 of the proliferation phase or on d 0 of the differentiation phase (d 4 of proliferation). Lipofectamine without miRNA was used as a control in addition to cells grown with no manipulation (Control). Cultures were collected for RNA extraction using Trizol at d 1 and 4 of growth and d 4 of differentiation.

miRNA PCR

miRbase was used to obtain miRNA sequences for *Ovis aries* and then miRNA sequences were matched in the TaqMan assay database (ThermoFisher). miRNA was converted to cDNA with the TaqMan miRNA reverse transcription kit (ThermoFisher). TaqMan Small RNA Assay kits (ThermoFisher) were used for miR-29a (assay no. 000412; catalog no. 4427975), miR-22-3p (assay no. 242214_mat; catalog no. 444886), miR-133 (assay no. 000458; catalog no. 4427975), miR-127 (assay no. 008411_mat; catalog no. 4440886), miR-299-5p (assay no. 000600; catalog no. 4427975), miR-1 (assay no. 000385; catalog no. 4427975), and miR-206 (assay no. 000510; catalog no. 4427975). The housekeeping gene U6 snRNA was selected and the U6 snRNA TaqMan Assay Kit (assay no. 001973; catalog no. 4427975; ThermoFisher) was used for normalization of miRNA gene expression for tissue samples. The Taqman PCR assay kit and a Quant Studio3 Real-Time PCR system were used for qPCR according to the manufacturer instructions.

Hoechst DNA assay

Cell culture proliferation was assessed using the procedures of Velleman et al. (2019) with modifications. The DNA content of samples was measured using Hoechst 33,342 fluorochrome (ThermoFisher). Cells were harvested daily starting on d 1 of proliferation with Trypsin-EDTA (0.25%) and stored at −80°C until assay. Cells were allowed to thaw on ice and then homogenized. The sample (100 μL) was combined with 100 μL of 0.2% (1 mg/ml) Hoechst dye in 0.1 M NaCl, 10 mM EDTA, 10 mM Tris with a pH 7.0. Plates were incubated in the dark for 10 min and fluorescence read at Ex; Em 330/80; 460/40 using a BioTek Synergy HT (Winooski, VT). A standard curve using purified double-stranded DNA was used to determine sample DNA concentrations. Experiments were conducted in duplicate with 3 replicate wells per sample. The intra-assay variance was < 9.6% and the inter-assay variance was 9.5%.

Cell culture immunofluorescence

The number of differentiated nuclei was assessed by antibody staining of myogenin (MYOG) positive nuclei. The expression of MYOG can be used as a marker for differentiated myoblast cells (Schmidt et al., 2019). Media was removed after 4 d of differentiation and cells were fixed with 4% paraformaldehyde at room temperature for 15 min. Cells were then permeabilized with 0.1% TritonX-100 for 10 min at room temperature and then blocked with a 3% BSA solution in PBS for 60 min at room temperature. Plates were incubated with a MYOG primary antibody 1:10 in PBS (Myogenin mouse IgG1, DHSB catalog no. F5D, RRID: AB_2146602) overnight at 4°C. Following incubation, plates were allowed to come to room temperature for 30 min. Primary antibody was removed with thorough washing and plates were incubated with a 1:1,000 Texas Red secondary antibody (goat anti-mouse IgG1, ThermoFisher catalog no. A-10530, RRID:AB_2534035) for 60 min protected from light at room temperature. Unbound secondary antibody was removed with thorough washing. Total nuclei were stained with Hoechst 33,342 (10 μg/ml, ThermoFisher) for 10 min

TABLE 1 Changes in body weight (BW), longissimus thoracis et lumborum (LM) weight, muscle fiber type and cross-sectional area by developmental time point.

	PN1 gd85	PN2 gd110	PN3 gd133	PW1 d42	PW2 d65	MAT d243	SEM
BW, kg	0.471[a]	2.28[b]	3.912[c]	19.566[d]	28.652[e]	56.90[f]	0.376
LM, g	6.30[a]	31.09[ab]	42.33[b]	—	—	884.15[c]	11.56
Muscle fiber type, %							
Type I	8.76[b]	8.71[b]	17.07[a]	—	—	7.81[b]	0.98
Type II	91.24[a]	91.29[a]	82.93[b]	—	—	92.19[a]	0.98
Type IIa	86.16[a]	81.12[a]	77.23[a]	—	—	30.68[b]	4.85
Type IIax	0[c]	9.59[bc]	13.98[b]	—	—	59.75[a]	4.37
Type IIx	13.84	8.29	8.78	—	—	9.57	1.55
Muscle fiber cross-sectional area, μm^2							
Type I	87.80[d]	144.26[c]	254.29[b]	—	—	2,429.77[a]	
Type II	70.76[d]	173.36[c]	263.54[b]	—	—	2,528.13[a]	
Type IIa	60.08[d]	117.18[c]	215.04[b]	—	—	1820.30[a]	
Type IIax		164.54[b]	397.84[b]	—	—	2,998.44[a]	
Type IIx	68.61[c]	137.25[c]	277.84[b]	—	—	3,185.46[a]	

[abcdef]Means in the same row with uncommon superscripts differ ($p < 0.05$).

protected from light at room temperature. Excess Hoechst dye was removed, and cells were imaged immediately. Twelve unique sample regions were imaged per well using a Cytation1 (BioTek) with a × 10 objective and a DAPI filer cube (DAPI, blue, EX; Em 377/50; 447/60) and a Texas Red filter cube (Texas Red, red, Ex; Em 586/15; 647/57). A single trained individual then counted the total nuclei and the total nuclei expressing MYOG. Results are expressed as the percentage of the total nuclei expressing MYOG.

Statistical analysis

Analysis of variance (ANOVA) followed by Fisher's Protected Least Significant Difference Test (FPLSD) was used to determine the effect of animal age (gd85, gd110, gd133, d42, d65 and d243) on lamb body weight, longissimus muscle mass, and qPCR. ANOVA and FPLSD were also used for muscle fiber histology cross-sectional area data, but the assumption of normality required was not met for these data. The data were averaged by image and several different distributions were used to perform the analysis. Fortunately, the different distributions all yielded similar results, and therefore results are presented in original scale for ease of interpretation. ANOVA was used to determine the effects of treatment and experiment on cell culture data, followed by *a priori* contrasts to compare treatment groups to the control. The Generalized Linear Mixed Model (GLIMIX) and General Linear Model (GLM) procedures of SAS (Version 9.4) of SAS 9.4 (SAS Institute) for the ANOVA, FPLSD, and contrast calculations. *p*-values less than 0.05 were considered evidence of statistical significance.

Comparison of miRNA expression analysis was conducted using the DESeq R package (1.8.3) and the Benjamini and Hochberg method was used to adjust *p* values.

Results

Lamb characteristics

Body weight increased ($p < 0.0001$) at each timepoint of development examined in this study (Table 1). Body weight mass increased by 113-fold from 0.5 kg at PN1 to 57 kg at MAT. Longissimus thoracis et lumborum (LM) weight increased ($p < 0.0001$) from PN1 to MAT by 139-fold. The weight of the LM was greater ($p < 0.05$) at PN3 compared to PN1 with PN2 being intermediate. The lambs were grown to near maturity, plateau of longissimus thoracis et lumborum muscles (MAT), which represents postweaning growth period.

Muscle fiber histology

Muscle fiber cross sectional images with Type I and II staining or Type IIa, IIx, and IIax are shown in Figure 1. Muscle fiber cross-sectional of Type I myofibers was greater ($p < 0.001$) at each timepoint during development. Overall hypertrophy of Type I myofibers increased from 88 μm^2 at PN1 to 2,430 μm^2 at MAT. Type I fibers represented about 8.43% of total myofibers at PN1, PN2, and MAT; however, type I myofiber percentage was greater ($p < 0.0001$) at PN3, 17.07%, compared to all other developmental timepoints. At each prenatal developmental stage, cross-sectional area increased by

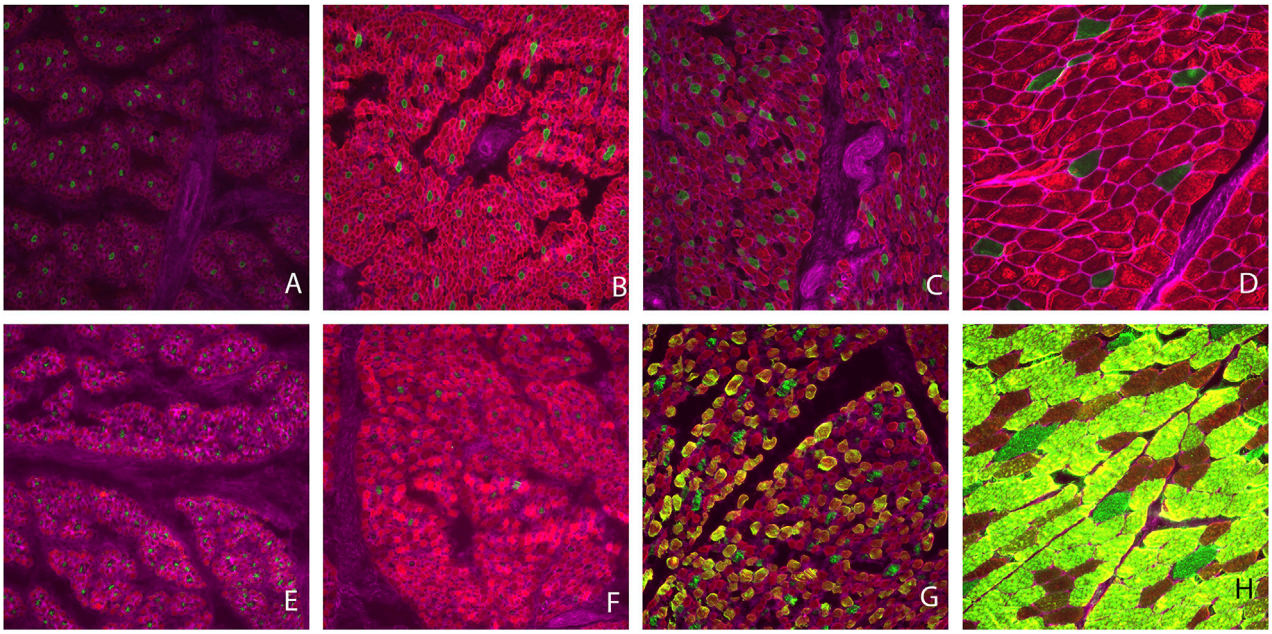

FIGURE 1
Muscle fiber cross sectional area images. Type I fibers are stained green and Type II fibers are red **(A–D)**. Type IIa fibers are stained red, Type IIx fibers are stained green and fibers expressing Type IIa and IIx proteins (Type IIax) are yellow in color **(E–H)**. Gestational d 85 samples **(A,E)**, gestational d 110 **(B,F)**, gestational d 133 **(C,G)**, maturity d 243 postnatal **(D,H)**.

64% at PN2 and by 76% at PN3, demonstrating that muscle fiber hypertrophy is on-going during the period of rapid fetal growth in the last trimester of gestation. Type II fiber area increased ($p < 0.0001$) at each development stage. Cross-sectional area of Type II fibers increased from 71 μm^2 at PN1 to 2,528 μm^2 at MAT. Type II fibers were further classified as Type IIa, IIx, and IIax (transitioning). Type IIa fiber size increased ($p < 0.0001$) at each development point evaluated from 60 μm^2 at PN1 to 1820 μm^2 at MAT. As a percentage of the total fibers, Type IIa fiber number was decreased ($p < 0.0001$) for the MAT developmental time point compared to all other times. Type IIx fibers size increased ($p < 0.0001$) as development progressed from prenatal to postnatal stage. Type IIx cross-sectional area did not differ between PN1 and PN2, however fiber size increased from PN2 to PN3 and PN3 to MAT. Type IIx fiber area increased from 69 μm^2 at PN1 to 3,185 μm^2 at MAT. Type IIx fibers as a percentage of the total fibers did not differ by developmental timepoint. Fibers that expressed both IIa and IIx proteins were classified as transitional fibers (IIax). No transitional fibers were found in PN1 samples. Fiber area of Type IIax fibers increased ($p < 0.01$) as development progressed. PN2 samples did not differ from PN3 fibers but cross-sectional area increased from PN3 to MAT. Type IIax fiber area increased from 164 μm^2 at PN2 to 2,998 μm^2 MAT. The percentage of Type IIax myofibers was similar during the prenatal stage (PN2 vs. PN3) but lower than MAT. The percentage of type IIa and IIax myofibers at MAT differed from the prenatal stage when Type IIax myofibers were non-existent or in low abundance.

miRNA sequencing

The total raw reads generated by sequencing was 396,602,151 with a minimum of 19,219,284 reads per individual sample and all samples had a Q30 of >97.00%. Reads containing >10% N (<0.000%), 5′ primer contaminants (0.005%), and/or did not contain the 3′ primer and the insert tag (0.842%) were excluded from the data. The 3′ primer sequence was trimmed and reads containing poly A/T/G/C (0.028%) were excluded. The remaining reads (99.125%) were used for mapping. Annotated reads were classified as known miRNA (41.80%), rRNA (0.14%), tRNA (0.02%), snRNA (0.02%), snoRNA (0.89%), repeat (6.03%), novel miRNA (0.02%; Supplementary Table S1), exon (±, 47.58%), intron (±, 2.40%), and other (1.10%) (Figure 2A). The largest portion was reads that mapped to exon regions with known miRNA being the second largest percentage. Reads length were also obtained and most reads ranged from 20–24 nt, with 22 nt being the frequency (Figure 2B). There was a high correlation between samples of the same developmental time point, indicating the reliability between samples (Figure 2C). Additionally, principal component analysis showed that developmental order could be captured, and

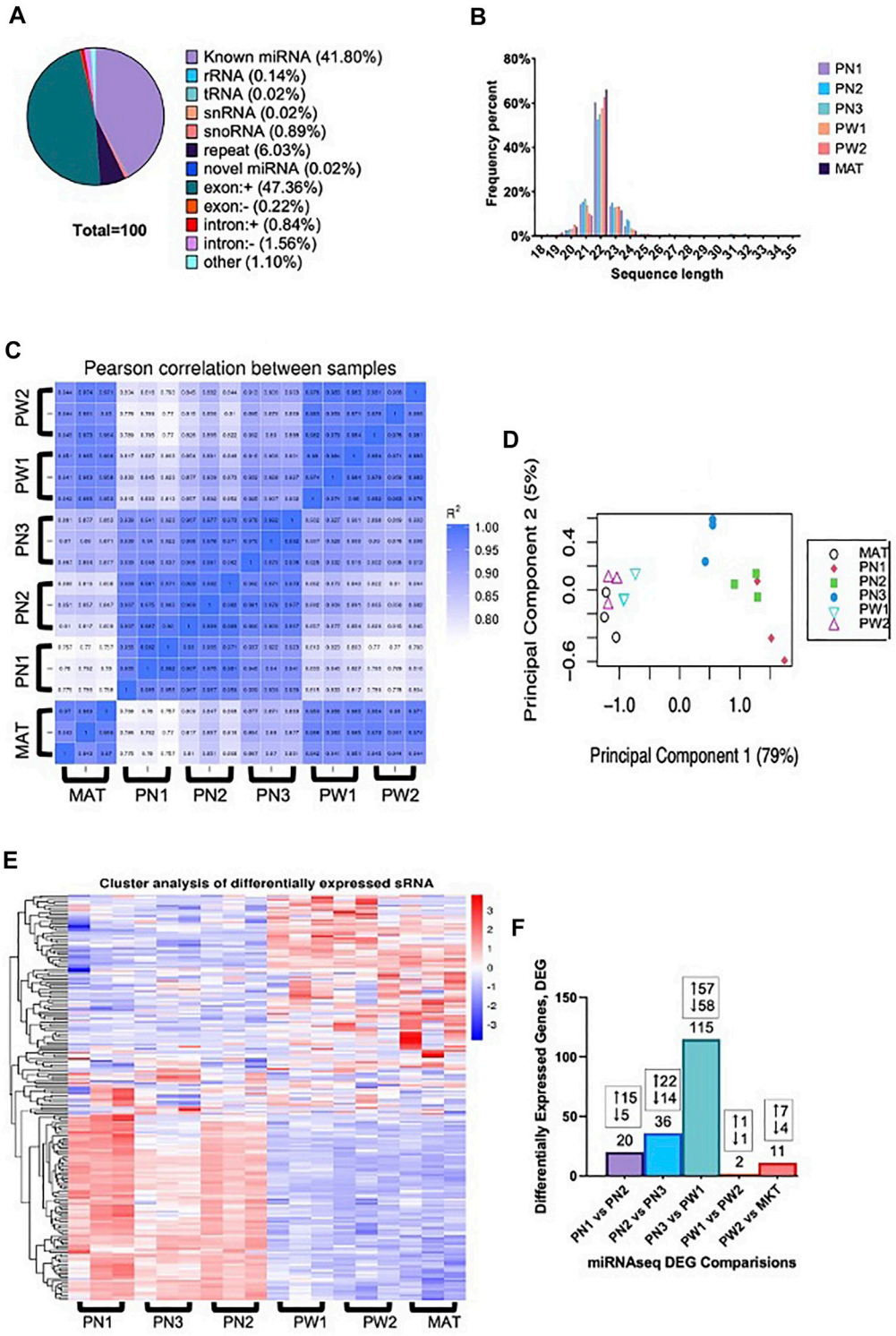

FIGURE 2
Small RNA analysis of ovine skeletal muscle at 6 developmental time points. **(A)** The classification of small RNA reads. **(B)** Distribution of small RNA sequence lengths from six developmental time points. **(C)** Correlation heat map of individual samples within developmental timepoints. **(D)** Principal component analysis of individual samples. **(E)** Hierarchical clustering analysis of individual samples within each developmental timepoint. **(F)** Number of differentially expressed miRNA from each comparison made with the number of up and downregulated miRNA denoted.

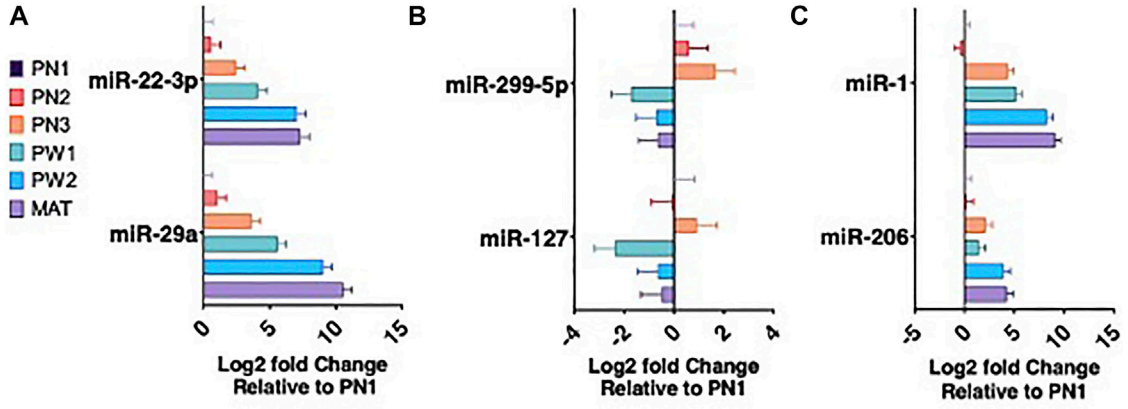

FIGURE 3
miRNA expression during six developmental time points. miRNA upregulated during development **(A)**. miRNA downregulated during development **(B)**. Muscle specific miRNA expression **(C)**.

a clear distinction was present between prenatal and postnatal samples (Figure 2D). This difference between pre and postnatal samples was also seen in the differentially expressed miRNA (Figure 2E).

There were 142 unique miRNA differentially expressed (P_{adj} < 0.05) between the five stages of longissimus muscle hypertrophy examined in this study (Figure 2F). No miRNA were differentially expressed at every growth stage examined but two miRNAs, miR-29a and miR-431, were differentially expressed in four comparisons. miR-29a was continuously upregulated from PN2 to MAT. miR-431 was down regulated from PN1 to PW1 and PW2 to MAT; however, miR-431 was not differentially expressed between PW1 and PW2. For validation of sequencing, miR-29a, -22-3p, -299-5p, and 127 were chosen due to their expression over several developmental timepoints and high or low abundance, respectively (Figures 3A,B). Expression of mir-29a and -22-3p increased (p < 0.05) during development. Overall, the increasing log2 fold change for miR-29a and -22-3p agreed with the sequencing results that showed upregulation during development (Figure 3A). miR-299-5p and -127 decreased (p < 0.05) in expression during postnatal development and this agreed with sequencing results (Figure 3B). Additional miRNA known to be present in muscle but not annotated in sequencing results, miR-1 and -206, were examined using qPCR (Figure 3C). miR-1 and -206 were both present at all developmental time points and expression increased (p < 0.05) as development progressed.

During the mid-prenatal stage (PN1 vs. PN2), 20 miRNA were differentially expressed (P_{adj} < 0.05) in this comparison (Table 2). miR-150 was up-regulated by 2.1-fold (P_{adj} < 0.0001) and miR-154b-3p was down-regulated by -2.4-fold (P_{adj} < 0.0001). Fourteen other miRNA were down-regulated (P_{adj} < 0.05) and four other miRNA were up-regulated (p < 0.05) from PN1 to PN2. Of these downregulated miRNA, miR-376, miR-17-5p and miR-431 have documented roles in skeletal muscle of the neonate and appear to alter satellite cell differentiation.

During the late prenatal stage of development (PN2 vs. PN3), 36 miRNA were differentially expressed (P_{adj} < 0.05) for this comparison (Table 3). miR-665-3p was down-regulated by -2.2-fold (P_{adj} < 0.0001) and novel_32 was up-regulated by 1.9- fold (P_{adj} < 0.0001). Thirteen additional miRNA were up-regulated (P_{adj} < 0.05) and 21 were down-regulated (P_{adj} < 0.05) during the late prenatal stage (PN2 vs. PN3). miR-133 and miR-143 were up-regulated and are known myomiRs with involvement in skeletal muscle hypertrophy.

During the transition from prenatal to postnatal development (PN3 vs. PW1), this stage had the most differentially expressed miRNA with 115 (Table 4). The largest magnitude (>3) log fold changes all came from the PN3 vs. PW1 comparison, miR-22-3p was up-regulated by 4.5-fold (P_{adj} < 0.0001) and novel_91 was down-regulated by -3.7-fold (P_{adj} < 0.0001). An additional 11 miRNA had a fold-change greater than 3, 7 were up-regulated and 4 were down regulated. Fifty-two miRNA were down-regulated (P_{adj} < 0.05) and 50 were up-regulated (P_{adj} < 0.05) with a fold-change < 3.

During the postnatal phase (PW1 vs. PW2), this stage had the smallest number of differentially expressed (P_{adj} < 0.05) miRNA with just two, miR-29a (up-regulated 0.8 fold) and miR-127 (down-regulated -0.6 fold), and this may be due to the short time duration between sampling (~25 days; Table 5). As longissimus muscle growth plateaus near maturity (PW2 vs. MAT), 11 miRNA were differentially expressed (Table 5). miR-431 was up-regulated 2.3-fold and novel_13 was down-regulated -1.9-fold for the PW2 vs. MAT comparison.

Target genes of differentially expressed miRNA were identified and the functional associations of genes were assessed with GOseq (Young et al., 2010). Between all 5 comparisons made, 195 terms were significantly enriched,

TABLE 2 Differentially expressed miRNA during mid prenatal phase (PN1 = gd85; PN2 = gd110) by significance level.

miRNA	PN1 TPM	PN2 TPM	log2FoldChange	$P_{adj.}$
oar-miR-150	91.79	485.40	2.1168	4.75E-08
oar-miR-154b-3p	104.76	13.03	−2.3920	8.88E-07
oar-miR-3959-3p	2,180.08	578.15	−1.6516	2.81E-04
oar-miR-487a-3p	140.56	37.32	−1.5813	3.04E-03
oar-miR-376d	402.22	152.21	−1.2468	5.96E-03
oar-miR-134-5p	741.58	351.42	−1.0009	6.12E-03
novel_159	1.40	14.19	1.7999	1.27E-02
oar-miR-665-3p	408.60	170.16	−1.1023	3.78E-02
oar-miR-496-5p	13.29	2.36	−1.4995	4.32E-02
oar-miR-1185-5p	71.02	25.14	−1.2216	4.32E-02
oar-miR-154a-3p	7,426.57	3,239.99	−1.0434	4.32E-02
novel_61	9.95	39.78	1.4153	4.32E-02
novel_7	2.25	12.75	1.5428	4.32E-02
oar-miR-376a-3p	526.98	197.21	−1.1641	4.39E-02
oar-miR-376e-3p	717.47	270.19	−1.1568	4.39E-02
oar-miR-17-5p	723.12	318.25	−1.0304	4.39E-02
oar-miR-431	7,283.58	2,116.71	−1.315	4.39E-02
novel_99	6.70	29.79	1.4065	4.57E-02
oar-miR-410-5p	52.07	17.95	−1.1921	4.98E-02
oar-miR-485-3p	1,178.44	592.23	−0.8902	4.98E-02

86 were from biological process, 42 were from cellular component, and 67 were from molecular function (Table 6; Supplementary Tables S2–S6). Fifty-nine terms were expressed in one comparison, 24 in 2 comparisons, 19 in 3 comparisons, 89 in 4 comparisons, and 4 in all 5 comparisons. The PN1 vs. PN2 comparison had 119 enriched terms, PN2 vs. PN3 had 121 enriched terms, PN3 vs. PW1 had 138 enriched terms, PW1 vs. PW2 had 4 enriched terms, and PW2 vs. MRT had 158 enriched terms.

Target genes of the of the 142 differentially expressed miRNA were annotated using the Kyoto Encyclopedia of Genes and Genomes to examine the miRNA relationship to cellular pathways (Table 7; Supplementary Tables S7–S11). A total of 35 pathways were enriched when all comparisons were examined. The PN1 vs. PN2 comparison had 16 enriched pathways, PN2 vs. PN3 had 17 enriched pathways, PN3 vs. PW1 had 21 enriched pathways, PW1 vs. PW2 had 2 enriched pathways, and PW2 vs. MKT had 21 enriched pathways. One pathway, Proteasome, was enriched in all 5 comparisons. Eight pathways were enriched in 4 comparisons, 5 in 3 comparisons, 4 in 2 comparisons, and 17 in only 1 comparison. The PN3 vs. PW1 comparison had enriched pathways with the highest rich factors (a ratio of genes enriched to total genes annotated in a pathway) when compared the same pathway in one or more of the 4 other comparisons; indicating that more genes were enriched in the PN3 vs. PW1 comparison when compared to the others.

Cell culture

Satellite cell culture experiments were conducted to examine loss of function for miR-29a on proliferation and differentiation. Cell proliferation rates were examined daily by measuring DNA content from d 1 to d 4 of the proliferation phase following AntagomiR-29a transfection and compared to Control cultures (Figure 4A). Following transfection on d 1, Lipofectamine treated cultures had reduced ($p < 0.05$) cell numbers when compared to Control. AntagomiR-29a treated cultures did not differ from the control. On d 2 of proliferation AntagomiR-29a 100 nM treated cultures tended ($p < 0.10$) to have reduced DNA content compared to Control cultures. AntagomiR-29a 300 nM treated cultures had increased ($p < 0.05$) DNA content compared to Control cultures on d 3. No cultures differed ($p > 0.05$) from Control cultures on d 4 of proliferation.

AntagomiR-29a treatment effect on satellite cell differentiation ability was assessed with MYOG staining (Figure 4B). Satellite cell differentiation was not altered ($p > 0.05$) by miRNA treatment during proliferation. AntagomiR 29a treatment during differentiation increased ($p < 0.05$) the percentage of nuclei expressing MYOG for AntagomiR 29a 100 and 300 nM treated cells compared to Control cultures. Lipofectamine treated cells did not differ Control cultures.

miR-29a expression was assessed on d 1 and 4 of proliferation and following 4 d of differentiation (Figures 4C–F). AntagomiR-29a at 300 nM reduced ($p < 0.05$) miR-29a expression 24 h

TABLE 3 Differentially expressed miRNA during mid prenatal phase (PN2 = gd110; PN3 = gd133) by significance level.

miRNA	PN2 TPM	PN3 TPM	log2FoldChange	$P_{adj.}$
oar-miR-665-3p	105.53	19.76	−2.1548	7.42E-07
oar-miR-136	4,205.65	12,564.74	1.4807	1.92E-05
oar-let-7f	232,325.25	497,336.61	1.0648	1.92E-05
oar-miR-758-3p	2,148.68	718.67	−1.4824	1.92E-05
oar-miR-376a-3p	122.33	31.74	−1.7540	1.92E-05
novel_32	26.48	121.52	1.9340	3.46E-05
oar-miR-154a-3p	2013.45	616.16	−1.5747	3.46E-05
oar-miR-431	1,318.53	327.11	−1.7979	3.46E-05
oar-miR-133	44,300.34	97,376.40	1.0930	5.05E-05
oar-miR-134-5p	217.18	88.23	−1.2304	5.05E-05
oar-miR-376d	94.20	30.84	−1.4645	2.30E-04
oar-miR-3959-3p	357.75	106.33	−1.5693	2.93E-04
oar-miR-1185-3p	712.52	113.66	−2.0861	3.55E-04
oar-miR-485-3p	365.87	128.05	−1.3896	3.55E-04
oar-miR-541-5p	685.94	351.68	−0.9286	5.67E-04
oar-miR-411a-3p	9,364.18	4,496.96	−1.0081	1.10E-03
oar-miR-29a	92.88	245.24	1.2835	1.71E-03
oar-miR-3957-5p	241.13	100.94	−1.1536	4.46E-03
oar-miR-376b-3p	254.12	83.64	−1.4026	4.55E-03
novel_91	5.83	32.93	1.8187	5.79E-03
oar-miR-143	1,154,220.57	2,416,323.96	0.9992	6.21E-03
oar-miR-541-3p	27.80	7.33	−1.5770	6.24E-03
novel_169	2.00	13.50	1.8854	6.32E-03
oar-miR-539-3p	147.10	61.36	−1.1402	9.63E-03
oar-let-7a	50,937.12	101,393.48	0.9319	1.09E-02
oar-miR-494-3p	4,633.28	2,740.92	−0.7292	1.15E-02
oar-let-7g	76,122.52	120,328.58	0.6411	1.30E-02
oar-miR-411b-3p	40.33	13.62	−1.3109	2.56E-02
novel_89	13.79	37.62	1.2308	2.67E-02
oar-miR-127	288,665.48	195,115.94	−0.5504	2.87E-02
oar-miR-412-3p	6,121.91	11,761.58	0.8756	3.03E-02
oar-miR-487a-3p	23.14	5.21	−1.5171	3.16E-02
oar-miR-410-5p	11.10	1.78	−1.5813	4.05E-02
oar-miR-376c-5p	887.36	1,509.02	0.7259	4.11E-02
novel_15	0.73	6.39	1.5986	4.57E-02
oar-miR-370-3p	87,715.07	34,345.31	−1.1449	4.82E-02

following transfection when compared to Control cultures, however AntagomiR-29a 100 nM treated cultures did not differ from Control cells (Figure 4C). Lipofectamine treated cells had increased miR-29a expression on d 1 of proliferation when compared to Control cultures. On d 4 of proliferation AntagomiR-29a 300 nM treated cultures had reduced ($p < 0.01$) miR-29a expression when compared to Control cultures (Figure 4D). Lipofectamine and AntagomiR-29a 100 nM cultures did not differ ($p > 0.05$) from Control cells on d4 of proliferation. Cells treated with either AntagomiR-29a at 100 nM or 300 nM during proliferation had reduced ($p < 0.01$) miR-29a expression following 4 d of differentiation when compared to Control cultures, while Lipofectamine cultures did not differ ($p > 0.05$; Figure 4E). Cells treated with AntagomiR-29a at 100 nM or 300 nM only during the differentiation stage had reduced ($p < 0.01$) miR-29a expression when compared to Control cultures (Figure 4F). Control and Lipofectamine cultures did not differ ($p > 0.05$) from each other on d 4 of differentiation.

TABLE 4 Differentially expressed miRNA during prenatal to postnatal transition phase (PN3 = gd133; PW1 = pd42) by significance level.

miRNA	PN3 TPM	PW1 TPM	log2FoldChange	$P_{adj.}$
oar-miR-22-3p	3,253.46	80,720.92	4.525	1.04E-57
oar-miR-299-5p	1,130.39	163.00	−2.753	3.26E-37
oar-miR-487b-3p	1,586.25	382.71	−2.0275	3.04E-24
oar-let-7g	55,592.12	134,263.09	1.2647	8.64E-18
oar-miR-30c	2,888.27	17,727.15	2.5525	2.01E-17
oar-miR-127	90,359.34	36,459.82	−1.3007	8.43E-17
oar-miR-432	4,637.76	964.83	−2.2213	1.17E-16
oar-miR-30d	58,769.57	287,068.30	2.2413	2.04E-16
oar-miR-29a	114.76	892.44	2.8509	2.86E-15
oar-miR-143	1,115,871.88	2,978,500.86	1.4042	2.94E-15
oar-miR-299-3p	365.94	73.79	−2.243	3.23E-14
oar-miR-381-3p	1,114,970.39	198,832.88	−2.417	3.64E-14
oar-miR-410-3p	1,324.49	146.52	−3.0324	6.13E-14
oar-miR-154a-3p	282.06	29.47	−3.1168	6.26E-14
oar-miR-3959-5p	2,487.10	760.65	−1.6855	3.08E-13
novel_101	2.42	56.15	4.0619	5.49E-13
oar-miR-376c-5p	702.86	105.15	−2.6425	6.86E-13
oar-miR-431	150.00	17.17	−3.0003	3.11E-12
oar-miR-16b	396.33	3,176.06	2.858	3.79E-12
oar-miR-495-3p	14,909.28	2,664.33	−2.3976	1.10E-11
oar-miR-493-5p	25,857.82	3,413.60	−2.7822	1.12E-11
oar-miR-27a	732.01	2,872.37	1.9279	1.35E-11
oar-miR-655-3p	5,093.71	575.75	−2.9609	7.15E-11
oar-miR-133	45,326.48	198,971.38	2.0734	1.01E-10
oar-miR-136	5,808.63	1,047.80	−2.3698	5.99E-10
novel_7	5.81	66.85	3.2284	8.29E-10
oar-miR-329b-3p	1,209.13	269.32	−2.088	3.31E-09
oar-miR-25	4,944.24	18,970.32	1.8852	4.35E-09
oar-miR-541-5p	162.78	45.44	−1.8002	5.87E-09
oar-miR-382-5p	5,232.22	1,504.11	−1.753	7.44E-09
oar-miR-191	3,644.91	11,054.01	1.5674	1.56E-08
oar-miR-150	351.46	2,376.73	2.592	1.86E-08
novel_159	3.66	39.97	3.14	4.37E-08
oar-miR-10b	295,096.57	791,364.41	1.3979	5.36E-08
oar-miR-103	902.93	4,755.78	2.2692	2.31E-07
oar-miR-125b	5,988.66	11,625.02	0.94814	4.41E-07
oar-miR-194	90.40	394.65	2.0266	9.84E-07
oar-miR-3956-5p	4,762.74	424.20	−3.0799	9.84E-07
novel_87	0.00	14.90	4.2219	5.24E-06
oar-miR-21	171,273.72	356,873.16	1.0442	7.52E-06
novel_4	12.28	78.51	2.4509	7.56E-06
oar-miR-379-5p	134,717.62	74,976.28	−0.83758	1.05E-05
oar-miR-382-3p	3,434.37	1,334.07	−1.3301	1.54E-05
oar-miR-221	32.74	233.10	2.5456	1.95E-05
oar-miR-30a-3p	1,360.59	2,175.92	0.67301	1.99E-05
novel_13	0.82	23.95	3.5678	2.31E-05
oar-miR-26a	142,269.96	387,849.86	1.4038	3.16E-05
oar-miR-369-3p	3,205.77	599.33	−2.2194	5.26E-05

(Continued on following page)

TABLE 4 (*Continued*) Differentially expressed miRNA during prenatal to postnatal transition phase (PN3 = gd133; PW1 = pd42) by significance level.

miRNA	PN3 TPM	PW1 TPM	log2FoldChange	$P_{adj.}$
oar-miR-3958-5p	179.07	36.70	−2.1109	5.26E-05
oar-miR-3956-3p	58.10	6.98	−2.6236	5.75E-05
oar-miR-495-5p	113.37	29.91	−1.7905	6.71E-05
novel_91	14.99	0.00	−3.6814	7.28E-05
oar-miR-380-3p	2,225.71	710.98	−1.5783	7.35E-05
novel_67	49.85	139.43	1.4286	1.08E-04
oar-miR-381-5p	25.66	3.39	−2.4986	1.52E-04
oar-miR-3955-5p	835.09	394.68	−1.0563	1.55E-04
oar-miR-107	128.68	391.89	1.5352	1.71E-04
novel_84	0.00	11.01	3.5774	2.40E-04
oar-miR-1185-3p	52.11	16.42	−1.5919	2.69E-04
oar-miR-3958-3p	47,442.40	20,242.12	−1.1938	3.39E-04
oar-miR-411a-3p	2067.40	546.75	−1.7827	5.15E-04
oar-miR-494-3p	1,270.31	755.52	−0.7418	6.25E-04
oar-miR-3955-3p	16.99	0.92	−2.9307	6.89E-04
oar-miR-181a	6,692.89	14,436.41	1.0794	9.16E-04
oar-miR-23a	2,455.76	7,624.23	1.5412	9.92E-04
novel_122	17.19	49.42	1.4476	1.07E-03
oar-miR-200c	3.14	20.69	2.3002	1.39E-03
novel_128	5.78	21.22	1.7154	1.48E-03
novel_54	0.00	4.71	3.0279	2.59E-03
oar-miR-543-3p	2,899.34	483.46	−2.1936	2.59E-03
oar-miR-376c-3p	259.56	85.30	−1.5059	2.70E-03
oar-miR-1193-5p	9.14	0.44	−2.7133	3.12E-03
oar-miR-329a-3p	31.82	8.82	−1.6675	3.34E-03
oar-miR-30b	1,431.93	7,886.11	2.0949	3.92E-03
oar-miR-493-3p	17,054.16	7,651.77	−1.1124	4.41E-03
oar-miR-329b-5p	23.91	5.34	−1.8633	5.17E-03
oar-miR-487a-5p	21.59	5.67	−1.6787	5.66E-03
oar-miR-17-5p	100.41	340.30	1.6048	5.69E-03
oar-let-7c	16,034.49	10,760.04	−0.56963	5.69E-03
oar-miR-655-5p	14.21	1.71	−2.3672	5.82E-03
oar-miR-370-5p	59.48	26.40	−1.1376	6.61E-03
oar-miR-30a-5p	56,262.60	97,321.10	0.77484	6.72E-03
novel_96	2.78	13.04	1.9389	7.16E-03
oar-miR-376a-3p	14.86	2.63	−2.0776	7.16E-03
oar-miR-376d	14.29	2.58	−2.0523	7.16E-03
novel_6	8.36	56.60	2.2011	7.43E-03
oar-miR-106a	17.22	56.22	1.5485	8.16E-03
novel_71	0.00	3.39	2.6493	9.51E-03
novel_83	0.00	3.50	2.6147	1.07E-02
oar-miR-487b-5p	22.13	5.47	−1.6954	1.09E-02
novel_61	13.52	42.26	1.483	1.10E-02
novel_42	0.20	4.84	2.5102	1.20E-02
oar-miR-412-3p	5,378.49	2,797.79	−0.91164	1.27E-02
oar-miR-323a-3p	917.06	352.11	−1.2845	1.33E-02
novel_8	7.16	33.85	1.867	1.40E-02
novel_75	9.16	27.85	1.4578	1.43E-02

(Continued on following page)

TABLE 4 (*Continued*) Differentially expressed miRNA during prenatal to postnatal transition phase (PN3 = gd133; PW1 = pd42) by significance level.

miRNA	PN3 TPM	PW1 TPM	log2FoldChange	$P_{adj.}$
oar-let-7f	229,818.32	311,018.30	0.43319	1.48E-02
oar-miR-26b	7,723.60	15,612.67	0.97488	1.48E-02
novel_5	37.21	89.02	1.186	1.50E-02
oar-miR-433-3p	486.83	246.10	−0.94394	1.50E-02
oar-miR-19b	909.29	1,537.82	0.74053	1.56E-02
oar-miR-412-5p	69.82	24.92	−1.3518	1.71E-02
novel_127	3.75	15.66	1.7598	1.77E-02
oar-miR-380-5p	95.19	49.81	−0.90109	2.05E-02
oar-miR-154b-5p	2,845.81	1,425.43	−0.95264	2.43E-02
novel_3	33.96	15.98	−1.0468	2.45E-02
oar-miR-409-5p	1,289.73	729.15	−0.79479	2.90E-02
novel_157	1.68	10.52	1.9707	2.92E-02
novel_52	0.20	4.45	2.2066	3.13E-02
oar-miR-10a	38,127.81	55,714.68	0.53872	3.50E-02
oar-miR-23b	3,386.13	6,868.51	0.96512	3.98E-02
novel_35	0.79	8.09	2.0227	4.54E-02
oar-miR-323b	63.49	13.28	−1.7337	4.57E-02
oar-miR-377-5p	27.26	9.33	−1.3625	4.99E-02
novel_85	0.00	2.71	2.0249	5.00E-02

TABLE 5 Differentially expressed miRNA during postnatal phase of development (PW1 = pd42; PW2 = pd60) and postweaning phase of development (PW2 = pd60; MAT = pd 240) by significance level.

miRNA	PW1 TPM	PW2 TPM	log2FoldChange	$P_{adj.}$
oar-miR-29a	435.77	814.59	0.82216	3.03E-02
oar-miR-127	17,782.67	11,042.48	−0.64633	3.10E-02
miRNA	**PW2 TPM**	**MAT TPM**	**log2FoldChange**	***Padj.***
oar-miR-29a	579.32	1954.82	1.6739	1.55E-09
oar-miR-29b	17.47	78.60	1.9496	1.42E-06
oar-miR-431	3.13	32.38	2.2537	1.45E-03
oar-miR-16b	1,405.30	478.61	−1.4019	2.00E-03
oar-miR-3959-5p	289.34	153.88	−0.86824	2.19E-02
oar-miR-412-3p	771.84	368.68	−0.98391	2.19E-02
oar-miR-411b-5p	197.62	81.17	−1.1539	2.19E-02
novel_13	14.96	0.88	−1.9055	2.19E-02
oar-miR-376e-5p	13.57	2.03	−1.7191	2.51E-02
oar-miR-543-3p	145.03	827.55	1.6478	3.81E-02
oar-miR-494-3p	248.53	118.80	−0.96596	4.73E-02

Discussion

Skeletal muscle hypertrophy is an intricate process that spans both the pre and postnatal developmental stages. miRNA are known to be involved in gene regulation and characterizing the transcriptomic changes that occur during development provides a more complete understanding of the mechanisms involved in hypertrophic muscle development. The current study covered a wide developmental range spanning from the conclusion of muscle fiber hyperplasia (PN1; gd 85) to near maturity (MAT).

10.3389/fgene.2022.988756

TABLE 6 Summary of enriched Gene Ontology terms from each comparison.

GO Accession	Description	Term type	P_{adj}
Enriched Terms PN1 v PN2			
GO:0003824	Catalytic activity	Molecular function	7.99E-13
GO:0008152	Metabolic process	Biological process	7.99E-13
GO:0005488	Binding	Molecular function	6.10E-10
GO:0016787	Hydrolase activity	Molecular function	6.07E-09
GO:0043167	Ion binding	Molecular function	1.02E-08
Enriched Terms PN2 v PN3			
GO:0003824	Catalytic activity	Molecular function	1.21E-16
GO:0008152	Metabolic process	Biological process	4.69E-14
GO:0016787	Hydrolase activity	Molecular function	1.73E-11
GO:0005488	Binding	Molecular function	1.54E-09
GO:0070011	Peptidase activity, acting on L-amino acid peptides	Molecular function	2.80E-09
Enriched Terms PN3 v PW1			
GO:0003824	Catalytic activity	Molecular function	2.07E-20
GO:0008152	Metabolic process	Biological process	1.36E-14
GO:0016787	Hydrolase activity	Molecular function	4.09E-12
GO:0005488	Binding	Molecular function	1.89E-10
GO:0008233	Peptidase activity	Molecular function	2.51E-09
Enriched Terms PW1 v PW2			
GO:0016787	Hydrolase activity	Molecular function	4.54E-03
GO:0008152	Metabolic process	Biological process	4.54E-03
GO:0003824	Catalytic activity	Molecular function	8.58E-03
GO:0005975	Carbohydrate metabolic process	Biological process	1.04E-02
Enriched Terms PW2 v MKT			
GO:0003824	Catalytic activity	Molecular function	2.28E-12
GO:0008152	Metabolic process	Biological process	1.03E-11
GO:0071704	Organic substance metabolic process	Biological process	2.95E-09
GO:0044238	Primary metabolic process	Biological process	1.25E-08
GO:0044237	Cellular metabolic process	Biological process	2.30E-07

Late gestation (gd 70–140 of gestation) is a period of exponential growth for the fetus and 80% of fetal growth occurs during this period (Rattray et al., 1974). The early postnatal period of development is noted for having increased growth efficiency compared to later postnatal growth (Greenwood and Bell, 2019). Lamb body weight increased as development progressed, with the largest percentage increase (300%) occurring during the transition from prenatal (PN3; gd 133) to postnatal (PW1; d 42) a period of approximately 56 days. Comparatively the post-weaning growth period (PW2; d 65 to MAT; d 243) was the longest at ~140 d and only resulted in a 97% body weight increase. From PN1 to MAT, muscle weight increased more than total body weight as a percentage, 12,528% and 10,349% respectively, indicating the importance of muscle hypertrophy in overall body growth.

Muscle fiber hypertrophy showed that there was an immense increase in muscle fiber area from PN1 to MAT. During prenatal hypertrophy, PN1 to PN3, Type II fibers were shown to have more hypertrophy from PN1 to PN3 than Type I fibers, 2.7- and 1.9-fold, respectively. Similar results were found during postnatal hypertrophy, PN3 to MAT, with Type II fibers having a 8.9 fold increase and Type I fibers increasing 8.6 fold in size. Within the Type II fibers, Type IIa and IIx showed a similar trend with a 2.6- and 3.0-fold increase during prenatal hypertrophy, and 7.5- and 10.5-fold increase during postnatal hypertrophy, respectively. Type IIax was not found in PN1 (gd 85) samples and could indicate that fiber transition does not start occurring until later in gestation. Postnatal hypertrophy of type IIax fibers was 6.5-fold, the lowest of the all the fibers classified. These findings are consistent with previous studies

TABLE 7 Summary of enriched KEGG pathways from each comparison.

ID	Description	P_{adj}
Enriched Pathways PN1 v PN2		
oas05140	Leishmaniasis	1.39E-02
oas04145	Phagosome	2.21E-02
oas05150	*Staphylococcus aureus* infection	2.21E-02
oas04210	Apoptosis	2.21E-02
oas04141	Protein processing in endoplasmic reticulum	2.21E-02
Enriched Pathways PN2 v PN3		
oas04142	Lysosome	1.09E-03
oas04141	Protein processing in endoplasmic reticulum	2.04E-03
oas05140	Leishmaniasis	2.04E-03
oas01100	Metabolic pathways	2.04E-03
oas04145	Phagosome	2.57E-03
Enriched Pathways PN3 v PW1		
oas04145	Phagosome	1.58E-03
oas04141	Protein processing in endoplasmic reticulum	3.10E-03
oas05140	Leishmaniasis	3.10E-03
oas05150	*Staphylococcus aureus* infection	3.10E-03
oas04976	Bile secretion	3.10E-03
Enriched Pathways PW1 v PW2		
oas04974	Protein digestion and absorption	4.15E-03
oas03050	Proteasome	2.31E-02
Enriched Pathways PW2 v MKT		
oas05140	Leishmaniasis	1.33E-03
oas05150	*Staphylococcus aureus* infection	2.24E-03
oas04152	AMPK signaling pathway	2.24E-02
oas05330	Allograft rejection	8.63E-02
oas04141	Protein processing in endoplasmic reticulum	1.17E-02

that show that, while Type I and II fibers are similar in size early in development, Type II fibers surpass Type I fibers in area at maturity (Wegner et al., 2000).

In the current study Type I fiber percentage was greater at PN3 (gd 133) compared to all other developmental time points. In cattle, Type I fiber percentage remained consistent from birth to 24 months of age, however Type IIa fiber percentage decreased with other myosin heavy chain isoforms increasing in percentage (Wegner et al., 2000). Similar findings have been shown in mice and pigs, with all studies noting that the transition from Type I to Type II fiber occurring early in the postnatal period (Wegner et al., 1993; Schiaffino et al., 2015). Muscle fiber type is determined based on the presence of myosin heavy chain isoforms which indicate the metabolic state (oxidative vs. glycolytic) of the individual muscle fibers (Pette and Staron, 1997). In the current study, Type IIa percentage was reduced at maturity compared to prenatal time points, while the percentage of Type IIax fibers increased at maturity. Muscle fiber type is not static and fibers can transition depending on factors like age, nutrition, and activity (Lefaucheur and Gerrard, 2000). Type IIa fibers are more oxidative than Type IIx fibers, so fibers expressing both proteins (Type IIax) would be an intermediate. The dramatic changes in fiber composition in the current study show that while growth is occurring so are metabolic alterations.

miRNA are a group of evolutionarily highly conserved genes that function in post-transcriptional regulation (Horak et al., 2016). The deep sequencing conducted in the current study found 41.80% of the raw reads mapped to known miRNA in the ovine genome. Additionally, a known myomiR, miR-133, was found and was differentially expressed during development. myomiR-1 and -206 were also identified with qPCR and showed increased expression as development progressed.

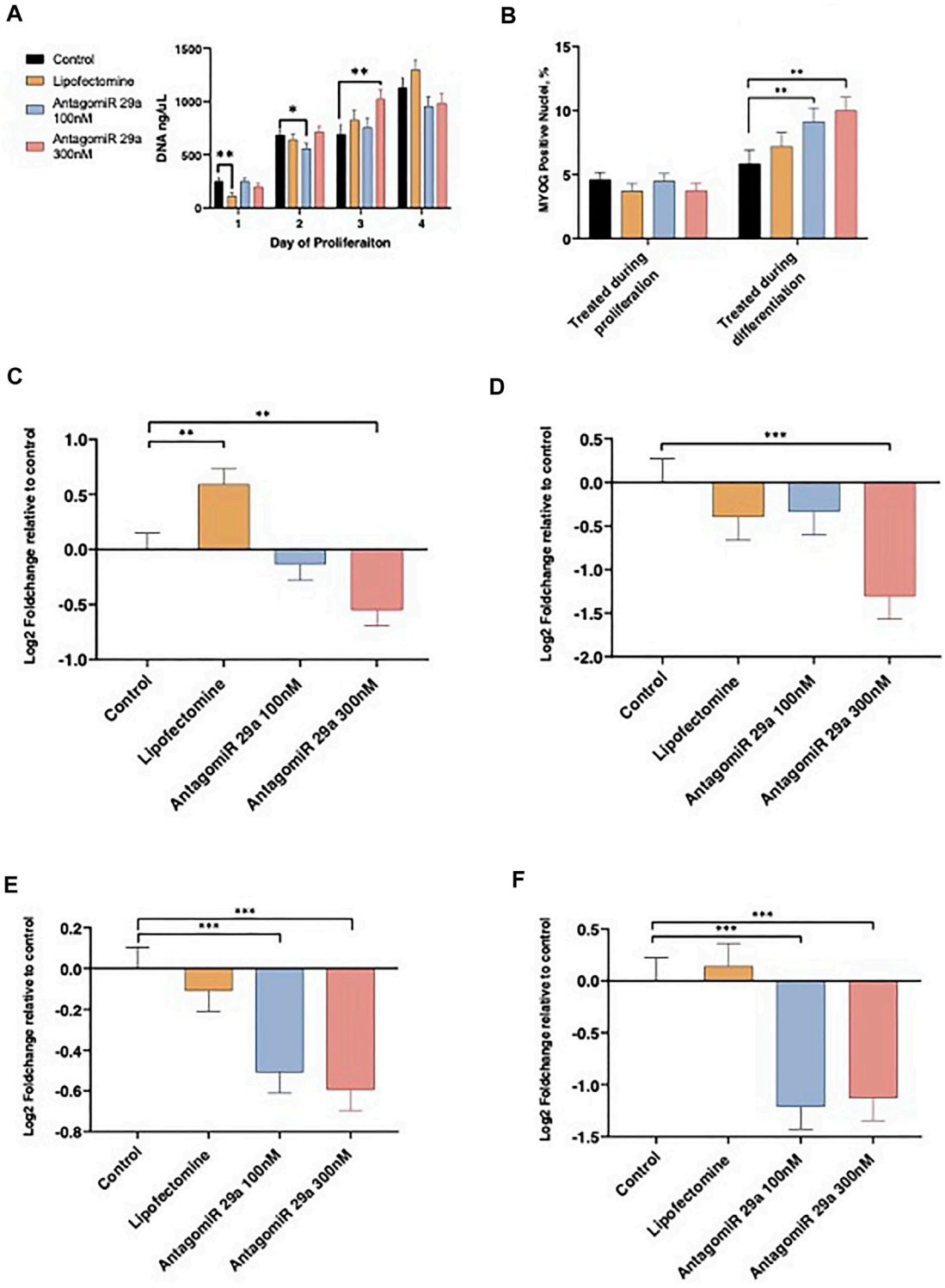

FIGURE 4
The effects of miR-29a inhibition on satellite cell proliferation, differentiation, and miRNA expression. Alterations from miR-29a inhibition to cell culture DNA content by day of proliferation **(A)**. miR-29a inhibition during proliferation or differentiation on the percentage of the total nuclei expressing MYOG **(B)**. miR-29a expression on d 1 of proliferation **(C)** and d 4 of proliferation **(D)**. miR-29a expression from cell cultures treated during proliferation **(E)** or differentiation **(F)**.

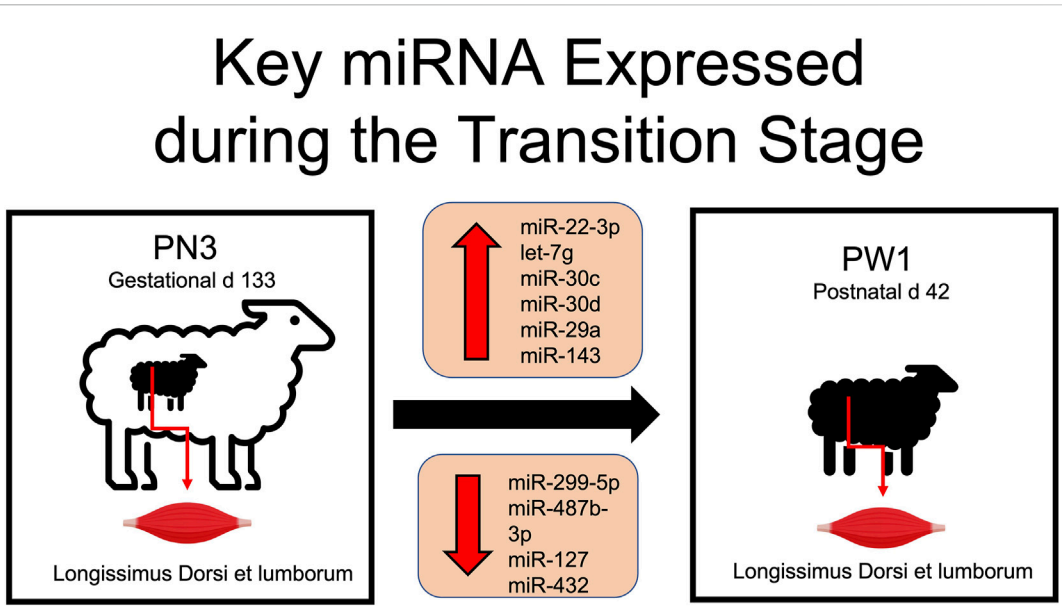

FIGURE 5
Differentially expressed miRNA involved in skeletal muscle hypertrophy during the transition from prenatal to postnatal development.

Human and bovine miR-1 and -206 have been identified in ovine samples through sequencing and were shown to be differentially expressed between breeds with higher muscle content compared to local sheep (Kaur et al., 2020). myomiRs are known to be expressed in high abundance in muscle tissue and have significant impact on muscle development (Horak et al., 2016).

miRNA profiles were altered by progressing muscle hypertrophy. There were 184 differentially expressed miRNA, 142 unique miRNA, from all 5 comparisons made (PN1 vs. PN2, PN2 vs. PN3, PN3 vs. PW1, PW1 vs. PW2, PW2 vs. MAT). The prenatal period (PN1 vs. PN2 and PN2 vs. PN3) had more adaptations to the miRNA profile compared to the postnatal period (PW1 vs. PW2 and PW2 vs. MAT; 56 vs. 13), even though the postnatal period was longer (48 vs. 161 d). The transitional period from prenatal to postnatal had the largest number of differentially expressed miRNA (115) reflecting that this period has increased transcriptomic change compared to the other developmental stages examined. Additionally, the transitional stage also had the largest log fold changes indicating that larger magnitude transcriptomic changes were occurring during this period. Similarly, the goat miRNA transcriptome has been characterized from gd 45 to d 90 postnatal at seven time points, with the most differentially expressed miRNA (184) observed from birth to d 90 of age (Ling et al., 2020). Examination of the porcine miRNA transcriptome during fetal development showed that miRNA transcripts increased as fetal muscle development progressed (McDaneld et al., 2009). miR-133 was found in high abundance in adult muscle tissue, and miR-22 and 143 were in abundance in adults and satellite cells. miR-29 was found in muscle and satellite cell cultures, however satellite cell cultures had higher abundance of the miRNA. Postnatally miR-29a was found to be upregulated and miR-127 was down regulated from weaning to maturity in pigs (Chen et al., 2020). A similar trend with miR-29a was found in the current study, however miR-127 was only down regulated during the prenatal to early postnatal comparisons (PN2 vs. PN3, PN3 vs. PW1, and PW1 vs. PW2). miR-22-3p was found in the transitional stage (PN3 vs. PW1) and had the largest log fold change (4.5). miR-22-3p has been previously reported in the skeletal muscle of sheep (Lie et al., 2014; Greene et al., 2019). Overexpression of miR-22-3p promotes myoblast differentiation and reduces proliferation in mouse myoblasts (Marzi et al., 2012). Similar results were seen in porcine satellite cells (Chen et al., 2020). miR-127 plus others have been selected for further testing as important miRNA and their potential role in muscle development and meat quality (Iqbal et al., 2020). miRNA-mRNA networks have shown that expression of miRNA is negatively correlated with the expression of mRNA targets (Ji et al., 2020; Ali et al., 2021).

miR-29a was differentially expressed in 4 of the 5 comparisons made in the current study and continually increased in expression level as development progressed. Ovine satellite cells were cultured to assess the loss of function of miR-29a and its impacts on proliferation and differentiation. miR-29a inhibition reduced cellular proliferation on d 2 but increased proliferation on d 3. AntagomiRs function through binding to the target miRNA and rendering it incapable of binding to mRNA (Broderick and Zamore, 2011; Stenvang et al., 2012). There is a level of cytotoxicity associated with the use of lipofectamine and this could explain initial reductions in cellular proliferation that were seen in all lipofectamine treated cultures (Wang J. Y. et al., 2018). Mouse myoblast, C2C12, proliferation is inhibited by pooled miR-29 family members, however differentiation

is promoted (Wei et al., 2013). miR-29 targets Akt3 and reduces the expression of mRNA and protein abundance. Ovine satellite cell differentiation capacity was increased by the inhibition of miR-29a. These results contrast with Wei et al. (2013) and show that even though miRNA family members are similar their biological function can vary between species. miR-29a is highly expressed in beta cells of the pancreatic islets and expression levels are associated with insulin resistance (Dalgaard et al., 2022). miR-29a has been shown to control cell proliferation in small cell lung cancer, hepatocellular carcinoma, and pancreatic ductal adenocarcinoma by targeting a variety of genes depending on cell type (Wang T. et al., 2018). More research is needed to explore the role of miR-29a in skeletal muscle development.

Muscle development is essential for both pre and postnatal development of offspring. Muscle fiber characteristics showed massive increases in fiber size and significant changes in muscle fiber type occur during pre and postnatal development. Alterations observed in the miRNA transcriptome add molecular evidence to the magnitude of changes occurring in skeletal muscle tissue during the transitional stage. The greatest change in miRNA expression occurred during the transition from prenatal to postnatal stage with 115 miRNA differentially expressed (DE) in comparison to other developmental time points only having from 2 to 36 DE. Key miRNA identified in this time period included miR-22-3p, -299-5p, -487b-3p, -30c, -127, -432, -30d, -29a, and -143 and let-7g (Figure 5). Of these, several have documented roles in myogenesis (miR-22-3p, -29a, -127, -432, -487b-3p), cardiomyocytes (miR-29a, -30c, -30d or let-7g), vascular smooth muscle (miR-143) or cell proliferation (miR-29a, -299-5p). More research is needed to determine the role of these miRNA in skeletal muscle hypertrophy and if they could be used to alter muscle growth or regeneration.

Data availability statement

The datasets presented in this study can be found in online repositories. The name of the repository and accession number can be found below: NCBI; GSE207055.

Ethics statement

The animal study was reviewed and approved by Clemson University Institutional Animal Care and Use Committee (AUP-2018-055 and AUP-2018-049).

Author contributions

MG performed sample collections, prepared muscle histology slides for imaging with the assistance of RP, extracted RNA, interpreted data, and composed the first draft of the manuscript. RP and TB performed immunofluorescence of muscle histology samples and imaged slides for analysis. WB aided with histology and cell culture data analysis. SD analyzed histology images, interpreted data, conceived the original research study, and was the principal investigator. All authors have read and approved the manuscript.

Funding

Technical contribution No. 7010 of the Clemson University Experiment Station. This material is based upon work supported by NIFA/USDA, under project number SC-1700580. This research was supported by South Carolina Center for Translational Research Improving Musculoskeletal Health NIH COBRE (P20GM121342), a National Institutes of Health Center of Biomedical Research Excellence (COBRE) funded by NIH/NIGMS (P20GM121342).

Acknowledgments

Appreciation is expressed to: J. L. Britt, S. M. Justice, M. C. Miller, R. Smith, B. Cochran and AVS 4920 Myostatin and Muscle undergraduate students for assistance with this research project. The SC-71 and BA-F8 antibodies developed by S. Schiaffino were obtained from the Developmental Studies Hybridoma Bank, created by the NICHD of the NIH and maintained at The University of Iowa, Department of Biology, Iowa City, IA 52242. The 6H1 antibody developed by C. Lucas was obtained from the Developmental Studies Hybridoma Bank, created by the NICHD of the NIH and maintained at The University of Iowa, Department of Biology, Iowa City, IA 52242. The research reported in this publication was conducted using a Leica DMi8 widefield microscope system, housed in the Clemson Light Imaging Facility (CLIF). CLIF is supported, in part, by the Clemson University Division of Research.

Conflict of interest

The authors declare that the research was conducted in the absence of any commercial or financial relationships that could be construed as a potential conflict of interest.

Publisher's note

All claims expressed in this article are solely those of the authors and do not necessarily represent those of their affiliated

organizations, or those of the publisher, the editors and the reviewers. Any product that may be evaluated in this article, or claim that may be made by its manufacturer, is not guaranteed or endorsed by the publisher.

Supplementary material

The Supplementary Material for this article can be found online at: https://www.frontiersin.org/articles/10.3389/fgene.2022.988756/full#supplementary-material

References

Ali, A., Murani, E., Hadlich, F., Liu, X., Wimmers, K., and Ponsuksili, S. (2021). Prenatal skeletal muscle transcriptome analysis reveals novel MicroRNA-mRNA networks associated with intrauterine growth restriction in pigs. *Cells* 10, 1007. doi:10.3390/cells10051007

Anderson, C., Catoe, H., and Werner, R. (2006). MIR-206 regulates connexin43 expression during skeletal muscle development. *Nucleic Acids Res.* 34, 5863–5871. doi:10.1093/nar/gkl743

Antoniou, A., Mastroyiannopoulos, N. P., Uney, J. B., and Phylactou, L. A. (2014). miR-186 inhibits muscle cell differentiation through myogenin regulation. *J. Biol. Chem.* 289, 3923–3935. doi:10.1074/jbc.M113.507343

Broderick, J., and Zamore, P. (2011). microRNA Therapeutics. *Gene Ther.* 18, 1104–1110. doi:10.1038/gt.2011.50

Cardasis, C. A., and Cooper, G. W. (1975). An analysis of nuclear numbers in individual muscle fibers during differentiation and growth: A satellite cell-muscle fiber growth unit. *J. Exp. Zool.* 191, 347–358. doi:10.1002/jez.1401910305

Chal, J., and Pourquié, O. (2017). Making muscle: Skeletal myogenesis *in vivo* and *in vitro*. *Development* 144, 2104–2122. doi:10.1242/dev.151035

Chen, J.-F., Mandel, E. M., Thomson, J. M., Wu, Q., Callis, T. E., Hammond, S. M., et al. (2006). The role of microRNA-1 and microRNA-133 in skeletal muscle proliferation and differentiation. *Nat. Genet.* 38, 228–233. doi:10.1038/ng1725

Chen, X., Zhao, C., Dou, M., Sun, Y., Yu, T., Pang, W., et al. (2020). Deciphering the miRNA transcriptome of Rongchang pig longissimus dorsi at weaning and slaughter time points. *J. Anim. Physiol. Anim. Nutr.* 104, 954–964. doi:10.1111/jpn.13314

Crist, C. G., Montarras, D., and Buckingham, M. (2012). Muscle satellite cells are primed for myogenesis but maintain quiescence with sequestration of Myf5 mRNA targeted by microRNA-31 in mRNP granules. *Cell Stem Cell* 11, 118–126. doi:10.1016/j.stem.2012.03.011

Dalgaard, L. T., Sorensen, A. E., Hardikar, A. A., and Joglekar, M. V. (2022). The microRNA-29 family - role in metabolism and metabolic disease. *Am. J. Physiol. Cell Physiol.* 323, C367–C377. doi:10.1152/ajpcell.00051.2022

Danoviz, M. E., and Yablonka-Reuveni, Z. (2012). "Skeletal muscle satellite cells: Background and methods for isolation and analysis in a primary culture system," in *Myogenesis Methods in Molecular Biology*. Editor J. X. DiMario (Totowa, NJ: Humana Press), 21–52. doi:10.1007/978-1-61779-343-1_2

Davis, T. A., and Fiorotto, M. L. (2009). Regulation of muscle growth in neonates. *Curr. Opin. Clin. Nutr. Metab. Care* 12, 78–85. doi:10.1097/MCO.0b013e32831cef9f

Enright, A. J., John, B., Gaul, U., Tuschl, T., Sander, C., and Marks, D. S. (2003). MicroRNA targets in Drosophila. *Genome Biol.* 5, R1. doi:10.1186/gb-2003-5-1-r1

Fahey, A. J., Brameld, J. M., Parr, T., and Buttery, P. J. (2005). Ontogeny of factors associated with proliferation and differentiation of muscle in the ovine fetus. *J. Anim. Sci.* 83, 2330–2338. doi:10.2527/2005.83102330x

Forterre, A., Komuro, H., Aminova, S., and Harada, M. (2020). A comprehensive review of cancer MicroRNA therapeutic delivery strategies. *Cancers* 12, 1852. doi:10.3390/cancers12071852

Friedländer, M. R., Mackowiak, S. D., Li, N., Chen, W., and Rajewsky, N. (2012). miRDeep2 accurately identifies known and hundreds of novel microRNA genes in seven animal clades. *Nucleic Acids Res.* 40, 37–52. doi:10.1093/nar/gkr688

Friedman, R. C., Farh, K. K.-H., Burge, C. B., and Bartel, D. P. (2009). Most mammalian mRNAs are conserved targets of microRNAs. *Genome Res.* 19, 92–105. doi:10.1101/gr.082701.108

Gharaibeh, B., Lu, A., Tebbets, J., Zheng, B., Feduska, J., Crisan, M., et al. (2008). Isolation of a slowly adhering cell fraction containing stem cells from murine skeletal muscle by the preplate technique. *Nat. Protoc.* 3 (9), 1501–1509.

Greene, M. A., Britt, J. L., Powell, R. R., Feltus, F. A., Bridges, W. C., Bruce, T., et al. (2019). Ergot alkaloid exposure during gestation alters: 3. Fetal growth, muscle fiber development, and miRNA transcriptome1. *J. Anim. Sci.* 97, 3153–3168. doi:10.1093/jas/skz153

Greenwood, P. L., and Bell, A. W. (2019). Developmental programming and growth of Livestock tissues for meat production. *Vet. Clin. North Am. Food Anim. Pract.* 35, 303–319. doi:10.1016/j.cvfa.2019.02.008

Horak, M., Novak, J., and Bienertova-Vasku, J. (2016). Muscle-specific microRNAs in skeletal muscle development. *Dev. Biol.* 410, 1–13. doi:10.1016/j.ydbio.2015.12.013

Houba, P., and Te Pas, M. F. W. (2004). "The muscle regulatory factors gene family in relation to meat production," in *Muscle development of Livestock animals* (Cambridge, MA: CABI), 201–223.

Hu, W., and Coller, J. (2012). What comes first: Translational repression or mRNA degradation? The deepening mystery of microRNA function. *Cell Res.* 22, 1322–1324. doi:10.1038/cr.2012.80

Iqbal, A., Ping, J., Ali, S., Zhen, G., Juan, L., Kang, J. Z., et al. (2020). Role of microRNAs in myogenesis and their effects on meat quality in pig — a review. *Asian-Australas. J. Anim. Sci.* 33, 1873–1884. doi:10.5713/ajas.20.0324

Ji, H., Wang, H., Ji, Q., Ji, W., Luo, X., Wang, J., et al. (2020). Differential expression profile of microRNA in yak skeletal muscle and adipose tissue during development. *Genes Genomics* 42, 1347–1359. doi:10.1007/s13258-020-00988-8

Kanehisa, M., Araki, M., Goto, S., Hattori, M., Hirakawa, M., Itoh, M., et al. (2008). KEGG for linking genomes to life and the environment. *Nucleic Acids Res.* 36, D480–D484. doi:10.1093/nar/gkm882

Kaur, M., Kumar, A., Siddaraju, N. K., Fairoze, M. N., Chhabra, P., Ahlawat, S., et al. (2020). Differential expression of miRNAs in skeletal muscles of Indian sheep with diverse carcass and muscle traits. *Sci. Rep.* 10, 16332. doi:10.1038/s41598-020-73071-7

Kostrominova, T. Y. (2011). Application of WGA lectin staining for visualization of the connective tissue in skeletal muscle, bone, and ligament/tendon studies. *Microsc. Res. Tech.* 74, 18–22. doi:10.1002/jemt.20865

Langmead, B., Trapnell, C., Pop, M., and Salzberg, S. L. (2009). Ultrafast and memory-efficient alignment of short DNA sequences to the human genome. *Genome Biol.* 10, R25. doi:10.1186/gb-2009-10-3-r25

Lefaucheur, L., and Gerrard, D. (2000). Muscle fiber plasticity in farm mammals. *J. Anim. Sci.* 77, 1. doi:10.2527/jas2000.77E-Suppl1b

Li, J., Reed, S. A., and Johnson, S. E. (2009). Hepatocyte growth factor (HGF) signals through SHP2 to regulate primary mouse myoblast proliferation. *Exp. Cell Res.* 315, 2284–2292. doi:10.1016/j.yexcr.2009.04.011

Lie, S., Morrison, J. L., Williams-Wyss, O., Suter, C. M., Humphreys, D. T., Ozanne, S. E., et al. (2014). Periconceptional undernutrition programs changes in insulin-signaling molecules and microRNAs in skeletal muscle in singleton and twin fetal sheep. *Biol. Reprod.* 90, 5. doi:10.1095/biolreprod.113.109751

Ling, Y., Zheng, Q., Jing, J., Sui, M., Zhu, L., Li, Y., et al. (2020). RNA-seq reveals miRNA role shifts in seven stages of skeletal muscles in goat fetuses and kids. *Front. Genet.* 11, 684. doi:10.3389/fgene.2020.00684

Mao, X., Cai, T., Olyarchuk, J. G., and Wei, L. (2005). Automated genome annotation and pathway identification using the KEGG Orthology (KO) as a controlled vocabulary. *Bioinformatics* 21, 3787–3793. doi:10.1093/bioinformatics/bti430

Marzi, M. J., Puggioni, E. M. R., Dall'Olio, V., Bucci, G., Bernard, L., Bianchi, F., et al. (2012). Differentiation-associated microRNAs antagonize the Rb–E2F pathway to restrict proliferation. *J. Cell Biol.* 199, 77–95. doi:10.1083/jcb.201206033

Mauro, A. (1961). Satellite cell of skeletal muscle fibers. *J. Biophys. Biochem. Cytol.* 9, 493–495. doi:10.1083/jcb.9.2.493

McDaneld, T. G., Smith, T. P., Doumit, M. E., Miles, J. R., Coutinho, L. L., Sonstegard, T. S., et al. (2009). MicroRNA transcriptome profiles during swine skeletal muscle development. *BMC Genomics* 10, 77. doi:10.1186/1471-2164-10-77

Pette, D., and Staron, R. S. (1997). Mammalian skeletal muscle fiber type transitions. *Int. Rev. Cytol.* 170, 143–223. doi:10.1016/s0074-7696(08)61622-8

Qadir, A. S., Woo, K. M., Ryoo, H.-M., Yi, T., Song, S. U., and Baek, J.-H. (2014). MiR-124 inhibits myogenic differentiation of mesenchymal stem cells via targeting Dlx5. *J. Cell. Biochem.* 115, 1572–1581. doi:10.1002/jcb.24821

Rattray, P. V., Garrett, W. N., East, N. E., and Hinman, N. (1974). Growth, development and composition of the ovine conceptus and mammary gland during pregnancy. *J. Anim. Sci.* 38, 613–626. doi:10.2527/jas1974.383613x

Rehfeldt, C., Te Pas, M. F. W., Wimmers, K., Brameld, J. M., Nissen, P. M., Berri, C., et al. (2011). Advances in research on the prenatal development of skeletal muscle in animals in relation to the quality of muscle-based food. I. Regulation of myogenesis and environmental impact. *Animal* 5, 703–717. doi:10.1017/S1751731110002089

Rupaimoole, R., and Slack, F. J. (2017). MicroRNA therapeutics: Towards a new era for the management of cancer and other diseases. *Nat. Rev. Drug Discov.* 16, 203–222. doi:10.1038/nrd.2016.246

Schiaffino, S., Reggiani, C., Akimoto, T., and Blaauw, B. (2021). Molecular mechanisms of skeletal muscle hypertrophy. *J. Neuromuscul. Dis.* 8, 169–183. doi:10.3233/JND-200568

Schiaffino, S., Rossi, A. C., Smerdu, V., Leinwand, L. A., and Reggiani, C. (2015). Developmental myosins: Expression patterns and functional significance. *Skelet. Muscle* 5, 22. doi:10.1186/s13395-015-0046-6

Schmidt, M., Schüler, S. C., Hüttner, S. S., von Eyss, B., and von Maltzahn, J. (2019). Adult stem cells at work: Regenerating skeletal muscle. *Cell. Mol. Life Sci.* 76, 2559–2570. doi:10.1007/s00018-019-03093-6

Stenvang, J., Petri, A., Lindow, M., Obad, S., and Kauppinen, S. (2012). Inhibition of microRNA function by antimiR oligonucleotides. *Silence* 3, 1. doi:10.1186/1758-907X-3-1

Velleman, S. G., Clark, D. L., and Tonniges, J. R. (2019). The effect of nutrient restriction on the proliferation and differentiation of Turkey pectoralis major satellite cells differing in age and growth rate. *Poult. Sci.* 98, 1893–1902. doi:10.3382/ps/pey509

Verma, M., Asakura, Y., and Asakura, A. (2019). Inhibition of microRNA-92a increases blood vessels and satellite cells in skeletal muscle but does not improve duchenne muscular dystrophy-related phenotype in mdx mice. *Muscle Nerve* 59, 594–602. doi:10.1002/mus.26433

Wang, J. Y., Shang, Q., Wang, D. D., Yan, W., Sha, H. H., Zhao, J. H., et al. (2018). miR-29a: a potential therapeutic target and promising biomarker in tumors. *Biosci. Rep.* 38 (1), BSR20171265. doi:10.1042/BSR20171265

Wang, T., Larcher, L., Ma, L., and Veedu, R. (2018). Systematic screening of commonly used commercial transfection reagents towards efficient transfection of single-stranded oligonucleotides. *Molecules* 23, 2564. doi:10.3390/molecules23102564

Wegner, J., Albrecht, E., Fiedler, I., Teuscher, F., Papstein, H.-J., and Ender, K. (2000). Growth- and breed-related changes of muscle fiber characteristics in cattle. *J. Anim. Sci.* 78, 1485–1496. doi:10.2527/2000.7861485x

Wegner, J., Fiedler, I., Klosowska, D., Klosowski, B., and Ziegan, B. (1993). Changes in the distribution of muscle fiber types in the M. longissimus dorsi of boars during growth, prepared by different histochemical methods. *Anat. Histol. Embryol.* 22, 355–359. doi:10.1111/j.1439-0264.1993.tb00231.x

Wei, W., He, H.-B., Zhang, W.-Y., Zhang, H.-X., Bai, J.-B., Liu, H.-Z., et al. (2013). miR-29 targets Akt3 to reduce proliferation and facilitate differentiation of myoblasts in skeletal muscle development. *Cell Death Dis.* 4, e668. doi:10.1038/cddis.2013.184

Wen, M., Shen, Y., Shi, S., and Tang, T. (2012). miREvo: an integrative microRNA evolutionary analysis platform for next-generation sequencing experiments. *BMC Bioinforma.* 13, 140. doi:10.1186/1471-2105-13-140

Young, M. D., Wakefield, M. J., Smyth, G. K., and Oshlack, A. (2010). Gene ontology analysis for RNA-seq: Accounting for selection bias. *Genome Biol.* 11, R14. doi:10.1186/gb-2010-11-2-r14

Zhang, W., Wang, S.-Y., Deng, S.-Y., Gao, L., Yang, L.-W., Liu, X.-N., et al. (2018). MiR-27b promotes sheep skeletal muscle satellite cell proliferation by targeting myostatin gene. *J. Genet.* 97, 1107–1117. doi:10.1007/s12041-018-0998-5

Zhao, Q., Kang, Y., Wang, H.-Y., Guan, W.-J., Li, X.-C., Jiang, L., et al. (2016). Expression profiling and functional characterization of miR-192 throughout sheep skeletal muscle development. *Sci. Rep.* 6, 30281. doi:10.1038/srep30281

Zhou, L., Chen, J., Li, Z., Li, X., Hu, X., Huang, Y., et al. (2010). Integrated profiling of microRNAs and mRNAs: microRNAs located on Xq27.3 associate with clear cell renal cell carcinoma. *PLoS One* 5, e15224. doi:10.1371/journal.pone.0015224

Zhu, L., Hou, L., Ou, J., Xu, G., Jiang, F., Hu, C., et al. (2019). MiR-199b represses porcine muscle satellite cells proliferation by targeting JAG1. *Gene* 691, 24–33. doi:10.1016/j.gene.2018.12.052

Zhu, M. J., Ford, S. P., Nathanielsz, P. W., and Du, M. (2004). Effect of maternal nutrient restriction in sheep on the development of fetal skeletal muscle. *Biol. Reprod.* 71, 1968–1973. doi:10.1095/biolreprod.104.034561

frontiers | Frontiers in Genetics

TYPE Original Research
PUBLISHED 18 October 2022
DOI 10.3389/fgene.2022.991606

OPEN ACCESS

EDITED BY
Sayed Haidar Abbas Raza,
Northwest A&F University, China

REVIEWED BY
Qianjun Zhao,
Institute of Animal Sciences (CAAS), China
Mei Liu,
Hunan Agricultural University, China
Kerong Shi,
Shandong Agricultural University, China

*CORRESPONDENCE
Fenghua Lv,
fenghualvbnu@gmail.com
Meiying Fang,
meiying@cau.edu.cn

SPECIALTY SECTION
This article was submitted to Livestock Genomics, a section of the journal Frontiers in Genetics

RECEIVED 11 July 2022
ACCEPTED 03 October 2022
PUBLISHED 18 October 2022

CITATION
Cui R, Kang X, Liu Y, Liu X, Chan S, Wang Y, Li Z, Ling Y, Feng D, Li M, Lv F and Fang M (2022), Integrated analysis of the whole transcriptome of skeletal muscle reveals the ceRNA regulatory network related to the formation of muscle fibers in Tan sheep. *Front. Genet.* 13:991606. doi: 10.3389/fgene.2022.991606

Integrated analysis of the whole transcriptome of skeletal muscle reveals the ceRNA regulatory network related to the formation of muscle fibers in Tan sheep

Ran Cui[1], Xiaolong Kang[2], Yufang Liu[3], Ximing Liu[1], Shuheng Chan[1], Yubei Wang[1], Zhen Li[1], Yao Ling[1], Dengzhen Feng[2], Menghua Li[1], Fenghua Lv[1]* and Meiying Fang[1]*

[1]Department of Animal Genetics and Breeding, National Engineering Laboratory for Animal Breeding, MOA Laboratory of Animal Genetics and Breeding, College of Animal Science and Technology, China Agricultural University, Beijing, China, [2]College of Agriculture, Ningxia University, Yinchuan, China, [3]Key Laboratory of Animal Genetics, Breeding and Reproduction of Ministry of Agriculture and Rural Affairs, Institute of Animal Science, Chinese Academy of Agricultural Sciences, Beijing, China

Meat quality is highly influenced by the kind of muscle fiber, and it can be significantly improved by increasing the percentage of slow-twitch fibers. It is still not known which genes control the formation of muscle fibers or how those genes control the process of forming in sheep until now. In this study, we used high-throughput RNA sequencing to assess the expression profiles of coding and noncoding RNAs in muscle tissue of Tan sheep and Dorper sheep. To investigate the molecular processes involved in the formation of muscle fibers, we collected two different muscle tissues, *longissimus dorsi* and *biceps femoris*, from Tan sheep and Dorper sheep. The *longissimus dorsi* of Tan sheep and Dorper sheep displayed significantly differential expression levels for 214 lncRNAs, 25 mRNAs, 4 miRNAs, and 91 circRNAs. Similarly, 172 lncRNAs, 35 mRNAs, 12 miRNAs, and 95 circRNAs were differentially expressed in the *biceps femoris* of Tan sheep and Dorper sheep according to the expression profiling. GO and KEGG annotation revealed that these differentially expressed genes and noncoding RNAs were related to pathways of the formation of muscle fiber, such as the Ca^{2+}, FoxO, and AMPK signaling pathways. Several key genes are involved in the formation of muscle fibers, including ACACB, ATP6V0A1, ASAH1, EFHB, MYL3, C1QTNF7, SFSWAP, and FBXL5. RT-qPCR

Abbreviations: ceRNA, competing endogenous RNA; DE, endogenoustially expressed genes; DEMs, Differentially expressed miRNAs; DELs, Differentially expressed lncRNAs; DECs, Differentially expressed circRNAs; GO, Gene Ontology; KEGG, Kyoto Encyclopedia of Genes and Genomes; qPCR, quantitative Polymerase Chain Reaction; ACACB, acetyl-CoA carboxylase beta; ATP6V0A1, ATPase H+ transporting V0 subunit a1; ASAH1, N-acylsphingosine amidohydrolase 1; EFHB, EF-hand domain family member B; MYL3, myosin light chain 3; FBXL5, F-box and leucine rileucine-richotein 5; SFSWAP, splicing factor SWAP; C1QTNF7, C1q and TNF relateTNF-rerelatedong non-coding RNAs; mRNAs, messenger RNAs; miRNAs, microRNAs; circRNAs, circular RNA; MyH7, myosin heavy chain 7; MyHC, myosin heavy chain, cardiac muscle complex.

verified that the expression patterns of randomly selected differentially expressed transcripts were highly consistent with those obtained by RNA sequencing. A total of 10 lncRNAs, 12 miRNAs, 20 circRNAs, and 19 genes formed lncRNA/circRNA-miRNA-gene networks, indicating that the formation of muscle fiber in Tan sheep is controlled by intricate regulatory networks of coding and noncoding genes. Our findings suggested that specific ceRNA subnetworks, such as circ_0017336-miR-23a-FBXL5, may be critical in the regulation of the development of muscle fibers, offering a valuable resource for future study of the development of muscle fibers in this animal species. The findings increase our understanding of the variety in how muscle fibers originate in various domestic animals and lay the groundwork for future research into new systems that regulate the development of muscle.

KEYWORDS

Tan sheep, skelete muscle, lncRNA, circRNA, ceRNA

Introduction

Meat quality is an important economic trait, and the ratio of muscle fibers is one of the most important factors affecting meat quality traits, which can be significantly improved by increasing the proportion of slow-twitch fibers. Skeletal muscle is composed of two types of muscle fibers that are classified as slow-twitch and fast-twitch fibers, which have different metabolic and contractile properties. Compared with fast-twitch fibers, slow-twitch fibers have higher oxidative metabolism capacity and higher mitochondrial content, so their proportions are positively correlated with various aspects of meat quality, such as tenderness, flavor, and juiciness (Doerr, 1971; RyuandB and Kim, 2005; Su et al., 2013). Ningxia Tan sheep are an important breed for fur in China (Kang et al., 2013; Liu et al., 2018), but with the decline of the fur market, they have gradually been bred for meat. Previous studies have shown that some meat quality indicators of Tan sheep were measured, such as pH, hydraulic power, meat color, shear force, cooked meat percentage, muscle fiber density, and diameter, while the relationship between the proportion of muscle fibers and meat quality traits in Tan sheep requires a more precise interpretation; in this study, we compared the proportions of slow-twitch fibers in Tan sheep and Dorper sheep. Studies have also found the heritability of the muscle fiber content ranged from 0.20 to 0.68 (Larzul et al., 1999), and molecular breeding is a key method used for the improvement of slow-twitch fiber content. However, no effective molecular markers for slow-twitch fiber content selection practices in sheep have yet been found.

A growing number of studies have revealed that noncoding RNAs are involved in transcriptional regulation (Kotb et al., 2015), cellular communication, and signal transduction (Kristensen et al., 2019) and play a variety of significant roles in muscle growth and development (Hong et al., 2019). Competing endogenous RNA (ceRNA) is a common physiological mechanism by which lncRNAs and circRNAs compete with miRNAs for binding (Salmena et al., 2011). Previous studies have demonstrated noncoding RNA and ceRNA regulation of myoblast differentiation and the formation of muscle fibers in mouse, chicken, and bovine species. For example, the intronic lncRNA SYISL recruits polycomb repressive complex 2 in C2C12 cells to suppress the expression of the fast-twitch fiber marker gene and myoblast differentiation (Jin et al., 2018). CircPTPN4 can function as a ceRNA to regulate nicotinamide phosphoribosyltransferase (*NAMPT*) expression by sponging miR-499-3p, thus participating in muscle fiber type switching in chicken primary myoblasts (Cai et al., 2022). The *longissimus dorsi* in cattle was shown to express CircMYBPC1 differently during adult and embryonic phases of development, and CircMYBPC1 interacted with the muscle gene MYHC by directly binding to miR-23a (Chen et al., 2021). Although many studies related to the formation of muscle fibers have been published, the detailed molecular mechanism remains unclear, especially in noncoding RNA and ceRNA in sheep.

The molecular process of the formation of muscle fibers in Tan sheep has not yet undergone a comprehensive examination. Therefore, clarifying the roles of the DEGs and noncoding RNAs can contribute to understanding the changes in the whole transcriptomes associated with the formation of muscle fibers in different sheep groups. In this study, the muscle fiber contents of *longissimus dorsi* and *biceps femoris* in Tan sheep and Dorper sheep were determined, and whole-transcriptome profiles in different groups (Tan sheep and Dorper sheep) and different tissues (*longissimus dorsi* and *biceps femoris*) of the same groups were obtained to compare the DEGs and noncoding RNAs. Finally, we built a thorough competing endogenous RNA (ceRNA) network to identify the genes that are most likely to be involved in the formation of muscle fibers. In-depth knowledge of the molecular processes underlying the development of muscle fibers in Chinese Tan sheep is provided in this report.

Materials and methods

Animal sample collection

Animal care and sample collection were authorized by the State Key Laboratory of Agricultural Biotechnology of the Agricultural University of China's Animal Welfare Committee and carried out by the June 2004 amendments to the Regulations on the Control of Experimental Animals (Ministry of Science and Technology). Three unrelated male Tan sheep were used in the experimental group, while three unrelated Dorper sheep were used in the control group. Both groups of sheep were bred in Ningxia, China, under identical conditions until they were 8 months old, at which point they were killed on the same day. From these six sheep, samples of the *longissimus dorsi* and *biceps femoris* were taken and kept in liquid nitrogen or at −80°C until needed.

Immunofluorescence staining experiment

To examine whether the proportion of slow-twitch fibers differed among different sheep groups, we performed immunofluorescence using a slow-twitch marker protein (MYH7 antibody). The fluorescein-labeled MYH7 antibody was used as a probe to detect the target antigen in the muscle tissue and to identify the location of the antigen. First, the frozen tissue of the *longissimus dorsi* and *biceps femoris* was sectioned. Slices of tissue were first fixed for 20 min at room temperature in 4% paraformaldehyde, followed by 20 min of penetration in 0.1% Triton X-100. Tissue sections were tagged overnight with an antibody (MYH7, 1/500) at 4°C following an hour of closure with 1% BSA. Tissue slices were washed three times with ×1 PBS the next day and then stained with Alexa Fluor 488-conjugated antibody (1/1,000) at room temperature for 1 h. Then, the tissue slices were washed with ×1 PBS, and 10 mg/ml Hoechst was added for 10 min.

RNA extraction and sequencing

Following the manufacturer's instructions, total RNA was extracted using TRIzol Reagent (Invitrogen, United States). RNA quality was evaluated using agarose gels at a 1% concentration. A K5500 spectrophotometer was used to measure the purity of the RNA (Kaiao, China). The Bioanalyzer 2100 system and the RNA Nano 6000 Assay Kit were used to measure RNA integrity and concentration (Agilent Technologies, United States). The mRNA/lncRNA/circRNA library was built using 5 μg of RNA from each sample. The HiSeq 4000 sequencing platform (Novogene, China) was used to build mRNA/lncRNA/circRNA sequencing libraries, and 150 bp paired-end reads were produced by the manufacturer's instructions.

To create the small RNA library, 3 μg of the sample's total RNA were employed. Using the NEBNext® Multiplex Small RNA Library Prep Set for Illumina® (NEB, United States) by the manufacturer's instructions, sequencing libraries were built. Using DNA High Sensitivity Chips, the Agilent Bioanalyzer 2100 system assessed the sequencing library's quality. The HiSeq 2500 sequencing platform (Novogene, China) was used to build small RNA sequencing libraries, and 50 bp single-end reads were produced. Fastq formatted raw data were initially processed using internal Perl programs.

Bioinformatic analysis

The gene modeling annotation files and the reference genome (Oar v3.1) were accessed from Ensembl (https://asia.ensembl.org/index.html). Bowtie2 (LangmeadandS and Salzberg, 2012) was used to build the index of the reference genome, and HISAT2 (Pertea et al., 2016) was used to align paired-end clean reads to the reference genome. The mapped readings of each muscle sample were put together using StringTie (Pertea et al., 2016) with a reference-based method. Then, to identify lncRNAs, we assessed the assembled transcripts according to five criteria. The following transcripts were eliminated: 1) those with exon numbers <2, 2) those with lengths ≤200 bp, 3) those with known non-lncRNA annotations, 4) those with fragments per kilobase of exon per million fragments mapped (FPKM) < 0.5, and 5) Phylogenetic codon substitution frequency (PhyloCSF) (Sun et al., 2013). PFAM-scan (Kong et al., 2007), coding-noncoding-index (CNCI) (Finn et al., 2008), and coding potential calculator (CPC) (Kellis and Jungreis, 2011) were used to separate mRNAs from lncRNAs. All of the aforementioned tools predict that novel protein-coding transcriptome candidates are transcripts with coding potential, while novel lncRNAs are transcripts without coding potential. To determine the expression level of mRNA in each sample, FPKM (fragments per million fragments per exome) of coding genes was calculated using Cuffdiff (Trapnell et al., 2010). Differential expression analysis was performed using DESeq (Likun et al., 2010), with a default significant difference of two for fold change and a q value of 0.05.

Bowtie aligned small RNA tags to reference sequences to examine the expression and distribution of small RNA within the genome (LangmeadandS and Salzberg, 2012). Bedtools (https://bedtools.readthedocs.io/) was used to search for known miRNAs by matching them to entries in miRBase (http://www.mirbase.org/). MiRDeep2 (Friedlnder et al., 2012) was used to analyze the remaining reads to predict novel miRNAs. The following criteria were used to evaluate the expression levels of miRNAs and circRNA using TPM (Transcripts Per Kilobase of exon model per Million mapped reads) (Zhou et al., 2010). DESeq (Likun et al., 2010) was used to evaluate the differential expression, with a fold change threshold of 2 and a p value of 0.05.

CircRNAs were screened using find_circ (Memczak et al., 2013) and CIRI2 (Yuan and Zhao, 2015), and known and new

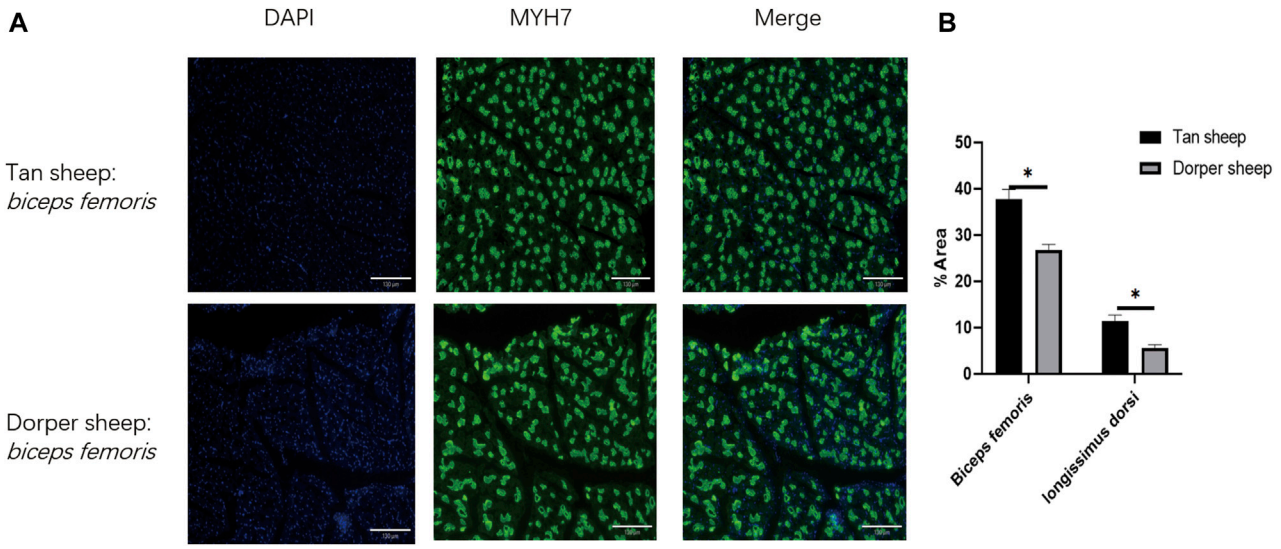

FIGURE 1
The difference of the slow-twitch fiber ratio of longissimus dorsi and Biceps femoris muscle between Tan sheep and Dorper sheep. **(A)** Frozen sections were immunofluorescently stained with MyH 17 antibody. "DAPI" is a staining solution suitable for the nuclear staining of common cells and tissues. "Merge" is to fuse the stained nucleus with the target protein. **(B)** Statistical chart of immunofluorescence staining results.

circRNAs in each sample were calculated (read count) and normalized with TPM (Zhou et al., 2010). Based on the distance from the corresponding circRNA along the genome sequence, the closest protein-coding genes for circRNAs were found to mark circular RNAs. Using circBase ID, which refers to circBase annotation, all known circRNAs were given names, and novel circRNAs were given names following the rank number listed. Exonic circRNA, intronic circRNA, antisense circRNA, intergenic circRNA, 3′UTR circRNA, 5′UTR circRNA, and ncRNA circRNA were the seven categories used to categorize all circRNAs (Memczak et al., 2013). The expression levels of circRNAs were quantified by the number of junction-spanning reads, and an absolute p value < 0.05 and fold change ≥2 were considered to be significantly differentially expressed. The coding potential of circRNAs was predicted using the presence or absence of an internal ribosome entry site (IRES) independent of the 5′ cap structure on the circRNA. IRES finder (Zhao et al., 2018) was used to predict whether circRNA sequences have potential elements of IRES.

Gene ontology and kyoto encyclopedia of genes and genomes enrichment analysis

DEGs, DE circRNA parental genes, DE lncRNAs, and DE miRNA target genes were subjected to functional and pathway enrichment analysis by Gene Ontology (GO) and Kyoto Encyclopedia of Genes and Genomes (KEGG) enrichment analysis. GOseq was based on the Wallenius noncentral hypergeometric distribution for GO enrichment analysis (Young et al., 2010). KOBAS v3.0 (Chen et al., 2011) was used to measure the statistical significance of enrichment in KEGG pathways.

Prediction of lncRNAs, miRNAs, and CircRNAs and construction of CeRNA network

10 kb upstream and downstream of the coding genes were identified as potential regulatory targets of lncRNAs. Expression of lncRNAs used for trans-acting prediction was co-expressed with mRNA rather than correlated with mRNA location. Using Pearson's correlation coefficients (r > 0.90 or r < −0.90) as a classifier, the expressed correlation between non-coding genes and genes was computed. Using miRanda (Enright et al., 2003), PITA (Marc et al., 2004), and RNAhybrid (Ventsislav et al., 2005), the prediction of miRNA target genes was carried out. The following threshold settings for PITA were established: maximum target length is 50,000; energy cut-off is 10, and 0.05 is the cut-off for the p-value. The following parameters were entered for RNAhybrid: utr: 3utr.fa; mir: mature. fa. To ensure the accuracy of our findings, we set the Smith-Waterman hybridization alignment match score higher than 140 and the minimum free energy of the duplex structure lower than −10. We created lncRNA/circRNA-miRNA–mRNA networks with lncRNA/circRNA acting as decoys, miRNA acting as the core, and mRNA acting as the target. Using Cytoscape (Michaele et al.,

2011), the lncRNA, circRNA, miRNA, and mRNA interactions were created and visualized.

Validation of differentially expressed transcripts

RT-qPCR validated the expression pattern of randomly selected differentially expressed transcripts from the longissimus dorsi and biceps femoris. FastKing gDNA Dispelling RT SuperMix and SuperReal PreMix Plus (Tiangen, China) mRNA detection assays were used for miRNA tests. The miRcute Plus miRNA First-strand cDNA Kit and miRcute Plus miRNA qPCR Kit (Tiangen, China) were used for microRNA tests. RT primers and a bespoke qRT–PCR quantitative kit (GenePharma, China) were used for circRNA detection. The RNase R- and control groups (without RNase R) were produced and translated into cDNA, and each circRNA was amplified using the primers indicated to visualize the back-splicing junction of the circRNA (Myriam and Gorospe, 2018; Heng et al., 2019). The back-splicing sites were then detected by sequencing the products. GAPDH and U6 small nuclear RNA genes were chosen as endogenous control genes (all primers are shown in Supplementary Table S12). Three biological replicates and triple reactions for each sample were used for all qPCR validations. Following amplification, the products were validated by agarose gel electrophoresis and Sanger sequencing, and the $2^{-\Delta\Delta Ct}$ method was used to determine the relative transcript abundance.

Cell culture and vector construction

Primary sheep myoblasts were isolated and cultured from embryo sheep leg muscle. Myoblasts and HEK293T cells (ATCC, United States) were cultured in high-glucose DMEM supplemented with fetal bovine serum (Hyclone, United States) and double antibiotics (1% penicillin and streptomycin). To induce myoblasts differentiation, cells were switched to a differentiation medium (DMEM; 2% horse serum) in nearly 90% confluence. Small interfering RNA (siRNA) against sheep circ_0017336 were designed and synthesized by Genepharma (Suzhou, China), and a nonspecific duplex was used as the control. Sheep myoblasts were transfected with 100 nM siRNA using Lipofectamine 2000. The si-circ_0017336 sequences are 5′-UUUGGAGAUAGCAGGGCUGTT-3′, 3′CAGCCCUGCUAUCUCCAAATT-5′. The fragment of the FBXL5 3′ UTR, including the binding site of miR-23a, was amplified and inserted into the psicheck2 vector (Promega, United States) at the 3′ end of the Renilla gene using restriction enzymes XhoI and NotI and T4 DNA ligase (TaKaRa, China). Psicheck2-FBXL5-M and psicheck2-FBXL5-W constructs were verified by sequencing.

Dual-luciferase reporter analysis

When the cell confluence reached about 80%, the miR-23a mimics and psicheck2-FBXL5-W or psicheck2-FBXL5-M were co-transfected into HEK293T cells using Lipofectamine 2000. After incubation for 24 h, Dual-luciferase activity was measured using an automatic microplate reader (Molecular Devices, United States), and the Renilla luciferase activity was normalized against firefly luciferase activity. The miR-23a mimics sequences are 5′-AUCACAUUGCCAGGGAUUUCC A-3′, 3′-GAAAUCCCUGGCAAUGUGAUUU-5′.

Analytical statistics

The means and standard error of the means are used to express data (SEM). Levene's test was used to check for homogeneity of variances, and then Student's *t*-test was used to determine significance. At $p < 0.05$, differences were deemed statistically significant.

Results

The proportion of slow muscle fibers in the *Biceps femoris* and *Longissimus dorsi* in sheep

According to the results of immunofluorescence staining, the proportions of slow-twitch fibers in the *longissimus dorsi* and *biceps femoris* of Tan sheep were 11.4% and 37.7%, respectively, and its proportions were 5.6% and 26.8% in the *longissimus dorsi* and *biceps femoris* of Dorper sheep. Tan sheep had considerably more slow-twitch muscle fibers than Dorper sheep did ($p < 0.01$) in their *longissimus dorsi* and *biceps femoris* (Figures 1A,B).

Blast analysis of transcriptome sequencing

The whole-transcriptome profiling of *longissimus dorsi* and *biceps femoris* tissues from Dorper sheep and Tan sheep were obtained to evaluate the genes involved in the formation of muscle fibers. The 12 samples used for the RNA sequencing libraries yielded an average of 95.74 million clean reads, and 83.55% to 90.07% of these reads were specifically aligned to the reference genome Oar v3.1. At least 85% of the readings were equal to or greater than Q30 (Supplementary Table S1-1). A total of 22,823 mRNAs, 224 known lncRNAs, and 22,373 unique lncRNAs were found in the muscle samples after additional filtering (Figure 2A) and removal of possible coding transcripts that were identified using CNCI, CPC, and PFAM (Figure 2B). The gene structure, expression, and sequence conservation of lncRNAs and protein-coding genes were

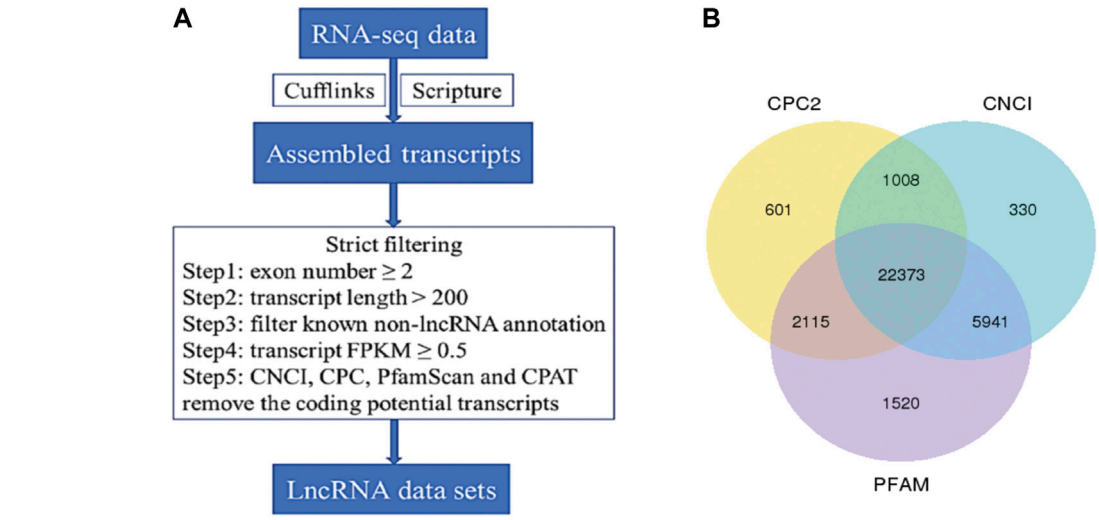

FIGURE 2
Identification of long non-coding RNAs (lncRNA) in muscle transcriptome. **(A)** Workflow for lncRNA identification. **(B)** Candidate lncRNAs were identified by using three applications: CNCI, coding-non-coding-index; CPC, coding potential calculator; PFAM-scan which detect and remove putative protein-coding transcripts.

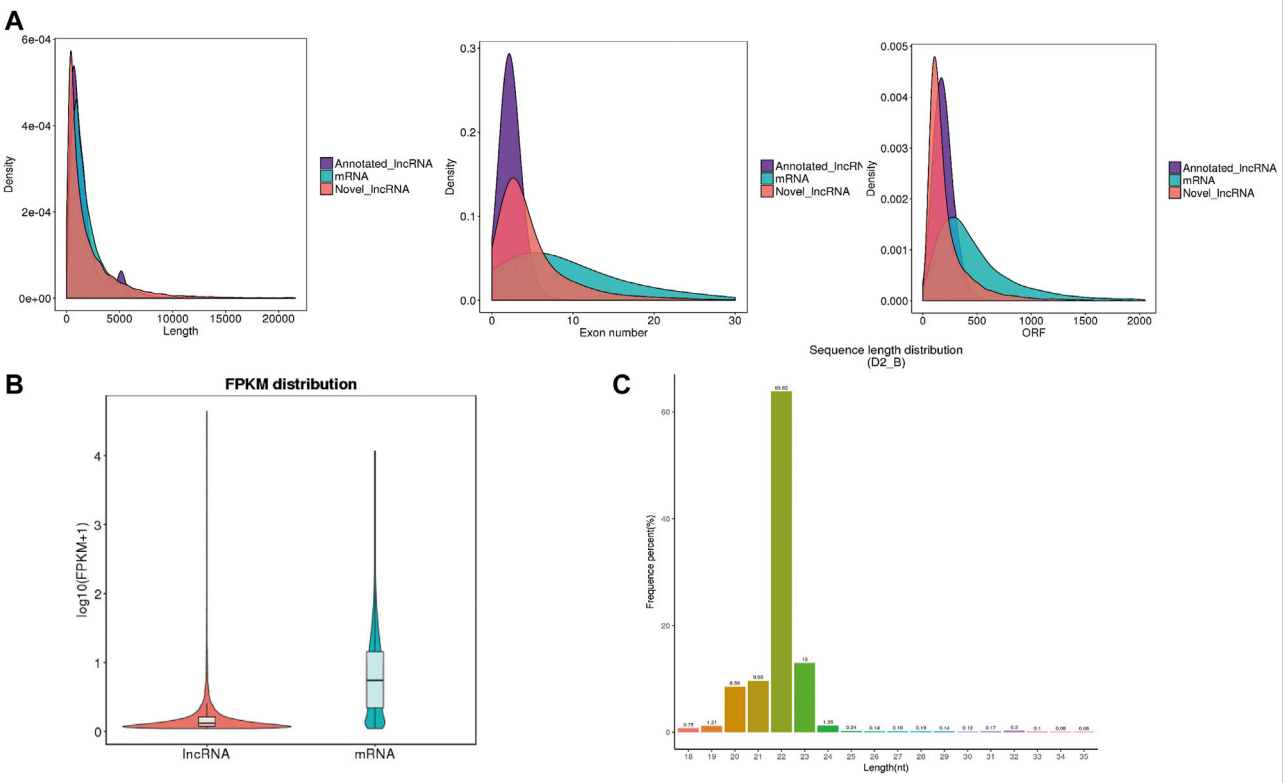

FIGURE 3
Genomic architecture and expression level of lncRNAs and miRNAs. **(A)** Comparison of mRNA transcript length, exon number and open reading frame (ORF) length. **(B)** Expression level of lncRNAs and mRNAs, calculated as log10(FPKM+1). **(C)** Length distribution of all identified small RNAS.

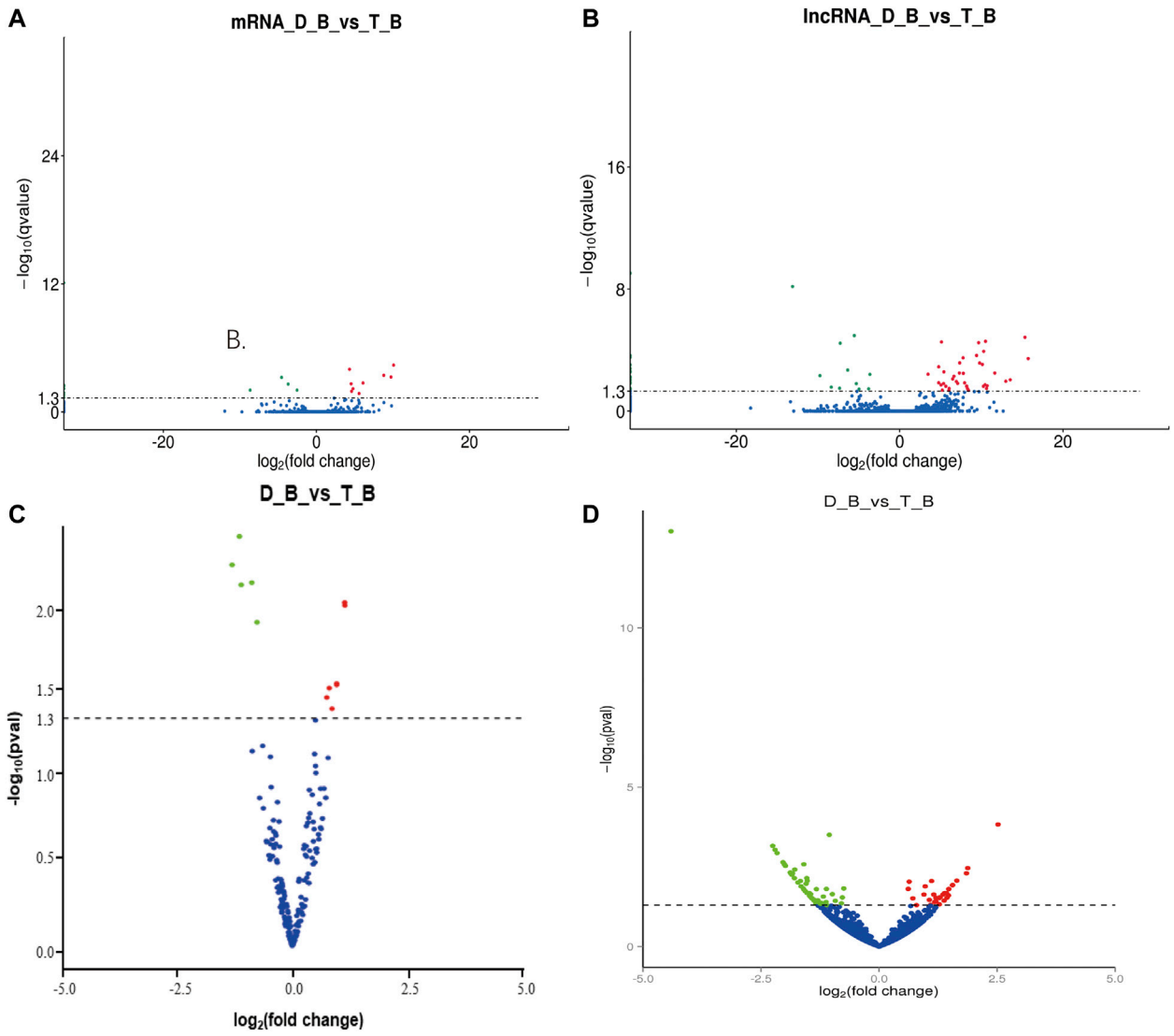

FIGURE 4
Differentially expressed mRNAs and non-coding RNAs in Tan sheep and Dorper sheep. **(A)** Expression profiles of mRNA in biceps femoris of Tan sheep and Dorper sheep. **(B)** Expression profiles of lncRNA in biceps femoris of Tan sheep and Dorper sheep. **(C)** Expression profiles of miRNA in biceps femoris of Tan sheep and Dorper sheep. **(D)** Expression profiles of circRNA in biceps femoris of Tan sheep and Dorper sheep. In the volcano plots, green points represent downregulated RNAs, while red points represent upregulated RNAS. "D_B" is the biceps femoris group of the Dorper sheep. "T_B" is the biceps femoris group of the Tan sheep.

compared. As lncRNA genomic characterizations were compared to those of mRNAs, it was discovered that the length range of their transcripts was similar; more lncRNAs had 2–4 exons than mRNAs, and they also had shorter open reading frames (ORFs) and lower FPKM values (Figures 3A,B).

With at least two independent reads crossing the back splice junction, a total of 3651 circRNAs were found. Exons, introns, and intergenic regions all serve as various circRNA source locations. Exons were more likely to produce circRNAs in this study; 3141 circRNAs were produced from exons of 1810 genes, whereas 197 circRNAs were produced from intronic regions of 175 genes, and our data indicated that the remaining circRNAs were intergenic. CircRNAs ranged in length from 192 nucleotides to 93,278 nucleotides and were mainly located on chromosome 1 (Supplementary Table S2). Interestingly, 4611 internal ribosome entry site (IRES) were predicted for circRNAs and that the highest score may reach 0.997 (Supplementary Table S12).

Additionally, for the small RNA-Seq libraries, rigorous filtering yielded an average of 16.02 million clean reads, with approximately 95% of these clean reads matched to the sheep reference sequence (Supplementary Table S1-2). Most clean reads ranged from 20 to 24 nt (Figure 3C). There were

238 known miRNAs in each sample, according to statistical statistics (Supplementary Table S2). A total of 141 mature miRNAs were annotated, and 97 new mature miRNAs were found (Supplementary Table S2).

Differential expression of genes and noncoding RNAs (LncRNAs, miRNAs, and circRNAs) between Tan sheep and Dorper sheep

In *biceps femoris* tissues, twelve DEGs were obtained between Tan sheep and Dorper sheep, where 11 were upregulated and 24 were downregulated (Supplementary Table S3; Figure 4A). Several DEGs were specifically expressed in Tan sheep, such as SFSWAP, or Dorper sheep, such as ASAH1. These genes may regulate the formation of muscle fibers.

Similarly, 172 DELs were discovered in the *biceps femoris* between Tan and Dorper sheep, of which 28 were upregulated and 144 were downregulated (Supplementary Table S5; Figure 4B). Several DE lncRNAs were particularly expressed in Tan sheep, including LNC 000295, LNC 000300, and LNC 000306, or Dorper sheep, including LNC_017854, LNC_02118,6, and LNC_015846. In the *biceps femoris*, there was a total of 15 differential expression miRNAs, of which 5 were upregulated and 7 were downregulated between Tan sheep and Dorper sheep (Supplementary Table S8; Figure 4C). MiR-133 (Martin et al., 2015), miR-370 (Zhang et al., 2021), and miR-148 (Yin et al., 2020) have been revealed to be important in the development of muscle fibers among these differentially expressed miRNAs. Additionally, 95 DECs were discovered in the *biceps femoris* between Tan sheep and Dorper sheep, of which 59 were upregulated and 36 were downregulated (Supplementary Table S10; Figure 4D).

In *longissimus dorsi* tissues, twenty-five DEGs were found between Tan sheep and Dorper sheep, including 12 upregulated and 13 downregulated in Tan sheep, which have more than 2-fold differential expression (Supplementary Table S3). These DEGs included F-box and leucine-rich repeat protein 5 (*FBXL5*) and myosin light chain 3 (*MYL3*), which are related to the regulation of the formation of muscle fibers. Several DEGs were specifically expressed in Tan sheep, such as FBXL5, or Dorper sheep, such as SFSWAP.

In all, 214 DELs were obtained in the *longissimus dorsi* tissues of Tan sheep and Dorper sheep, of which Tan sheep had 101 upregulated and 113 downregulated DELs (Supplementary Table S5). Several DE lncRNAs were specifically expressed in Tan sheep, such as LNC_003872, LNC_01870,8, and LNC_021269, or Dorper sheep, such as LNC_008982, LNC_00889,6, and LNC_001693. These lncRNAs may control how muscle fibers are formed. Three known miRNAs were expressed overall at lower levels in Tan sheep than in Dorper sheep, whereas one known miRNA was expressed at higher levels (Supplementary Table S8). One of these miRNAs with variable expression, miR-23a, has been linked to the development of muscle fibers (Chen et al., 2021). In the *longissimus dorsi* tissues of Tan sheep and Dorper sheep, a total of 91 DECs were also discovered, of which 45 were upregulated and 46 were downregulated (Supplementary Table S10).

Functional analysis of differentially expressed transcripts

GO and KEGG pathway analysis were carried out to assess the potential roles of differentially expressed genes, lncRNAs, miRNAs, and circRNAs. Three functional categories were carried out of the GO pathways for DEGs (biological process, cellular component, and molecular function). The biological processes involved in the development of muscle fibers, such as calcium ion transport (GO: 0006816), oxidation-reduction process (GO: 0055114), muscular system process (GO: 0003012), and regulation of myoblast differentiation (GO: 0045661), were also significantly enriched. The CAMP signaling pathway and metabolic pathways were significantly enriched according to KEGG enrichment analysis (Supplementary Table S4; Figures 5A,B). The development of muscle fibers also includes several important metabolic and myoblast differentiation-related genes, including ATP6V0A1 and MYL3.

Two separate algorithms—cis (genomic location) and trans (expression correlation)—were used to predict the target genes of the identified lncRNAs to elucidate their potential roles in the formation of muscle fibers, 2,154 cis-acting lncRNAs target a total of 720 genes among them, while 446 trans-acting lncRNAs have a total of 163 target genes. The GO pathway of cis-lncRNAs was highly enriched in negative regulation of glycolysis (GO: 0006110), muscle fiber development (GO: 0048741), and ATPase activity (GO: 0042623), and skeletal muscle contraction (GO: 0003009) (Supplementary Table S6). KEGG enrichment was significantly enriched in the metabolic pathway muscle atrophy; GO annotation of trans-lncRNAs was significantly enriched in positive regulation of skeletal muscle tissue development (GO: 0048643) and muscle cell differentiation (GO: 0042692); KEGG enrichment was significantly enriched in glycolysis, TCA cycle, and Wnt signaling pathway (Supplementary Table S7). GO annotation and KEGG enrichment analysis of the targets showed miRNAs were mainly enriched in metabolic pathways (Supplementary Table S9). The parental genes of DE circRNAs were largely enriched in myofibrils (GO: 0030016) and glycogen metabolic pathways (GO: 0005977), according to GO analysis. DE circRNAs were primarily enriched in the Ca^{2+} signaling pathways, FoxO signaling pathways, and AMPK signaling pathways, according to KEGG pathway analysis (Supplementary Table S11).

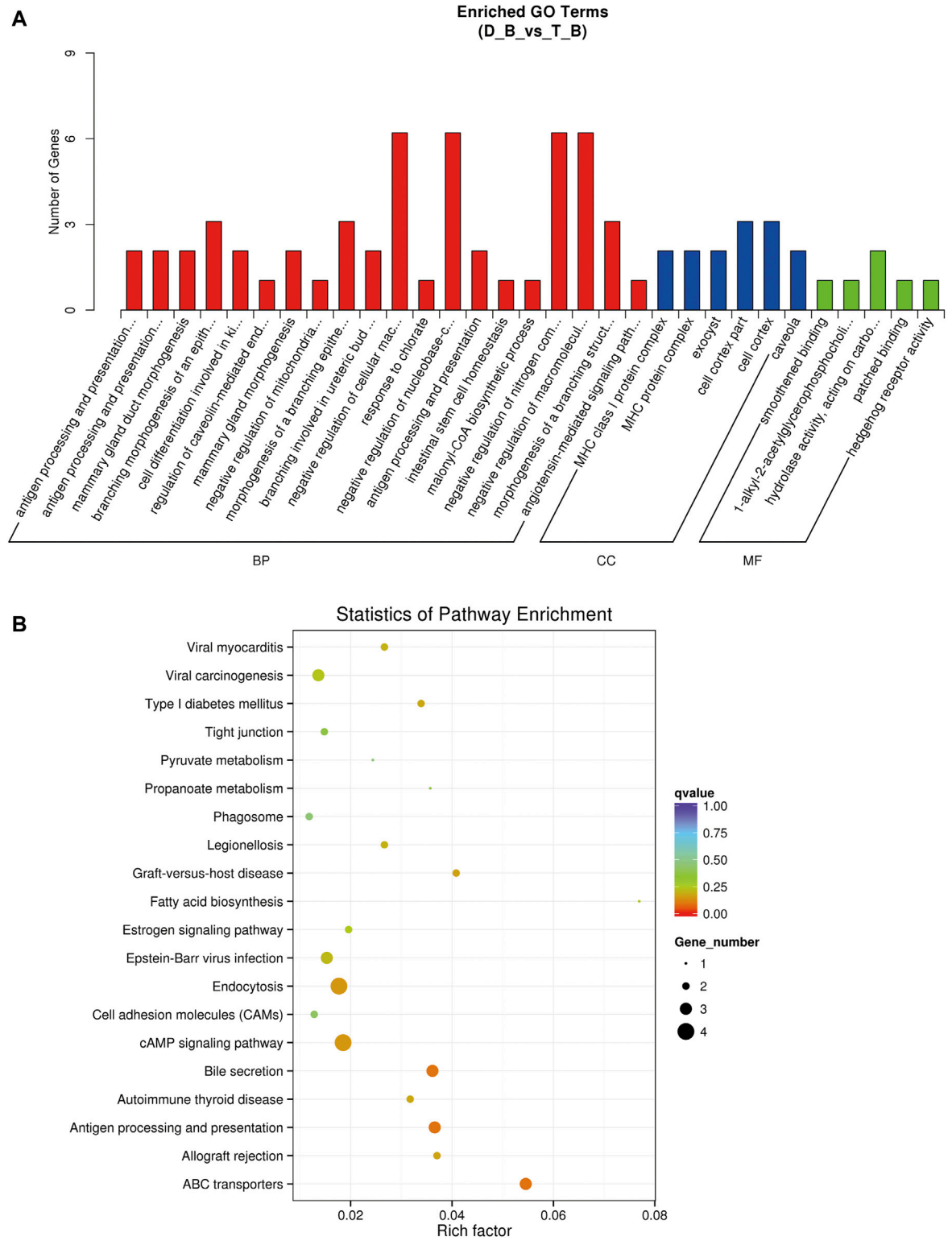

FIGURE 5
GO and KEGG enrichment analysis in biceps femoris of Tan sheep and Dorper sheep. **(A)** GO enrichment annotation of mRNAs. **(B)** KEGG annotation of mRNAs. "D_B"is the biceps femoris group of the Dorper sheep. "T_B" is the biceps femoris group of the Tan sheep.

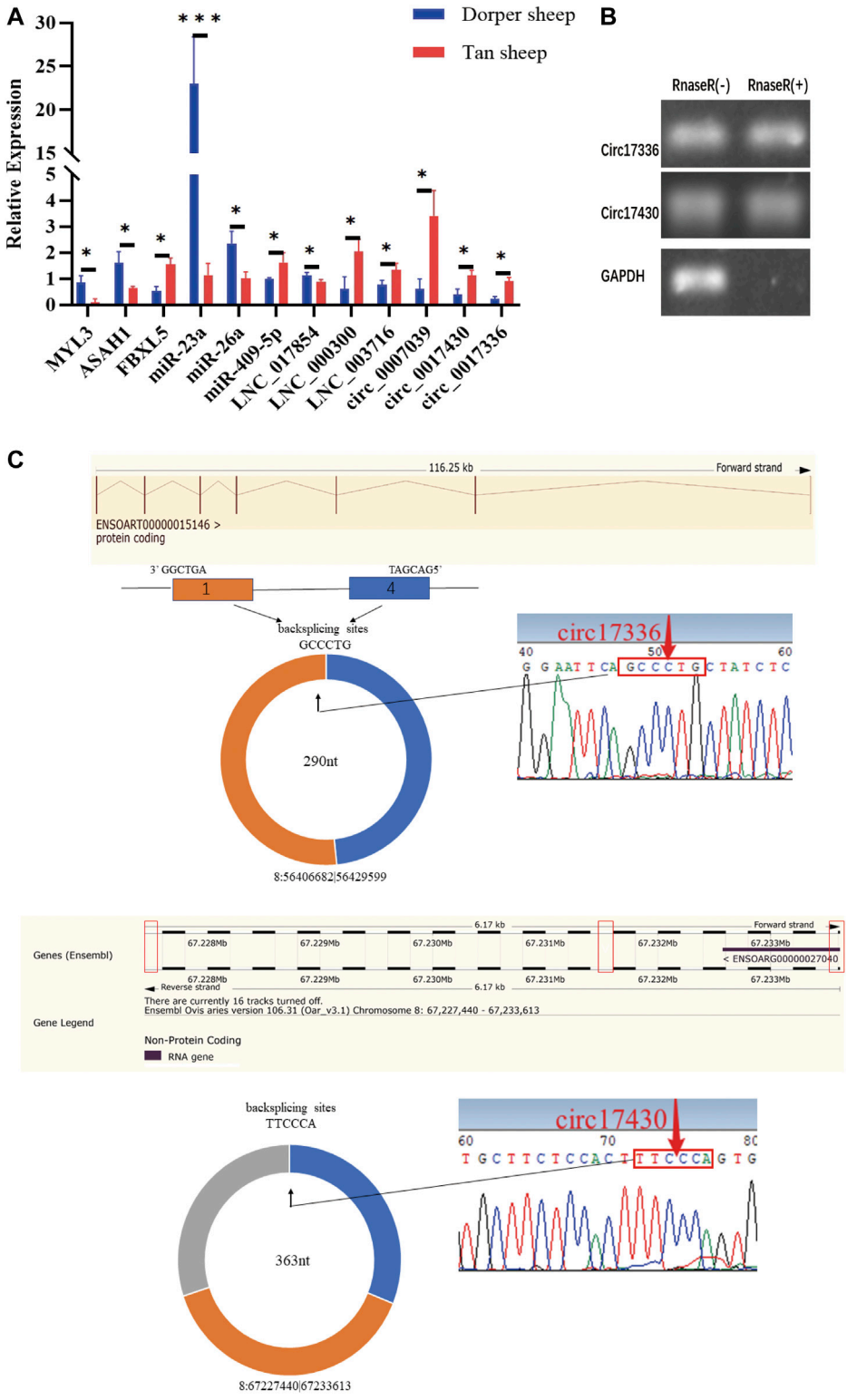

FIGURE 6
(A) The expression levels of mRNA, miRNA, lncRNA and circRNA were verified by qPCR. **(B)** The results obtained from use of Rnase R indicate that the expression levels of circ_0017336 and circ_0017430 are resistant to Rnase R. "Rnase R (+)" indicates RNA treated with RNase R: "Rnase R (–)" indicates untreated RNA. **(C)** The backsplice junctions of circ_0017336 and circ_0017430 were verified with Sanger sequencing. The red arrows indicate head-to-tail back-splicing sites of circRNAs.

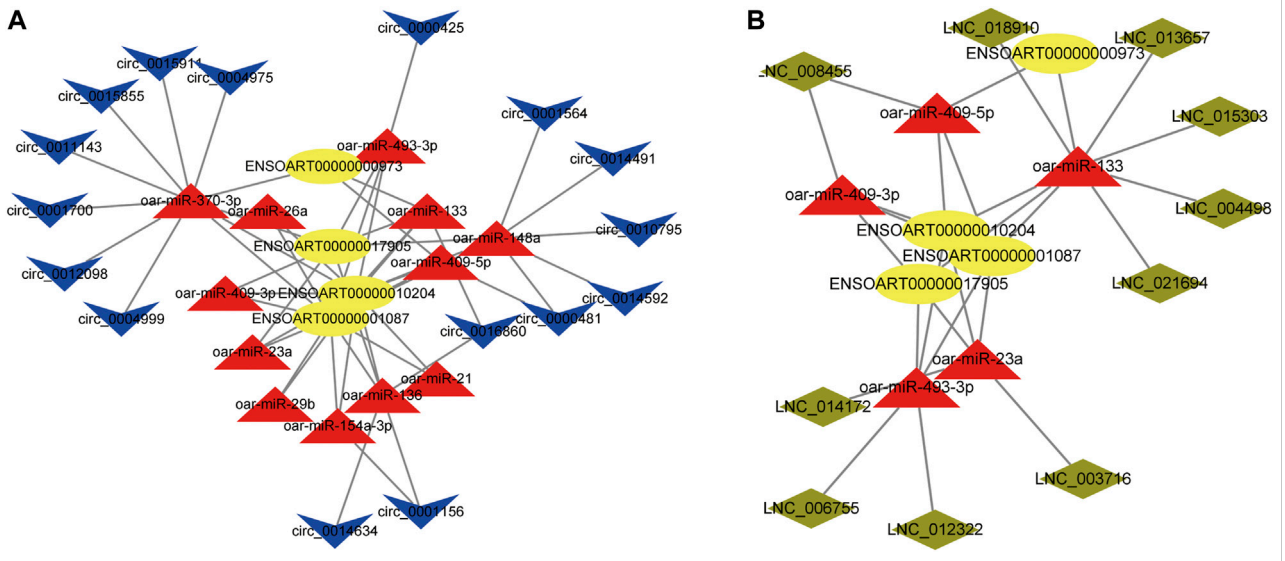

FIGURE 7
(A) CircRNA-miRNA-mRNA interaction network specifically expressed in Tan sheep. **(B)** LncRNA-miRNA-mRNA interaction network specifically expressed in Tan sheep. The ovals, triangles, parallelograms and V types represent mRNAs, miRNAs, lncRNAs and circRNAs, respectively.

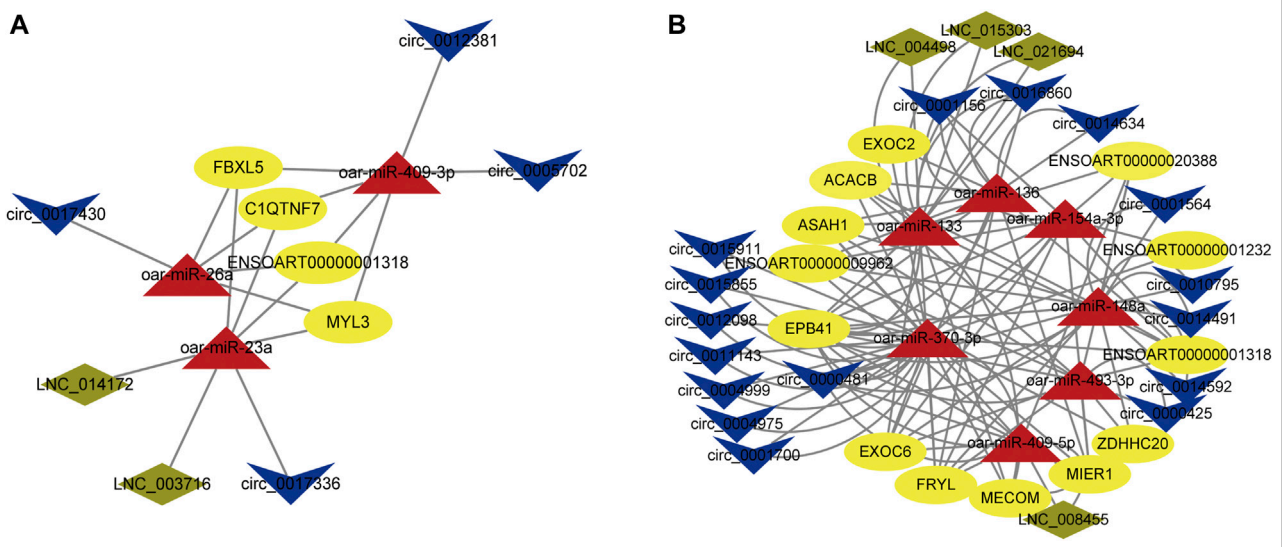

FIGURE 8
ceRNA network construction in differnt muscle tissues. **(A)** LncRNA/circRNA-miRNA-mRNA interaction network was constructed based on different expression levels in the longissimus dorsi of Tan sheep and Dorper sheep. **(B)** LncRNA/circRNA-miRNA-mRNA interaction network was constructed based on different expression levels in the biceps femoris of Tan sheep and Dorper sheep. The ovals, triangles, parallelograms and V types represent mRNAs, miRNAs, lncRNAs and circRNAs respectively.

Validation of differentially expressed transcript expression

To validate the RNA-seq results, *MYL3*, *ASAH1*, miR-409-5p, circ_0017336, circ_0007039, LNC_0017854, LNC_003716, and LNC_000300 were selected, and their expression patterns in *biceps femoris* tissue of Tan sheep and Dorper sheep were examined using qPCR. *FBXL5*, miR-23a, miR-26a, and circ_0017430 were also selected, and their expression patterns in *the longissimus dorsi* of Tan sheep and Dorper sheep were examined using qPCR (Figure 6A). RT–qPCR verified that the expression patterns of randomly above differentially expressed

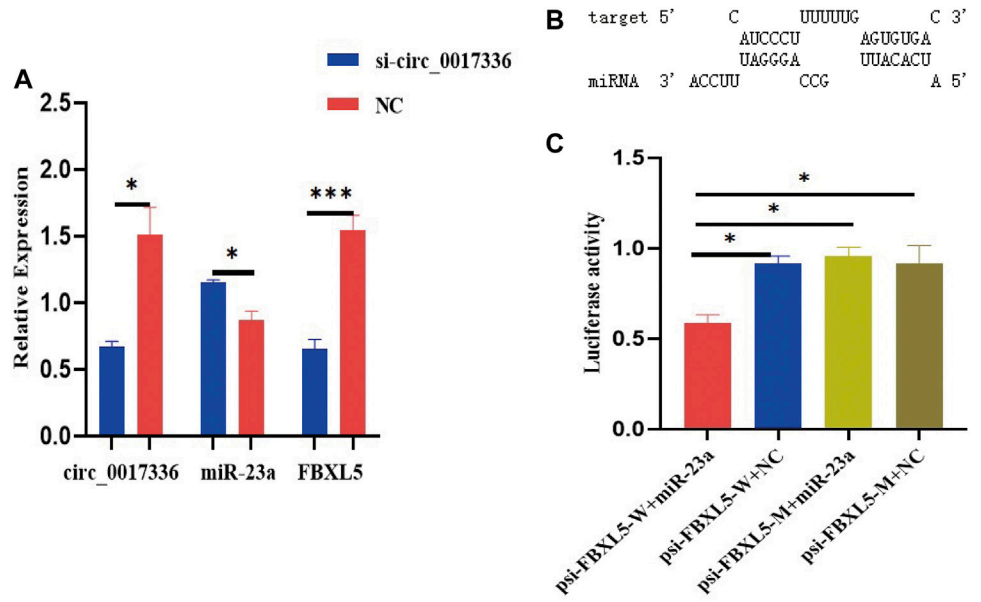

FIGURE 9
(A) si-circ_0017336 promotes the expression of miR-23a and inhibits the exprsion of FBXLS in sheep myoblasts. **(B)**. The binding sites of miR-23a and FBXLS were predicted by RNAhybrid software. **(C)** Dual-luciferase reporter gene experiments verified that miR-23a directly targets FBXL5. indicates $p < 0.05$, ***indicates $p < 0.001$, NC is the control group.

transcripts were highly consistent with those obtained by RNA sequencing. Notably, RNase R digestion assays further demonstrated that circ_0017336 and circ_0017430 had a circular structure (Figure 6B), and the back splice junctions of circRNAs were confirmed before validation (Figure 6C).

Construction of CeRNA regulatory network

We found lncRNA and circRNA gene pairs with miRNA binding sites based on the ceRNA hypothesis, and we constructed lncRNA–miRNA-gene pairs and circRNA-miRNA-genes with lncRNA and circRNA acting as decoys, miRNA as the core, and mRNA as the target. The ceRNA network generated above was then visualized with Cytoscape software, using various shapes to represent various types of RNAs. The specific circRNA-miRNA-gene networks and lncRNA–miRNA-gene networks closely related to the formation of muscle fibers in Tan sheep are shown in Figures 7A,B and a summary table listing all possible functioning ceRNA networks was added to Supplementary Table S14. Furthermore, from the ceRNA network, we observed some ceRNA subnetworks, which showed that circ_0017336 and its target FBXL5, ACACB and EXOC6 "talked" to each other through the same miR-23a response elements, whereas LNC_014172 and LNC_003716 "talked" to their targets through miR-23a response elements, respectively. Therefore, we speculate that these subnetworks may play a key role in the formation of muscle fiber.

In addition, we also constructed ceRNA networks in the *longissimus dorsi* and *biceps femoris* tissues. In the *longissimus dorsi*, the network shows possible interactions among 2 DE lncRNAs, 3 DE miRNAs, 4 DE circRNAs, and 4 DE mRNAs (Figure 8A; Supplementary Table S14). For example, circ_0017336 were identified as ceRNA of miR-23a, which targeted MYL3, FBXL5, and C1QTNF7; LNC_003716 and LNC_014172 regulated ENSOART00000001318 by competing miRNA response elements of miR-23a. The network depicts potential connections among 4 DE lncRNAs, 7 DE miRNAs, 16 DE circRNAs, and 13 DE mRNAs in the *biceps femoris* (Figure 8B; Supplementary Table S14). For instance, ASAH1 and circ_0000481 potentially create a ceRNA network through miR-409-5p as a bridge. These findings imply that genes and noncoding genes that exhibit differential expression in Tan sheep and Dorper sheep might work together to control the formation of muscle fibers *via* an interaction network, and their regulatory patterns are also different in different tissue sites.

miR-23a directly bound FBXL5

To investigate whether circ_0017336 acts as a competing endogenous RNA in sheep myoblasts, the interfering fragment si-circ_0017336 was transfected into sheep myoblasts to

significantly inhibit the expression level of circ_0017336. The changes of miR-23a and FBXL5 expression level were detected after 3 days of differentiation of myoblasts treated with si-circ_0017336, and it was found that the interference of circ_0017336 significantly increased the expression of miR-23a in skeletal muscle cells, but suppressed the expression of FBXL5 (Figure 9A). To further validate the targeting relationship between miR-23a and FBXL5, the prediction software RNAhybrid revealed that FBXL5 had putative miR-23a binding sites (Figure 9B). To verify whether miR-23a directly targets FBXL5, miR-23a mimics were co-transfected with psi-CHECK2 dual-luciferase reporters containing the 3′UTR of FBXL5 into 293T cells for luciferase activity analysis, and we found that overexpression of miR-23a reduced the luciferase activity (Figure 9C). These results revealed that FBXL5 could indeed bind miR-23a directly.

Discussion

The formation of muscle fibers is a polygenic trait in sheep, mainly determined by genetic factors, and is an important determinant of meat quality characteristics. Previous studies have revealed a closely association of the type of muscle fiber with meat quality traits due to the effects on the postmortem metabolic rate in the conversion of muscle to meat. The association between more slow-twitch fibers and better meat quality has been observed in a variety of species, including sheep (Valin et al., 1982), pigs (Bowker et al., 2005; Zhou et al., 2021), chickens (Ouyang et al., 2017), and calves (Maltin et al., 1998). Two mechanisms have been suggested for the muscle fiber pattern in Tan sheep. According to the research mentioned above, one theory proposes that the difference in the amount of slow-twitch fiber, with Tan sheep having more and Dorper sheep having less, is what causes the phenotypic. An alternative explanation claims that the difference is the result of an epigenetic regulatory process, possibly involving noncoding RNAs.

Given that some essential genes linked to specific phenotypes or significant biological processes have been identified using high-throughput RNA sequencing, it may be possible to understand the mechanisms underlying the formation of muscle fiber patterns. Numerous muscle tissue transcription profiles in animals have been studied using RNA sequencing, but similar studies have not been conducted in Tan sheep. To determine the critical elements involved in the formation of muscle fibers, we evaluated, for the first time, the differences in the expression profiles of mRNAs, lncRNAs, and circRNAs in the *longissimus dorsi* and *biceps femoris* tissues of two sheep breeds. Additionally, we found that a more complex ceRNA regulatory network is formed in the *longissimus dorsi* than in the *biceps femoris*. As studies have shown that slow-twitch fibers have higher mitochondrial content and oxidative phosphorylation capacity, and the ratio of slow-twitch fibers in the *longissimus dorsi muscle* is higher than that in the *biceps femoris* muscle, which makes it possible that the *longissimus dorsi* muscle has more glycolysis, oxidative phosphorylation, ad some metabolism-related genes to form a more complex ceRNA regulatory network.

Different metabolic and contractile characteristics exist between slow-twitch and fast-twitch fibers. Fast-twitch fibers have low oxidative metabolism and low mitochondrial content, while slow-twitch fibers have a high oxidative capability and large mitochondrial content. FBXL5, a member of the F-box protein family, regulates iron homeostasis in cells and systems by promoting the degradation of iron regulatory protein 2, and is an essential sensor for bioavailable iron (Ruiz and Bruick, 2014; Moroishi et al., 2014). The lack of iron in the body is closely related to the quality and function of skeletal muscle (Scherbakov et al., 2019), and we think that the formation of muscle fibers may be affected by the regulation of iron content by FBXL5. The acetyl-CoA carboxylase beta (ACACB) and ATPase H+ transporting V0 subunit a1 (ATP6V0A1) genes were significantly upregulated in Tan sheep, both of which were enriched in the oxidative phosphorylation pathway and consistent with the fact that Chinese native sheep have a better flavor than sheep from other regions. The main function of EFHB is to bind calcium ions (Rosado, 2021), triggering a Ca^{2+}-dependent transport pathway (Wu et al., 2002; Chin, 2005), causing the formation of skeletal muscle fibers. Additionally, MYL3 showed differential expression in the muscle tissues of Tan sheep and Dorper sheep, which was consistent with earlier research that also deemed these genes to be key candidates for muscle growth and development (Ouyang et al., 2017). According to GO analysis, MYL3 is mostly involved in muscle contraction. Additionally, the specific roles of SFSWAP and two novel transcripts (ENSOART00000001243 and ENSOART00000001318) are unknown and are differentially expressed in both tissues. While ENSOART00000001243 and ENSOART00000001318 are downregulated in both *longissimus dorsi* and *biceps femoris* tissues, SFSWAP was interestingly increased in *longissimus dorsi* tissues but downregulated in *biceps femoris* tissues. The varied functions of these genes during the formation of these two tissues may be related to these consistent or inconsistent trend changes in expression trends, which are worthy of future analysis.

Noncoding RNAs act as epigenetic regulators of the expression of protein-coding genes in eukaryotes, which can control the expression at both transcriptional and post-transcriptional stages (Kornienko et al., 2013), and the large-scale ceRNA networks composed of noncoding RNAs and mRNA are important for regulation in various physiological and pathological processes (Salmena et al., 2011; Ala et al., 2013). Numerous miRNAs are important regulators of the growth of muscle fibers. For instance, miR-23a affects the expression of the MYHC gene and the development of muscle cells (Wang et al., 2012; Chen et al., 2021). The constructed ceRNA network results also demonstrated that DE circRNAs competed with miR-23a for binding and may function as ceRNAs to regulate the levels of ACACB, FBXL5, and EXOC6, respectively. This confirms the significance of miR-23a not only in its functions but also as a bridge in the ceRNA mechanism for the formation of muscle fibers. We hypothesized that several subnetworks within the network, such as circ_0017336-miR-23a-FBXL5, may be extremely

important in controlling the formation of muscle fibers. RT-qPCR results showed that there was a ceRNA relationship between circ_0017336 and miR-23a as well as FBXL5 during sheep myogenic differentiation, and the dual luciferase reporter systems further verified that miR-23a directly targets FBXL5 for regulation. However, their roles and relationships still require confirmation. Our knowledge of the formation of muscle fiber phenotypes in sheep is expected to progress with the identification of new functions for lncRNAs and circRNAs.

Taken together, our data provide evidence for interactions that have high functional specificity in the formation of muscle fibers and that are consistent with the ceRNA hypothesis. This study provides new insights into the complex molecular mechanisms underpinning sheep meat traits variation but understanding exactly how the different type of muscle fiber are formed in the Tan sheep and Dorper sheep will require additional experiments.

Conclusion

The current study paints a thorough picture of the differences between Tan sheep and Dorper sheep in the whole-transcriptome profiles of the *longissimus dorsi* and *biceps femoris* tissues. Tan sheep had much more slow-twitch fibers than Dorper sheep had in their *longissimus dorsi* and *biceps femoris*. Among two sheep breeds, 60 DEGs were discovered, including ACACB, ATP6V0A1, ASAH1, EFHB, MYL3, C1QTNF7, SFSWAP, and FBXL5. Act according to our research, numerous lncRNAs, miRNAs, and circRNAs play a crucial role in crucial biological processes related to the development of muscle fiber pathways, such as the FoxO signaling pathway, the AMPK signaling pathway, and the Ca^{2+} signaling pathway. We also created the first lncRNA/circRNA-miRNA-gene interaction network based on the differentially expressed transcripts from muscle tissues, where some networks, such as circ_0017336-miR-23a-FBXL5, may be crucial in the control of muscle fiber creation. Our findings have established future investigations on the molecular mechanisms underlying muscle fiber development by identifying possible regulators and molecular regulatory networks that may be connected to the production of muscle fibers in sheep.

Data availability statement

The datasets presented in this study can be found in online repositories. The names of the repository/repositories and accession number(s) can be found in the article/Supplementary Material.

Ethics statement

The animal study was reviewed and approved by animal welfare committee of the State Key Laboratory for Agro-biotechnology of China Agricultural University (approval number XK257).

Author contributions

XK, YuL, XL, YaL and DF carried out the tests; RC, SC, YW, and ZL carried out the data analysis; ML, FL, and MF conceptualized the study and supervised the experiments. RC, YW, and ZL also created the figures and tables. All authors reviewed and approved the final version of the manuscript.

Funding

The National Key Research and Development Program of China (2021YFD1200900) and the Program of Agricultural Breeding in the Ningxia Hui Autonomous Region provided financial assistance for this work (No. nxnyyz20150101).

Conflict of interest

The reviewer QZ declared a shared affiliation with the author(s) YuL to the handling editor at time of review.

The authors declare that the research was conducted in the absence of any commercial or financial relationships that could be construed as a potential conflict of interest.

Publisher's note

Supplementary material

The Supplementary Material for this article can be found online at: https://www.frontiersin.org/articles/10.3389/fgene.2022.991606/full#supplementary-material

References

Ala, U., Karreth, F. A., Bosia, C., Pagnani, A., Taulli, R., Leopold, V., et al. (2013). Integrated transcriptional and competitive endogenous RNA networks are cross-regulated in permissive molecular environments. *Proc. Natl. Acad. Sci. U. S. A.* 110 (18), 7154–7159. doi:10.1073/pnas.1222509110

Bowker, B. C., Swartz, D. R., Grant, A. L., and Gerrard, D. (2005). Myosin heavy chain isoform composition influences the susceptibility of actin-activated S1 ATPase and myofibrillar ATPase to pH inactivation. *Meat Sci.* 71, 342–350. doi:10.1016/j.meatsci.2005.04.014

Cai, B., Ma, M., Zhou, Z., Kong, S., Zhang, J., Zhang, X., et al. (2022). circPTPN4regulates myogenesis via the miR-499-3p/NAMPTaxis. *J. Anim. Sci. Biotechnol.* 13 (1), 2. doi:10.1186/s40104-021-00664-1

Chen, X., Mao, X., Huang, J., Ding, Y., Wu, J., Dong, S., et al. (2011). Kobas 2.0: A web server for annotation and identification of enriched pathways and diseases. *Nucleic Acids Res.* 39, 316–322. doi:10.1093/nar/gkr483

Chen, M., Wei, X., Song, M., Jiang, R., Huang, K., Deng, Y., et al. (2021). Circular RNA circMYBPC1 promotes skeletal muscle differentiation by targeting MyHC. *Mol. Ther. Nucleic Acids* 24, 352–368. doi:10.1016/j.omtn.2021.03.004

Chin, E. R. (2005). Role of Ca2+/calmodulin-dependent kinases in skeletal muscle plasticity. *J. Appl. Physiol.* 99 (2), 414–423. doi:10.1152/japplphysiol.00015.2005

Doerr, C. R. AshmoreandL. (1971). Comparative aspects of muscle fiber types in different species. *Exp. Neurol.* 31 (3), 408–418. doi:10.1016/0014-4886(71)90243-3

Enright, A., John, B., Gaul, U., Tuschl, T., Sander, C., and Marks, D. S. (2003). MicroRNA targets in Drosophila. *Genome Biol.* 5 (11), R1. doi:10.1186/gb-2003-5-1-r1

Finn, R. D., Tate, J., Mistry, J., Coggill, P. C., Sammut, S. J., Hotz, H. R., et al. (2008). The Pfam protein families database. *Nucleic Acids Res.* 32 (1), D281–D288. doi:10.1093/nar/gkm960

Friedlnder, M. R., Mackowiak, S. D., Li, N., Chen, W., and Rajewsky, N. (2012). miRDeep2 accurately identifies known and hundreds of novel microRNA genes in seven animal clades. *Nucleic Acids Res.* 40 (1), 37–52. doi:10.1093/nar/gkr688

Heng, L., Yin, H., Jing, Y., Yan, X., Chen, W., Jiang, C., et al. (2019). Profiles analysis reveals circular RNAs involving zebrafish physiological development. *J. Cell. Physiol.* 234 (9), 15922–15933. doi:10.1002/jcp.28250

Hong, L., Gu, T., He, Y., Zhou, C., Hu, Q., Wang, X., et al. (2019). Genome-wide analysis of circular RNAs mediated ceRNA regulation in porcine embryonic muscle development. *Front. Cell Dev. Biol.* 7 (289), 289. doi:10.3389/fcell.2019.00289

Jin, J., Lv, W., Xia, P., Xu, Z. Y., Zheng, A. D., Wang, X. J., et al. (2018). Long noncoding RNA SYISL regulates myogenesis by interacting with polycomb repressive complex 2. *Proc. Natl. Acad. Sci. U. S. A.* 115 (42), E9802–E9811. doi:10.1073/pnas.1801471115

Ruiz, J. C., and Bruick, K. (2014). F-box and leucine-rich repeat protein 5 (FBXL5): Sensing intracellular iron and oxygen. *J. Inorg. Biochem.* 133, 73–77. doi:10.1016/j.jinorgbio.2014.01.015

Kang, X., Liu, G., Liu, Y., Xu, Q., Zhang, M., and Fang, M. (2013). Transcriptome profile at different physiological stages reveals potential mode for curly fleece in Chinese tan sheep. *PLoS One* 8 (8), e71763. doi:10.1371/journal.pone.0071763

Kellis, M., and Jungreis, I. (2011). PhyloCSF: A comparative genomics method to distinguish protein coding and non-coding regions. *Bioinformatics* 27 (13), i275–i282. doi:10.1093/bioinformatics/btr209

Kong, L., Zhang, Y., Ye, Z., Liu, X. Q., Zhao, S. Q., Wei, L., et al. (2007). CPC: Assess the protein-coding potential of transcripts using sequence features and support vector machine. *Nucleic Acids Res.* 35, W345–W349. doi:10.1093/nar/gkm391

Kornienko, A. E., Guenzl, P. M., Barlow, D. P., and Pauler, F. M. (2013). Gene regulation by the act of long non-coding RNA transcription. *BMC Biol.* 11 (2), 59–350. doi:10.1186/1741-7007-11-59

Kotb, A., Amaresh, P., Supriyo, D., Grammatikakis, I., Kim, J., Ding, J., et al. (2015). Circular RNAs in monkey muscle: Age-dependent changes. *Aging* 7 (11), 903–910. doi:10.18632/aging.100834

Kristensen, L. S., Andersen, M. S., Stagsted, L., Ebbesen, K. K., Hansen, T. B., and Kjems, J. (2019). The biogenesis, biology and characterization of circular RNAs. *Nat. Rev. Genet.* 20 (7), 675–691. doi:10.1038/s41576-019-0158-7

LangmeadandS, B., and Salzberg, L. (2012). - Fast gapped-read alignment with Bowtie 2. *Nat. Methods* 9 (4), 357–359. doi:10.1038/nmeth.1923

Larzul, C., Roy, P. L., Gogué, J., Talmant, A., Jacquet, B., Lefaucheur, L., et al. (1999). Selection for reduced muscle glycolytic potential in Large White pigs. II. Correlated responses in meat quality and muscle compositional traits. *Genet. Sel. Evol.* 31 (1), 61. doi:10.1186/1297-9686-31-1-61

Likun, W., Zhixing, F., Xi, W., Wang, X., and Zhang, X. (2010). DEGseq: an R package for identifying differentially expressed genes from RNA-seq data. *Bioinforma. Oxf. Engl.* 26 (1), 136–138. doi:10.1093/bioinformatics/btp612

Liu, Y., Zhang, J., Xu, Q., Kang, X., Wang, K., Wu, K., et al. (2018). Integrated miRNA-mRNA analysis reveals regulatory pathways underlying the curly fleece trait in Chinese tan sheep. *BMC Genomics* 19 (1), 360. doi:10.1186/s12864-018-4736-4

Maltin, C. A., SinclairandP, K. D., Warriss, D., Grant, C. M., Porter, A. D., Delday, M. I., et al. (1998). The effects of age at slaughter, genotype and finishing system on the biochemical properties, muscle fibre type characteristics and eating quality of bull beef from suckled calves. *Anim. Sci.* 66 (2), 341–348. doi:10.1017/s1357729800009462

Marc, R., Peter, S., Matthias, H., and Giegerich, R. (2004). Fast and effective prediction of microRNA/target duplexes. *RNA (New York, NY)* 10 (10), 1507–1517. doi:10.1261/rna.5248604

Martin, H., Jan, N., and Julie, B.-V. (2015). Muscle-specific microRNAs in skeletal muscle development. *Dev. Biol.* 410 (1), 1–13. doi:10.1016/j.ydbio.2015.12.013

Memczak, S., Jens, M., Elefsinioti, A., Torti, F., Krueger, J., Rybak, A., et al. (2013). Circular RNAs are a large class of animal RNAs with regulatory potency. *Nature* 495 (7441), 333–338. doi:10.1038/nature11928

Michaele, S., Keiichiro, O., Johannes, R., Wang, P. L., and Ideker, T. (2011). Cytoscape 2.8: New features for data integration and network visualization. *Bioinforma. Oxf. Engl.* 27 (3), 431–432. doi:10.1093/bioinformatics/btq675

Moroishi, T., Yamauchi, T., Nishiyama, M., and Nakayama, K. I. (2014). HERC2 targets the iron regulator FBXL5 for degradation and modulates iron metabolism. *J. Biol. Chem.* 289, 16430–16441. doi:10.1074/jbc.M113.541490

Myriam, P. A. C., and Gorospe, M. (2018). Detection and analysis of circular RNAs by RT-PCR. *Bio. Protoc.* 8 (6), e2775. doi:10.21769/BioProtoc.2775

Ouyang, H., Wang, Z., Chen, X., Yu, J., Li, Z., and Nie, Q. (2017). Proteomic analysis of chicken skeletal muscle during embryonic development. *Front. Physiol.* 8, 281. doi:10.3389/fphys.2017.00281

Pertea, M., Kim, D., Pertea, G. M., Leek, J. T., and Salzberg, S. L. (2016). Transcript-level expression analysis of RNA-seq experiments with HISAT, StringTie and Ballgown. *Nat. Protoc.* 11 (9), 1650–1667. doi:10.1038/nprot.2016.095

Rosado, J. A. (2021). SARAF and EFHB modulate store-operated Ca 2+ entry and are required for cell proliferation, migration and viability in breast cancer cells. *Cancers* 13, 4160. doi:10.3390/cancers13164160

RyuandB, Y. C., and Kim, C. (2005). The relationship between muscle fiber characteristics, postmortem metabolic rate, and meat quality of pig longissimus dorsi muscle. *Meat Sci.* 71 (2), 351–357. doi:10.1016/j.meatsci.2005.04.015

Salmena, L., Poliseno, L., Tay, Y., Kats, L., and Pandolfi, P. P. (2011). A ceRNA hypothesis: The rosetta stone of a hidden RNA language? *Cell* 146 (3), 353–358. doi:10.1016/j.cell.2011.07.014

Scherbakov, N., Sandek, A., Valentova, M., Mayer, A., von Haehling, S., Jankowska, E., et al. (2022). Iron deficiency and reduced muscle strength in patients with acute and chronic ischemic stroke. *J. Clin. Med.* 11 (3), 595. doi:10.3390/jcm11030595

Su, L., Li, H., Xin, X., Duan, Y., Hua, X. Q., and Jin, Y. (2013). Muscle fiber types, characteristics and meat quality. *Adv. Mat. Res.* 2203 (634-638), 1263–1267. doi:10.4028/www.scientific.net/amr.634-638.1263

Sun, L., Luo, H., Bu, D., Zhao, G., Yu, K., Zhang, C., et al. (2013). Utilizing sequence intrinsic composition to classify protein-coding and long non-coding transcripts. *Nucleic Acids Res.* 41 (17), e166. doi:10.1093/nar/gkt646

Trapnell, C., Williams, B. A., Pertea, G., Mortazavi, A., Kwan, G., van Baren, M. J., et al. (2010). Transcript assembly and quantification by RNA-Seq reveals unannotated transcripts and isoform switching during cell differentiation. *Nat. Biotechnol.* 28 (5), 511–515. doi:10.1038/nbt.1621

Valin, C., Touraille, C., Vigneron, P., and Ashmore, C. R. (1982). Prediction of lamb meat quality traits based on muscle biopsy fibre typing. *Meat Sci.* 6 (4), 257–263. doi:10.1016/0309-1740(82)90036-5

Ventsislav, R., Vesselin, B., and Nikiforov, M. I. (2005). MicroInspector: A web tool for detection of miRNA binding sites in an RNA sequence. *Nucleic acids Res.* 33, W696–W700. doi:10.1093/nar/gki364

Wang, L., Chen, X., Zheng, Y., Li, F., Lu, Z., Chen, C., et al. (2012). MiR-23a inhibits myogenic differentiation through down regulation of fast myosin heavy chain isoforms. *Exp. Cell Res.* 318 (18), 2324–2334. doi:10.1016/j.yexcr.2012.06.018

Wu, H., Kanatous, S. B., Thurmond, F. A., Gallardo, T., Isotani, E., Bassel-Duby, R., et al. (2002). Regulation of mitochondrial biogenesis in skeletal muscle by CaMK. *Science* 296 (5566), 349–352. doi:10.1126/science.1071163

Yin, H., He, H., Cao, X., Shen, X., Han, S., Cui, C., et al. (2020). MiR-148a-3p regulates skeletal muscle satellite cell differentiation and apoptosis via the PI3K/AKT signaling pathway by targeting Meox2. *Front. Genet.* 11 (4), 512. doi:10.3389/fgene.2020.00512

Young, M., Wakefield, M. J., Smyth, G. K., and Oshlack, A. (2010). Gene ontology analysis for RNA-seq: Accounting for selection bias. *Genome Biol.* 11 (2), R14. doi:10.1186/gb-2010-11-2-r14

Yuan, G., and Zhao, J. (2015). Ciri: An efficient and unbiased algorithm for de novo circular RNA identification. *Genome Biol.* 16 (1), 4. doi:10.1186/s13059-014-0571-3

Zhang, P., Du, J., Guo, X., Wu, S., He, J., Li, X., et al. (2021). LncMyoD promotes skeletal myogenesis and regulates skeletal muscle fiber-type composition by sponging miR-370-3p. *Genes* 12 (4), 589. doi:10.3390/genes12040589

Zhao, J., Wu, J., Xu, T., Yang, Q., He, J., and Song, X. (2018). IRESfinder: Identifying RNA internal ribosome entry site in eukaryotic cell using framed k-mer features. *J. Genet. Genomics* 45 (7), 403–406. doi:10.1016/j.jgg.2018.07.006

Zhou, L., Chen, J., Li, Z., Li, X., Hu, X., Huang, Y., et al. (2010). Integrated profiling of MicroRNAs and mRNAs: MicroRNAs located on Xq27.3 associate with clear cell renal cell carcinoma. *PLoS One* 5 (12), e15224. doi:10.1371/journal.pone.0015224

Zhou, X., Liu, Y., Zhang, L., Kong, X., and Li, F. (2021). Serine-to-glycine ratios in low-protein diets regulate intramuscular fat by affecting lipid metabolism and myofiber type transition in the skeletal muscle of growing-finishing pigs. *Anim. Nutr.* 7 (7), 384–392. doi:10.1016/j.aninu.2020.08.011

frontiers | Frontiers in Genetics

TYPE Original Research
PUBLISHED 15 November 2022
DOI 10.3389/fgene.2022.1019687

OPEN ACCESS

EDITED BY
Rajwali Khan,
University of Agriculture, Pakistan

REVIEWED BY
Bojiang Li,
Shenyang Agricultural University, China
Xiaojun Liu,
Henan Agricultural University, China
Hamayun Khan,
University of Agriculture, Pakistan

*CORRESPONDENCE
Qing-Xia Lu,
luqingxia82@163.com
Bao-Song Xing,
bsxing@126.com

†These authors have contributed equally to this work

SPECIALTY SECTION
This article was submitted to Livestock Genomics, a section of the journal Frontiers in Genetics

RECEIVED 15 August 2022
ACCEPTED 27 October 2022
PUBLISHED 15 November 2022

CITATION
Wang J, Chen J-F, Ma Q, Mo D-L, Sun J-J, Ren Q-L, Zhang J-Q, Lu Q-X and Xing B-S (2022), Identification and characterization of circRNAs related to meat quality during embryonic development of the longissimus dorsi muscle in two pig breeds. *Front. Genet.* 13:1019687. doi: 10.3389/fgene.2022.1019687

Identification and characterization of circRNAs related to meat quality during embryonic development of the longissimus dorsi muscle in two pig breeds

Jing Wang[1†], Jun-Feng Chen[1†], Qiang Ma[1], De-Lin Mo[2], Jia-Jie Sun[3], Qiao-Ling Ren[1], Jia-Qing Zhang[1], Qing-Xia Lu[1*] and Bao-Song Xing[1*]

[1]Henan Key Laboratory of Farm Animal Breeding and Nutritional Regulation, Institute of Animal Husbandry and Veterinary Science, Henan Academy of Agricultural Sciences, Zhengzhou, China, [2]State Key Laboratory of Biocontrol, School of Life Sciences, Sun Yat-sen University, Guangzhou, China, [3]Guangdong Provincial Key Laboratory of Animal Nutrition Control, Guangdong Laboratory for Lingnan Modern Agriculture, National Engineering Research Center for Breeding Swine Industry, College of Animal Science, South China Agricultural University, Guangzhou, China

Meat quality, an important economic trait, is regulated by many factors, especially by genetic factors, including coding genes, miRNAs, and lncRNAs. Recent studies have elucidated that circRNAs also play a key role in muscle development and lipid deposition. However, the functions and regulatory mechanisms of circRNAs in meat quality remain mostly unknown. The circRNA expression profiles between Huainan pigs (Chinese indigenous pigs, fat-type, Huainan HN) and Large White pigs (Western commercial pigs, lean-type, LW) in the longissimus dorsi (LD) muscle at 38, 58, and 78 days post conception (dpc) were compared by sequencing. In total, 39,887 circRNAs were identified in 18 samples, and 60, 78, and 86 differentially expressed circRNAs (DECs) were found at the three stages mentioned above between these two breeds. The parent genes of DECs were enriched in myogenesis, proliferation, adipogenesis and muscle fiber-type transition. The circRNA-miRNA interaction networks included 38 DECs and 47 miRNAs, and these miRNAs were involved in muscle development and lipid metabolism. Two shared DECs (circ_0030593 and circ_0032760) of these three stages were selected, their head-to-tail junction sites were validated by Sanger sequencing, and RT–qPCR results suggested that these two DECs might be involved in intramuscular fat deposition. These findings provide a basis for understanding the role of circRNAs in meat quality.

KEYWORDS

pig, circRNA, muscle development, lipid deposition, ceRNA

Introduction

Pork is the predominant source of dietary protein worldwide. At present, the pork production can largely meet market's demand, and higher requirements for pork quality has been put forward. Compared with the Western commercial pig breeds, Chinese indigenous pig breeds generally exhibit better meat quality, including bright meat color, thin muscle fibers and high intramuscular fat content. The differences in meat quality traits between Chinese indigenous breeds and Western commercial breeds provide good material for studying the genetic differences in meat quality traits. Screening new regulatory factors for meat quality is of great economic value to genetically improve meat quality traits.

A muscle fiber is the smallest functional unit of skeletal muscle, and its thickness, density, type and intramuscular fat content all influence meat quality. Muscle development involves a complex set of cellular and developmental processes that is regulated by many genes, transcription factors, and noncoding RNAs. Some studies have compared the expression of mRNAs, miRNAs and lncRNAs in different pig breeds at different developmental stages. For example, Cai et al. compared transcriptomic differences in longissimus dorsi (LD) muscle between Mashen (MS) and Large White (LW) pigs at 0, 90 and 180 days after birth and found that growth genes were associated with a faster growth rate in LW, while genes related to fatty acid synthesis were associated with higher intramuscular fat deposition in MS (Cai et al., 2020). Zhao et al. compared transcriptome differences between Lantang (LT) and Landrace (LR) pigs from 35 days post conception (dpc) to 180 days post-natal (dpn), confirming that 49–77 dpc is critical for muscle phenotype formation and that GSK3B may be involved in later myogenesis in LR, with some myogenic inhibitors also potentially contributing to the slower muscle differentiation rate in LT (Zhao et al., 2011). He et al. compared the expression of miRNAs in LD muscle of MS and LW at 35 dpc and identified 87 differentially expressed miRNAs, which were enriched in muscle contraction, WNT, mTOR, and MAPK (He et al., 2017). Herein, our team preliminarily compared lncRNA expression differences in LD muscle between Huainan (HN) and LW pigs at 38, 58, and 78 dpc. The results suggested that the most active period of muscle development between these two breeds was different, being more active at 58 dpc in the HN and 78 dpc in the LW. LncRNAs also participated in earlier myogenesis, shorter proliferation and higher intramuscular fat (IMF) deposition in HN. The PI3K/Akt and cAMP pathways are associated with IMF deposition (Wang et al., 2020a).

Circular RNA, having a covalent closed-loop structure, was first observed by electron microscopy in 1976, and by 2012, a large number of circRNAs had been discovered using high-throughput sequencing technology. Recent studies have shown that circRNAs are involved in the regulation of meat traits, such as circTAF8 (Li et al., 2021a), circCCDC91 (Zhao et al., 2022), circUBE2Q2 (Zhao et al., 2022), and circSVIL (Yue et al., 2022), which are involved in muscle development, and circPPARA (Li et al., 2022a), circINSR (Shen et al., 2020), and circ-ATXN2 (Song et al., 2021), which are associated with lipid deposition. Porcine circMYLK4 was also identified as a regulator of fast/slow myofibers (Cao et al., 2022). These studies have determined the functions of some circRNAs in different species, but studies on porcine circRNAs are limited, with most of them only performing differential expression profiling analysis and ceRNA network construction. For example, Hong et al. analyzed circRNA expression profiles in LD muscle of Duroc pigs at 33, 65 and 90 dpc and found circRNAs with higher expression levels at 33 dpc (Hong et al., 2019). Li et al. compared circRNA expression in LD muscle of Ningxiang pigs at 30, 90, 150 and 210 dpn and found that differentially expressed circRNAs (DECs) were enriched in muscle development and fatty acid biosynthesis signaling pathways (Li et al., 2021b). Jin et al. compared the whole transcriptional profiles of 47 different skeletal muscles in adult pigs and identified 48,232 circRNAs, elucidating the molecular regulatory differences in energy metabolism and contractile properties of different skeletal muscle sites (Jin et al., 2021). Wang et al. screened 66 DECs in the LD muscle between adult HN and Duroc×(Landrace×Yorkshire) (DLY) pigs that are involved in myogenesis, lipogenic differentiation and flavor through Wnt, the transition between fast and slow fibers, and alanine, aspartate and glutamate metabolism pathways (Wang et al., 2019a). Li et al. compared the expression of circRNAs in the LD muscle of MS pigs and LW pigs at 1, 90 and 180 days of age and screened 327 DECs enriched in TGF-β, MAPK, FoxO and other signaling pathways related to skeletal muscle growth and fat deposition (Li et al., 2021c).

In most species, the number of muscle fibers becomes fixed during the embryonic period, making this time critical for meat quality. Previous studies have indicated that primary muscle fibers are formed from 30 to 60 dpc, while secondary muscle fibers are formed from 54 to 90 dpc. Studies on the effect of porcine circRNAs on muscle development have made comparisons between different stages in the same pig breed or between different breeds in one developmental stage or different developmental stages after birth. However, circRNA expression differences in the LD muscle between fatty and lean pigs at embryonic stages have not been reported. HN pigs, an excellent indigenous Chinese pig breed, were included in "The fine local livestock and poultry breeds record of Henan province" in 1986 and are famous for their heat resistance, roughage resistance, large litter size, and particularly high intramuscular fat content. To date, the effect of circRNAs on muscle development in the embryo stage of Huainan pigs has not been reported. Therefore, RNA sequencing technology and bioinformatics methods were first applied to identify DECs in LD muscle between HN pigs (Chinese indigenous breed, fat type)

and LW pigs (Western commercial breed, lean type) at different embryonic developmental stages, and functional validation and regulatory mechanism analysis were performed for shared DECs at different stages. The results of this study provide fundamental material for studying the mechanisms of circRNAs in porcine muscle development.

Materials and methods

Experimental animals and tissue collection

All pigs were fed by Henan Xing Rui Agricultural and Animal Husbandry Technology Co., Ltd (Henan Province, China). Five HN and five LW sows in their second or third parity were selected and artificially inseminated with sperm from the same breed (with the same genetic background). At 38, 58, and 78 dpc, one sow from each breed was slaughtered following national and institutional guidelines for the ethical use and treatment of animals in experiments. At 38 dpc, it was difficult to identify female and male fetuses by appearance, so all of the fetuses were immediately removed from the uteri and used for sample collection. The sexes of these fetuses were identified by the SRY gene, and then three male and three female fetuses were selected for sequencing. At 58 and 78 dpc, three male and three female fetuses were selected by appearance and used for sample collection. For all fetuses, the LD muscle tissue was collected from the same area and snap frozen in liquid nitrogen until further use. Existences and expressional levels of identified circRNAs were detected between eleven different tissues from adult HN pigs, including the heart, liver, spleen, lung, kidney, gut, stomach, LD muscle, subcutaneous adipose, intramuscular adipose, and abdomen adipose. The LD muscles were sampled from forty Duroc × (Landrace × Yorkshire) adult pigs with high IMF (>6%) and forty with low IMF (<3%), separately, and then the differences of the circRNAs' expression between the high IMF pigs and low IMF pigs were detected.

RNA isolation, quality control and library preparation

According to the manufacturer's instructions, TRIzol reagent (Invitrogen Life Technologies, Carlsbad, United States) was used to isolate total RNA from LD muscle samples. For each stage of both breeds, one male RNA sample and one female RNA sample were mixed, and three mixed RNA samples were used for sequencing. A NanoDrop ND-1000 (Implen, Westlake Village, CA, United States), Agilent 2,100 Bioanalyzer (Agilent Technologies, United States) and denaturing agarose gel electrophoresis were used to test the purity, concentration and integrity, respectively, of the isolated RNA. Samples with high RNA integrity number (RIN) values (larger than eight) were used for library preparation. Ribosomal RNA was removed from the total RNA using the Ribozero™ rRNA Removal Kit (Epicenter, United States). Then, linear RNA was removed using an RNAse R kit (Epicenter, United States). The rRNA-free and linear RNA-free RNA was used to generate sequencing libraries with the NEBNext® Ultra™ Directional RNA Library Prep Kit (NEB, Ipswich, MA, United States).

CircRNA sequencing and circRNA identification

The Illumina HiSeqTM 2,500 platform (Novogene, Beijing, China) was used to sequence the generated libraries. TopHat2 software (v2.1.1) was used to map the clean data to the porcine reference genome (Sscrofa11.1). Find_circ algorithms (Rao et al., 2021) and CIRI2 (Gao et al., 2018) were used to identify circRNAs from the unmapped reads (read count ≥2). The expression levels of circRNAs are shown as transcripts per kilobase per million mapped reads (TPM). According to the mapping region to the annotated gene, circRNAs were classified as exonic, intronic, and intergenic circRNAs.

Principal component analysis and hierarchical clustering

PCA of circRNA expression profiles was conducted using the R packages FactoMineR and Facto Extra. Hierarchical clustering of circRNAs was generated using the R package heatmap.

Identification of DECs and analysis of their functional differences in circRNA expression

HN and LW animals at 38, 58, and 78 dpc were analyzed using the DEseq2 package (Love et al., 2014), and $|\log2\text{foldchange}| \geq 1$ and $p_{adj} \leq 0.05$ were used to identify DECs. DECs' parental genes were subjected to Gene Ontology (GO) and Kyoto Encyclopedia of Genes and Genomes (KEGG) analyses using the DAVID tool (http://david.abcc.ncifcrf.gov/), and $p < 0.05$ was considered significant.

DEC-miRNA network construction

MiRanda software (v3.3a) was used to predict potential binding sites of miRNA to DECs, as previously described (Wang et al., 2019b). The miRNAs were derived from the LD muscle between HN and LW at 38, 58, and 78 dpc, and these

TABLE 1 Primers used for RT–PCR.

Name	Sequence (5′-3′)	Size (bp)
circ_0030593	F: GTCCGAGGGCAGTGGACTGG	123
	R: GGCTTGATGCAGCAGCACTT	
circ_0011630	F: AATGGCATTTCCAGGAGGTT	123
	R: TTGTCAGACTCCATGGTACTT	
circ_0002895	F: GTGACATGGAGTCCATCATC	166
	R: ATGACGAATTGAATTCTGCT	
circ_0032760	F: CTGAACCACTGAGCGCTGAG	121
	R: ACGGCGCAGAGGTCAAGAAG	
circ_0025881	F: GCAAAACACACTCAGATGAT	126
	R: CTTGTCCATTAATTCGTTCTTC	
circ_0028985	F: CCATCGATATCCAGGTTGTTGAG	129
	R: TCAGTGATGCCGTACTGGAA	
PPAR gamma	F: AGGACTACCAAAGTGCCATCAAA	142
	R: GAGGCTTTATCCCCACAGACAC	
FABP4	F: ATGAAAGAAGTGGGAGTGG	156
	R: ATCAAATTCCTGGCCCAATT	
AdipoQ	F: CGATTGTCAGTGGATCTGACG	151
	R: CAACAGTAGCATCCTGAGCCCT	
GLUT4	F: TAAGACAAGATGCCGTCGGG	136
	R: GAGAAGACGGCGAGGACAAG	
ADD1	F: CGATTCGCCCCTGAGAACAC	129
	R: CTGGGACCATTCAGCCTCTC	
GAPDH	F: ACCAGGTTGTGTCCTGTGAC	94
	R: AGCTTGACGAAGTGGTCGTT	

results have not been published before. Cytoscape (V3.2) software was used to visualize the potential DEC-miRNA regulatory network.

Reverse transcription quantitative PCR

According to the manufacturer's instructions, the Prime Script RT reagent Kit with gDNA Eraser (TaKaRa, Dalian, China) was used to convert total RNA to cDNA using random primers. A SYBR Green PCR kit (TaKaRa, Dalian, China) was used to perform qPCR. The outward-facing primers were used for circRNA identification. GAPDH was used as an internal control. All primers used for RT–qPCR are shown in Table 1. Each qPCR experiment was performed in triplicate, and the fold-changes of circRNAs were calculated using the $2^{-\triangle\triangle Ct}$ method (Xu et al., 2017).

Culture and differentiation of porcine intramuscular adipocytes

Following previously described methods (Chen et al., 2017), intramuscular adipocytes were isolated from porcine LD muscle and cultured in normal medium, defined here as DMEM/F12 supplemented with 10% FBS and antibiotics (100 IU/ml penicillin and 100 μg/ml streptomycin) at 37°C and 5% CO_2 (Day 0, D0).

Differentiation was induced as follows: differentiation medium I ("normal medium" supplemented with 5 μg/ml insulin, 1 mM DEX, and 0.5 mM IBMX) was changed 48 h after 100% confluence (Day 2, D2). Two days later, differentiation medium II ("normal medium" supplemented with 5 μg/ml insulin) was changed (Day 4, D4). Two days later, the normal medium was changed (Day 6, D6).

CircRNA overexpression

Circ_0030593 was amplified to construct the pCD2.1-circ_0030593 overexpression vector (Geneseed, Guangzhou, China). When the intramuscular adipocytes reached 70%–80% confluence, the pCD2.1-circ_0030593 and pCD2.1 empty vectors were transfected using DharmaFect 2 (Dharmacon, Lafayette, CO, United States) at a final concentration of 7 μL/mL, and the medium was changed 12 h later. Overexpression efficiency was assessed 24 h after transfection. Four days (D4) and six days (D6) after differentiation, the cells were harvested for RT–qPCR of several adipogenesis marker genes and Oil Red O staining.

Statistical analysis

The R statistical package (version 3.6.1) was used to analyze the data. The results are presented as the mean ± standard error, and a p-value <0.05 was considered statistically significant.

Results

Basic features of CircRNAs

A total of 39,887 circRNAs were identified from 18 samples. The length of the circRNAs ranged from 150 to 98,866 nucleotides (nt), 30.87% of which were larger than 10,000 nt, and for circRNAs less than 10,000 nt, those with lengths of 200–500 comprised the highest percentage (Figure 1A). These circRNAs were distributed across all chromosomes, with chromosome one having the most circRNAs (4,255) and chromosome Y having the fewest circRNAs (only 18) (Figure 1B). Based on chromosome location, these circRNAs can be classified into exonic, intergenic and intronic circRNAs. In each sample at each stage in both breeds, the most circRNAs were located in intronic regions, and the fewest circRNAs were located in intergenic regions (Figure 1C).

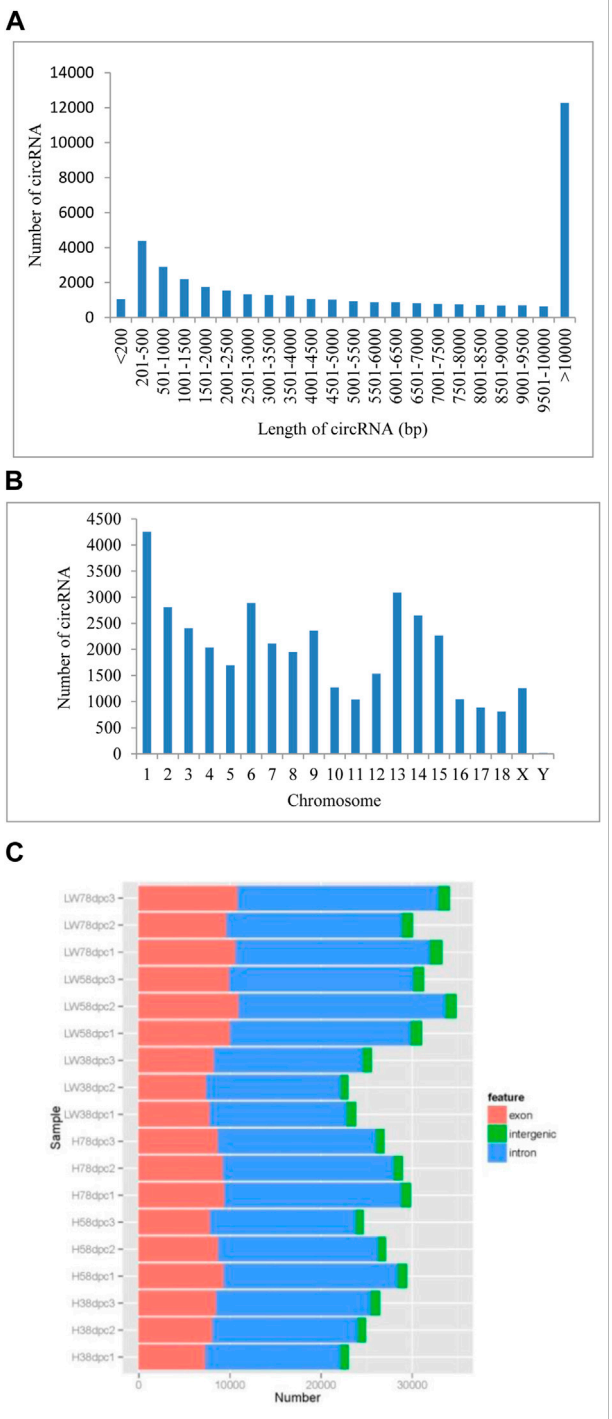

FIGURE 1
The genomic features of novel circRNAs in LD muscle of HN and LW at different embryonic periods **(A)** Length distribution of novel circRNAs. **(B)** Chromosome distribution of novel circRNAs. **(C)** Classification of the novel circRNAs.

Differential expression of circRNA between HN and LW pigs

As shown by PCA (Figure 2A) and the heatmap (Figure 2B), the 18 samples clustered together at the same stage in the same breeds, and it is evident that the genetic relationship of three samples of HN78dpc are far away from other samples, followed by LW38dpc and H58dpc, while nine samples of LW58dpc, H38dpc, and LW78dpc were closer together. Comparing these two breeds, the number of DECs for the three stages were 60, 78 and 86, respectively, and in each stage, there were more downregulated DECs than upregulated DECs (Figures 2C–E). There were four shared DECs in all three stages: circ_0032738, circ_0010646, circ_0030593, and circ_0032760 (Figure 2F). Compared these four shared DECs with our previous results between HN and DLY, and it was found that the expressional difference of circ_0010646 and circ_0030593 between HN and DLY were also significantly, and both of these circRNAs showed lower expressional level in HN (Wang et al., 2019a).

Functional enrichment analyses of DECs

The GO results indicated that at 38 dpc, the parent genes of DECs were mainly enriched in the transportation of folic acid, vitamins, and the location of mitochondria and muscle development-related pathways, such as adult heart development and myofibril assembly (Figure 3A). In 58 dpc, synthesis, metabolism, and regulation of lipoprotein were enriched, along with cholesterol transport, cell differentiation and Fas pathways (Figure 3B). At 78 dpc, the genes were mainly enriched in muscle development-related pathways, such as muscle filament sliding, myofibril assembly, actin filament-based process, muscle contraction, striated muscle cell development, muscle cell development, and striatal muscle contraction, in addition to the Fas pathway (Figure 3C).

As shown in Figure 4, the KEGG results indicated that muscle development-related pathways were enriched in different stages, involving hypertrophic cardiomyopathy (HCM), cardiomyopathy (DCM), viral myocarditis dilation, adrenergic signaling in cardiomyocytes, and cardiac muscle contraction. Meanwhile, adipose differentiation- and lipid deposition-related pathways were also enriched, such as PI3K-Akt, cAMP, Wnt, type I diabetes mellitus, cholesterol metabolism, cGMP-PKG, sphingolipid metabolism, and the TCA cycle. In addition, muscle fiber type transition-related pathways were enriched, such as AMPK, Wnt, and thyroid hormone.

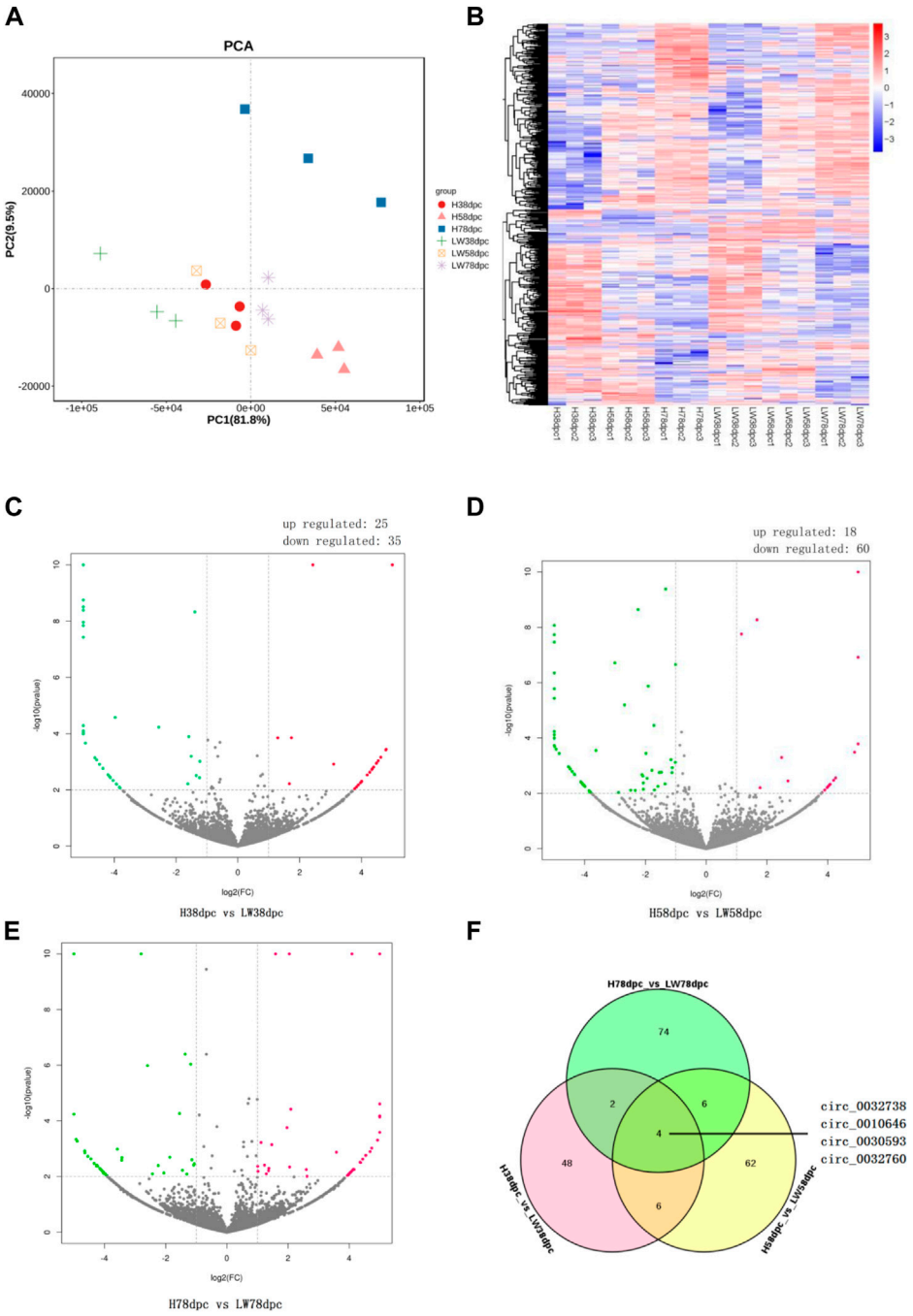

FIGURE 2
Principal component analysis (PCA) plot **(A)** and heatmap **(B)** of all detected circRNAs from 18 samples. Volcano plots of differential circRNAs between HN and LW pigs at 38 dpc **(C)**, 58 dpc **(D)**, and 78 dpc **(E)**. **(F)** Venn diagrams of DECs between HN and LW at different stages.

DEC-miRNA network construction

All DECs in the three stages in HN and LW pigs were subjected to interaction analysis with miRNA (Figure 5). A total of 38 DECs corresponding to 47 miRNAs were selected, and their interactions were made into a network with a total of 271 edges, of which miR-4331-3p corresponded to the most circRNAs (36 circRNAs), while circ_0035380 had the most target miRNAs (27 miRNAs).

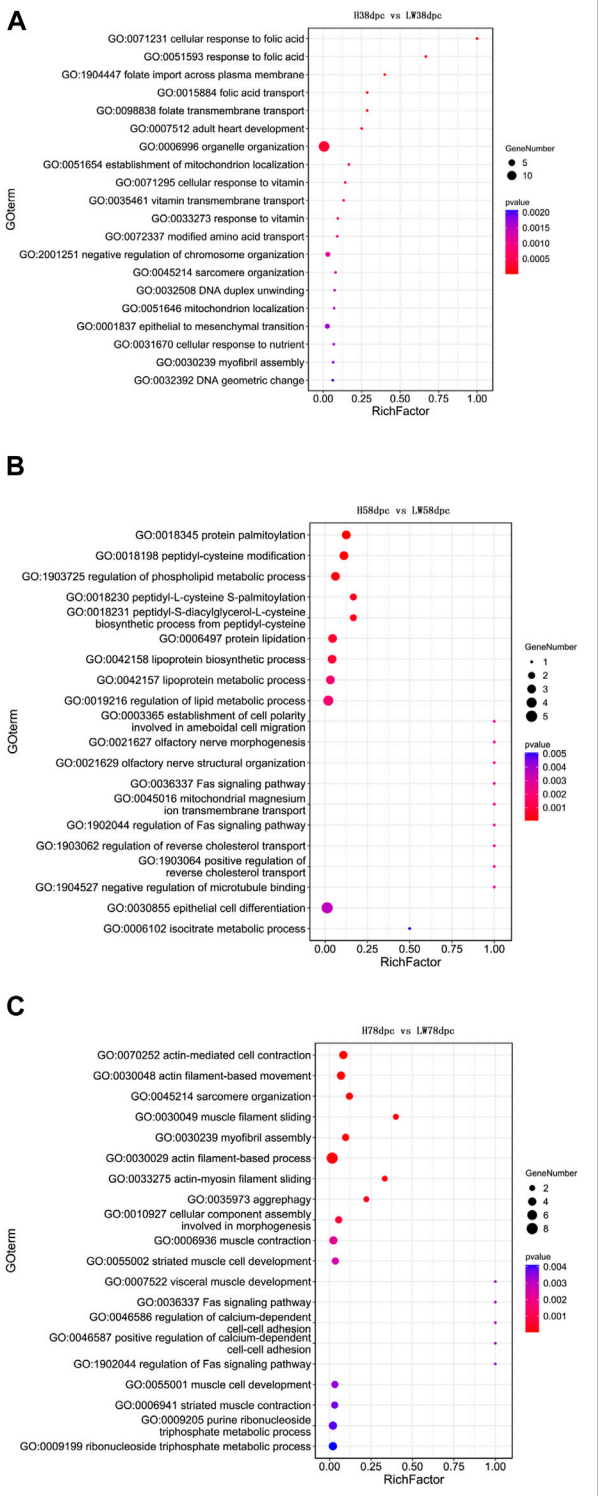

FIGURE 3
GO enrichment analyses based on parent genes of differential circRNAs at 38 dpc **(A)**, 58 dpc **(B)**, and 78 dpc **(C)**.

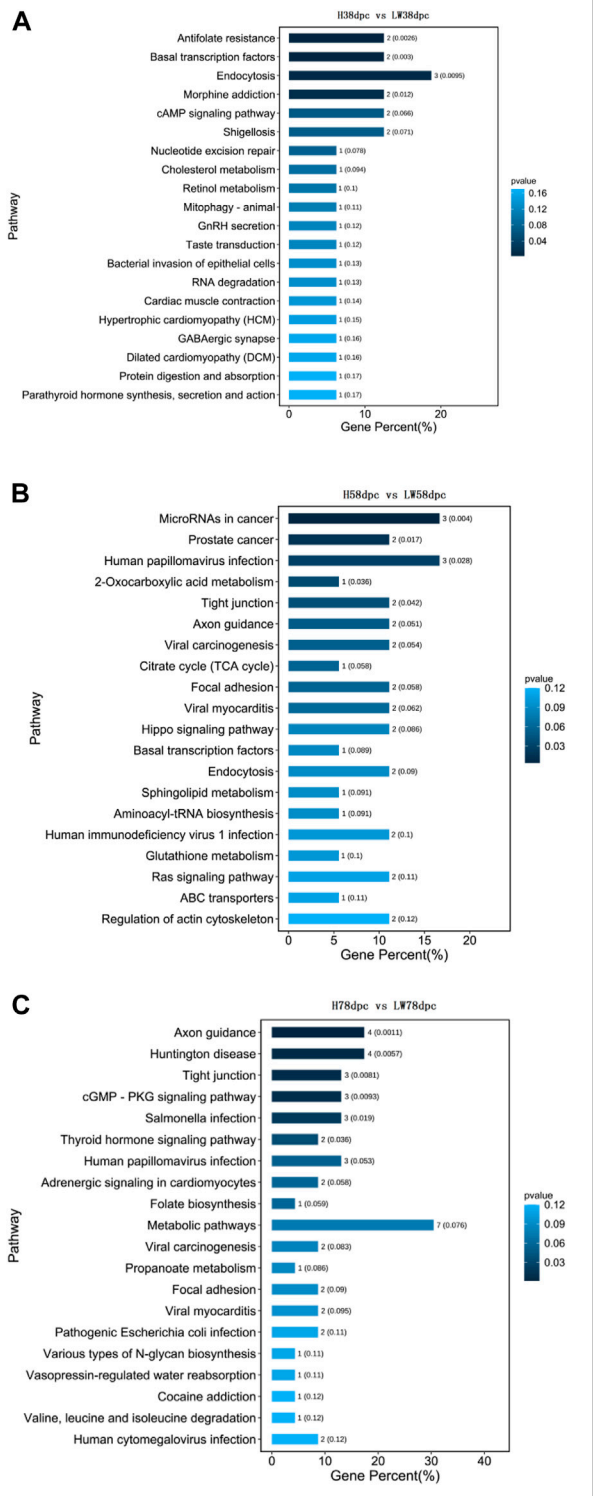

FIGURE 4
KEGG pathway analysis based on parent genes of differential circRNAs at 38 dpc **(A)**, 58 dpc **(B)**, and 78 dpc **(C)**.

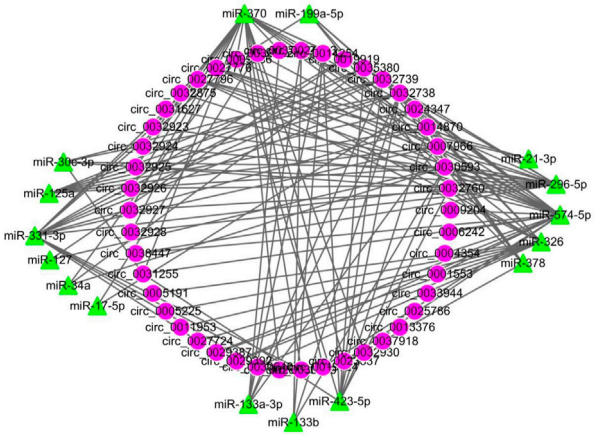

FIGURE 5
The circRNA-miRNA network of all differentially regulated circRNAs between HN and LW at 38 dpc, 58 dpc, and 78 dpc. Circular nodes represent circRNAs; triangular nodes represent miRNAs.

Validation of cric_0030593 and circ_0032760

The junction sites of circ_0030593, circ_0025881, circ_0011630, circ_0028985, circ_0032760 and circ_0002895 were confirmed by PCR amplification and sequencing (Figure 6A). The RT–PCR results revealed that these circRNA expression patterns were consistent with the RNA-seq results (Figures 6B–E). Two shared DECs were subjected to tissue expression profiling, and circ_0030593 was most highly expressed in intramuscular adipose and subcutaneous adipose tissues (Figure 7A). Circ_0032760 was most highly expressed in adipose tissues, with the highest concentration found in intermuscular adipose tissue, followed by muscle tissue (Figure 7A). It was found that both circRNAs showed highest expressional levels in intramuscular adipose tissue, indicating that these two DECs might play an important role in intramuscular fat deposition, so we firstly verified their regulation role in adipogenesis of porcine intramuscular adipocytes. To further evaluate the role of circ_0032760 and circ_0002895 in IMF deposition, a potential correlation with IMF content of LD muscle was examined in another cohort comprising 40 DLY pigs with high IMF and 40 with low IMF. The results revealed that circ_0030593 exhibited higher expression levels in the low IMF group than in the high IMF group ($p < 0.01$), but the expressional difference of circ_0032760 between these two groups was not significant ($p > 0.05$) (Figure 7B). Further overexpression of circ_0030593 in porcine primary intramuscular adipocytes, the expression of circ_0030593 was significantly upregulated, but the expression of its parental gene ZDHH7 was not affected (Figure 7C). And oil red O staining suggested that elevated expression of circ_0030593 had an inhibitory effect on lipid deposition (Figures 7D,E). The RT–qPCR results suggested that upregulation of circ_0030593 inhibited lipogenic differentiation, and the expression of PPAR gamma, FABP4, AdipoQ, GLUT4 and ADD1 was downregulated (Figure 7F).

Discussion

Pork is the most commonly consumed meat in the world, and pork production has largely met the demand. Currently, consumers are increasingly interested in meat quality, so screening for key regulatory factors related to meat quality has significant economic value. Many studies have identified meat quality-related circRNAs, such as those regulating myoblast proliferation and differentiation (circMYBPC1 (Chen et al., 2021), circ-FoxO3 (Li et al., 2019), and circEch1 (Huang et al., 2021)) and those regulating fat deposition (circINSR (Shen et al., 2020), circ-PLXNA1 (Wang et al., 2020b), and circPTK2 (Ding et al., 2021)). Most studies on porcine circRNAs have only performed differential expression analyses, such as screening DECs in LD muscle between obese and lean pigs at one developmental stage (Wang et al., 2019b; Li et al., 2021c; Li et al., 2022a) or screening DECs in different muscle fiber types (Li et al., 2020; Jin et al., 2021). In contrast, research about specific DECs' molecular regulatory mechanisms is limited; however, it was reported that circTUT7 regulates HMG20B expression through miR-30a-3p and thus affects embryonic development of skeletal muscle (Hong et al., 2019). Furthermore, circPPARA promotes intramuscular adipogenesis *via* miR-429 and miR-200b (Li et al., 2022a). Therefore, this study compared circRNA expression in LD muscle between HN and LW pigs at different embryonic stages (38, 58, and 78 dpc) and performed functional enrichment and ceRNA regulatory network analysis of DECs. In addition, a preliminary analysis of the molecular regulatory mechanisms of shared DECs at different stages was performed. Considering the animal welfare and economic cost, in current study 3 litters were taken from the same sow, genetically unrelated litters could be sampled to further validate the conclusions in this study. But the results of the current study still provide some material for understanding the role of circRNAs in meat quality.

Most circRNAs regulate expression of their parental gene, which in turn affects related traits. Therefore, in this study, DECs' parental genes were subjected to GO and KEGG analysis. Previous studies have shown that there are significant differences in embryonic muscle development between Chinese indigenous pig breeds and Western commercial breeds. Zhao et al. compared embryonic developmental differences in LD muscle between LT (obese) and LR (lean) breeds and found that the primary fibers emerged at 35 dpc and

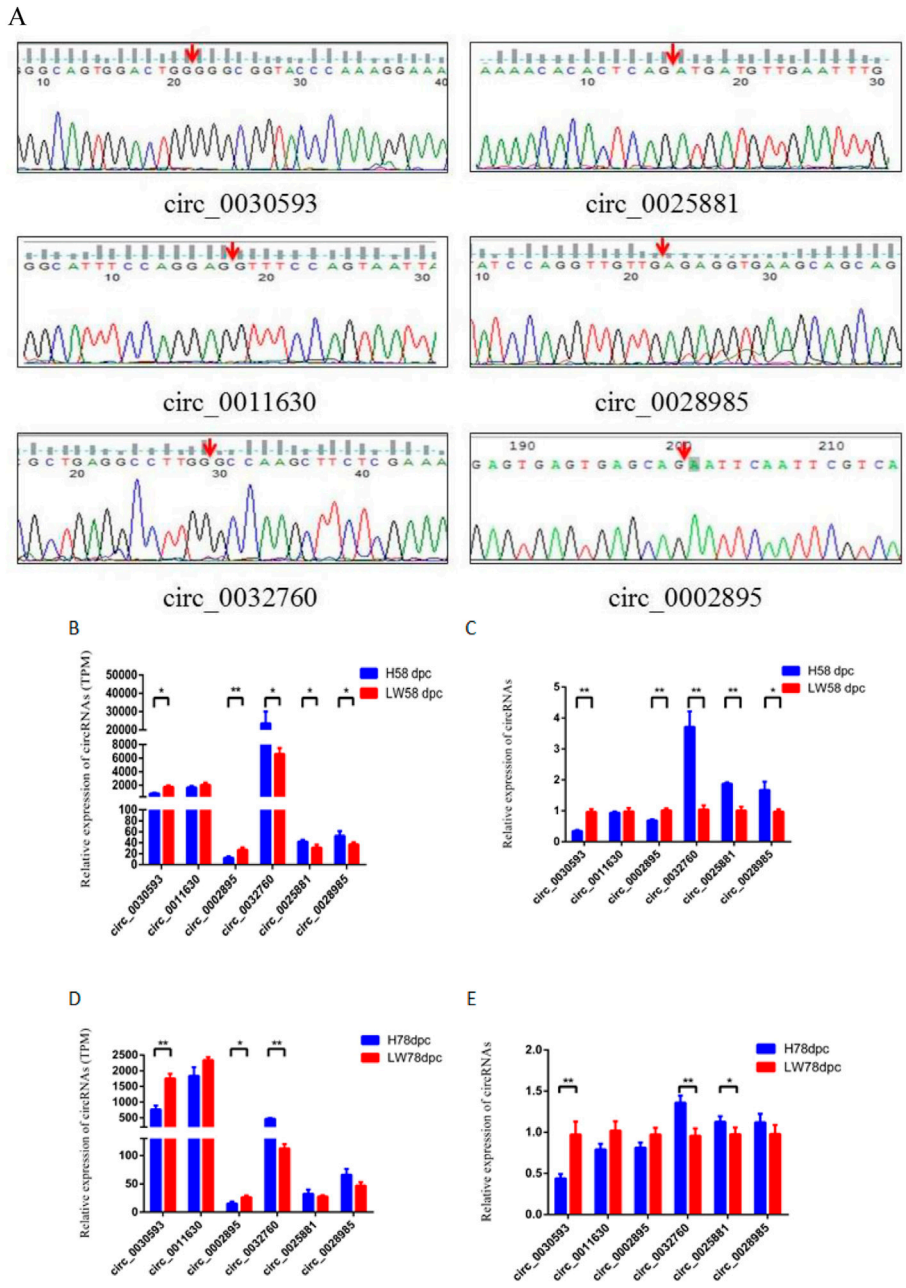

FIGURE 6
Validation of differently expressed circRNAs **(A)** The back-splicing junction sequence of circRNAs by sanger sequencing using the convergent primers. RNA sequecing **(B,D)** results and RT-qPCR results **(C,E)** of six differently expressed circRNAs between HN and LW at 58 dpc and 78 dpc.

49 dpc, respectively. At 49 dpc, secondary muscle fibers could be detected in both breeds, but at 91 dpc, LT had fewer muscle fiber numbers and smaller muscle fiber diameters (Zhao et al., 2011). Similarly, the number and density of myoblasts in TC were greater than those in YK pigs at 30 dpc (Zhao et al., 2015). These studies indicate that during the embryonic period, compared to Western commercial pig breeds, Chinese indigenous pig breeds exhibit earlier myogenesis, shorter proliferation, and consequently lower meat production. In the present study, many muscle development-related signaling pathways were enriched, with HCM and DCM being consistently upregulated in HN. The transcription and metabolism of folic acid were enriched at 38 dpc, and it was reported that folic acid is necessary for the proliferation and

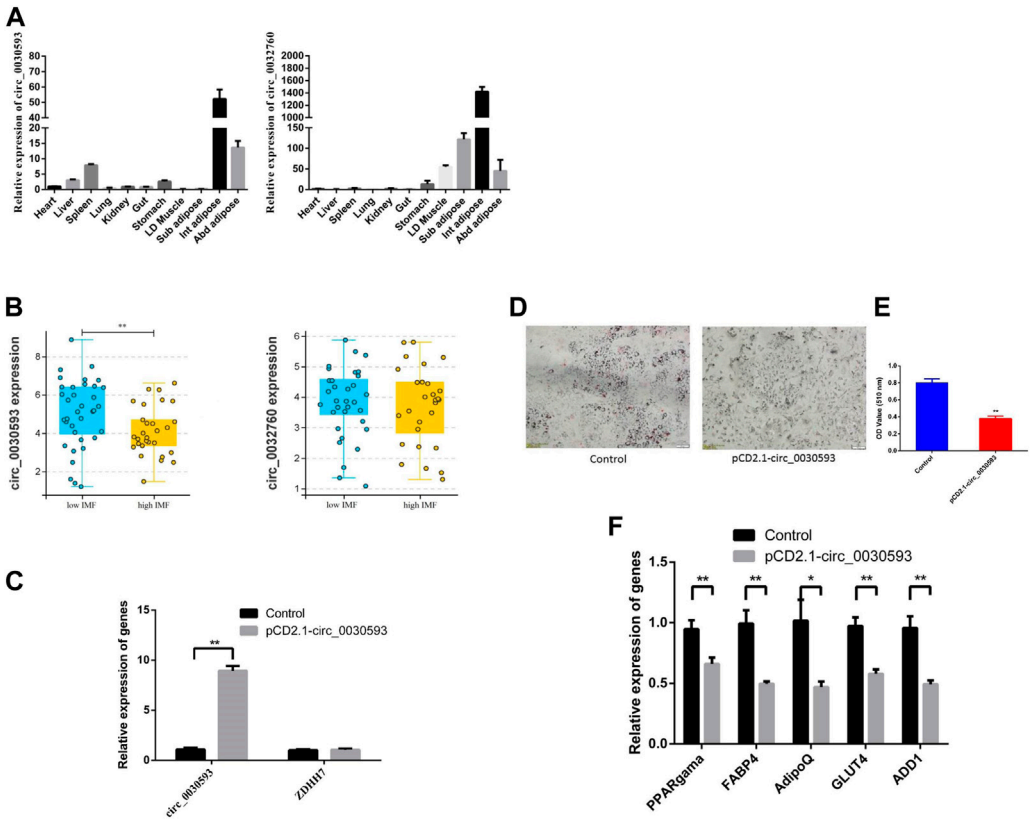

FIGURE 7
Function validation of differently expressed circRNAs **(A)** The expression level of circ_0030593 and circ_0032760 in different tissues by RT-qPCR. **(B)** circ_0030593 and circ_0032760 expression in longissimus dorsi muscle from high IMF and low IMF pigs **(C)**The effect of pCD2.1-circ_0030593 on expression of circ_0030593 and its parent gene ZDHH7. Overexpression of circ_0030593 inhibited adipogenesis by Oil Red O staining **(D)**, OD value **(E)** and RT-qPCR **(F)**.

differentiation of myoblasts (Hwang et al., 2018). In contrast, the Wnt pathway, which promotes myogenic differentiation (Zhou et al., 2015), was significantly upregulated at both 38 and 58 dpc. These results are consistent with earlier myogenic differentiation and proliferation in Chinese indigenous pig breeds. Rap1 (Li et al., 2018), adhesion junctions (Ghosh et al., 2022), tight junctions (Kusch et al., 2009), ras (Tyurin-Kuzmin et al., 2020) and other signaling pathways associated with myoblast proliferation and muscle development were downregulated at 58 dpc and/or 78 dpc. These results suggest that at 58 dpc and 78 dpc, muscle development in the HN was less active than that in the LW, consistent with previous findings that Chinese indigenous pig breeds exhibit slower muscle development than Western commercial breeds during the later embryonic period (Zhao et al., 2011). This result is also consistent with our previous studies on lncRNAs (Wang et al., 2020a).

It has been reported that during the later embryonic development period, intramuscular fat deposition in Chinese indigenous pigs is different from that in Western commercial breeds (Zhao et al., 2015). In the present study, multiple pathways associated with adipose differentiation and lipid deposition were enriched at different stages, such as the cAMP pathway, which inhibits adipogenesis and promotes lipolysis (Liu et al., 2017), was upregulated at 38 dpc and downregulated at 78 dpc. The cGMP/PKG pathway, which promotes adipogenesis (Chen et al., 2007), displayed higher expression at 78 dpc. The estrogen pathway, which inhibits IMF deposition (Renaville et al., 2012), was downregulated at both 38 and 78 dpc. The Fas signaling pathway, which is involved in intramuscular fat deposition (Cui et al., 2012), was enriched at 58 and 78 dpc. Other pathways associated with lipid metabolism, such as type I diabetes mellitus, cholesterol metabolism, and sphingolipid metabolism, were upregulated in HN at different developmental periods. These results coincide with the higher IMF content in Chinese indigenous pig breeds.

Muscle fiber type also affects meat quality, such as meat color and tenderness (Lee et al., 2010). The proportion of muscle fiber types was found to be different between Chinese and Western commercial pig breeds (Kunej et al., 2005; Huang et al., 2016). In this research, AMPK exhibited lower expression in HN at 78 dpc, and

Wnt displayed higher expression levels in HN at 38 and 58 dpc. Both of these pathways can promote a fast-to-slow fiber type shift (Tee et al., 2009; Liu et al., 2016). The thyroid hormone pathway, which affects muscle fiber type, was also enriched (Salvatore et al., 2014).

CircRNAs can also function as miRNA sponges. For example, circ-FoxO3 inhibits C2C12 myoblast cell differentiation by sponging miR-138-5p (Li et al., 2019). CircINSR inhibits preadipocyte adipogenesis by regulating Foxo 1 and EPT 1 *via* miR-15/16 (Shen et al., 2020). CircHIPK3 promotes the proliferation and differentiation of myoblasts by sponging miR-7 (Gao et al., 2021). CircFUT10 promotes adipocyte proliferation *via* the let-7-PPARGC1B (peroxisome proliferator-activated receptor γ coactivator 1-β) pathway (Jiang et al., 2020). In the current study, the DEC-miRNA network included 62 nodes (44 circRNAs and 16 miRNAs) and 141 edges, of which miR-370 had the most target circRNAs (23 circRNAs) and circ_0032738 had the most miRNA binding sites (12 miRNAs). Therefore, these DECs might participate in the regulation of meat quality by sponging these miRNAs.

To validate the RNA sequencing results, 6 circRNAs were confirmed by amplification with convergent primers. Expression of these circRNAs at the 58 dpc and 78 dpc stage was analyzed by RT–qPCR, and the results were consistent with the sequencing results. To determine how these circRNAs regulate muscle development or fat deposition, two shared DECs (circ_0030593 and circ_0032760) were selected for functional verification. Both circRNAs showed the highest expression levels in intramuscular adipose tissue, indicating that these two DECs might play an important role in intramuscular fat deposition, so we first verified their regulatory role in the adipogenesis of porcine intramuscular adipocytes. The expression difference of circ_0030593 between the high and low IMF group was significant ($p < 0.05$), suggesting that circ_0030593 may have an inhibitory effect on intramuscular fat deposition. Further overexpression experiments in porcine primary intramuscular adipocytes confirmed that elevating circ_0030593 inhibited lipid deposition. However, the mechanism of circ_0030593 is still not entirely clear. Circ_0030593 contains binding sites for many miRNAs associated with adipogenesis and lipid deposition, such as the miRNAs promoting adipogenesis and lipid deposition (miR-574-5p (Li et al., 2022b), miR-326 (Feng et al., 2020), miR-296-5p (Cazanave et al., 2011), and miR-378 (Podkalicka et al., 2022)) and miRNAs inhibiting lipid deposition (miR-125a (Xu et al., 2018), miR-127 (Gao et al., 2019), miR-34a (Wang et al., 2020c), miR-199a-5p (Alexander et al., 2013; Shi et al., 2014), and miR-370 (Chu et al., 2021; Zhang et al., 2021)). Therefore, circ_0030593 may be involved in regulating lipid deposition and thereby affecting intramuscular fat deposition by binding these miRNAs, but the specific miRNA or miRNAs need to be verified using dual luciferase, RIP and ChIRP assays in future research.

In conclusion, circRNA expression differences in LD muscle between HN and LW pigs at different embryonic stages were compared, and a DEC-miRNA network was constructed. The results indicated that circRNAs participate in the regulation of embryonic muscle development differences between HN and LW by regulating myogenesis, proliferation, adipogenesis and muscle fiber transformation. We also identified a novel circRNAs circ_0030593, that showed the highest expression levels in intramuscular adipose tissue, and in primary intramuscular adipocytes, it inhibited lipid deposition. These results provide basic material for understanding the effect of circRNA on meat quality.

Data availability statement

The datasets presented in this study can be found in online repositories. The names of the repository/repositories and accession number(s) can be found below: https://www.ncbi.nlm.nih.gov/, SRP243554.

Ethics statement

The animal study was reviewed and approved by the Institutional Animal Care and Use Committee (IACUC).

Author contributions

Conceptualization, JW, Q-XL, and B-SX; Funding acquisition, JW and J-FC; Investigation, JW, QM, and J-FC; Methodology and Validation, QM, J-JS, Q-LR, and J-QZ; Resources, JW, J-FC, and J-QZ; Writing—original draft, JW and J-FC; Writing—review and editing, JW, D-LM, Q-XL, and B-SX. All authors have read and agreed to the published version of the manuscript.

Funding

This study was funded by the National Key R&D Program of China (2021YFD1301200), National Natural Science Foundation of China (31601927), Henan Excellent Youth Fund Project (222300420051), Financial Budget Project of Henan Province (212102110010), Special Fund for Science and Technology Innovation Team in Henan Academy of Agricultural Science (2022TD34), and Independent Innovation Fund Project in Henan Academy of Agricultural Science (2022ZC42, XMZC202103).

Conflict of interest

The authors declare that the research was conducted in the absence of any commercial or financial relationships that could be construed as a potential conflict of interest.

Publisher's note

References

Alexander, M.-S., Kawahara, G., Motohashi, N., Casar, J.-C., Eisenberg, I., Myers, J.-A., et al. (2013). MicroRNA-199a is induced in dystrophic muscle and affects WNT signaling, cell proliferation, and myogenic differentiation. *Cell Death Differ.* 20 (9), 1194–1208. doi:10.1038/cdd.2013.62

Cai, C.-B., Li, M., Zhang, Y.-W., Meng, S., Yang, Y., Gao, P.-F., et al. (2020). Comparative transcriptome analyses of longissimus thoracis between pig breeds differing in muscle characteristics. *Front. Genet.* 11, 526309. doi:10.3389/fgene.2020.526309

Cao, H.-G., Liu, J.-M., Du, T.-N., Liu, Y.-H., Zhang, X.-Y., Guo, Y., et al. (2022). Circular RNA screening identifies circMYLK4 as a regulator of fast/slow myofibers in porcine skeletal muscles. *Mol. Genet. Genomics.* 297 (1), 87–99. doi:10.1007/s00438-021-01835-5

Cazanave, S.-C., Mott, J.-L., Elmi, N.-A., Bronk, S.-F., Masuoka, H.-C., Charlton, M.-R., et al. (2011). A role for miR-296 in the regulation of lipoapoptosis by targeting PUMA. *J. Lipid Res.* 52 (8), 1517–1525. doi:10.1194/jlr.M014654

Chen, C.-W., Chen, L.-K., Huang, T.-Y., Yang, D. A.-O., Liu, S.-Y., Tsai, P.-J., et al. (2007). Nitric oxide mobilizes intracellular Zn^{2+} via the GC/cGMP/PKG signaling pathway and stimulates adipocyte differentiation. *Cardiovasc Res.* 75 (2), 426–433.

Chen, F.-F., Xiong, Y., Peng, Y., Gao, Y., Qin, J., Chu, G.-Y., et al. (2017). miR-425-5p inhibits differentiation and proliferation in porcine intramuscular preadipocytes. *Int. J. Mol. Sci.* 18 (10), 2101. doi:10.3390/ijms18102101

Chen, M.-J., Wei, X.-F., Song, M.-M., Jiang, R., Huang, K.-W., Deng, Y.-F., et al. (2021). Circular RNA circMYBPC1 promotes skeletal muscle differentiation by targeting MyHC. *Mol. Ther. Nucleic Acids* 24, 352–368. doi:10.1016/j.omtn.2021.03.004

Chu, Y.-X., Yao, Y., and Li, X. (2021). MiR-370 enhances cell cycle and represses lipid accumulation in porcine adipocytes. *Anim. Biotechnol.* 32 (3), 334–342. doi:10.1080/10495398.2019.1697278

Cui, H.-X., Zheng, M.-F., Liu, R.-R., Zhao, G.-P., Chen, J.-L., and Wen, J. (2012). Liver dominant expression of fatty acid synthase (FAS) gene in two chicken breeds during intramuscular-fat development. *Mol. Biol. Rep.* 39 (4), 3479–3484. doi:10.1007/s11033-011-1120-8

Ding, Z.-Y., Sun, D.-Y., Han, J., Shen, L., Yang, F., Sah, S., et al. (2021). Novel noncoding RNA CircPTK2 regulates lipolysis and adipogenesis in cachexia. *Mol. Metab.* 53, 101310. doi:10.1016/j.molmet.2021.101310

Feng, Y.-T., Zhou, L.-T., Peng, Y., Yang, Y.-T., Fan, T.-Y., Jiang, X., et al. (2020). The role of miR-326 in adipogenic differentiation of human adipose-derived stem cells by targeting C/EBPα *in vitro*. *Anat. Rec.* 303 (7), 2054–2060. doi:10.1002/ar.24281

Gao, M.-J., Li, X., Yang, Z.-J., Zhao, S., Ling, X.-X., Li, J.-J., et al. (2021). circHIPK3 regulates proliferation and differentiation of myoblast through the miR-7/TCF12 pathway. *J. Cell. Physiol.* 236 (10), 6793–6805. doi:10.1002/jcp.30363

Gao, Y., Wang, Y.-Q., Chen, X.-C., Peng, Y., Chen, F.-F., He, Y.-L., et al. (2019). MiR-127 attenuates adipogenesis by targeting MAPK4 and HOXC6 in porcine adipocytes. *J. Cell. Physiol.* 234 (12), 21838–21850. doi:10.1002/jcp.28660

Gao, Y., Zhang, J.-Y., and Zhao, F.-Q. (2018). Circular RNA identification based on multiple seed matching. *Brief. Bioinform.* 19 (5), 803–810. doi:10.1093/bib/bbx014

Ghosh, D., Ghosh, S., and Chaudhuri, A. (2022). Deconstructing the role of myosin contractility in force fluctuations within focal adhesions. *Biophys. J.* 121 (9), 1753–1764. doi:10.1016/j.bpj.2022.03.025

He, D.-T., Zou, T.-D., Gai, X.-R., Ma, J.-D., Li, M.-Z., Huang, Z.-Q., et al. (2017). MicroRNA expression profiles differ between primary myofiber of lean and obese pig breeds. *PLoS One* 12 (7), e0181897. doi:10.1371/journal.pone.0181897

Hong, L.-J., Gu, T., He, Y.-J., Zhou, C., Hu, Q., Wang, X.-W., et al. (2019). Genome-wide analysis of circular RNAs mediated ceRNA regulation in porcine embryonic muscle development. *Front. Cell Dev. Biol.* 7, 289. doi:10.3389/fcell.2019.00289

Huang, K.-W., Chen, M.-J., Zhong, D.-D., Luo, X.-E., Feng, T., Song, M.-M., et al. (2021). Circular RNA profiling reveals an abundant circEch1 that promotes myogenesis and differentiation of bovine skeletal muscle. *J. Agric. Food Chem.* 69 (1), 592–601. doi:10.1021/acs.jafc.0c06400

Huang, Y.-N., Ao, Q.-W., Jiang, Q.-Y., Guo, Y.-F., Lan, G.-Q., and Jiang, H.-S. (2016). Comparisons of different myosin heavy chain types, AMPK, and PGC-1α gene expression in the longissimus dorsi muscles in Bama Xiang and Landrace pigs. *Genet. Mol. Res.* 15 (2). doi:10.4238/gmr.15028379

Hwang, S.-Y., Kang, Y.-J., Sung, B., Jang, J.-Y., Hwang, N.-L., Oh, H.-J., et al. (2018). Folic acid is necessary for proliferation and differentiation of C2C12 myoblasts. *J. Cell. Physiol.* 233 (2), 736–747. doi:10.1002/jcp.25989

Jiang, R., Li, H., Yang, J.-M., Shen, X.-M., Song, C.-C., Yang, Z.-X., et al. (2020). circRNA profiling reveals an abundant circFUT10 that promotes adipocyte proliferation and inhibits adipocyte differentiation via sponging let-7. *Mol. Ther. Nucleic Acids* 20, 491–501. doi:10.1016/j.omtn.2020.03.011

Jin, L., Tang, Q.-Z., Hu, S.-L., Chen, Z.-X., Zhou, X.-M., Zeng, B., et al. (2021). A pig BodyMap transcriptome reveals diverse tissue physiologies and evolutionary dynamics of transcription. *Nat. Commun.* 12 (1), 3715. doi:10.1038/s41467-021-23560-8

Kunej, T., Wu Xl Fau - Berlic, T.-M., Berlic Tm Fau - Michal, J.-J., Michal Jj Fau - Jiang, Z., Jiang, Z., and Fau - Dovc, P. (2005). Frequency distribution of a Cys430Ser polymorphism in peroxisome proliferator-activated receptor-gamma coactivator-1 (PPARGC1) gene sequence in Chinese and Western pig breeds. *J. Anim. Breed. Genet.* 122 (1), 7–11. doi:10.1111/j.1439-0388.2004.00498.x

Kusch, A., Tkachuk, S., Tkachuk, N., Patecki, M., Park, J., Dietz, R., et al. (2009). The tight junction protein ZO-2 mediates proliferation of vascular smooth muscle cells via regulation of Stat1. *Cardiovasc. Res.* 83 (1), 115–122. doi:10.1093/cvr/cvp117

Lee, S.-H., Joo, S.-F., and Ryu, Y.-C. (2010). Skeletal muscle fiber type and myofibrillar proteins in relation to meat quality. *Meat Sci.* 86 (1), 166–170. doi:10.1016/j.meatsci.2010.04.040

Li, B.-J., He, Y., Wu, W.-J., Tan, X.-F., Wang, Z.-H., Irwin, D.-M., et al. (2022). Circular RNA profiling identifies novel circPPARA that promotes intramuscular fat deposition in pigs. *J. Agric. Food Chem.* 70 (13), 4123–4137. doi:10.1021/acs.jafc.1c07358

Li, B.-J., Yin, D., Li, P.-H., Zhang, Z.-K., Zhang, X.-Y., Li, H.-Q., et al. (2020). Profiling and functional analysis of circular RNAs in porcine fast and slow muscles. *Front. Cell Dev. Biol.* 8, 322. doi:10.3389/fcell.2020.00322

Li, B., Yang, J.-Z., He, J., Gong, Y., Xiao, Y., Zeng, Q.-H., et al. (2021). Spatiotemporal regulation and functional analysis of circular RNAs in skeletal muscle and subcutaneous fat during pig growth. *Biol. (Basel)* 10 (9), 841. doi:10.3390/biology10090841

Li, K., Huang, W.-C., Wang, Z.-J., Chen, Y.-F., Cai, D.-F., and Nie, Q.-H. (2021). circTAF8 regulates myoblast development and associated carcass traits in chicken. *Front. Genet.* 12, 743757. doi:10.3389/fgene.2021.743757

Li, M., Zhang, N., Zhang, W.-F., Hei, W., Cai, C.-B., Yang, Y., et al. (2021). Comprehensive analysis of differentially expressed circRNAs and ceRNA regulatory network in porcine skeletal muscle. *BMC Genomics* 22 (1), 320. doi:10.1186/s12864-021-07645-8

Li, Q., Teng, Y.-F., Wang, J., Yu, M., Li, Y.-Q., and Zheng, H. (2018). Rap1 promotes proliferation and migration of vascular smooth muscle cell via the ERK pathway. *Pathol. Res. Pract.* 214 (7), 1045–1050. doi:10.1016/j.prp.2018.04.007

Li, X.-Y., Li, C.-Y., Liu, Z.-J., Ni, W., Yao, R., Xu, Y.-R., et al. (2019). Circular RNA circ-FoxO3 inhibits myoblast cells differentiation. *Cells* 8 (6), 616. doi:10.3390/cells8060616

Li, Y.-Y., Li, J.-Y., Yu, H.-B., Liu, Y.-X., Song, H.-X., Tian, X.-X., et al. (2022). HOXA5-miR-574-5p axis promotes adipogenesis and alleviates insulin resistance. *Mol. Ther. Nucleic Acids* 27, 200–210. doi:10.1016/j.omtn.2021.08.031

Liu, G.-N., Li, M.-H., Xu, Y.-T., Wu, S., Saeed, M., and Sun, C. (2017). ColXV promotes adipocyte differentiation via inhibiting DNA methylation and cAMP/PKA pathway in mice. *Oncotarget* 8 (36), 60135–60148. doi:10.18632/oncotarget.18550

Liu, J., Liang, X.-J., Zhou, D.-X., Lai, L., Xiao, L.-W., Liu, L., et al. (2016). Coupling of mitochondrial function and skeletal muscle fiber type by a miR-499/Fnip1/AMPK circuit. *EMBO Mol. Med.* 8 (10), 1212–1228. doi:10.15252/emmm.201606372

Love, M.-I., Huber, W., and Anders, S. (2014). Moderated estimation of fold change and dispersion for RNA-seq data with DESeq2. *Genome Biol.* 15 (12), 550. doi:10.1186/s13059-014-0550-8

Podkalicka, P., Mucha, O., Kaziród, K., Szade, K., Stępniewski, J., Ivanishchuk, L., et al. (2022). miR-378 affects metabolic disturbances in the mdx model of Duchenne muscular dystrophy. *Sci. Rep.* 12 (1), 3945. doi:10.1038/s41598-022-07868-z

Rao, A., Arvinden, V.-R., Ramasamy, D., Patel, K., Meenakumari, B., Ramanathan, P., et al. (2021). Identification of novel dysregulated circular RNAs in early-stage breast cancer. *J. Cell. Mol. Med.* 25 (8), 3912–3921. doi:10.1111/jcmm.16324

Renaville, B., Piasentier, E., Bacciu, N., and Prandi, A. (2012). Association of the estrogen receptor 1 and 2 polymorphisms with fat distribution in heavy pigs. *Livest. Sci.* 146 (1), 54–58. doi:10.1016/j.livsci.2012.02.021

Salvatore, D., Simonides, W.-S., Dentice, M., Zavacki, A.-M., and Larsen, P.-R. (2014). Thyroid hormones and skeletal muscle-new insights and potential implications. *Nat. Rev. Endocrinol.* 10 (4), 206–214. doi:10.1038/nrendo.2013.238

Shen, X.-M., Tang, J., Ru, W.-X., Zhang, X.-Y., Huang, Y.-Z., Lei, C.-Z., et al. (2020). CircINSR regulates fetal bovine muscle and fat development. *Front. Cell Dev. Biol.* 8, 615638. doi:10.3389/fcell.2020.615638

Shi, X.-E., Li, Y.-F., Jia, L., Ji, H.-L., Song, Z.-Y., Cheng, J., et al. (2014). MicroRNA-199a-5p affects porcine preadipocyte proliferation and differentiation. *Int. J. Mol. Sci.* 15 (5), 8526–8538. doi:10.3390/ijms15058526

Song, X.-H., He, N., Xing, Y.-T., Jin, X.-Q., Li, Y.-W., Liu, S.-S., et al. (2021). A novel age-related circular RNA circ-ATXN2 inhibits proliferation, promotes cell death and adipogenesis in rat adipose tissue-derived stromal cells. *Front. Genet.* 12, 761926. doi:10.3389/fgene.2021.761926

Tee, J.-M., van Rooijen, C., Boonen, R., and Zivkovic, D. (2009). Regulation of slow and fast muscle myofibrillogenesis by Wnt/beta-catenin and myostatin signaling. *PLoS One* 4 (6), e5880. doi:10.1371/journal.pone.0005880

Tyurin-Kuzmin, P.-A., Kalinina, N.-I., Kulebyakin, K.-Y., Balatskiy, A.-V., Sysoeva, V.-Y., and Tkachuk, V.-A. (2020). Angiotensin receptor subtypes regulate adipose tissue renewal and remodelling. *FEBS J.* 287 (6), 1076–1087. doi:10.1111/febs.15200

Wang, J., Chen, M.-Y., Chen, J.-F., Ren, Q.-L., Zhang, J.-Q., Cao, H., et al. (2020). LncRNA IMFlnc1 promotes porcine intramuscular adipocyte adipogenesis by sponging miR-199a-5p to up-regulate CAV-1. *BMC Mol. Cell Biol.* 21 (1), 77. doi:10.1186/s12860-020-00324-8

Wang, J., Ren, Q.-L., Hua, L.-S., Chen, J.-F., Zhang, J.-Q., Bai, H.-J., et al. (2019). Comprehensive analysis of differentially expressed mRNA, lncRNA and circRNA and their ceRNA networks in the longissimus dorsi muscle of two different pig breeds. *Int. J. Mol. Sci.* 20 (5), 1107. doi:10.3390/ijms20051107

Wang, J., Ren, Q.-L., Hua, L.-S., Chen, J.-F., Zhang, J.-Q., Bai, H.-J., et al. (2019). Comprehensive analysis of differentially expressed mRNA, lncRNA and circRNA and their ceRNA networks in the longissimus dorsi muscle of two different pig breeds. *Int. J. Mol. Sci.* 20 (5), E1107. doi:10.3390/ijms20051107

Wang, L.-D., Liang, W.-S., Wang, S.-S., Wang, Z.-X., Bai, H., Jiang, Y., et al. (2020). Circular RNA expression profiling reveals that circ-PLXNA1 functions in duck adipocyte differentiation. *PLoS One* 15 (7), e0236069. doi:10.1371/journal.pone.0236069

Wang, W.-W., Li, X.-X., Ding, N., Teng, J., Zhang, S., Zhang, Q., et al. (2020). miR-34a regulates adipogenesis in porcine intramuscular adipocytes by targeting ACSL4. *BMC Genet.* 21 (1), 33. doi:10.1186/s12863-020-0836-7

Xu, T.-Y., Wu, J., Han, P., Zhao, Z.-M., and Song, X.-F. (2017). Circular RNA expression profiles and features in human tissues: A study using RNA-seq data. *BMC Genomics* 18 (6), 680. doi:10.1186/s12864-017-4029-3

Xu, Y., Du, J.-J., Zhang, P.-W., Zhao, X., Li, Q., Jiang, A.-A., et al. (2018). MicroRNA-125a-5p mediates 3T3-L1 preadipocyte proliferation and differentiation. *Molecules* 23 (2), 317. doi:10.3390/molecules23020317

Yue, B.-L., Yang, H.-Y., Wu, J.-Y., Wang, J., Ru, W.-X., Cheng, J., et al. (2022). circSVIL regulates bovine myoblast development by inhibiting STAT1 phosphorylation. *Sci. China. Life Sci.* 65 (2), 376–386. doi:10.1007/s11427-020-1908-2

Zhang, P.-W., Du, J.-J., Guo, X.-Y., Wu, S., He, J., Li, X.-R., et al. (2021). LncMyoD promotes skeletal myogenesis and regulates skeletal muscle fiber-type composition by sponging miR-370-3p. *Genes (Basel)* 12 (4), 589. doi:10.3390/genes12040589

Zhao, J., Zhao, X.-Y., Shen, X.-X., Zhang, Y., Zhang, Y., Ye, L., et al. (2022). CircCCDC91 regulates chicken skeletal muscle development by sponging miR-15 family via activating IGF1-PI3K/AKT signaling pathway. *Poult. Sci.* 101 (5), 101803. doi:10.1016/j.psj.2022.101803

Zhao, X., Mo, D.-L., Li, A.-N., Gong, W., Xiao, S.-Q., Zhang, Y., et al. (2011). Comparative analyses by sequencing of transcriptomes during skeletal muscle development between pig breeds differing in muscle growth rate and fatness. *PLoS One* 6 (5), e19774. doi:10.1371/journal.pone.0019774

Zhao, Y.-Q., Li, J., Liu, H.-J., Xi, Y., Xue, M., Liu, W.-H., et al. (2015). Dynamic transcriptome profiles of skeletal muscle tissue across 11 developmental stages for both Tongcheng and Yorkshire pigs. *BMC Genomics* 16 (1), 377. doi:10.1186/s12864-015-1580-7

Zhou, Y.-F., Zhou, Z., Zhang, W., Hu, X.-M., Wei, H.-K., Peng, J., et al. (2015). SIRT1 inhibits adipogenesis and promotes myogenic differentiation in C3H10T1/2 pluripotent cells by regulating Wnt signaling. *Cell Biosci.* 5, 61. doi:10.1186/s13578-015-0055-5

Frontiers in Veterinary Science

Transforms how we investigate and improve animal health

The third most-cited veterinary science journal, bridging animal and human health with a comparative approach to medical challenges. It explores innovative biotechnology and therapy for improved health outcomes.

Discover the latest Research Topics

See more →

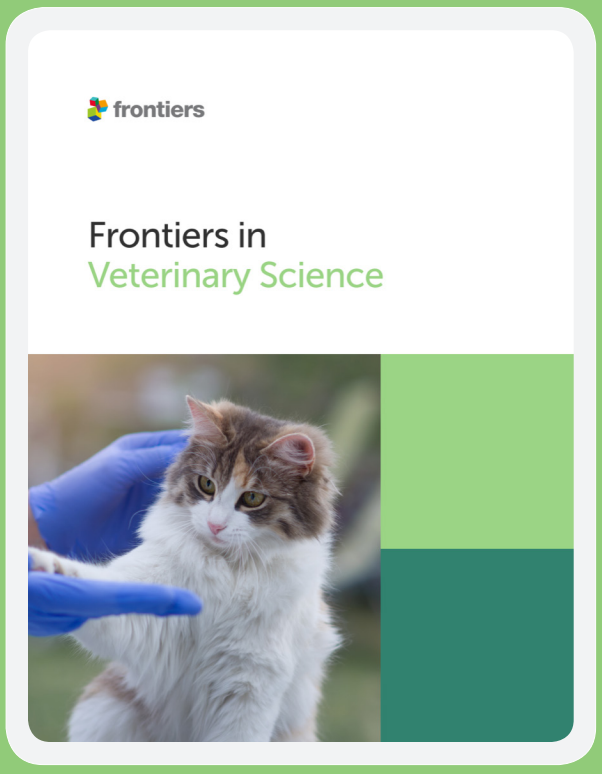

Frontiers

Avenue du Tribunal-Fédéral 34
1005 Lausanne, Switzerland
frontiersin.org

Contact us

+41 (0)21 510 17 00
frontiersin.org/about/contact